

On the role of districts as renewable energy hubs

Présentée le 8 avril 2022

Faculté des sciences et techniques de l'ingénieur
Groupe SCI STI FM
Programme doctoral en énergie

pour l'obtention du grade de Docteur ès Sciences

par

Luise MIDDELHAUVE

Acceptée sur proposition du jury

Prof. D. Dujic, président du jury
Prof. F. Maréchal, directeur de thèse
Prof. U. Eicker, rapporteuse
Dr K. Orehounig, rapporteuse
Prof. C. Ballif, rapporteur

“Alles, was man tun muss, ist, die richtige Taste zum richtigen Zeitpunkt zu treffen.”

“All one has to do is hit the right key at the right time.”

J. S. Bach

Acknowledgments

It is easy. "All one has to do is hit the right key at the right time" - a quote from my favorite composer Johann Sebastian Bach about him playing every existing instrument. The beauty of his statement is, that it is timeless, connects the 18th century to the 21st and puts the process of writing a software-based PhD thesis in a different light. "It is easy, we have everything" would be the matching quote from my professor, supervisor, mentor, Doktorvater François, whom I want to thank first. I am not as humble as Bach and admit it was not as easy for me, but without your guidance, it would have been much harder. I thank you for always having an open door for discussions and for having my back in any kind of situation.

It would also have been much harder without the great team at IPESE, which started as a group of colleagues but became a circle of friends, which I do not want to miss. The very first colleagues I have met at IPESE were Paul, Nils and Sébastien at a day somewhere in November 2017. Thank you, Paul, for laying the groundwork for this thesis with your own research and for patiently answering my millions of questions at the beginning. Thank you, Sébastien, for opening my eyes to how to present results in a fancy way, especially parallel coordinates, before I even had started in the lab. Nils, I am very grateful for your input about PV orientation and all the connected ladybugs and grasshoppers in this world.

When I officially started as a PhD student in February 2018, I found a great team at IPESE, people from all over the world. Each lunch became a social event, a colorful mix of cultures which often had us laughing with tears. Thank you to the experienced generation of PhDs Sophia, Victor, Stefano, Dilan for welcoming and integrating me without any hesitation. Hür and Raluca, we were an amazing team for organizing the IPESEski weekend. The amount of food we bought and cooked that weekend was unprecedented and conveniently freed us from the workshop. Thank you, Julia, for the deal we made about via ferratas, the fun at the summer school in Champéry, and for the visit to fête des vignerons, which I will always remember. Xiang, thank you for your unique sense of humor and for experiencing ECOS 2021 together. Fred, thank you for your kind nature and pleasant train rides to Sion, discussing the heat pumps of today. Thank you Shanshan for the best dumpling night Sion has seen as of today. Thank you, Rafael, for not being blind and Alessio for dreaming about the digitalization of the power grid. Thank you also to the new generation of PhDs Jonas, Dorsan and Cédric for being the future of the lab and for making REHO a success story. Of course, I want to acknowledge all the masterstudents, which were challenging me with their curious questions and

Acknowledgments

who contributed to the research: Nataljia, Nils, Alexander, Max, Jules, Tobia, Yann and Cédric. Only talking about PhDs and Masterstudents I would miss a very important part of the lab: our post-docs. Thank you Tivi, Shivom, Alberto, Luc, Theo and Ermanno for your support and experience, which helped me finding my way in the research community. Thank you Maziar for being my literally closest friend in Vevey and for all the energizing bike rides, carrying watermelons and wine bottles uphill to ensure our refreshing break. Francesco, you guided and helped me to publish, without you, this journey would have been a much longer one. You have always said “I just help to make your work shine” but it was more than that, thank you. Ivan, although not “my” post-doc, I am very grateful that you have always found the time to discuss results, English phrases, Catan strategies and for leaving behind a lifetime supply of turmeric. Our lab has the true experts of pressing the right key at the right time: Gillian, Cyrille, Michel, Cédric, thank you for being the backbone of our IT support, which made the 1234 look small. Sylvie and Evelyn, our “front office”, thank you for all your support and the laughter we shared, although confronted with hideous bureaucracy, real estate agencies or missing washing machines. Next to the front office is “Manuele’s office”. Thank you Manuele for your contribution about the life-cycle assessment of energy systems in this thesis. Our lab has a twin lab at EPFL, the GEM: Thank you Guillaume for all the fun we had, while sitting in the jury at the oral exams of the course MOES. Priscilla and Manuel thank you for the good time with many weird jokes when we shared the train ride to Montreux.

This thesis was made possible in context of national research projects, where I met many partners in academics and the industry. First and foremost, thank you, Jordan and Lionel, for your input about PV placement, load disaggregation and all your feedback. Having someone to discuss outside the lab was very enriching. Thank you to Arnoud for the low barrier to needed data and measurements and Andreea for believing in our research and continuing the collaboration at IPESE.

Writing a PhD thesis during a pandemic was challenging in many ways. The last two years were defined by lockdowns and home-office, and I felt more isolated than ever. I am very grateful for the support of my family and friends, which helped me reaching the goal of submitting this thesis. A gigantic thank you to Bonnie and Katie, who reviewed parts of this thesis in their spare time. Not only did the English language improve drastically, but your help and comments made me feel much less of a lonely fighter. Thank you also to my friends, who have came the long way to Switzerland to see me: Janin, Vivien, Moa, Hannah and Madeleine. Thank you, Daniel, for being my first Swiss friend and for your immediate help when I was looking for an apartment. There have been many ups and downs in my PhD journey, which no one has followed as closely as you, Francesca. Without any explanation needed you have always understood my situation. We often joked about 1 soul 2 bodies, but actually it is your nature to see the situation from not expected angles, which I value immensely.

Thank you to my parents, Milo and Georg, and my sister Helene, who were there for me throughout the entire journey; from the very beginning to the surprise visit at the very end. Thank you for counseling me on all my pros and cons on whether or not to accept this PhD position; I think we came the right decision. Helene, thank you for being the decoration queen and for making me feel

Acknowledgments

at home even at my new place in Switzerland.

Frederik, this is it, we made it. It is not “I made it”, it is “we made it”. We traveled 84782km (two times around the globe!) to see each other, spending about 900hrs on the train or in the car. We made it through 4 years, 2 countries and 1 pandemic. This was only possible because of your love and patience. We made it. Thank you.

Vevey, 22.02.2022

Lise Middelhaave

Abstract

Although inevitable, the process of transforming urban areas into sustainable living environments presents many challenges. The decentralization of the energy system, the interconnection of multiple energy carriers, and the need to account for conflicting interests renders it a complex task. As key stakeholders, authorities often lack appropriate decision tools to frame and encourage the transition and to monitor the impact of implemented policies.

This work aims to provide useful insights into the role of districts as renewable energy hubs by showing requirements and highlighting constraints, leading to an increase in renewable energy penetration. The benefits and trade-offs between centralized and decentralized renewable energy hubs are emphasized to contribute to the ongoing discussion regarding sustainable urban planning. Mathematical programming is used to build a multi-objective optimization platform that integrates several renewable technologies with a special focus on solar integration. Specifically, this approach includes the role of the orientation of photovoltaic (PV) panels and the use of facades, including mounting partly shadowed PV panels and receiving solar heat gain. A decomposition algorithm (Dantzig–Wolfe) is used to bypass the computation effort associated with centralized energy hubs at the district scale.

The results highlight that a low-emission electrical grid mix has a high impact on sustainable design of renewable energy hubs at the building scale and led to less independent system configurations. Optimally integrating of solar systems had a significant impact on their interaction with the electrical grid: rotating the panels 20° westwards reduced the grid exchange peak by 50% while increasing cost by only 8.3%. Moreover, the studied district could achieve carbon neutrality based on PV energy alone, whereas self-sufficiency is more ambitious than confirmed the importance of storage systems: even with 100% round-trip efficiency of storage systems, the required ratio of area covered in PV modules to the energy reference area (ERA) was $A_{pv}/A_{ERA} = 0.44$ and 16 % of available facades were needed to be covered with PV modules. However, energy demand reduction through thermal renovation would allow self-sufficiency with half of the PV and storage capacity. Overall, this work demonstrates that moving from a decentralized to coordinated and centralized design strategy allows a higher electrification rate and an increased integration of renewable energy in the district for the same total expenses. The centralized investment strategy differed most from the decentralized strategy for PV panels; using the centralized strategy, a wide range of PV installation on less-optimal surfaces became economically interesting. The most economically convenient solution to overcome

Abstract

transformer limitations were district storage for peak shaving and photovoltaic curtailment. The cost increase were around 600 CHF per kWyr annual capacity shortage, regardless of the considered district energy system.

Keywords: District energy system, Multi-objective optimization, Photovoltaics, Renewable energy integration, Interconnection of energy carriers

Zusammenfassung

Die Transformation städtischer Gebiete hin zu nachhaltigen Lebensräumen ist unvermeidlich und der Prozess mit zahlreichen Herausforderungen verbunden. Die Aufgabe ist komplex aufgrund der Dezentralisierung des Energiesystems, der Verbindung mehrerer Energieträger, sowie der Berücksichtigung widersprüchlicher Interessen. Den Behörden als Hauptakteuren fehlen oft geeignete Entscheidungshilfen, um diesen Übergang zu gestalten, zu fördern und die Auswirkungen der umgesetzten Maßnahmen zu kontrollieren.

Ziel dieser Arbeit ist es, nützliche Einblicke in die Rolle von Bezirken als *renewable energy hubs* zu geben, indem die Anforderungen aufzeigt und die Randbedingungen hervorhoben werden, die zu einer Erhöhung der Marktdurchdringung von erneuerbaren Energien führen. Die Vorteile und Kompromisse zwischen zentralen und dezentralen *renewable energy hubs* werden analysiert, um einen Beitrag zur laufenden Diskussion über nachhaltige Stadtplanung zu leisten.

Mit Hilfe mathematischer Programmierung wird eine multikriterielle Optimierungsplattform erstellt, die mehrere erneuerbare Technologien integriert. Besonderer Fokus liegt dabei auf der Integration von Solarenergie. Der Ansatz umfasst insbesondere die Rolle der Fassaden einschließlich der Ausrichtung von teilweise beschatteten PV-Paneele. Ein Dekompositionsalgorithmus (Dantzig–Wolfe) wird verwendet, um den Berechnungsaufwand zu reduzieren, der mit zentralisierten *renewable energy hubs* auf Bezirksebene verbunden ist.

Die Ergebnisse zeigen, dass ein emissionsarmer Strommix einen großen Einfluss auf die nachhaltige Gestaltung von *renewable energy hubs* auf der Gebäudeebene hat und zu weniger unabhängigen Systemkonfigurationen führt. Die optimale Integration von Solarsystemen hatte einen signifikanten Einfluss in Verbindung mit dem Stromnetz: Eine Drehung der Paneele um 20° nach Westen reduzierte Netzaustauschspitzen um 50%, während die Gesamtkosten nur um 8,3% stiegen. Darüber hinaus konnte der untersuchte Stadtteil allein mit PV-Strom CO₂-Neutralität erreichen, wohingegen die Selbstversorgung ehrgeiziger war, was die Bedeutung von Speichersystemen bestätigte: Selbst bei einem Gesamtwirkungsgrad der Speichersysteme von 100% betrug das erforderliche Verhältnis zwischen der mit PV-Modulen bedeckten Fläche und der Gesamtfläche $A_{pv} / A_{ERA} = 0.44$, und es mussten 16% der verfügbaren Fassaden mit PV-Modulen bedeckt werden. Eine Reduzierung des Energiebedarfs durch thermische Sanierung würde jedoch eine Selbstversorgung mit bereits der Hälfte der PV- und Speicherkapazität ermöglichen. Insgesamt zeigt diese Arbeit, dass der Wechsel von einer dezentralen zu einer koordinierten und zentralisierten Strategie eine höhere Elektrifizierungsrate und eine stärkere Integration erneuerbarer Energien bei gleichen Gesamtkosten im Bezirk

Zusammenfassung

ermöglicht. Für PV-Paneele ist der Unterschied zwischen einer zentralisierten und einer dezentralen Investitionsstrategie am größten; mit der zentralisierten Strategie wurde eine Installation von PV-Anlagen auf weniger optimalen Flächen wirtschaftlich interessant. Die wirtschaftlich günstigste Lösung zur Überwindung der Transformatormehrbelastungen waren Stadtteil-Speicher zur Spitzenlastreduzierung und Beschränkung der PV-Einspeisung. Die Mehrkosten beliefen sich auf etwa 600 Franken pro kWyr jährlicher Kapazitätsknappheit, unabhängig vom Energiesystem des Stadtteils.

Schlüsselwörter: Energiesysteme, multikriterielle Optimierung, Photovoltaik, erneuerbare Energie, Multienergiesysteme

Contents

Acknowledgments	i
Abstract (English/German)	v
Table of content	ix
List of figures	xiii
List of tables	xvii
Acronyms and abbreviations	xix
List of symbols	xxiv
Introduction	1
Environmental impact of district energy systems	1
What are renewable energy hubs?	3
Contributions and novelty	4
Chapter 1: Renewable energy hubs at the building scale	5
Chapter 2: Photovoltaic panel orientation in renewable energy hubs	5
Chapter 3: Facades in interconnected renewable energy hubs	6
Chapter 4: Computational reduction for renewable energy hubs at the district scale	6
Chapter 5: Renewable energy hubs at the district scale	7
1 Renewable energy hubs at the building scale	9
1.1 Introduction	10
1.2 Method	11
1.2.1 Energy system	12
1.2.2 Energy demand	15
1.2.3 Energy system technologies	17
1.2.4 Problem objectives	18
1.2.5 Key performance indicators	20
1.2.6 Case study	27

Contents

1.3	Results and discussion	30
1.3.1	Global warming potential	30
1.3.2	Impact of system boundaries	32
1.3.3	Dimensional reduction	34
1.4	Conclusion	38
2	Photovoltaic panel orientation in renewable energy hubs	41
2.1	Introduction	42
2.2	State-of-the-art	42
2.2.1	Multi-objective optimization framework of building energy systems	42
2.2.2	Simulation and optimization of solar based energy systems	43
2.2.3	Modeling of photovoltaic panel orientation and directed irradiation	45
2.2.4	Gaps and contributions	46
2.3	Method	46
2.3.1	Irradiation modeling	47
2.3.2	Orientation of PV panel	48
2.3.3	Flat roofs and shading	49
2.3.4	Model integration PV Panel	52
2.3.5	Case study	53
2.4	Results and discussion	54
2.4.1	PV panel integration in renewable energy hubs at the building scale	54
2.4.2	Optimal orientation and the role of self-consumption	56
2.4.3	Comparison with flat roof assumption	57
2.4.4	Impact on the grid	59
2.5	Conclusion	63
3	Facades in interconnected renewable energy hubs	65
3.1	Introduction	66
3.1.1	State-of-the-art	66
3.1.2	Gaps and contributions	69
3.2	Method	69
3.2.1	Decentralized district energy system	70
3.2.2	Expansion of the validity range for PV installations	72
3.2.3	Solar irradiation and shading among buildings	74
3.2.4	Solar heat gains	77
3.2.5	Data-driven approach	77
3.2.6	Case study area	78
3.3	Results and discussion	80
3.3.1	What is the potential of energy generation from PV in the district?	80

Contents

3.3.2 Are PV installations on facades needed to become carbon neutral?	82
3.3.3 How much electricity can be generated locally and cost-efficiently?	83
3.3.4 How much PV is needed to achieve self-sufficiency?	85
3.3.5 How much energy storage is needed to achieve self sufficiency?	86
3.4 Conclusion	88
4 Computational reduction for centralized energy systems	91
4.1 Introduction	92
4.2 Time-series aggregation	92
4.2.1 State-of-the-art	92
4.2.2 Gaps and contributions	93
4.2.3 Method	94
4.2.4 Case study	95
4.2.5 Results and discussion	96
4.2.6 Main findings	102
4.3 Decomposition algorithm	104
4.3.1 State-of-the-art	104
4.3.2 Gaps and contributions	106
4.3.3 General structure	107
4.3.4 Algorithm	113
4.3.5 Case study	116
4.3.6 Results and discussion	116
4.3.7 Main findings	122
5 Renewable energy hubs at the district scale	125
5.1 Introduction	126
5.1.1 State-of-the-art	126
5.1.2 Gaps and contributions	128
5.2 Method	129
5.2.1 Key performance indicators	129
5.2.2 Centralized units	132
5.2.3 Centralized constraints	132
5.2.4 Case study	133
5.3 Results	134
5.3.1 What is the potential of a centralized design strategy?	134
5.3.2 Optimal investment strategy for photovoltaic panels	140
5.3.3 Grid-aware integration of renewable energy	147
5.4 Conclusion	152

Contents

Conclusion	155
Limitations and future perspectives	158
Appendix	161
A (Chapter 1)	163
B (Chapter 2)	171
C (Chapter 3)	175
D (Chapter 4)	179
E (Chapter 5)	181

List of figures

1	Strategy for the development of electricity generation from photovoltaic (PV) systems in Switzerland through the year 2050.	2
1.1	Schematic overview of a renewable energy hub at the building scale.	11
1.2	Quality of the data reduction technique for different number of k-medoid clusters . .	28
1.3	Clustering results for external temperature and global irradiation	29
1.4	Trade off between total annual expenses and global warming potential.	30
1.5	Relative share of operational global warming potential (GWP) to the total GWP for different cost scenarios.	31
1.6	Influence of the grid mix on the optimal design of renewable energy hubs.	32
1.7	Exergy efficiency and renewable energy share for various system configurations of renewable energy hubs	33
1.8	Impact of system boundaries for evaluation global warming potential (GWP).	34
1.9	Variable correlation plot of the principal component analysis of key performance indicators.	35
1.10	Result of K-medoids clustering of the technology decisions within the 8000 different optimal solutions for 40 residential renewable energy hubs.	37
2.1	Annual total irradiation, visualized for skydome of Geneva, Switzerland.	47
2.2	Annual irradiation on oriented PV modules on the climate zone of Geneva	49
2.3	Geometric relation between the distance between two modules and the sun elevation. .	50
2.4	Distance d between the modules for determining the inter-modular shading depending on the relative azimuth orientation	50
2.5	Irradiation loss of PV panel shading for different design limiting angles	51
2.6	Optimal integration of PV panels in renewable energy hubs.	55
2.7	Optimal distribution of PV installation for different roofs.	56
2.8	Optimal PV orientation for different installed capacities on a flat roof.	57
2.9	Error caused by assuming horizontal PV panels to optimal PV orientation for a district .	58
2.10	The need of PV panels of one renewable energy hub at the building scale in Switzerland to reach self-sufficiency with re-imports.	60

List of figures

2.11 Distribution of PV installation and orientation for total cost optimization of 40 buildings with individual load profiles	62
2.12 Distribution of PV installation and orientation for total cost optimization of 40 buildings with individual load profiles and real roof orientations.	63
3.1 Overview of a decentralized district energy system.	71
3.2 Visualization of the need for piece-wise linearization of the cost function for PV panels	73
3.3 Exemplary visualization of the geometry for a Facade to a Building and the sky-limiting angle.	74
3.4 Outline sketch of different azimuth angles.	75
3.5 Details of the case study area.	79
3.6 Economically best PV installation for 31 residential buildings.	81
3.7 Results of the multi-objective optimization of 31 buildings in one low-voltage grid. . .	82
3.8 Economic analysis of PV panel installation following a centralized investment strategy.	83
3.9 Variation of the PV yearly generation to achieve break-even as a function of feed-in and demand prices.	84
3.10 The influence of PV installations to reach self-sufficiency.	86
3.11 Key identifiers of a storage system to store surplus PV electricity for different efficiency strategies.	87
3.12 State of charge of a storage system aiming at self-sufficiency for different levels of PV penetration.	88
4.1 Procedure of time-series aggregation	93
4.2 Overview of the iterative procedure for systematic input data reduction	94
4.3 Key performance indicators (KPIs) of the k-medoids clustering	96
4.4 Demonstration of Part 1 of the algorithm, case study with one building	97
4.5 Demonstration of Part 1 of the algorithm, case study with five buildings	98
4.6 Overview of unit decisions for the aggregated problem (AP) with a different number of typical periods.	99
4.7 Multi-objective optimization of one the energy system for one building	99
4.8 Comparison of multi objective optimization with and without detected outlier	100
4.9 The role of outliers on the electricity exchange	101
4.10 Computation time of aggregated time-series and operation problem	101
4.11 Translation of the Dantzig–Wolfe decomposition principle to the design and operation optimization of centralized energy systems.	107
4.12 Application of the Dantzig–Wolfe algorithm in multi objective optimization	113
4.13 Dantzig–Wolfe decomposition algorithm.	114
4.14 Impact of different strategies on the termination of the iteration.	117
4.15 Convergence of the Dantzig–Wolfe decomposition.	118

4.16 Computational effort	119
4.17 Comparison of the objective function for the compact and decomposed formulation .	120
4.18 Comparison of the unit decisions for the compact and decomposed formulation . .	120
4.19 Dual variable π and electricity exchange of a district	121
4.20 Dual variable β during the multi-objective optimization (MOO)	122
5.1 Multi-objective optimization of a residential district with 31 buildings.	134
5.2 Single-objective optimization of a residential district with 31 buildings	136
5.3 Electricity exchange in the district from the perspective of the buildings and the transformer for each design strategy.	137
5.4 Comparison of identical TOTEX optimal solutions for a residential district with 31 buildings	138
5.5 Comparison of optimal unit decisions for solutions with identical TOTEX but different design strategies.	139
5.6 Resource exchange of a residential district with 31 buildings.	139
5.7 Economic analysis of PV installations in the district	140
5.8 Order of optimal PV panel installations on roofs in case study district. All buildings are connected to the same low-voltage transformers.	141
5.9 Economic analysis of PV panel installation following a centralized investment strategy	142
5.10 Variation of the PV yearly generation to achieve break-even as a function of feed-in and demand prices of electricity.	143
5.11 Required PV panel installation to achieve self-sufficiency and carbon neutrality. . . .	144
5.12 Required PV panel integration for different district scenarios	146
5.13 Analysis of two storage systems.	148
5.14 Load duration curve on the local low-voltage transformer.	149
5.15 Peak reduction for decentralized and centralized design strategy.	150
5.16 Limitation imposed by the local transformer for different self-sufficient district scenarios.	151
5.17 Options for overcoming the local transformer limitation.	151
5.18 Impact of the Swiss goals for 2050 for PV deployment.	159
A.1 Relevant building data for different typical days.	168
A.2 Contribution of each KPI to dimension 1 and 2 of the principle component analysis. .	169
B.1 Influence of tilt angle orientation on partly shaded panel	171
B.2 Footprint of PV panels on roof, visualization of changing limiting angle along panel. .	172
B.3 Clustering results for external temperature, global irradiation, and weekdays.	172
B.4 Relevant district data for different typical days.	173
C.1 Relevant district data for different typical days.	175

List of figures

D.1	Details about detected typical days and outliers.	179
E.1	Resource exchanges at district level for the detected TOTEX optimum according to two different optimization strategies.	181
E.2	Resource exchange at transformer level for increasing investment cost. Renewable energy hub without electricity storage systems.	182
E.3	Electricity demand profile at the transformer for different typical days.	182
E.4	Annual electricity demand profile at the transformer.	183
E.5	Annual generated electricity per installed area of PV panels.	183
E.6	Economic analysis of PV panel installation following a centralized investment strategy for different scenarios.	184
E.7	Required PV panel installation to achieve self-sufficiency and carbon neutrality for the district scenario considering a refurbished building stock.	185
E.8	Required PV panel installation to achieve self-sufficiency and carbon neutrality for the district scenario including cogeneration.	186
E.9	The influence of peak shaving on the optimal orientation of PV panels for the centralized design strategy.	186

List of tables

1.1	Overview of energy system technologies.	17
1.2	Overview of common KPIs of decentralized energy systems.	26
1.3	Overview input data of the case study for 40 buildings.	27
2.1	Building parameters for a typical single-family house with large available roof surface.	53
3.1	Literature overview of solar irradiation modeling on buildings.	68
3.2	List of necessary data layers.	78
3.3	Overview input data for 31 buildings. All buildings are connected to the same low-voltage grid.	79
3.4	Overview of identified solutions for a future decentralized district. Self-sufficiency (SS), round-trip efficiency η of the electric storage system.	89
4.1	Difference of the CPU time of the proposed approach to the state-of-the-art.	102
4.2	Limitation of decomposition approaches	106
4.3	Dantzig-Wolfe Algorithm and the corresponding part in the decomposition of district energy systems	108
4.4	Example of a primal and a corresponding dual problem.	110
4.5	Multi objective optimization with Dantzig-Wolfe Algorithm.	112
5.1	Literature review on the optimization of urban energy system problems.	127
5.2	Limits and constraints for the integration of PV panels.	147
A.1	Global warming potential and renewable energy share factors related to the grid.	163
A.2	GWP factor of transmission and combustion of natural gas in Switzerland.	163
A.3	Performance efficiencies for assessing current operating cost based on demand values.	164
A.4	Parameter data for modeling photovoltaic panels.	164
A.5	Global warming potential to the construction of energy system technologies.	165
A.6	Economic parameters of energy system technologies.	165
A.7	Bounds of the unit sizes of the energy system technologies.	165
A.8	Considered second law efficiency for different temperature levels of the heat pump.	166
A.9	Considered part load limit for different temperature levels of the heat pump.	166

List of tables

A.10 Annual demand for different building categories and types according to national standard norms.	166
A.11 Building details of the case study.	167
A.12 Weather data clustering results.	168
B.1 Weather data clustering results including weekdays.	172
C.1 Building related data, building type and category.	176
C.2 Building related data, energy related values are annual.	177
C.3 Available surface share for PV installations on facades and roofs.	177

Acronyms and abbreviations

ADMM	alternating direction method of multipliers
AP	aggregated problem
AR	annual revenues
AVE	avoided emissions
BA	battery
BES	building energy system
BO	boiler
CAPEX	capital expenses
CAVE	cost of avoided emissions
CC	current cost
CHP	combined heat and power
COP	coefficient of performance
CPT	carbon payback time
DES	district energy system
DHW	domestic hot water
EH	electrical heater
EMS	energy management system
ERA	energy reference area
GHG	greenhouse gas
GHI	global irradiation
GIS	geographic information systems
GM	grid multiple
GU	grid usage
GWP	global warming potential
HP	heat pump
HVAC	heating, ventilation and air conditioning
IPCC	Intergovernmental Panel on Climate Change
IRR	internal rate of return
KPI	key performance indicator
LCA	life cycle assessment

Acronyms and abbreviations

LCoE	levelized cost of electricity
LDC	load duration curve
MAE	mean average error
MAPE	mean average percentage error
MILP	mixed-integer linear programming
MOO	multi-objective optimization
MP	master problem
NG	natural gas
NLP	non linear programming
NPV	net present value
OCC	occupancy
OGD	open government data
OP	operating problem
OPEX	operational expenses
PHS	pumped hydro storage
PV	photovoltaic
PVC	photovoltaic curtailment
PVP	photovoltaic penetration
RES	renewable energy share
RMSD	root mean square deviation
SC	self-consumption
SH	space heating
SOFC	solid oxide fuel cell
SOO	single-objective optimization
SP	subproblem
SS	self-sufficiency
SSE	sum of squared errors
STO	storage
TOTEX	total expenses
TSA	time-series aggregation

List of symbols

Parameters

A	area	[m ²]
C	heat capacity coefficient	[kW/m ² K]
F	bound of validity range of unit sizes	[◊]
Φ	specific heat gain	[kW/ m ²]
Q	thermal power	[kW]
T	temperature	[K]
U	heat transfer coefficient	[kW/m ² K]
V	volume	[m ³]
α	azimuth angle	[°]
b	baremodule	[-]
β	limiting angle	[°]
c	energy tariff	[currency/kWh]
c_p	specific heat capacity	[kJ(/ (kg K)]
d	distance	[m]
d_p	frequency of periods per year	[d/yr]
d_t	frequency of timesteps per period	[h/d]
e	electric power	[kW/m ²]
ϵ	elevation angle	[°]
η	efficiency	[-]
$f_{b,r}$	spatial fraction of a room in a building	[-]
f^s	solar factor	[-]
f^u	usage factor	[-]
g	global warming potential streams	[kg _{CO2,eq} /kWh]
γ	tilt angle	[°]
g^{glass}	ratio of glass per facades	[-]
h	height	[m]
i	interest rate	[-]
i^{c1}	fixed investment cost	[currency]

List of symbols

i^{c^2}	continuous investment cost	[currency/ \diamond]
i^{g^1}	fixed impact factor	[kg _{CO2,eq}]
i^{g^2}	continuous impact factor	[kg _{CO2,eq} / \diamond]
irr	irradiation density	[kWh/m ²]
l	lifetime	[yr]
m	mass	[kg]
n	project horizon	[yr]
n	number/ quantity	[\cdot]
pd	period duration	[h]
ϕ	solar gain fraction	[kW/ m ²]
q	thermal power	[kW/m ²]
ρ	density	[kg/m ³]
s	shading factor	[\cdot]
x	coordinate, pointing east	[\cdot]
y	coordinate, pointing north	[\cdot]
z	coordinate, pointing to the zenith	[\cdot]

Variables

C	cost	[currency]
E	electricity	[kW(h)]
G	global warming potential	[kg _{CO2,eq}]
H	natural gas or fresh water	[kW(h)]
Q	thermal energy	[kWh]
R	residual heat	[kWh]
T	temperature	[K]
f	sizing variable	[\diamond]
λ	decomposition decision variable, master problem	[\cdot]
y	decision variable, binary	[\cdot]

Dual Variables

$[\beta]$	epsilon constraint for multi-objective optimization
$[\mu]$	incentive to change design proposal
$[\pi]$	cost or global warming potential of electricity

Superscripts

A	appliances
B	building
L	light

List of symbols

P	people
bat	battery
bes	building energy system
cap	capital
chp	combined heat and power unit
cw	cold water
-	demand
dhw	domestic hot water
el	electricity
era	energy reference area
ext	external
gain	heat gain
ghi	global horizontal irradiation
gr	grid
hp	heat pump
int	internal
inv	investment
irr	irradiation
max	maximum
min	minimum
net	netto
ng	natural gas
op	operation
pv	photovoltaic panel
r	return
ref	reference
rep	replacement
s	supply
SH	space heating
stat	static
+	supply
tot	total
TR	transformer

Indexes

0	nominal state
<i>II</i>	ref. to second law of thermodynamics
<i>I</i>	ref. to first law of thermodynamics

List of symbols

b	building
f	facades
i	iteration
k	temperature interval
l	linearization interval
p	period
pt	patch
r	replacement
t	timestep
u	unit

Sets

A	set of azimuth angles
B	set of buildings
O	set of orientation
F	set of facades
I	set of iterations
K	set of temperature levels
L	set of linearization intervals
P	set of typical periods
R	set of units which need replacement
R	set of roofs
S	set of skydome patches
T	set of timesteps
U	set of units
Y	set of tilt angles

Introduction

Overview

- Future perspectives for districts in the context of the energy transition
- Literature gaps in modeling energy hubs
- Definition of renewable energy hubs
- Contributions and novelty of this thesis

This thesis is structured in five chapters. A general overview of the environmental impact of district energy systems is first provided, including an analysis of the current situation and future perspectives and aims. This overview then develops into a glimpse into the state-of-the-art of energy hubs, providing the main literature gaps that are then addressed in this thesis. The novel concept of a renewable energy hub at different scales is then defined.

Environmental impact of district energy systems

Today, it is broadly acknowledged that climate change is a threat to both human and natural ecosystems and that the increasing greenhouse gas emissions from anthropogenic activities are at the root of the warming of the climate [1]. Among all human-related activity sectors, buildings accounted for 36% of the global final energy use and 39% of the greenhouse gas emissions in 2018 [2]. Among the latter, residential buildings globally accounted for 61% of the final energy use and 41% of the emissions. Furthermore, over 50% of the global final energy use in residential buildings is related to space and water heating [2, 3]. Therefore, decarbonizing the building stock requires a holistic approach, that considers both electrical and thermal end uses of the energy demand.

The consensus among researchers around the globe is that mitigation pathways to limit global warming should be characterized by the improvement of energy conservation and efficiency, the de-carbonization of electricity, and the electrification of end-uses [4–6]. Regarding the decarbonization of the building stock, switching to electrical heating, ventilation and air conditioning (HVAC) systems allows a higher conversion efficiency and improves the integration of locally generated renewable energy, such as by installing photovoltaic (PV) panels on rooftops [1, 3]. The building sector has been forecasted to experience the highest direct electrification rates among energy end-use sectors,

Introduction

as it is predicted to reach 73% by 2050 from the 2019 32% [5]. As a result, the electricity demand of buildings is expected to double by 2050 [5]. Electrifying the building stock has the potential to lower local pollutant emissions and increase the energy system efficiency, especially when coupled with the use of local renewable energy sources [7, 8]. The installation of rooftop PV is a cost-convenient choice in many parts of the world, even in absence of subsidies [9]. In Switzerland, the production of electricity from solar energy is the most cost-effective way of expanding electricity production capacities in terms of cents per kilowatt-hour [10]. As of 2019, more than 90% of the solar potential on the top of roofs worldwide remained unexploited [9], whereas only 3.5% of the electricity demand remained met by photovoltaic electricity, in Switzerland [10].

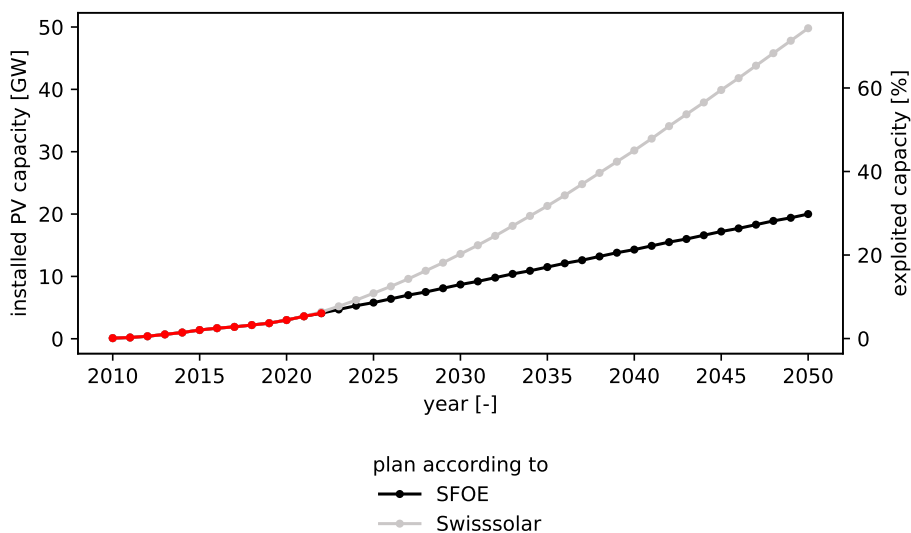


Figure 1 – Strategy for the development of electricity generation from photovoltaic (PV) systems in Switzerland through the year 2050. Plan according to Swiss Federal Office of Energy (SFOE) [11] and Swissolar, the Swiss Solar Energy Professionals Association [12].

Therefore, national authorities are aiming to drastically increase the electricity generation from solar energy resources in the coming years. In Switzerland, the National Energy Act 2050 specified an aim of more than 11 TWh production of renewable energy excluding hydropower by 2035 [11]. Using the simplified assumption that 1 MWh electricity is annually generated by 1 kW of installed capacity of PV systems in Switzerland [12], this extrapolates to an aim of 20 GW of installed PV capacity by the year 2050 (Figure 1). In contrast, the national association Swissolar has recommended a drastically increased aim of 50 GW [12]. The potential of PV systems on building surfaces has been estimated as approximately 67 GW in Switzerland [12]. Both thus require a drastic increase in exploited capacity from the 2021 usage of approximately 5% to approximately 30% (SFOE) or 70% (Swissolar). Further, these aims demand an investigation of the impact of this strategy on the decentralized energy systems of districts.

Volatile power generation caused by the fluctuation of solar irradiation challenges the capacity of the electrical power grid. Therefore, in addition to maximizing the electricity generated from the sun, the interaction of the building energy system with the electrical power grid should be reduced by maximizing self-consumption while decreasing the grid's energy demand. At the same time, a holistic approach is necessary to consider multiple energy carriers in order to supply not only electricity but also the thermal service demand to buildings. These requirements can be fulfilled by considering renewable energy hubs.

What are renewable energy hubs?

In light of the energy transition, the energy system is moving toward a distributed system characterized by a high level of interconnectivity among energy carriers. This transition has led to an increased popularity in the concept of energy hubs. According to Geigl et al. [13], an energy hub is a unit where multiple energy carriers can be converted, conditioned, and stored. A review on energy hubs with more than 100 contributions in the field has been provided by Mohammadi et al. [14], where they define an energy hub as a place where the production, consumption, storage, and conversion of multiple energy carriers happens. Energy hubs can be classified according to their sector, e.g., residential or industrial. Additionally, two scales of energy hubs can be considered, micro or macro energy hubs, where a macro system comprises a collection of micro energy hubs controlled by a central unit [14]. The energy system of a residential building is a micro hub; several buildings can be allocated to one macro hub [15]. Energy hubs have shown a great potential to improve and increase the usage of renewable energy technology in a system [16], such as the use of the implementation of regional energy hubs with a high share of wind to avoid the curtailment of renewable energy sources [16]. Recently, researchers have focused on optimally operating loads within the energy hub, including scheduling, but without considering the optimal investment of equipment for the energy hub [15]. However, Maroufmashat et al. [17] analyzed the interactions between collection of energy hubs while considering differing pre-defined energy hub scenarios. Their result demonstrated an increasing importance of interaction as the number of hubs considered increased, up to a maximum of three interconnected energy hubs. Upscaling a collection to contain several interconnected energy hubs, however, poses a computational problem; solving these optimization problems thus requires computational reduction methods, such as the alternating direction method of multipliers (ADMM) [18] or heuristic methods [19].

Different researchers have used slightly varied definitions of an energy hub. The consensus is that an energy hub is a place that has in-flows and out-flows and considers the interconnection of multiple energy carriers through conversion and storage units. Another important aspect involves the aim of optimally controlling the operation of an energy hub to reach a certain goal. In this work, this concept is expanded to a renewable energy hub.

A renewable energy hub

- is a center of optimally interconnected energy carriers;
- contains conversion and storage units;
- maximizes its own usage of renewable energy resources;
- is embedded in a superior network;
- is considered at different scales. The decisive factor is the level at which investment decisions are made.

Although some researchers have recently aimed to use an energy hub to optimize the integration of renewable energy, the concept of a renewable energy hub is a novel term presented in this thesis. The definition of a renewable energy hub is further detailed in the following section about contributions and novelty.

Contributions and novelty

Unlike in prior studies, renewable energy hubs at different scales are addressed in this work. This work contributes to the state-of-the-art by introducing renewable energy hubs, which is including investment decisions within the concept of an energy hub and focuses on maximizing the usage of renewable energy resources.

The level at which the investment decisions are taken is the decisive factor to define the scale of the renewable energy hub. Two different scales are analyzed within this work: the building and the district scale. When investment decisions are taken from the perspective of a building owner, the renewable energy hub is at the building scale. When investment decisions are taken for the community, the renewable energy hub is considered at the district scale. Therefore, a district can either be considered as a collection of renewable energy hubs at the building scale or as one energy hub at the district scale. The former corresponds to a decentralized design strategy, the latter to a centralized one. Building energy systems are generally considered as decentralized or distributed energy systems within a city district, where a city district is defined as a collection of buildings that are all allocated to a single low-voltage transformer of the electrical grid. Unlike current state-of-the-art, the interactions between decentralized energy systems are highlighted in both versions of the design strategy of the district energy system and distributed loads are not aggregated.

A renewable energy hub maximizes the usage of energy from renewable sources to satisfy the self-demand, causing interaction between the renewable energy hub and the superior network. This work provides a detailed consideration of solar energy within renewable energy hubs, thereby bridging the gap between studies that consider the accurate simulation of oriented irradiation and those that optimize solar integration in building energy systems. The resulting approach applied in this work can clarify the exchanges inside the renewable energy hub. To overcome computational

issues caused by the large problem size of renewable energy hubs at the district scale, a deterministic decomposition method is developed to perform the centralized multi-objective optimization (MOO) of several dozen buildings.

These contributions are outlined in five chapters of the thesis as follows. Perspectives and outlook are then summarized in the conclusion.

Chapter 1: Renewable energy hubs at the building scale

How are renewable energy hubs defined at the building scale?

What performance indicators should be used to describe renewable energy hubs?

As part of their mission to lead the renewable energy transition and ensure energy independence and security of supply in the context of decarbonizing the energy mix and/or phasing out nuclear energy, policy makers and energy operators have the responsibility of selecting indicators. Engineers have thus been asked to propose key performance indicators (KPIs) that quantify the positive impact of operation strategies and efficient technology solutions that harvest and distribute more renewable resources while minimizing the environmental impact and overall costs. In this chapter, the concept of renewable energy hubs at the building scale is introduced. A wide range of alternative solutions are generated using mixed-integer linear programming (MILP) and MOO to search the decision space of decentralized energy systems. Machine learning techniques, including principle component analysis and k-medoids clustering, are applied to identify major trends, thus supporting multi-criteria decision making.

Chapter 2: Photovoltaic panel orientation in renewable energy hubs

What is the impact of the orientation of PV panels on renewable energy hubs and the grid?

The integration of renewable energy sources, particularly PV panels, is becoming an increasingly widespread solution for reducing the carbon footprint of a building energy system (BES). However, the volatility inherent in their electricity generation and its mismatch with the typical demand patterns are cause for concern, particularly from the viewpoint of the management of the power grid. Compared with existing renewable energy hub approaches reported in literature, the contribution of PV panels is modeled in more detail, including a more accurate solar irradiation model and the shading effect among panels. Compared with existing studies in PV modeling, the interaction between the PV panels and the remaining units of the BES, including the effects of optimal scheduling, is considered.

Chapter 3: Facades in interconnected renewable energy hubs

What is the role and potential of facades in decentralized energy hubs?

The intersection of BES and the solar potential on building facades has not yet been adequately investigated. Accordingly, PV panel orientation possibilities are investigated in combination with a shadow model from the surroundings in the optimization approach of energy hubs at the building scale in Chapter 3. The economic and environmental rationale for installing PV panels on facades is also analyzed. The role of PV systems in urban districts, and particularly of facade-mounted PV systems, is addressed by focusing on the amount of PV that is needed to reach self-sufficiency and that can be installed while being economically beneficial. The district is optimized in a decentralized fashion as a collection of renewable energy hubs at the building scale. Thereby, the amount of electricity generated from the district is estimated that, from the perspective of the electricity grid, needs to be distributed or stored, as well as the related costs. Although general conclusions cannot be drawn based on a single study, a methodological approach to address the highlighted gap in the literature is suggested; the proposed method is then applied to a specific case study to showcase its potential. The chosen case study area is a typical peri-urban district on the outskirts of Geneva, Switzerland.

Chapter 4: Computational reduction for renewable energy hubs at the district scale

What is the best method to overcome runtime issues when generating centralized energy hub designs?

The optimal design and scheduling of energy systems with a high share of renewables is a complex and computationally demanding task. The mismatch of supply and demand of energy requires the consideration of time-series with a resolution of a few minutes, whereas each system has a lifetime of multiple decades. Additionally, this chapter aims to tackle renewable energy hubs at the district scale, which includes several dozen distributed energy systems. Two algorithms are thus proposed in Chapter 4 to systematically reduce the computational efforts of energy hubs at the district scale. The first algorithm reduces the input data by exploiting the two-stage nature of the optimal design and planning of the system and sequentially performing k-medoids clustering. Unlike the state-of-the-art, the influence of varying the number of typical periods is not examined on the quality of the clustering algorithm but on the objective function and the integer decisions. The second algorithm is a decomposition approach of the model formulation itself. The Dantzig–Wolfe decomposition algorithm is identified to be most suitable for the decomposition of renewable energy hubs at the district scale. Thus, a direct contribution to the state-of-the-art is a formulation for MOO that also allows an improvement of the initialization of the algorithm. The method is then validated using the compact, undecomposed, model formulation of the problem.

Chapter 5: Renewable energy hubs at the district scale

What are the potential and limitations of centralized renewable energy hubs at the district scale?

The integration of renewable energy technology in district energy systems is a common interest in order to meet challenges connected to the energy transition. The optimal planning of these district energy systems is a computational intensive task, as each building in the district has its own energy system installed that exchanges resources with the community. In this chapter, the previously proposed and validated Dantzig–Wolfe decomposition is applied to ease the computational efforts of renewable energy hubs at the district scale. The proposed method contributes to the state-of-the-art in district energy modeling, as it allows entire low-voltage grids to be considered in a deterministic approach. Further, this approach includes the MOO of the thermal and electric systems. The proposed centralized approach furthermore allows the consideration of both centralized and distributed energy units in the district, as well as the inclusion of centralized constraints such as the capacity of the local low-voltage transformer. The resulting centralized design strategy is compared to the decentralized design strategy presented in Chapter 3, where a collection of renewable energy hubs are considered at the building scale. To highlight the benefits at the district scale, both methods are applied to a typical peri-urban district in the area of Geneva, Switzerland. The benefits of this strategic, community-based design of renewable energy hubs at the district scale are highlighted. Additionally, the grid-aware integration of solar energy in energy hubs at the district scale is further analyzed.

Renewable energy hubs at the building scale

Overview

- Modeling and optimization framework of renewable energy hubs at the building scale
- Integration of a smart heating system
- Definition, reduction and correlation of KPIs
- Focus on global warming potential with hourly resolution

The content of this chapter is mainly published in [20] and partly available in the supplementary information of publication [21].

Policy makers and energy operator have the responsibility to select indicators for their mission to lead the renewable energy transition ensuring energy independence and security of supply in the context of decarbonisation of the energy mix and and/or nuclear phase-out with increasing cost for flexibility. Engineers are therefore asked to propose models and KPIs allowing to quantify the positive impact of operation strategies and efficient technology solutions to harvest and distribute more renewable resources, while minimizing the environmental impact and overall costs. The goal of this chapter is to propose a modeling framework of renewable energy hubs at the building scale and to classify the performance of possible solutions. A wide-range of alternative solutions are generated using Mixed Linear Integer Programming (MILP) and Multi Objective Optimization (MOO) to capture the decision space. Machine learning techniques, like principle component analysis and k-medoids clustering, are applied to identify the major trends, thus supporting multi – criteria decision making. Results highlight the importance of (i) setting appropriate system boundaries, (ii) using at least hourly resolution and (iii) constructional footprint to characterize renewable energy hubs. Low emission electrical grid mix had a high impact on design strategies and was in conflict with decentralized, self-sufficient energy systems. Including life cycle assessment (LCA) of the system showed besides operational emission, the constructional footprint was significantly contributing to the total Global Warming Potential (GWP), especially in modern energy system designs.

1.1 Introduction

Efficient use of energy, promotion of domestic renewable energy and security of supply are recurrent themes of energy policies with implication in the building sector, which is accountable for around 36% of the total final world energy consumption [2]. In addition, the electricity demand in this sector is expected to increase by more than 70% by 2050 [5], highlighting the importance to strategically plan the interaction between households with electricity power grid. The renewable energy hub, promotes its own consumption of locally produced electricity and therefore aims to minimize the interaction with the superior network. The first research question, which is addressed in this chapter, is: *How are renewable energy hubs defined at the building scale?*. The first chapter of the thesis is introducing the concept of a renewable energy hub at the building scale. The definition of the considered energy systems is built upon preceding work from Stadler [22] and Girardin [23]. Thereby, the aim is to demonstrate a holistic integration of the thermal demand side management, with a smart heating strategy of the building.

In order to plan, measure, and decide, the framework of a renewable energy hub needs key performance indicators (KPIs). Energy and environment strategies are developed and evaluated with KPIs, which vary not only in definition but also between stakeholders. The magnitude of available indicators is immense, research contributions are available that took a subset of the indicators and focused only on the definition of the KPIs and their comparison [24]. Research groups which focused on the development of whole frameworks measured the performance with indicators such as total cost and equivalent CO₂ emission [22, 25, 26]. In contrast, researcher focusing on the development on single energy units favored technical performance indicators [27]. A large diversity exists for KPIs describing the security of energy supply. Stakeholder distinguish between political relation, self-sufficiency and also robustness of the system [28]. Some KPIs in this category are introduced project-specific, which makes it difficult to compare the performances of different frameworks.

The second research question, which is addressed in this chapter is: *What performance indicators should be used to describe renewable energy hubs?*. This chapter thus aims at bridging a gap between identification of a minimum necessary set of indicators and evaluation of the impact of KPIs on the description of a solution. Therefore, a large variation of common KPIs in the literature is collected and major trends are analyzed with machine learning techniques. Special focus is on the evaluation of the global warming potential (GWP). Contribution to the state-of-the-art is the consideration of hourly values of the electrical grid mix instead of the yearly averages.

1.2 Method

The goal of this chapter is to introduce a strategic way to generate decentralized energy system designs and to show their interactions with their environment. Thus, the renewable energy hub in form of a building energy system (BES) is defined in a first step. To identify a decision space, a mixed-integer linear programming (MILP) optimization approach is adopted, where the types and sizes of the different components of the BES are considered as optimization variables.

In a second step, a selection of conflicting KPIs are collected to assist the decision making among different design proposals. Therefore, multi-objective optimization (MOO) is performed with ecological, economical, technical and security indicators as objective. In order to be computationally able to conduct a MOO, data reduction techniques is performed in a final step.

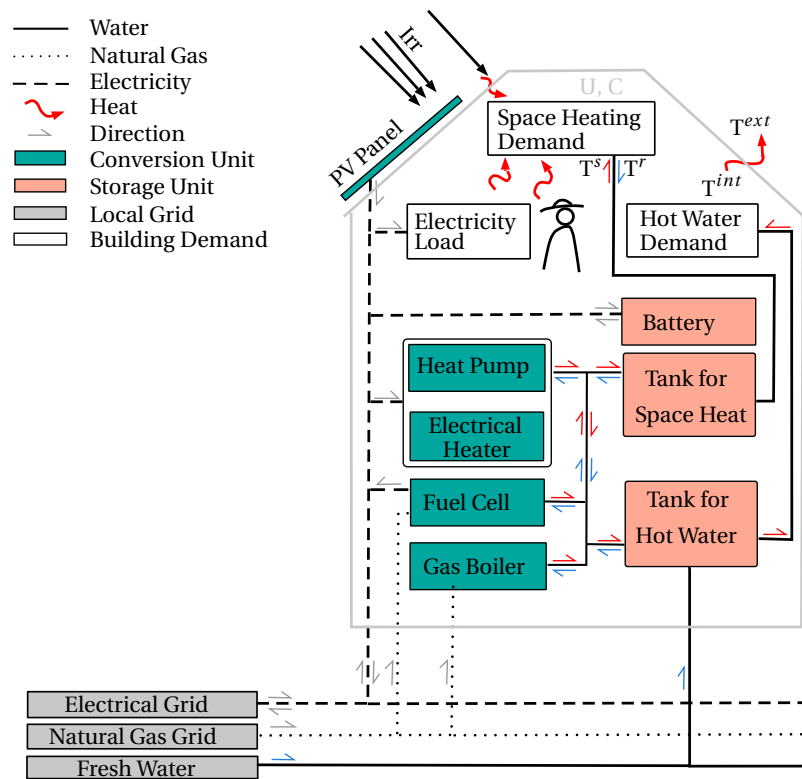


Figure 1.1 – Schematic overview of a renewable energy hub at the building scale, which is also considered as a decentralized energy system.

The BES modeling framework is illustrated in Figure 1.1. Heating requirements can be satisfied by an air-water heat pump (HP), electrical heater (EH), a combined heat and power (CHP) unit in form of a fuel cell, and a gas boiler (BO). Energy is stored in either a stationary battery (BA), domestic hot water and buffer storage (STO) or the building envelope. Photovoltaic (PV) panels act as renewable energy sources. The decentralized energy system is interconnected to the main energy distribution networks: the natural gas, electricity and fresh water grids.

Three types of energy demands are considered: space heating (SH), domestic hot water (DHW), and electricity. Uncontrollable load profiles of electricity and DHW profiles are direct inputs to the framework and can be generated using standardized profiles according to norms or measurements in a pre-processing step. In contrast, the SH demand is modelled within the framework itself in order to include the control strategy of the energy management system (EMS) and the possibility of a thermal renovation of the building. The SH demand is impacted by factors such as the conductive heat losses through the building envelope, the heat capacity of the building and the heat gains from occupants, electric appliances and solar irradiation. Furthermore, space heating demand is characterized by the desired comfort temperature of the rooms, the nominal return and supply temperature of the heat distribution system and the control strategy of latter. This work builds upon the methods developed by [23] for the thermal demand of the buildings and upon [22] for BES design.

1.2.1 Energy system

The challenge in solving the BES modeling framework relies within identifying both the design of each conversion and storage unit and the associated yearly load scheduling with sufficient precision in a reasonable computing time. In addition, the problem formulation should allow accounting for the existence of competing objectives. For these reasons, the optimal integration of the building energy technologies is formulated as a MOO problem using MILP. Unit sizes and installation decisions are used as the main optimization variables of interest. To clearly differentiate decision variables from input parameters, bold typeset is used to represent all decision variables. As all sets are predefined, normal and capital typeset is used. The main problem sets are: the set of buildings B , the set K of all different temperature levels of the heating system, the set of available conversion and storage units U ; the different days of the year are represented by periods in the set P , to which hourly timesteps are allocated and contained in set T .

Sizing constraints The main equation for sizing and scheduling problem units are described by Equations 1.1.

$$y_{b,u} \cdot F_u^{min} \leq f_{b,u} \leq y_{b,u} \cdot F_u^{max} \quad (1.1a)$$

$$f_{b,u,p,t} \leq f_{b,u} \quad (1.1b)$$

$$y_{b,u,p,t} \leq y_{b,u} \quad (1.1c)$$

$$\forall b \in B \quad \forall u \in U \quad \forall p \in P \quad \forall t \in T$$

The decision to purchase a unit is represented by the binary variable y , whereas the continuous variable f represents the unit size. The upper and lower bound (F^{min}, F^{max}) for unit installations

1.2. Method

are also necessary for identifying the validity range for the linearization of the cost function of the unit [29].

Energy balances The energy system of the building includes all the different unit technologies that are used to fulfil the building's energy demand.

$$\dot{E}_{b,p,t}^{gr,+} + \sum_{u \in U} \dot{E}_{b,u,p,t}^+ = \dot{E}_{b,p,t}^{gr,-} + \sum_{u \in U} \dot{E}_{b,u,p,t}^- + \dot{E}_{b,p,t}^B \quad (1.2a)$$

$$\dot{H}_{b,p,t}^{gr,+} = \sum_{u \in U} \dot{H}_{b,u,p,t}^- \quad \forall b \in B \quad \forall p \in P \quad \forall t \in T \quad (1.2b)$$

The superscript + indicates outgoing flows like the supply of each grid or unit, whereas – marks an incoming flow, also often referred to as demand unit or feed-in to the grids. The electricity demand of the building E^B is uncontrollable and a input requirement that needs to be satisfied. Energy can be exchanged with the electricity grid E^{gr} in both ways (Equation 1.2a), whereas water and gas grids H can only supply (Equation 1.2b).

The heat cascade ensures that heat requirements are supplied, while the second law of thermodynamic is satisfied. The hot streams S_h and cold streams S_c are sorted in increasing temperature intervals k [22].

$$\dot{R}_{k,b,p,t} - \dot{R}_{k+1,b,p,t} = \sum_{u_h \in S_h} \dot{Q}_{u_h,k,b,p,t}^- - \sum_{u_c \in S_c} \dot{Q}_{u_c,k,b,p,t}^+ \quad (1.3a)$$

$$\dot{R}_{1,b,p,t} = \dot{R}_{n_k+1,b,p,t} = 0 \quad \forall k \in K \quad \forall b \in B \quad \forall p \in P \quad \forall t \in T \quad (1.3b)$$

In Equation 1.3a the residual heat R_k is cascaded to the next interval ($k+1$). Equation 1.3b closes the thermal balance by ensuring that no heat is cascaded to the highest or lowest interval [22]. To ensure that no energy is accumulated between different periods, cyclic constraints are imposed both on the indoor temperature and on thermal and electrical energy storage systems. Cyclic constraints ensure that the state is reset to its initial status at the end of each period [22].

Heating distribution system The thermal loads are included into the heat cascade to satisfy the second law of thermodynamics. As the thermal load of space heating $\dot{Q}^{SH,-}$ is a variable, variable return and supply temperatures would lead into non-linearity. Therefore, a set of discretized substreams are defined which are constrained by the nominal operation of the hydronic heating system [22]. These discretized thermal streams can be activated or not, and be scaled in magnitude to correspond in sum to the thermal stream $\dot{Q}^{SH,-}$, which is satisfying the space heating demand

[22]. Thereby, the heat transfer rate $c_p \cdot \dot{m}$ of the nominal state serves as an upper bound for the sum of the transfer rates of the substreams. The temperature of the discretized streams is predefined in fixed intervals around the supply and return temperatures of the nominal state. The nominal operation is described in its main points in following equations.

$$A_b^{era} \cdot \dot{q}_{b,p,t}^{stat,SH} = c_p \cdot \dot{m}_b \cdot (T_{b,p,t}^s - T_{b,p,t}^r) \quad \forall b \in \mathbf{B} \quad \forall p \in \mathbf{P} \quad \forall t \in \mathbf{T} \quad (1.4)$$

The nominal return and supply temperatures are obtained with a static heating model $\dot{q}^{stat,SH}$ (Equation 1.4). The static heating model balances the heat gains and losses similar to the energy balance in the building, but without the influence of capacities or overheating. Thus in the following, the desired indoor temperature T_0^{int} is fixed.

$$A_b^{era} \cdot \dot{q}_{b,p,t}^{stat,SH} = \dot{Q}_{b,p,t}^{gain} - U_b \cdot A_b^{era} \cdot (T_{b,0}^{int} - T_{p,t}^{ext}) \quad \forall b \in \mathbf{B} \quad \forall p \in \mathbf{P} \quad \forall t \in \mathbf{T} \quad (1.5)$$

The three unknown parameters, the mass flow \dot{m} and the return and supply temperatures T^r and T^s are calculated with two additional assumptions.

$$c_p \cdot \dot{m}_b = \frac{\dot{Q}_{b,0}}{T_{b,0}^s - T_{b,0}^r} \quad (1.6a)$$

$$\dot{Q}_{b,0} = U_b \cdot A_b^{net} \cdot (T_{b,0}^{int} - T_0^{ext}) \quad \forall b \in \mathbf{B} \quad (1.6b)$$

First assumption is, that the control strategy aims at keeping the mass flow constant. This allows to assess the heat transfer fluid rate by the design conditions (Equations 1.6a and 1.6b). The design condition is determined by the coldest external temperature, for which the heating system is designed and devised without additional internal gains. The nominal supply and return temperatures at design state vary for each building category and are influenced by the renovation state and age of the building. The temperatures are derived from the energy signature model, described in detail by Girardin [23].

$$\dot{Q}_{b,p,t}^{stat,SH} = (UA)_b^{hex} \cdot \frac{T_{b,p,t}^s - T_{b,p,t}^r}{\ln \left(\frac{T_{b,p,t}^s - T_0^{int}}{T_{b,p,t}^r - T_0^{int}} \right)} \quad \forall b \in \mathbf{B} \quad \forall p \in \mathbf{P} \quad \forall t \in \mathbf{T} \quad (1.7)$$

The second assumption is, that the heat exchange model for buildings is describing the thermal heat transfer [23]. Later assumption allows to calculate the nominal return and supply temperatures.

1.2. Method

This leads to the last Equation 1.7, which is needed to define the nominal state.

$$(UA)_b^{hex} = \dot{Q}_{b,0} \cdot \frac{\ln\left(\frac{T_{b,0}^s - T_{b,0}^{int}}{T_{b,0}^r - T_{b,0}^{int}}\right)}{T_{b,0}^s - T_{b,0}^r} \quad \forall b \in \mathbf{B} \quad (1.8)$$

The overall heat transfer coefficient U_b^{hex} and the heat exchange area A_b^{hex} of the heating system is characteristic for each building, which are calculated on the design condition (Equation 1.8).

1

1.2.2 Energy demand

Three types of energy demands are considered in the model: space heating (SH), domestic hot water (DHW), and uncontrollable electricity (such as for lightning or appliances). These demands are satisfied within the renewable energy hub, importing energy or exploiting resources that are available. They are included in the energy balances (Equation 1.2); all thermal loads are also respected in the heat cascade to satisfy the second law of thermodynamics (Equation 1.3).

Space heating demand The general form of the SH demand can be expressed by the first order dynamic model of buildings [22].

$$\dot{Q}_{b,p,t}^{SH} = \dot{Q}_{b,p,t}^{gain} - U_b \cdot A_b^{era} \cdot (T_{b,p,t}^{int} - T_{p,t}^{ext}) - C_b \cdot A_b^{era} \cdot (T_{b,p,t+1}^{int} - T_{b,p,t}^{int}) \quad \forall b \in \mathbf{B} \quad \forall p \in \mathbf{P} \quad \forall t \in \mathbf{T} \quad (1.9)$$

In Equation 1.9, \dot{Q}^{gain} represents internal heat gains from appliance, people and solar irradiation and A^{era} the energy reference area (ERA), which has to be heated. The overall heat transfer coefficient U consists of the heat transfer by conduction and air renewal, whereas the thermal heat capacity C describes the response time of the internal temperature [30]. The internal building temperature T^{int} is considered as a variable to be optimized. This allows the building heat capacity to work as an additional, free thermal storage for the building energy system, thus making it possible to use available surplus electricity, which was generated onsite. Clearly, comfort should also be taken into account: this is achieved through the introduction of a penalty cost in the optimization problem objective at each hour when the indoor temperature exceeds pre-defined bounds. These penalty costs are deduced in a post-computing step.

$$\dot{Q}_{b,p,t}^{gain} = \dot{Q}_{b,p,t}^{int} + \dot{Q}_{b,p,t}^{irr} \quad \forall b \in \mathbf{B} \quad \forall p \in \mathbf{P} \quad \forall t \in \mathbf{T} \quad (1.10)$$

The heat gain has two main contributions: internal gains resulting from the usage of the building

(\dot{Q}^{int}) , and solar irradiation (\dot{Q}^{irr}) (Equation 1.10).

$$\dot{Q}_{b,p,t}^{int} = A_b^{net} \cdot \sum_{r \in \text{Rooms}} f_{b,r} \cdot f_{r,p}^u \cdot (\Phi_{r,p,t}^P + \Phi_{r,p,t}^{A+L}) \quad \forall b \in \mathcal{B} \quad \forall p \in \mathcal{P} \quad \forall t \in \mathcal{T} \quad (1.11)$$

The internal gains (Equation 1.11) mainly represent the immediate consequence of people occupancy (superscript P) and of the usage of electric appliances and lights (superscript $A+L$). Demand profiles for the different building and room usages can be found in standard norms [31]. The total gains for each building result from the sum of the gains of each room in the building. $f_{b,r}$ represents the fraction of the total building's surface allocated to each room r . A usage factor f^u is used to account for monthly/weekly variations related to the specific usage of each building and room type [31]. The internal gains are normalized to the internal net surface of the building A^{net} , calculated as the heated surface without the base surface of inner and outer walls.

$$\dot{Q}_{b,p,t}^{irr} = A_b^{era} \cdot \phi^{irr} \cdot irr_{b,p,t}^{ghi} \quad \forall b \in \mathcal{B} \quad \forall p \in \mathcal{P} \quad \forall t \in \mathcal{T} \quad (1.12)$$

The solar gains are connected to a solar gain factor ϕ , which describes how much global irradiation is received as heat by the building.

Domestic hot water demand Typical DHW demand is stated in standardized national norms [31, 32]. Similar to the internal heat gains, the DHW profile is specific to each room type and usage.

$$Q_b^{dhw,-} = A_b^{net} \cdot \sum_{r \in \text{Rooms}} f_{b,r} \cdot f_{r,p}^u \cdot V_r^{dhw,ref} \cdot \frac{n^{ref}}{A_r^{net}} \cdot c_p^{dhw} \cdot \rho^{dhw} (T^{dhw} - T^{cw}) \quad \forall b \in \mathcal{B} \quad (1.13)$$

In Equation 1.13, the factor n^{ref}/A_r^{net} expresses the number of reference units per net surface of the specific room. The cold water temperature is assumed to be constant at $T^{cw} = 10^\circ\text{C}$, whereas the hot water temperature has to be delivered at $T^{dhw} = 60^\circ\text{C}$ to meet sanitary standards. The thermodynamic properties ρ^{dhw} and c_p^{dhw} are the density and the specific heat capacity of water, respectively. The daily profiles are derived from the occupancy profiles in combination with the activity profiles of the rooms [31].

Electricity demand When measured data is not available, the electricity demand can be calculated based on the profiles provided by national standard norm [31].

$$\dot{E}_{b,p,t}^B = A_b^{net} \cdot \sum_{r \in \text{Rooms}} f_{b,r} \cdot f_{r,p}^u \cdot \dot{e}_{r,p,t}^{A+L} \quad \forall b \in \mathcal{B} \quad \forall p \in \mathcal{P} \quad \forall t \in \mathcal{T} \quad (1.14)$$

1.2. Method

The electricity demand of the appliances and light of the different rooms are combined in the e^{A+L} term (Equation 1.14). The net surface of the building A^{net} , the share of specific room types $f_{b,r}$ and the usage $f_{r,p}^u$ factor lead to the uncontrollable load of the building E^B .

1.2.3 Energy system technologies

The modeling of energy systems technologies of buildings was demonstrated as a contribution to the state-of-the-art by Stadler [22] and are integrated in the renewable energy hub. In this section only an overview of the energy system technologies is provided. The nature of the input and output streams, and the reference unit of each technology are detailed in Table 1.1. The reference unit is the physical unit of the sizing variable f (see Equation 1.1). The thermal systems for providing DHW and SH must be separated in order to apply to hygienic standards. Furthermore, both service requirements are on different temperature levels.

Table 1.1 – Overview of energy system technologies, based on the work by Stadler [22].

technology	input stream	output stream	reference unit
energy conversion technologies			
gas boiler	natural gas	heat	[kW _{th}]
heat pump	ambient heat, electricity	heat	[kW _e]
electrical heater SH	electricity	heat	[kW _{th}]
electrical heater DHW	electricity	heat	[kW _{th}]
PV panel	solar irradiation	electricity	[kW _p]
cogeneration [†]	natural gas	electricity, heat	[kW _e]
energy storage technologies			
thermal storage SH	heat	heat	[m ³]
thermal storage DHW	heat	heat	[m ³]
battery	electricity	electricity	[kWh]

[†] model based on a solid oxide fuel cell

The gas boiler and the electrical heaters are implemented using a static conversion efficiency of 0.98 and 0.99, respectively. The heat pump is modeled using the ideal coefficient of performance and the second law efficiency that accounts for irreversibilities. The ideal coefficient of performance is modeled with variable return and supply temperatures. To avoid non-linearities, the streams of the heat pump are discretized. The main heat source, which is considered in this work, is ambient air. Different heat sources can be considered by changing the source temperature and the second law efficiency. The cogeneration unit is modeled using a nominal thermal and electrical conversion efficiency of 0.59 and 0.27, respectively. A minimum load of 50% and a minimum operation duration of 3h is considered. The energy conversion efficiencies decline linearly until the minimum partload, where the efficiencies are 0.58 and 0.20. The PV panels are modeled considering

the energy conversion of global solar irradiation to electricity. The reference efficiency is 0.17, which varies with the temperature of the modules. Thermal solar panels, which can satisfy the demand of DHW, are also included in the modeling framework presented by Stadler [22]. It was more beneficial to provide the DHW with the combination of the heat pump and PV panels. Additionally, the roof surface is limited and the installation of PV panels were prioritized by the solver. Therefore, the thermal solar panels were only chosen in extreme grid tariff scenarios, where additionally the installation of heat pumps were prohibited a priori. Hence, thermal panels are not further focused on in this work.

1

The thermal storage systems are implemented considering water as medium, which is discretized in three temperature levels. The electricity storage system is modeled as lithium battery with a minimum and a maximum state-of-charge of 0.2 and 0.8, respectively. The discharge and charge efficiency is considered to be 0.9.

1.2.4 Problem objectives

The design of decentralized energy systems can be considered optimal from various perspectives. In this work, focus lies on minimizing economic indicators (operational expenses (OPEX), capital expenses (CAPEX) and total expenses (TOTEX)). Additionally, the minimization of the total GWP can be considered as objective. As objectives can be generally competing (solutions with high CAPEX have low OPEX, and vice versa), the problem can be approached using a MOO approach. The MOO problem is implemented using the ϵ -constraint method to generate Pareto curves. For example, minimizing OPEX can be considered as the first main problem objective and different optimization problems are solved, where the CAPEX is constrained at incrementally increasing values. The same principle is then repeated after inverting the roles of the two objectives.

Annual operating expenses The annual OPEX consist of the expenses and gains related to the interaction with the local electricity and natural gas grids. The price for fresh water supply is considered to be neglectfully small and is not included in the calculation of annual OPEX.

$$C_b^{op} = \sum_{p \in P} \sum_{t \in T} \left(c_{p,t}^{el,+} \cdot \dot{E}_{b,p,t}^{gr,+} - c_{p,t}^{el,-} \cdot \dot{E}_{b,p,t}^{gr,-} + c_{p,t}^{ng,+} \cdot \dot{H}_{b,p,t}^{gr,+} \right) \cdot d_t \cdot d_p \quad \forall b \in B \quad (1.15)$$

In Equation 1.15, $c^{el,+}$, $c^{el,-}$ and $c^{ng,+}$ represent the electricity purchase and selling prices, and the natural gas purchase price; $\dot{H}^{gr,+}$ represents the energy flow of natural gas purchased from the grid for building b at time step t and typical period p ; similarly, $\dot{E}^{gr,+}$ and $\dot{E}^{gr,-}$ represent the electricity flows from and to the grid. Annual values are integrated over each typical period p and accounted with their frequency d .

1.2. Method

Annual capital expenses The annual CAPEX include the investment and replacement costs of the unit technologies with different expected lifetimes.

$$C_b^{cap} = \frac{i(1+i)}{(1+i)^n - 1} \cdot (C_b^{inv} + C_b^{rep}) \quad (1.16a)$$

$$C_b^{inv} = \sum_{u \in U} b_u \cdot (i_u^{c1} \cdot y_{b,u} + i_u^{c2} \cdot f_{b,u}) \quad (1.16b)$$

$$C_b^{rep} = \sum_{u \in U} \sum_{r \in R} \frac{1}{(1+i)^{r \cdot l_u}} \cdot (i_u^{c1} \cdot y_{b,u} + i_u^{c2} \cdot f_{b,u}) \quad \forall b \in B \quad (1.16c)$$

1

In Equation 1.16a, expenses are annualized over the project time horizon n using the project interest rate i [29, ch. 10]. The parameters i^{c1} and i^{c2} represent the linear version of the unit cost function with bare module b [22]. If the project horizon exceeds the lifetime of a unit (l), the unit must be replaced and purchased again (Equation 1.16c). For units with a lifetime greater than or equal to the project time horizon, the total number of replacements (R) is zero.

Annual total expenses The annualized TOTEX is expressed as combination of CAPEX and OPEX (Equation 1.17).

$$C_b^{tot} = C_b^{cap} + C_b^{op} \quad \forall b \in B \quad (1.17)$$

Global warming potential The Intergovernmental Panel on Climate Change (IPCC) refers to emissions by their CO₂ equivalence [3]. Commonly, when investigating the ecological footprint, the greenhouse gas emissions per unit of final energy (e.g.; g_{CO₂} / kWh of produced electricity) are considered [26]. In this approach, the footprint of batteries and thermal storage cannot be considered. Additionally, the impact factors are based on different efficiencies and amortization cannot be compared to the unit choices.

$$G_b^{tot} = G_b^{bes} + G_b^{op} \quad \forall b \in B \quad (1.18)$$

To overcome these issues, the GWP is divided into the share coming from the operation G^{op} and the construction of the building energy system G^{bes} to derive the total annual global warming potential G^{tot} (Equation 1.18).

$$G_b^{op} = \sum_{p \in P} \sum_{t \in T} \left(g_{p,t}^{el} \cdot \dot{E}_{b,p,t}^{gr,+} - g_{p,t}^{el} \cdot \dot{E}_{b,p,t}^{gr,-} + g_{p,t}^{ng} \cdot \dot{H}_{b,p,t}^{gr,+} \right) \cdot d_p \cdot d_t \quad \forall b \in B \quad (1.19)$$

Equation 1.19 details the GWP from the system's operations in $\text{CO}_{2,eq}$, where the period and time-dependent parameters $g_{p,t}$ are account for the GWP per kWh consumed electricity E [33]. It is common practice to use average values, as for accounting for the GWP per consumed natural gas H . Therefore, the different resulting contributions to the GWP are considered. The parameter d_t accounts for the duration of each timestep within a period and d_p for the duration or frequency of each period within one year.

$$G_b^{bes} = \sum_{u \in U} \frac{1}{l_u} \cdot (i_u^{g1} \cdot y_{b,u} + i_u^{g2} \cdot f_{b,u}) \quad \forall b \in B \quad (1.20)$$

The GWP of the building energy system G^{bes} is expressed in Equation 1.20. The parameters i^{g1} and i^{g2} represent the linear unit cost function in terms of GWP. The database ecoinvent documents the environmental impact of energy processes and materials and provides life cycle assessments of the different technologies [34]. The allocation system model and when available Swiss data is chosen. To assess the GWP of different unit technologies, the indicator "GWP 100a" of the method "IPCC 2013" documented in the online version 3.6 of ecoinvent is adopted. This indicator considers greenhouse gas emissions based on the GWP published by the IPCC for a time horizon of 100 years.

1.2.5 Key performance indicators

The performance of the renewable energy hub is measured according to large number of different indicators in the literature. The KPIs vary between studies, which makes it a challenge to compare the result of different systems. Following section is defining and collecting a comprehensive bandwidth of KPIs, with the aim to demonstrate their correlations and to reduce their necessary number. The KPIs are divided in four subgroups: Environmental, economical, technical and security indicators. All previously mentioned objectives serve as KPI, which are the GWP associated to operation and the system technologies (Equations 1.18, 1.19, 1.20), the OPEX (Equation 1.15), CAPEX (Equation 1.16a) and TOTEX (Equation 1.17). KPIs are expressed in normal text font in order to distinguish them from variables and parameters of the model formulation. The following equations are expressed in annual values to ease readability, although the operation and the exchanges of renewable energy hub are analyzed in hourly values.

Technical indicators Technical indicators evaluate the performance of the energy system from the perspective of the energy conversion technologies. In general, these indicators measure the energetic effort to fulfill the service requirements of SH, DHW and electricity. Common point of discussion is how and if renewable energy sources should be included in the balance or not. For this reason, following definitions of energy and exergy efficiency are defined for both system boundaries, PV panels, or solar irradiation, included (η^{pv}) and excluded (η). The energy efficiency is

1.2. Method

the effectiveness of the system or the application of the first law of thermodynamics [35].

$$\eta_I = \frac{E^{B,-} + Q^{SH,-} + Q^{dhw,-}}{E^{gr,+} + E^{pv,+} - E^{gr,-} + H^{gr,+}} \quad (1.21)$$

In Equation 1.21, the electricity demand of the building E^B is solely the uncontrollable demand, which is together with the demand for domestic hot water Q^{dhw} , a service requirement. The demand for space heating Q^{SH} is variable as it depends on the heating strategy of the building.

The exergy efficiency is evaluating the thermodynamic performance of the system respecting the second law of thermodynamics [35]. One challenge for the exergy efficiency is the correct system boundaries. One possibility is to assume that the space heating services are delivered at the temperature of the room [36]. Another possibility would be to consider supply and return temperature, which represents a system boundary at the convector itself.

$$\eta_{II} = \frac{E^{B,-} + E^{QSH,-} + E^{Qdhw,-}}{E^{gr,+} + E^{pv,+} - E^{gr,-} + E^{Hgr,+}} \quad (1.22)$$

In Equation 1.22, the exergy content of the DHW demand E^{Qdhw} is accounted at 328K and the one for SH at the current indoor temperature, which depends on the heating strategy. Reference temperature for the Carnot factor is the time-dependent external temperature. The exergy content of methane is used for the one of natural gas $E^{Hgr,+}$. Chemical exergy values of methane are available in [36, ch.11].

Including the PV panels within the system boundaries means not to directly account for the electricity the system receives from the panels but for the incoming energy in form of solar irradiation. This includes not only the evaluation of the energy conversion efficiency of the PV panels but also the level of PV curtailment.

$$\eta_I^{pv} = \frac{E^{B,-} + Q^{SH,-} + Q^{dhw,-}}{E^{gr,+} - E^{gr,-} + H^{gr,+} + A^{pv} * irrghi} \quad (1.23)$$

In Equation 1.23, the area of installed PV panels and the global solar irradiation $irrghi$ are replacing the former electricity from PV panels (compare Equation 1.21).

$$\eta_{II}^{pv} = \frac{E^{B,-} + E^{QSH,-} + E^{Qdhw,-}}{E^{gr,+} - E^{gr,-} + E^{Hgr,+} + E^{Hgr,+} + A^{pv} * E^{irr}} \quad (1.24)$$

In Equation 1.24, the exergy value of solar irradiation E^{irr} is referenced at the temperature of the sun 6000K [27].

For energy systems relying on heat pumps, the coefficient of performance (COP) is an important metric.

$$\text{COP}_{b,p,t} = \frac{Q_{b,p,t}^{hp,+}}{E_{b,p,t}^{hp,-}} \quad \forall b \in B \quad \forall p \in P \quad \forall t \in T \quad (1.25a)$$

$$\text{COP}_b = \frac{\sum_t Q_b^{hp,+}}{\sum_t E_b^{hp,-}} \quad \forall b \in B \quad (1.25b)$$

1

In Equation 1.25a, the COP is calculated with the energy consumption $E^{hp,-}$ and the heat delivered $Q^{hp,+}$ by the heat pump at every timestep. The COP is changing with the operation condition in each timestep, but can also be expressed as annual average with the sum over the electric consumption $E^{hp,-}$ and the annual heat delivered $Q^{hp,+}$ (Equation 1.25b). The COP is specific to the renewable energy hub of each building b .

Security indicators The following performance indicators evaluate the security of the supply. This comprises of two aspects, the degree of autonomy like the self-sufficiency (SS) as well as the stress level on the distribution grid like the grid usage (GU).

$$SS = \frac{E^{chp,+} + E^{pv,+} - E^{gr,-}}{E^{chp,+} + E^{pv,+} - E^{gr,-} + E^{gr,+}} \quad (1.26)$$

SS is the share of electricity demand, which can be covered by onsite generated electricity [37] (Equation 1.26).

$$SC = \frac{E^{chp,+} + E^{pv,+} - E^{gr,-}}{E^{chp,+} + E^{pv,+}} \quad (1.27)$$

self-consumption (SC) is the share of the onsite generated electricity, which is consumed by the decentralized energy system itself [37] (Equation 1.27).

$$GU_b^\pm = \max_{p,t} \left(\frac{E_{b,p,t}^{gr,\pm}}{\max_{p,t} (E_{b,p,t}^{B,-})} \right) \quad \forall b \in B \quad (1.28)$$

The GU describes the interaction with the grid in respect to the maximum uncontrollable load of the building. The uncontrollable load is excluding the demand for heating. Therefore, this indicator

1.2. Method

evaluates the impact of a system design on the grid. Equation 1.28 defines the GU according to [25].

$$\text{PVC} = \frac{E^{pv,gen} - E^{pv,+}}{E^{pv,gen}} \quad (1.29)$$

The photovoltaic curtailment (PVC) factor is share of the total amount of PV energy that is curtailed from the PV generation $E^{pv,gen}$ (Equation 1.29) [25].

$$GM_b^\pm = \max_p \left(\frac{\max_t \dot{E}_{p,t}^{gr,\pm}}{\frac{1}{pd_p} \sum_t (\dot{E}_{p,t}^{gr,\pm})} \right) \quad \forall b \in B \quad (1.30)$$

The grid multiple (GM) limits the peak power of the grid to the average demand of a period [38]. It constrains the height of the peak demand relative to the average usage during the time. A GM = 2 maximal allows a peak twice as high as average grid supply (+) or feed-in (-). Equation 1.30 defines the GM, where pd is the total duration of a period.

Economical indicators The net present value (NPV) is the absolute value of the investment in the present. This KPI is neither accounting for nor evaluating the runtime of the project. Several studies use NPV to asses the value of the proposed investment plan for energy systems [25, 39].

$$NPV = -(\mathbf{C}^{inv} + \mathbf{C}^{rep}) + \frac{(1+i)^n - 1}{i(1+i)^n} \cdot (-C^{op} + C^{op,ref}) \quad (1.31)$$

In Equation 1.31, cashflows are balanced in the present. Therefore, the CAPEX does not need to be annualized, whereas the difference of the proposed OPEX C^{op} , to the of current one $C^{op,ref}$ needs to be accumulated over the project horizon n and accounted with the project interest rate i [29, ch. 10].

The internal rate of return (IRR) is the discount rate to which the NPV would become zero, hence would become profitable. The higher the IRR the more profitable and safer is the planned investment.

$$IRR = i \quad | \quad NPV(i) = 0 \quad (1.32)$$

In contrast to NPV the IRR respects the runtime of the project and is not an absolute value (Equation 1.32). For example, the IRR can be used as objective to analyse the optimal PV size [40].

Annual revenues (AR) are the benefit from selling the generated electricity to the grid and from avoiding electricity import [40].

$$AR = (c^{el,+} \cdot SC + c^{el,-} \cdot (1 - SC)) \cdot (E^{pv,+} + E^{chp,+}) \quad (1.33)$$

In this study, electricity can be generated by CHP and PV panels, hence their operation is the only one considered in Equation 1.33. SC is the share of onsite generated electricity which is consumed by the decentralized energy system itself .

The leveled cost of electricity (LCoE) is the true cost of onsite consumed electricity. It respects also the investment in the energy system infrastructure. The definition of LCoE is controversial and therefore included in different versions.

$$1 \quad \text{LCoE}^I = \frac{C^{cap,pv} + C^{cap,bat} - E^{pv,+} \cdot (\text{SC} \cdot c^{el,+} + (1 - \text{SC}) \cdot c^{el,-})}{E^{pv,+}} \quad (1.34)$$

The first version (LCoE^I) is balancing the cost of the electricity generated onsite (Equation 1.34). Operation costs are the annual rewards, similar to Equation 1.33. Degradation and maintenance is neglected, however replacement costs are included in the capital expenses C^{cap} , in case the technologies reach their end of life and need to be replaced. If LCoE^I is a positive value, the investment of battery and PV is profitable. LCoE^I is only considering the generated electricity and the investment from PV panels and batteries, as including CHP in the calculation would neglect combined heating services. The performance indicator is defined according to the review made by branker et al. [41].

$$\text{LCoE}^{II} = \frac{C^{cap,pv} + C^{cap,bat} + c^{el,+} \cdot E^{gr,+} - c^{el,-} \cdot E^{gr,-}}{E^B} \quad (1.35)$$

Instead of evaluating the electricity cost of a utility, the second definition of LCoE evaluates the electricity cost of the whole project (Equation 1.35) [25]. However, this definition is only applicable for systems without CHP and heat services based on electricity.

The cost of avoided emissions (CAVE) are economic value of avoided emission.

$$\text{CAVE} = \frac{C^{tot,ref} - C^{tot}}{G^{tot,ref} - G^{tot}} \quad (1.36)$$

Equation 1.36 is closely related to Equation 1.40 and avoided emissions (AVE). The reference system is the current energy system which is accounted by its current costs $C^{tot,ref}$ and connected emissions $G^{tot,ref}$, which are resulting from satisfying current annual electricity, SH and DHW demand.

Environmental indicators There is a great variety of KPIs to determine and rate ecological performance of energy systems in open literature. Some are collected and presented in the review [24]. The focus of this study are energy systems for residential buildings. Therefore, the categories are reduced to GWP and the use of renewable energy sources.

1.2. Method

The renewable energy share (RES) gives the information to which part renewable energy sources are used to provide the required energy supply. Additionally, to the grid supply the generated electricity on site from PV panels is considered to be 100% renewable.

The photovoltaic penetration (PVP) measures how much of the total electricity demand of the building and the units could be covered by generated electricity from photovoltaic panels (Equation 1.37). This KPI is not measuring actually self-consumption or includes the operation of the PV panels; it rather gives information about the installed capacity of renewable energy resources in form of PV electricity in the renewable energy hub.

$$PVP = \frac{E^{pv,gen}}{E^{pv,+} + E^{chp,+} - E^{gr,-} + E^{gr,+}} \quad (1.37)$$

The carbon payback time (CPT) indicates how many years a renewable technology has to be operated to pay off the GWP, which is connected to its construction.

$$CPT^{pv} = \frac{G^{bes,pv}}{\sum_{b \in B} \sum_{p \in P} \sum_{t \in T} (g_{p,t}^{el} \cdot E_{b,p,t}^{pv,+}) \cdot d_t \cdot d_p} \quad (1.38)$$

In Equation 1.38, the CPT is calculated based on the indirect emissions of all installed PV panels $G^{bes,pv}$ and on the avoided emission while operating them [24].

$$CPT^{pv,bat} = \frac{G^{bes,pv} + G^{bes,bat}}{\sum_{b \in B} \sum_{p \in P} \sum_{t \in T} (g_{p,t}^{el} \cdot E_{b,p,t}^{pv,+}) \cdot d_t \cdot d_p} \quad (1.39)$$

When focusing on the electrical side of the energy system, a common combination are PV panels together with electrical storage systems. Therefore, the CPT in Equation 1.39 is accounting for the indirect emission of both installed PV panels $G^{bes,pv}$ as well as electric batteries $G^{bes,bat}$.

The difference of GWP between the current energy system and the proposed design are the AVE [42, ch.8].

$$AVE = G^{tot,ref} - G^{tot} \quad (1.40)$$

In Equation 1.40, the emissions of the reference system $G^{op,ref}$ are calculated based on current annual energy demand of electricity, SH and DHW in combination with typical impact factors, which can be found in the appendix.

Table 1.2 – Overview of common KPIs of decentralized energy systems, including abbreviation (abbr.) used in this work, symbol, physical unit to associated mathematical equation (equ.), and reference (ref.) to useful literature. Chosen currency is Swiss Francs (CHF), which corresponds to the currency of the case study.

description	abbr.	symbol	unit	equ.	ref.
technical indicators					
coefficient of performance (HP)	COP	COP_b	[·]	(1.25)	[35]
energy efficiency (1st law efficiency)	-	η^I	[·]	(1.21)	[36]
exergy efficiency (2st law efficiency)	-	η^{II}	[·]	(1.22)	[36]
energy efficiency, PV panels included	-	$\eta^{I,pv}$	[·]	(1.23)	[27]
exergy efficiency, PV panels included	-	$\eta^{II,pv}$	[·]	(1.24)	[27]
security indicators					
grid multiple demand	GM	GM^-	[·]	(1.30)	[22]
grid multiple supply	GM	GM^+	[·]	(1.30)	[22]
grid usage demand	GU	GU^-	[·]	(1.28)	[25]
grid usage supply	GU	GU^+	[·]	(1.28)	[25]
photovoltaic curtailment	PVC	-	[·]	(1.29)	[25]
self-consumption	SC	-	[·]	(1.27)	[37]
self-sufficiency	SS	-	[·]	(1.26)	[37]
economical indicators					
annual capital expenses	CAPEX	C^{cap}	[CHF/yr]	(1.16a)	[29]
annual operation expenses	OPEX	C^{op}	[CHF/yr]	(1.15)	[29]
annual investment costs	-	C^{inv}	[CHF/yr]	(1.16b)	[29]
annual replacement costs	-	C^{rep}	[CHF/yr]	(1.16c)	[29]
annual revenues	AR	-	[CHF/yr]	(1.33)	[40]
annual total expenses	TOTEX	C^{tot}	[CHF/yr]	(1.17)	[29]
cost of avoided emissions	CAVE	-	[CHF/kg _{CO2,eq}]	(1.36)	[42]
internal rate of return	IRR	-	[·]	(1.32)	[29]
levelized cost of electricity (definition 1)	LCoE	$LCoE^I$	[CHF/kWh]	(1.34)	[41]
levelized cost of electricity (definition 2)	LCoE	$LCoE^{II}$	[CHF/kWh]	(1.35)	[25]
net present value	NPV	-	[CHF]	(1.31)	[29]
environmental indicators					
avoided emission	AVE	-	[kg _{CO2,eq} /yr]	(1.40)	[42]
carbon payback time PV systems	CPT	CPT^{pv}	[yr]	(1.38)	[24]
carbon payback time PV & battery systems	CPT	$CPT^{pv, bat}$	[yr]	(1.39)	[24]
global warming potential from operation	GWP	G^{op}	[kg _{CO2,eq} /yr]	(1.19)	[43]
global warming potential from BES	GWP	G^{bes}	[kg _{CO2,eq} /yr]	(1.20)	[43]
photovoltaic penetration	PVP	-	[·]	(1.37)	[25]
renewable energy share	RES	-	[·]	(·)	[24]
total global warming potential	GWP	G^{tot}	[kg _{CO2,eq} /yr]	(1.18)	[43]

1.2. Method

1.2.6 Case study

The generation of renewable energy hub designs and the evaluation of associated KPIs is demonstrated by performing MOO of 40 different residential buildings. The main input data are detailed in Table 1.3. The buildings are defined by their usage type, their renovation stage and their size in terms of ERA and net surface. The characteristic input parameter are derived from publicly available databases of the national building stock [44, 45].

Table 1.3 – Overview input data of the case study for 40 buildings. Additional input information is the current main energy carrier, used for providing hot water and space heating services, considered carrier: heating oil, natural gas, electricity, solar irradiation.

		multi family house	multi family house	single family house	single family house	
building type ⁺		I	I	II	II	
building category ⁺		existing	standard	existing	standard	
number of buildings		8	2	26	4	
total net surface	A^{net}	6400	970	6500	1400	m^2_{net}
total energy ref. area	A^{era}	8000	1200	8200	1800	m^2_{era}
design supply temperature	T_0^s	65	41.5	65	41.5	°C
design return temperature	T_0^r	50	33.9	50	33.9	°C
overall heat transfer factor [†]	U	1.8 ± 0.3	0.83 ± 0	1.74 ± 0.24	0.83 ± 0	$W/(m^2_{era} K)$
heat capacity factor [†]	C	120 ± 0	120 ± 0	120 ± 0	120 ± 0	$Wh/(m^2_{era} K)$
solar gain factor [†]	ϕ	0.06 ± 0.015	0.0120 ± 0	0.06 ± 0.013	0.0120 ± 0	-
annual electricity demand	E^B	22	20	22	19	kWh/m^2_{net}
annual hot water demand	Q^{dhw}	25	25	19	19	kWh/m^2_{net}
annual internal heat gain	Q^{int}	30	32	29	29	kWh/m^2_{net}
annual current cost [†]	C^{op}	27 ± 4	16 ± 3	32 ± 13	20 ± 1	CHF/m^2_{era}

⁺ according Swiss standard norm [31]

[†] average values \pm standard deviation. Detailed building data is available in the appendix.

The heating system requirements are characterized by the design return and supply temperatures of the heating network, the overall heat transfer factor, the capacity factor, and the solargain factor that are derived by the method developed by Girardin [23]. In a pre-processing step, the annual demand profiles for domestic hot water and electricity are derived according to previously presented methods (Section 1.2.2). Additionally, the desired indoor temperature is assumed to be 20 °C for all buildings. Additional input information is the main energy carrier which is currently used to supply thermal service demands. This information is used to estimate current cost and GWP of the building energy system inplace.

Data reduction The hourly timesteps of a typical annual profile, leads to 8760 data points per year. This leads, together with the complexity of the model, to computationally untraceable models. Reducing the size of the data representing the energy demand of the renewable energy hub and weather conditions is required. The aggregation of time-series to typical periods is specifically popular, as patterns occur naturally in the supply and demand of energy, which arise in the time dimension through hourly, daily and seasonal cycles. A recent comprehensive review by Hoffman et al. [46], who analyzed data reduction techniques that were applied for modeling energy systems in 130 different publications. Schütz et al. [47] compared different aggregation methods for the selection of typical demand days, such as k-means, k-medians, k-centers, k-medoids, seasonal and monthly based classifications. Hoffman et al. and Schütz et al. [46, 47] demonstrated that the more intuitive aggregation methods of seasons or months led to significantly larger errors than machine learning methods for the same computation time. Algorithms within the latter category performed similarly well, although k-medoids were most reliable for approximating costs. Therefore, k-medoids clustering algorithm is chosen and performed. Typical days are identified based on two variables: global irradiation and ambient temperature. Typical weather data is available from the EnergyPlus open source database [48]. Packages in the programming language R are available and used to perform the clustering [49]. First, the input data is normalized and converted to a distance matrix, using the function *distNumeric*, provided by the package *kmed*. Then, the k-medoids clustering is performed using the function *wcKMedoids* of the package *WeightedCluster* with the method *PAMonce*. Figure 1.2 shows the quality of the preformed data clustering on global irradiation and ambient temperature for Geneva, Switzerland, with different number of clusters.

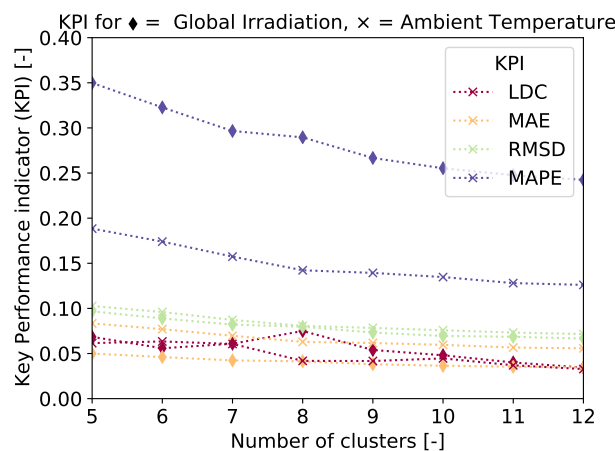


Figure 1.2 – Quality of the data reduction technique for different number of k-medoid clusters: load duration curve (LDC), mean average error (MAE), root mean square deviation (RMSD) and mean average percentage error (MAPE). Selected number of clusters is 10 additional to two extreme periods. Typical weather data for Geneva Switzerland [48].

Based on the information presented in Figure 1.2, yearly operation was based on 10 typical days,

1.2. Method

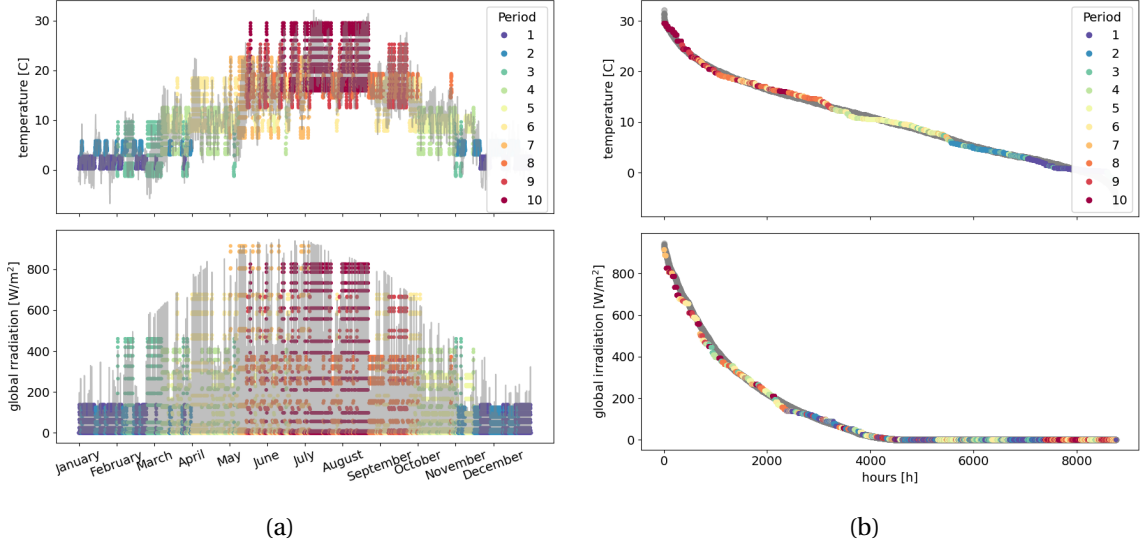


Figure 1.3 – Clustering results for external temperature and global irradiation [48] a) classification of different periods over the year b) load duration curve.

since this appears as a good compromise between the key performance indicators and the expected computational requirements. Figure 1.3 visualizes the reconstructed annual profiles of solar irradiation and outdoor temperature for the result of the k-medoids clustering. To ensure that no energy is accumulated between different periods, cyclic constraints are imposed both on the indoor building temperature and on the thermal and electrical energy storage systems. Cyclic constraints reset the state to its initial status at the end of each period [22].

1.3 Results and discussion

The aim of the result section is to provide an answer to the research question of this chapter *What performance indicators should be used to describe renewable energy hubs?*. The answer is given in several parts. At first, points concerning single KPIs are discussed. Special focus is thereby given to controversial aspects of the GWP. Subsequently, dimensional reduction is performed to reveal most influential measures to describe renewable energy hubs.

1

1.3.1 Global warming potential

The total GWP is usually in trade-off with TOTEX. Low TOTEX scenarios have high total GWP and vice-versa (Figure 1.4). For a typical Swiss residential building, the cheapest TOTEX scenario was around 17 CHF/m² ERA. This scenario was equipped with a heat pump, a gas boiler for thermal peak loads, thermal storage, and a few PV panels. The biggest contribution to reduce GWP was the total replacement of natural gas with electricity, by increasing the installed capacity of the heat pump and using electrical heaters for thermal peak loads. To reduce the total GWP even further, priority was given to consuming a higher share of electricity generated on site, by increasing the amount of PV panels and installing electricity storage in form of lithium batteries (Figure 1.4). Considering only GWP associated to the operation of the systems was underestimating the total GWP by 5% for the low cost scenarios (Figure 1.4b). The electrification of the renewable energy hub with the preference in the self-consumption onsite generated electricity increased the importance of the GWP associated to the construction of units for the energy system. Neglecting these contributions caused an annual error of more than 40% for systems with low GWP (Figure 1.4b).

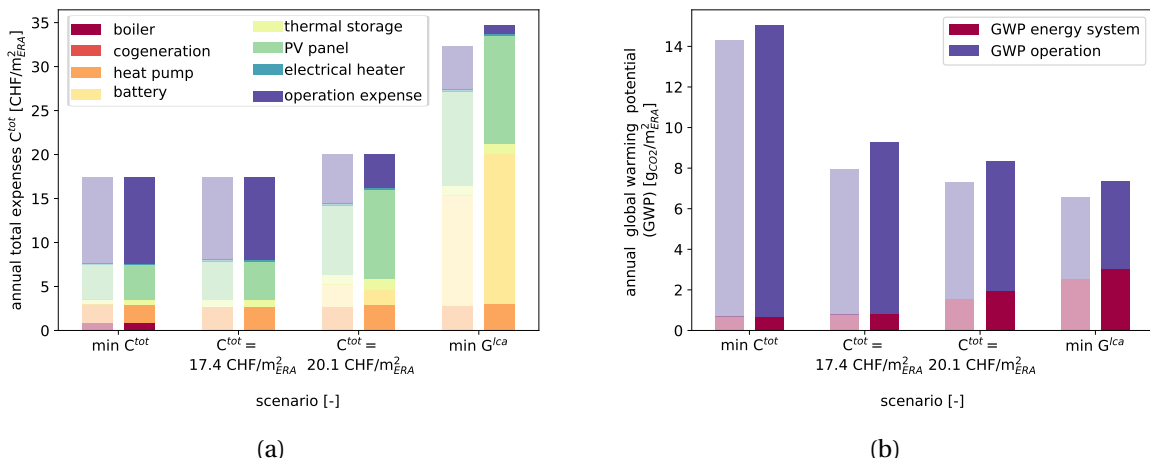


Figure 1.4 – The trade off between (a) total annual costs and (b) emission for renewable energy hubs. MOO of a typical Swiss building effected from average emission values of Swiss grid mix (light) and dynamic profiles (dark)

1.3. Results and discussion

Impact of resolution Usual studies do not consider the resolution of the GWP per consumed electricity from the grid and use annual average values. Figure 1.4b and 1.5 visualize the difference for assuming annual averages or an hourly resolution. The hourly values were based on the Swiss grid mix from 2019, which showed a higher related environmental impact during winter days than during summer [33].

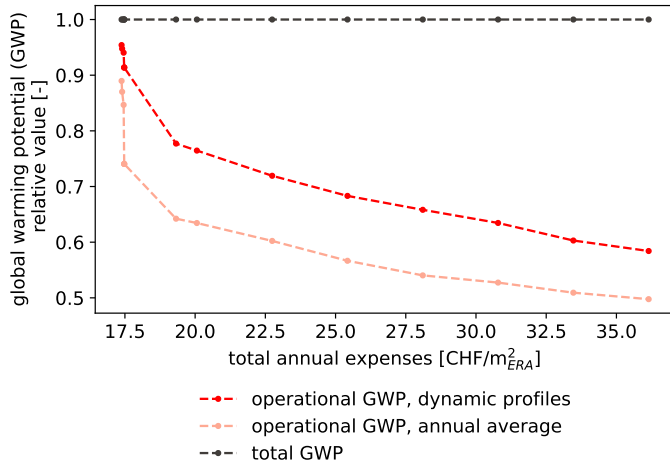


Figure 1.5 – Relative share of operational global warming potential (GWP) to the total GWP for different cost scenarios. Impact of different resolution of GWP, which is related to the electricity consumed from the power grid.

The highest energy demand for renewable energy hubs was noticed during winter, due to the demand for space heating. As this was concurring with the time of high impact factors of electricity, the total GWP was generally underestimated by around 10% when assuming an average value (Figure 1.5). Furthermore, different energy system configurations were identified to be optimal for the renewable energy hub. To increase the self-consumed electricity in winter months had a higher priority when an hourly resolution was considered; thus in this situation PV systems and batteries were chosen to a greater share (Figure 1.4a).

Impact of grid mix The GWP connected to the grid mix had a high impact on the solutions. It influenced not only the decision making of single renewable energy hubs, but also revealed different national strategies. Next to the weather, which is impacting the thermal demand or the solar potential, the grid mix of different countries impacts the solution. For demonstration purposes, economic input parameters, such as the investment costs of equipment or grid tariffs were assumed to be identical between the countries. Figure 1.6 shows Pareto optimal configurations for renewable energy hub at the building scale for four exemplary different European countries.

For countries with high emission mix on the grid, optimal solutions focused on decentralized, local

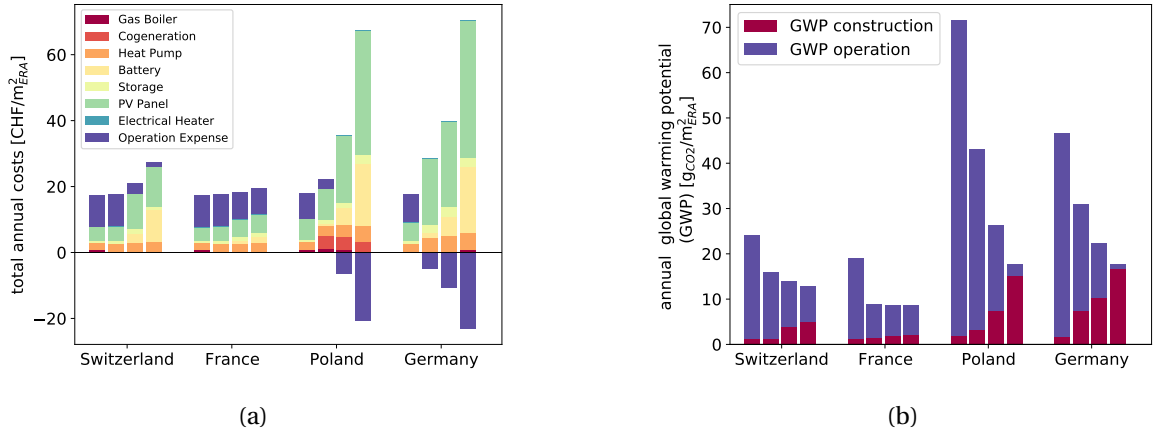


Figure 1.6 – Influence of the grid mix on the optimal design of renewable energy hubs. Comparison of different energy system configurations for a typical residential building in four European countries. Four Pareto optimal points between (a) total annual costs and (b) annual emission for each country.

generation and consumption of electricity. This strategy accepted the high constructional footprint of technologies like PV panels and batteries. For countries, like Poland, where the GWP of the electricity exceeds the impact of burning natural gas, it was suggested to invest into decentralized cogeneration technologies like solid oxide fuel cells (SOFCs) (Figure 1.6a). Next to the geographical context, this example can also be understood as the demonstration of the impact of the project horizon. The project horizon was considered to be 20 years, a time period in which the grid mix is most likely developing towards a less polluted electricity mix in context of the energy transition. In this case, a future, low GWP associated grid mix, is presented by the values considered for France (Figure 1.6). In this situation, it was more profitable for both, annual emission and cost, to consume the electricity from the grid rather than to focus on a decentralized production.

1.3.2 Impact of system boundaries

The choice of system boundaries was influencing not only absolute values, but also the relative trend of performance indicators. Two examples are presented in the following.

The first example is demonstrating the different system boundaries when analyzing the exergy efficiency of a renewable energy hub. Studies focusing on the energy conversion of solar irradiation commonly use an average temperature of the sun around 6000K to determine the exergy efficiency of the system [27, 50]. In contrast, other studies exclude the solar irradiation from the exergy efficiency and directly balance the exergy generated from the solar system. Figure 1.7 compares both definitions with respect to the RES and total annual costs of different energy system configurations. For comparability reason, system solutions using natural gas were excluded and buildings with similar renovation states were compared.

1.3. Results and discussion

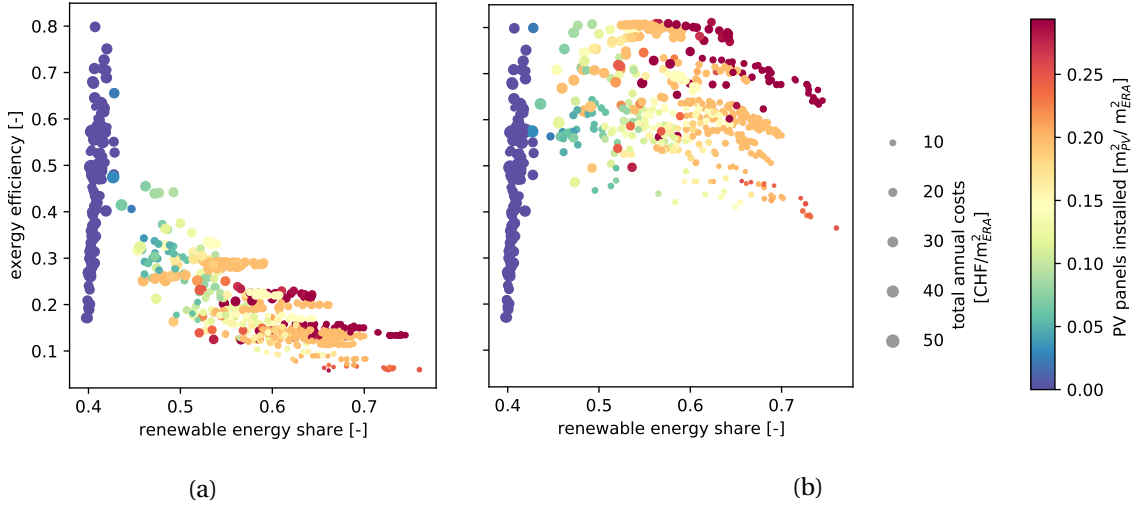


Figure 1.7 – Exergy efficiency and renewable energy share for various system configurations of renewable energy hubs, which consist of different sizes for installed HP, EH, PV panels, STO and BA. The capacity of installed PV panels is normalized by the energy reference area (ERA) of each building. Comparison of two different definitions of exergy efficiency: a) Including the conversion of irradiation, inside the system boundaries and b) Excluding the conversion of irradiation.

For electrical systems without PV panels the RES was constant and the exergy efficiency increased when substituting electrical heater with heat pumps to satisfy heating demand. Increasing the share of PV panels, led to an increase in RES and to very different behavior of the exergy efficiency for the two versions. The low exergy efficiency of the PV panels decreased the overall exergy efficiency drastically when the solar irradiation was included inside the system boundaries. In that case, the exergy evaluation of different system configuration was dominated by the installed size of PV panels per ERA. Solar irradiation is a resource which enters the renewable energy hub free of charge. Additionally, the exergy efficiency of PV systems is mainly interesting for developer of the solar system itself. If solar irradiation is nevertheless included in the exergy balance, the exergy efficiency for generating the electricity on the grid should also be considered to lead to consistent results. However, latter data at hourly resolution was not publicly available. Therefore, the exergy efficiency is considered excluding the balance of the energy conversion in PV panels in the rest of the thesis.

The second example is demonstrating the importance of appropriate system boundaries when evaluating the GWP of energy systems. The total GWP considers the environmental footprint of the renewable energy hub. As previously demonstrated, the contribution from both, the construction and the operation of the energy system should be considered. However, there are two different perspectives possible. One perspective is, to consider the total effort which is needed to satisfy the energy demand of the renewable energy hub itself. The other option is to include the impact of the renewable energy hub within its the superior network. The difference lies in accounting the locally produced and exported resources. Figure 1.8 shows the evaluation of the GWP for TOTEX scenarios

of one typical renewable energy hub at the building scale.

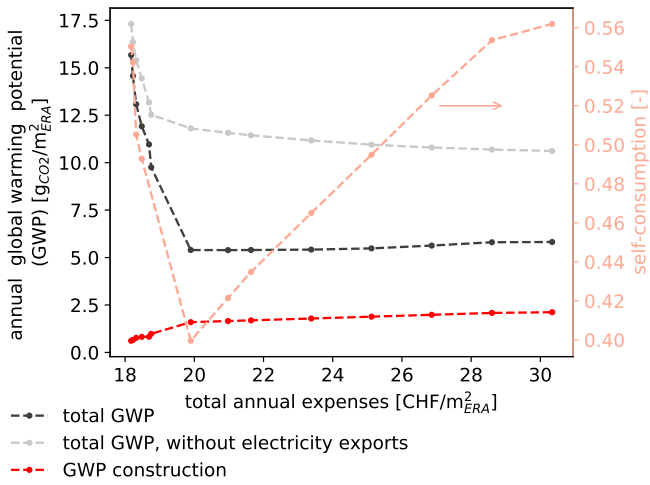


Figure 1.8 – Impact of system boundaries for evaluation global warming potential (GWP). Comparison of the total GWP as defined in Equation 1.18 to the GWP when exports are not considered as avoidance.

At around 20 CHF/m² ERA, the capacity of installing PV panels was exceeded and the focus was on increasing SC rates by installing storage systems. Nevertheless, the SC rate of the electricity produced onsite was not exceeding 60% in detected solutions (Figure 1.8). If the total GWP was considering the exported electricity as avoidance of equivalent emissions, the total annual GWP was approximately 6 gCO₂,eq/m² ERA. If exported electricity was not included in the balance (Equation 1.18), the GWP was around 12 gCO₂,eq/m² ERA, increased by a factor 2. The operation of the electricity grid is characterized by the synchronization of consumption and generation of electricity. The electricity, which is fed into the grid by the renewable energy hub, is avoiding the production of same amount of electricity at current grid mix. Therefore, these exports are always accounted for in the balance of the GWP in the rest of the thesis.

1.3.3 Dimensional reduction

The aim of this section is to explore the decision space and support the multi-criteria decision making. Over 8000 different solutions were generated by considering each indicator in a multi-parametric optimisation framework for 40 renewable energy hubs. Analyzed KPIs are listed in Table 1.2. In accordance with the results of previous section, the GWP of operation was considered with dynamic impact profiles only and the exergy efficiency was excluding the energy conversion in PV panels. The correlation between the different indicators is demonstrated by performing a principal component analysis of the decision space. The principal component analysis was performed using the function *prcomp* provided by the programming language R [51]. A principal

1.3. Results and discussion

component is a dimension in which the most substantial variance in the data is noticeable. It can be understood as defining an axis of a new coordinate system, which is used to allocate each data point. Figure 1.9 shows the correlation plot of the KPIs in the first two dimensions of the principal component analysis.

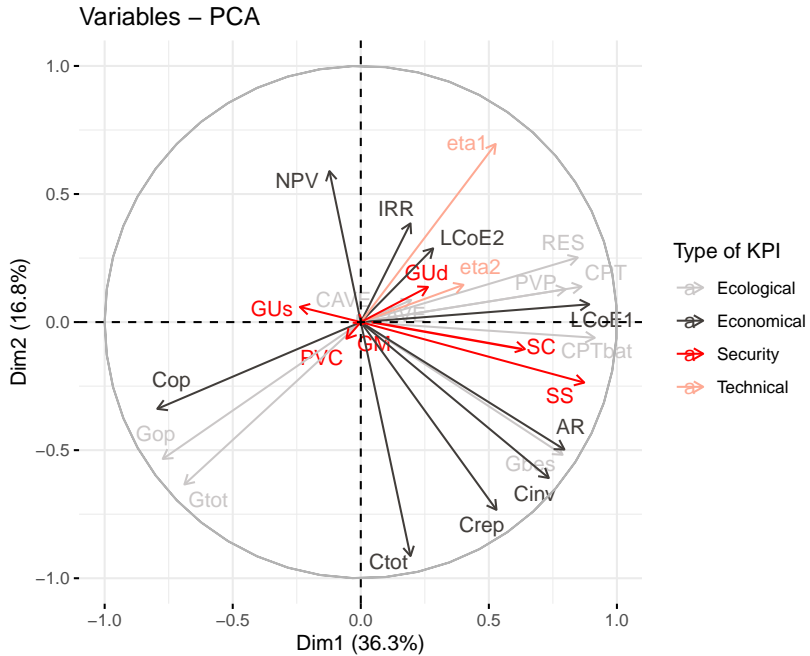


Figure 1.9 – Variable correlation plot of the principal component analysis. Positive correlated KPIs are grouped together, not correlated are perpendicular, inverse correlated are 180° opposite. Distance from the origin gives the impact of the KPI itself.

Each dimension corresponds to a principle component, they are ordered with declining significance. The first dimension was explaining 36.3% of the variance, the second 16.8% (Figure 1.9). The variations of the following dimensions are even smaller and not very informative, hence the correlation is further analyzed based on the first two dimensions.

Influential KPIs The distance to the origin reveals the quality of the indicator and its contribution to define a solution. The longer the arrow in the correlation plot (Figure 1.9), the more specific is this indicator to describe the performance of the renewable energy hub. In other words, for the KPIs represented by short arrows, for example concerning the security of the grid (GM, GU, PVC), many different solutions existed, with the same value of this KPI. These KPIs did not clearly describe a solution. However, they revealed the potential of a renewable energy hub to meet these KPIs. For example, in order respecting a limit on the GU, it is possible to

change the operation for a wide range of detected solutions.

Correlated KPIs Strongly correlated indicators are grouped together, for example G^{bes} , AR and C^{inv} . This correlation was due to the fact that the system with the highest environmental footprint allocated to the construction had batteries and PV panels installed, which were also the most expensive units. The solutions characterized by batteries and PV panels gave priority to local generation and consumption of electricity from renewable energy sources, which is also measured by the AR. This correlation also confirmed the previous finding (Figure 1.4). For more expensive system configurations, which usually consist of a larger share of PV and battery, constructional emissions could not be neglected.

Another correlation can be observed between the OPEX (C^{op}) and the GWP of the operation (G^{op}). Main contributor to both, OPEX and operational GWP, were the resources imported and exported by the system. However, the vectors were not as close as the previous example due to the high GWP of natural gas compared to the electricity but the inverse correlation of cost (1:2.5) in Switzerland.

Inverse correlated KPIs In Figure 1.9, inverse correlated KPIs are visualized by arrows which are opposite to each other. One example is the correlation of NPV and total costs (C^{tot}). The higher the total cost of the proposed energy system, the lower was the net present value of the system. The OPEX of the current installed energy system played a minor role in this context (see Equation 1.31). Figure 1.9 also shows the intuitive relation between systems with increased RES, which also had a higher PVP but OPEX were reduced as well as the operational GWP.

Uncorrelated KPIs Uncorrelated KPIs are positioned in an 90° angle from each other in Figure 1.9. These KPIs are best suited to pin-point a solution. They are also predestined to serve as objectives during MOO. The sum of replacement and investment cost are CAPEX and were perpendicular to the operating expenses C^{op} . Therefore, the CAPEX - OPEX pareto curve is well suited to investigate the decision space of renewable energy hubs.

The value of these results is two-fold: On one hand this method revealed redundant indicators. Therewith, it supports decision maker to select a subset of essential indicators. On the other hand the method allowed for the identification, which KPIs contributed the most to define a solution and should not be neglected. The impact of these results are demonstrated in the following. Typical solutions were derived by performing a k-medoids clustering of the more than 8000 different MOO solutions for the 40 buildings of the case study. A subset of uncorrelated indicators were then used to evaluate the performance of identified typical systems.

The typical energy system configurations which were identified are outlined in the following:

- Medoid 1 - system based on natural gas boiler
- Medoid 2 - heat pump and small installed capacities of PV panels and storage systems
- Medoid 3 - heat pump, PV panels, large electrical and small thermal storage capacities

1.3. Results and discussion

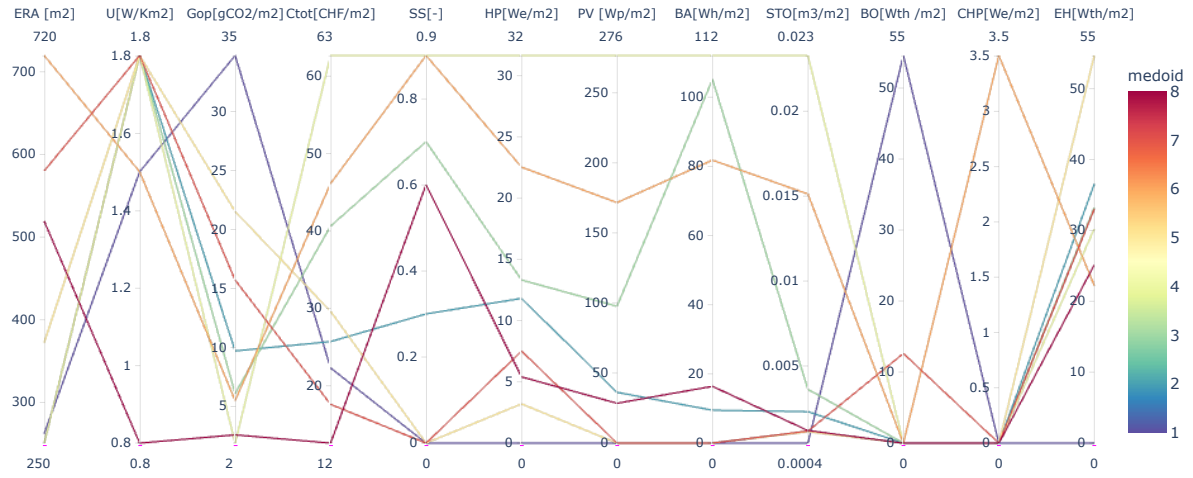


Figure 1.10 – Result of K-medoids clustering of the technology decisions within the 8000 different optimal solutions for 40 residential renewable energy hubs. Visualized building related parameter are the heated surface [m^2] and the heat transfer coefficient U to describe the renovation state [23]. Three uncorrelated KPIs are selected (compare Figure 1.9).

- Medoid 4 - large capacities of installed heat pump, PV panels and storages
- Medoid 5 - related to Medoid 1, instead of gas boiler, based on heat pump and electrical heater
- Medoid 6 - only solution with cogeneration units installed, additional to heat pump, PV panels and large storage systems.
- Medoid 7 - system based on heat pump and gas boiler. No PV panels or batteries.
- Medoid 8 - system based on heat pump, PV and small storage systems, modern building

These typical solutions can be all well described by the presented KPIs in Figure 1.10 (GWP of the operation, total costs and self-sufficiency) and the correlation analysis of the remaining KPIs (Figure 1.9). In the following three examples are provided.

Medoid 1 describes a typical solution for a residential building, which is based on natural gas boiler (Figure 1.10). The GWP of the operation was highest and the SS lowest among the other medoid solutions. As demonstrated with Figure 1.9, allocated GWP and costs of the system's operation were correlated. Therefore, it can be concluded that the OPEX were also highest for the type of systems, represented by Medoid 1.

The performance of Medoid 4 is described by the highest total expenses and SS among the typical solutions. The analysis of the correlation of KPIs (Figure 1.9), allowed for the conclusion that this system had the lowest net present value, but also highest annual revenues. As the system had low GWP associated to operation, the OPEX of Medoid 4 was low as well. The system of Medoid 4 had large capacities of heat pumps, PV and storage systems installed.

The lowest total expenses and GWP of the operation is presented by Medoid 8, which is describing a

system for a renovated renewable energy hub. Smaller capacities of heat pumps, PV and storage systems were installed with respect to Medoid 3. Nevertheless, both systems represented by their medoids led to similar values in SS.

1.4 Conclusion

The renewable energy hub at the building scale was defined in a mixed-integer linear programming (MILP) approach. The renewable energy hubs were connected to the electricity grid, natural gas grid and water grid and the aim is to satisfy the demand for space heating, domestic hot water and electricity. The following conversion technologies were implemented: air-water heat pumps, gas boiler, PV panels, electrical heater and CHP units in form of solid-oxide fuel cells. Additionally, renewable energy hubs could be equipped with thermal storage systems and batteries. As the building was modeled according to the first order dynamic building model, heat can also be stored in the building itself. A possibility was implemented to include a smart heating strategy, which preheats the building at times of surplus electricity from renewable sources. Annual time-series in the input data was reduced to ten typical days with hourly timesteps. A MOO framework was used to capture the decision space. Considering the state-of-the-art in building energy system modeling, 31 different KPIs were defined. The analysis of these measures was structured in two parts. The first part was looking at individual KPIs, whereas the reduction of necessary KPIs and typical renewable energy hub configurations was addressed in the second part.

In the first part, different controversial aspects of describing the GWP of renewable energy hubs were highlighted. Neglecting the footprint associated to the construction of the energy system technologies, introduced an error of 5% for basic equipped systems. The error was increasing in relevance for modern, decentralized systems, where the footprint accounted for more than 40% of the total GWP. The common way of estimating the GWP which is connected to electricity consumption from the grid is to use average values. The comparison to hourly values associated to the Swiss grid mix from 2019, showed that this was underestimating the total GWP by more than 10%. With average impact factors, the renewable energy hub gave too little priority to self-consume generated electricity in winter months, which was influencing the optimal design strategy. The GWP associated to the electricity exchange to the electrical grid had a great impact on the optimal design strategy of renewable energy hubs. The lower the imported emissions were of the electricity, the lower were the incentives to install independent, decentralized solutions, which rely on renewable energies and storage systems but are high in constructional GWP. Two examples about the importance of system boundaries were demonstrated: The inclusion of the environmental impact of the energy conversion in PV panels and the inclusion of the electricity exports when balancing the total GWP of the system. First part led to the conclusion that the appropriate definition of the GWP should include the constructional footprint of the energy system equipment, dynamic impact profiles of the grid, and should consider exports as avoidance of equivalent emission. The exergy efficiency

1.4. Conclusion

of the system was defined without considering the electrical efficiency of the PV panels. Limiting factor of including this aspect was the missing exergy values associated to the electricity grid.

In the second part, machine learning techniques, like principle component analysis and k-medoids clustering, were applied to identify the major trends, and supporting multi – criteria decision making. More than 8000 different solutions were generated by considering 40 typical residential buildings in a multi parametric optimization framework. Some KPIs were identified to be more influential (like TOTEX) than other (like GU). Direct and inverse correlation of the KPIs was demonstrated. This analysis revealed that a few KPIs were enough to give a holistic picture of the performance of renewable energy hubs. The principle component analysis also clearly identified two separate dimensions for CAPEX and OPEX. Therefore, they are mainly chosen objectives for the MOO in the following chapters of this thesis. Eight typical system configurations were identified through k-medoids clustering of the solutions. It was demonstrated how a selection of uncorrelated KPIs enables the full evaluation of these different typical solutions.

This analysis is however valid for the considered values of the specific economic costs and environmental impacts. Future extension of this work would be to perform an uncertainty analysis of the KPIs and their correlation by, for example, carry out a monte carlo analysis. Interesting influences are for example the CO₂-taxes on electricity, which might gain importance over the coming years. At the same time, the investment costs of PV panels and batteries might decrease. This could change the fact that some KPIs are correlated and some are not. For example, the emission and the cost that are related to the operation of the renewable energy hub are likely to still be correlated, even with higher CO₂-taxes. In contrast, the total cost and costs that are allocated to the operation might become more correlated with the reduction of the investment costs of PV panels and batteries.

Further improvement is to provide a larger variety of social KPIs and to include exergy-based indicators of the grid mix. The KPIs were focused on considered the optimal inclusion of renewable energies in form of PV panels. However, the actual available roof area was simplified and considered as horizontal. The aim of the following Chapter 2 is to overcome this limitation.

Photovoltaic panel orientation in renewable energy hubs

Overview

- Integration of oriented PV panels in MILP for modeling and optimization of BES
- Inclusion of inter-modular shading and load scheduling
- Impact of PV panel orientation on the design strategy of renewable energy hubs
- Different strategies for subsidizing the installation of PV panel impacting the optimal orientation

The content of this chapter is published in [52] and [53].

The integration of renewable energy sources, and particularly of photovoltaic (PV) panels, is becoming an increasingly widespread solution for reducing the carbon footprint of renewable energy hubs. However, the volatility of the energy generation and its mismatch with the typical demand patterns are cause for concern, particularly from the viewpoint of the management of the power grid. This chapter aims to show the influence of the orientation of PV panels and to provide support to the decision making process. Compared with existing approaches of renewable energy hubs at the building scale, the contribution of PV panels is modeled in more detail, including a more accurate solar irradiation model and the shading effect among panels. Compared with existing studies in PV modeling, the interaction between the PV panels and the remaining units of the building energy system (BES), including the effects of optimal scheduling is considered. The results confirmed the relevant influence of PV panels' azimuth and tilt on the performance of BES. Whereas south-orientation remained the most preferred choice, west-oriented panels better matched the demand when compared with east-oriented panels. An appropriate choice of orientation was shown to benefit the grid: rotating the panels 20° westwards can, together with an appropriate scheduling, reduce the peak power of the exchange with the power grid by 50% while increasing total cost by only 8.3%. Including the more detailed modeling of the PV energy generation demonstrated that assuming horizontal surfaces can lead to inaccuracies of up to 20% when calculating operating expenses and electricity generated, particularly for high levels of PV penetration.

2.1 Introduction

It is today widely accepted that climate change is a threat to both human and natural ecosystems, and that the increasing greenhouse gas emissions from anthropogenic activities are at the root of the warming of the climate [1]. Among all human-related activity sectors, buildings accounted for 36% of the global final energy use and 39% of the greenhouse gas emissions in 2018 [2]. Among the latter, residential buildings globally accounted for 61% of the final energy use and 41% of the emissions. Furthermore, over 50% of the global final energy use in residential buildings is related to space and water heating [2, 3].

To decrease carbon emissions, several solutions have been suggested to increase carbon efficiency while fulfilling heating requirements for residential buildings. Whereas several researchers have focused on reducing the demand, another solution is to move away from high-carbon fossil fuels, thereby switching from natural gas and oil to low carbon fuels such as green electricity. In particular, switching to electrical HVAC systems allows a higher conversion efficiency and improves the integration of locally generated renewable energy, such as by installing PV panels on rooftops [1, 3]. However, volatile power generation caused by the fluctuation of solar irradiation challenges the capacity of the electrical power grid. Therefore, in addition to maximizing the energy generated from the sun, it is important to reduce the interaction of the BES with the electrical power grid. The renewable energy hub is giving priority to self-consumption of locally produced electricity. The aim of this chapter is to propose a framework for renewable energy hubs which integrates the aspect of optimally design and schedule a high share of solar energy resources.

2.2 State-of-the-art

The overview about the state of the art is structured into three research areas of main interest in the following. The first one is looking at current status of the multi-objective optimization (MOO) framework of BES, which is the underling system structure of the considered renewable energy hub. The second part is summarizing the current state of the art of energy systems which focus on the integration of solar based energy resources. The last and third part is providing an overview of simulation techniques of oriented irradiation. This section closes with stating the resulting gaps of the literature and the scientific contribution of this chapter.

2.2.1 Multi-objective optimization framework of building energy systems

The vast number of alternative solutions available to reduce the carbon footprint of BES makes the choice of the appropriate system a complex decision. For this reason, several studies dealing with energy system optimization have focused on it. In particular, when renewable energy generation is involved, the target is to identify economical and environmental friendly solutions for BESs that

cover thermal and electricity demand while protecting the grid and therewith secure the supply.

Consequently, many similar BES optimization problems exist and are generally characterized by having multiple, competing objectives. The most common include capital expenses (CAPEX), operational expenses (OPEX), and global warming potential (GWP). This forces researchers to adopt a MOO approach. The MOO of BES has been the focus of extensive research over the past years [22, 26, 38, 54–59].

Within the framework of BES optimization, many models have included PV panels as one alternative for distributed energy generation. In most cases, the electricity generated by PV panels has been modeled by an efficiency converting solar radiation to electricity. Because of the need to reduce model complexity, these models are generally relatively simple. It is common to use the total irradiation, often referred to as global irradiation, to model the incoming solar radiation, which corresponds to assuming horizontal panels [60].

In general, studies focusing on the energy system have not accounted for varied panel orientation, and only the most detailed PV models have included the influence of different ambient conditions (such as external temperature) on the efficiency of the conversion [55, 58, 61] or on panel degradation [39].

A detailed literature review has revealed no prior investigation on the role of the incident angle of solar irradiation on PV panels, with the exception of thermal solar panels, where the roof orientation was set as the orientation of the thermal solar panel [59].

2.2.2 Simulation and optimization of solar based energy systems

The increasing penetration of solar energy in the electricity network has confronted the grid operators with new challenges. The demand during solar noon hours is decreasing, whereas the demand after sunset is increasing, causing a sharp ramp in evening hours. Within this context, adapting the supply to match demand has become a compelling task [62].

Research in the field of solar-based energy systems, however, has shown that panel/roof orientation and tilt have a substantial influence on the energy generation potential of PV panels, and that altering these variables can help to provide a better match between the demand and the energy availability from the PV modules. Thereby, researchers have focused on the optimal sizing of PV panels and batteries, maximizing objectives like the internal rate of return [40] or minimizing costs [25].

Van der Stel et al. [63] proposed a MILP framework to analyze PV–Battery system in techno-economical terms based on real demand and PV profiles with different orientations taken from smart meter measurements of 39 residential buildings in The Netherlands. The authors demonstrated that although the increased self-consumption was the main contributor to annual saving, centralized

and decentralized storage systems are economically infeasible. Unsurprisingly, high feed-in tariffs result in a larger optimal size for PV panels. Similarly, Holweger et al. [25] demonstrated the impact of different price signals on the optimal unit size and grid impact. Their optimization framework included storage and curtailment options but the orientation of the PV was fixed. Hartner et al. [40] have not included storage or curtailment options and used a simulation tool to assess the electricity profiles generated by PV panels.

Varying the orientation of the PV modules allows for a better match between the demand and energy availability from the PV modules, thus resulting in higher self-consumption and, hence, higher revenues, without the need for batteries. The economic advantage of self-consuming the energy produced by the PV modules instead of selling it to the grid operator largely depends on country-specific attributes, such as price profiles and the amount of generated electricity [64–66]. However, given the challenges of grid stability arising from a more widespread adoption of distributed electricity generation, most countries are reducing the compensation for feeding in energy to the grid to promote self-consumption and, hence, reduce strong demand variations.

Litjens et al. [64] showed that self-consumption is highest at 212° azimuth and 26° tilt for residential buildings in Netherlands. Similar results were obtained in the United Kingdom by Mondol et al. [65] and by Lahnaoui et al. [66], who concluded that west-oriented PV systems have a higher share of directly consumed electricity than east-oriented systems for residential demand patterns in Germany. On the other hand, the maximum electricity generation was achieved for south-oriented systems (approximately 180° azimuth) and with a tilt angle approximately 30° . Although these values can change based on the system location (latitude and weather patterns), similar results have been found by researchers in Austria [40], The Netherlands and the UK [64, 65]. A maximum variation of the optimal orientation of about 7° towards the west and higher tilt angles were identified due to weather influence [64].

Not all researchers, however, have agreed with the result that slightly west-oriented panels are the most optimal configuration. A recent study by [67] investigated the impact of the orientation of PV modules on the grid, including the effects on grid losses and PV curtailment. Their results identified that the optimal orientation is the one that maximizes the annual generated electricity (south, 35° tilt in Belgium). Although this high generation also causes the highest curtailment and grid losses, changing the orientation did not lead to more useful energy. The authors also found, however, that changing the tilt angle had a higher impact on the grid than on the generation and thus suggested to lower tilt angles for more constrained grids [67].

Other researchers have confirmed that, although it might not be the most economically convenient choice, it is possible to contribute to preserving grid stability by changing the orientation. Sadineni et al. [68], referring to a case study in the United States of America (USA), showed that the combination orientating the PV modules to the west and load scheduling of the cooling demand can

reduce the peak by more than 60%, although the most economical orientation at flat price profiles remains south. These results were confirmed by Rhodes et al. [69], who evaluated the optimal placement of PV panels at a national level in the USA. They found that orientating the PV panels towards the south led to the maximum energy generated. Differently from Sadineni et al. [68], however, they also showed that shifting the orientation 20°–50° westwards increased the economic value of the generated PV electricity by 1%–7%. A further increase in the tilt and in the westward orientation was also identified as the optimal "peak placement", as the system produced 24% more energy during peak demand hours [69].

However, as the optimal integration of PV and battery systems was the focus in the aforementioned studies, historical measurements of the electric demand have been commonly applied or the remaining technologies and the renovation state of the building is fixed a priori, leading to predefined demand profiles from the buildings.

2.2.3 Modeling of photovoltaic panel orientation and directed irradiation

As highlighted in the previous section, the positioning of the PV modules (orientation and tilt angle) can significantly impact the model design of how such systems perform once included in the BES. This highlights the need for including models accounting for these effects on the energy generation profile of a solar panel.

Accessing the orientation of solar irradiation is important for urban planners to find the best building concepts and designs and to evaluate the solar potential of surfaces. An overview of detailed models for determining solar incident values was provided by Hafez et al. [70], who focused on the optimal tilt angle and on how it varies with the location and season. Starting from the assumption that orientation is considered as optimal when the received irradiation is maximal, Hafez et al. [70] presented optimal tilt angles from case studies from all over the world.

Irradiation models are generally classified into two categories. Isotropic models assume a uniform intensity of diffuse radiation over the skydome, whereas anisotropic sky models do not. Different models have been proposed [60, 70, 71]. It is unfortunately controversial whether isotropic or anisotropic models are more accurate, and literature in the field shows conflicting results. In general, anisotropic models are more detailed and computationally intensive, but have been found more accurate by the majority of case studies (e.g. [72, 73]). However, others, such as Shukla et al. [74], concluded that isotropic models provide a higher degree of accuracy.

Focusing on solar orientation modeling in an urban context, Freitas et al. [75] provided an overview of empirical and computational solar radiation models and concluded that numerical radiation algorithms connected with geographic information systems (GIS) tools represent the most appropriate trade-off between accuracy and computational time. The application of a GIS based approach

to evaluate solar potential including topographic impact was demonstrated by Bremer et al. [76] for a city in Austria, by Ko et al. [77] for Taiwan and by Verso et al. [78] for a city in Spain. However, Verso et al. [78] did not model shading, as only the best roofs were considered for PV installation. Vulkan et al. [79] developed an open source package in R to model shading effects on building surfaces in Israel and concluded that south oriented facades could contribute significantly to annual electricity generation. The handling of shading on rooftops has been identified to be one of the main distinction of different assessments of solar potential in Switzerland [80]. Assouline et al. [81] proposed an approach using machine learning to extrapolate missing data using a combination of support vector machines and GIS to access the annual potential of Switzerland. Their method to assess monthly mean values in a high spatial resolution is included in the Swiss national project to determine the solar potential and to provide guidelines to building owners [82]. Although these studies have the focus on different orientation of single roofs, the aspect of the connected energy system remains a minor focus.

2.2.4 Gaps and contributions

Based on the aforementioned literature review, there exists gap in the state-of-the-art at the intersection between a) studies focusing on BES, which only include a very simplified representation of the energy generated by PV panels, and b) studies focusing on the optimal placement of PV panels, which never include how this affects, and is affected by, the integration with other parts of the BES. This chapter therefore aims to investigate the following research questions:

What is the impact of the orientation of PV panels on renewable energy hubs and the grid?

- What is an optimal placement of PV panels (orientation and tilt) from the perspective of renewable energy hubs and of the grid? How does it depend on problem parameters such as the load profile and the characteristics of the building?
- What are the principles that should be adopted when choosing the placement of increasing quantities of PV panels on the roof of the building?
- What is the magnitude of the error induced by the assumption of only horizontally installed PV panels in renewable energy hubs at the building scale?
- How are different policies for subsidizing the installation of PV panels impacting the "optimal" orientation?

2.3 Method

The research questions of this chapter are addressed by integrating a more detailed modeling framework of the incoming solar irradiation and the orientation of the PV panels in renewable energy hubs at the building scale. The renewable energy hub is modelled according to mixed-integer linear programming (MILP) approach presented in Chapter 1.2. This method section is

2.3. Method

first addressing how incoming irradiation is modelled, then how the orientation of PV panels is considered, followed by the integration of inter-modular shading effects on flat roofs. The method section ends with the demonstration how the more detailed modeling of oriented PV panels is integrated in the framework of renewable energy hubs. In the following, parameter are expressed with normal font, variables in bold font. Additional required sets in this chapter are the set of considered roofs $r \in R$, azimuth angles $\alpha \in A$ and title angles $\gamma \in Y$. A pair of azimuth and title angles is used to describe the orientation of one skydome patch $pt \in S$ or defines the set of possible orientations O of PV modules.

2.3.1 Irradiation modeling

The modeling of the incident solar irradiation is achieved through the discretization of the skydome into 145 patches, each containing information about the irradiation density in a given time horizon [83]. This approach is based on the anisotropic irradiation model, developed by Perez et al. [84], which accounts for direct and anisotropic diffuse irradiation from clear to partly clouded skies. Figure 2.1 visualizes the cumulative sky approach for one typical year in Geneva, Switzerland. Equa-

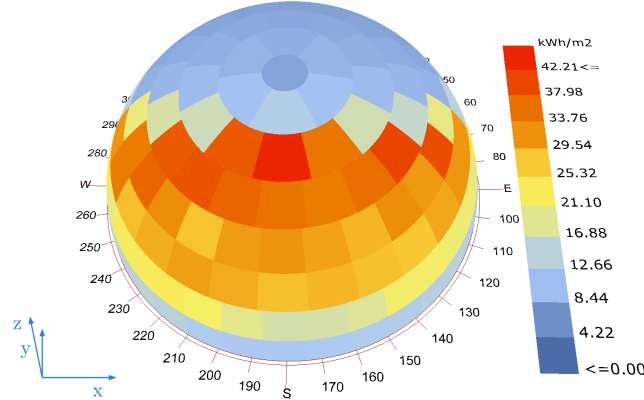


Figure 2.1 – Annual total irradiation, visualized for skydome of Geneva, Switzerland. Typical weather data from [48].

tion 2.1 expresses the irradiation coming from one patch irr_{pt} in the coordinates of the skydome x_{sd}, y_{sd}, z_{sd} , where α represents the azimuth angle of the sky-direction and ϵ is the elevation angle of one patch pt . Thereby, x_{sd} points to the east, y_{sd} to the north and z_{sd} to the zenith, and the azimuth angle increases clockwise starting from the north, where $\alpha = 0$. The elevation angle increases counterclockwise from $\epsilon = 0$ for patches with no elevation in the sky (compare with Fig. 2.1).

$$\vec{irr}_{pt} = irr_{pt} \cdot \begin{pmatrix} -\sin \alpha_{pt} \cdot \cos \epsilon_{pt} \\ -\cos \alpha_{pt} \cdot \cos \epsilon_{pt} \\ -\sin \epsilon_{pt} \end{pmatrix} \forall \{(\alpha_{pt}; \epsilon_{pt}) | pt \in S\} \quad (2.1)$$

2.3.2 Orientation of PV panel

If x_{pv}, y_{pv}, z_{pv} define the coordinate system of the PV panel, then z_{pv} is perpendicular to the panel and represents the direction where the irradiation is of relevance for the photoelectric effect, and x_{pv}, y_{pv} set up the plane of the PV module itself. Orienting the PV panel in the x_{sd}, y_{sd}, z_{sd} coordinate system of the skydome means to rotate the PV panel twice. The rotation axis of the azimuth orientation is always the z_{sd} axis of the skydome. In contrast, the tilt rotation is always around the x_{pv} of the panel. If the azimuth rotation is carried out first, the second rotation is around the new \tilde{x}_{pv} of the PV panel. If the tilt rotation is carried out first, the z_{sd} axis has to be expressed in dependence of the first rotation around x_{pv} . Whereas the azimuth rotation is clockwise (negative), tilt rotation is counterclockwise (positive). This leads to the rotation matrix Γ shown in Equation 2.2.

2

$$\Gamma_{\tilde{x}_{pv}} \cdot \Gamma_{z_{sd}} = \Gamma_{z_{sd}} \Gamma_{x_{pv}} = \begin{bmatrix} \cos \alpha_{pv} & -\sin \alpha_{pv} & 0 \\ \sin \alpha_{pv} \cdot \cos \gamma_{pv} & \cos \alpha_{pv} \cdot \cos \gamma_{pv} & -\sin \gamma_{pv} \\ \sin \alpha_{pv} \cdot \sin \gamma_{pv} & \cos \alpha_{pv} \cdot \sin \gamma_{pv} & \cos \gamma_{pv} \end{bmatrix}$$

$$\forall \alpha_{pv} \in A, \forall \gamma_{pv} \in Y \quad (2.2)$$

The combination of Equation 2.1 and the rotation matrix Γ leads to Expression 2.3 for the incident irradiation density irr along the negative z_{pv} axis of the PV module. Therefore, the pair $(\alpha_{pt}, \epsilon_{pt})$ uniquely defines the position of one patch pt within the skydome and $(\alpha_{pv}, \gamma_{pv})$ the orientation of the PV panel. Taking only positive values allows filtering out the contribution of irradiation coming from behind the panel. The irradiation thus calculated is integrated over the whole skydome.

$$irr_{pv}(\alpha_{pv}, \gamma_{pv}) = (-1) \cdot \sum_{pt=1}^S irr_{pt}(\alpha_{pv}, \gamma_{pv})$$

$$= \sum_{pt=1}^S irr_{pt} \cdot \max[(\sin \alpha_{pv} \cdot \sin \gamma_{pv} \cdot \sin \alpha_{pt} \cdot \cos \epsilon_{pt} + \cos \alpha_{pv} \cdot \sin \gamma_{pv} \cdot \cos \alpha_{pt} \cdot \cos \epsilon_{pt} + \cos \gamma_{pv} \cdot \sin \epsilon_{pt}), 0]$$

$$\forall \alpha_{pv} \in A, \forall \gamma_{pv} \in Y \quad (2.3)$$

Figure 2.2 shows the irradiation received by the PV modules, whereas Figure 2.1 shows a visualization of the irradiation coming from the skydome. For a flat, horizontal panel, the incoming irradiation is independent of the azimuth angle. For azimuth angles, where the sun is never positioned over the year, annual irradiation density is strictly increasing with lowering the tilt angle and maximal for tilt angle $\gamma_{pv} = 0$ (horizontal panels). The situation changes for PV orientation between east (azimuth: 90°) and west (azimuth: 270°). Starting from a vertical panel, decreasing the tilt leads to an increase in the irradiation density. The annual irradiation is maximized at a tilt angle of 35° for

2.3. Method

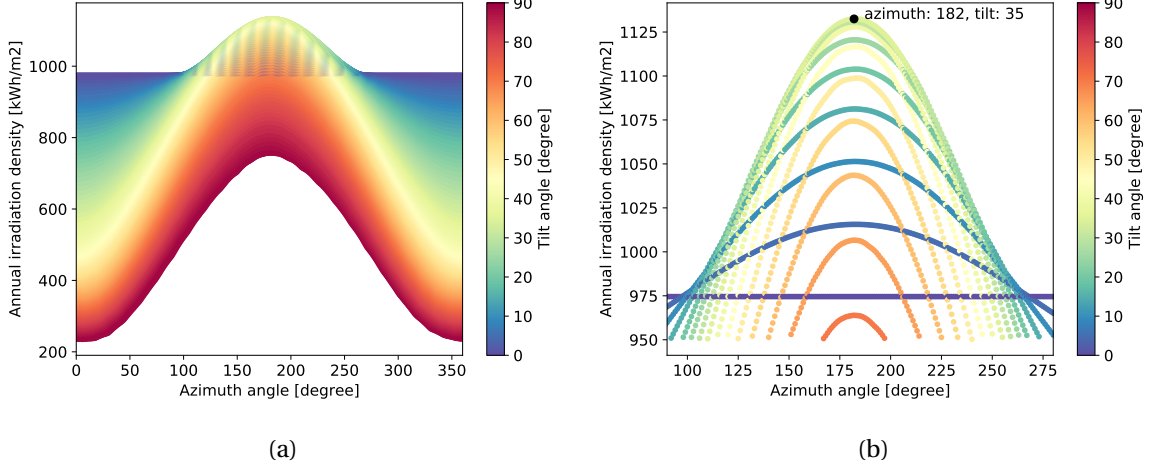


Figure 2.2 – a) Annual irradiation on oriented PV modules in the climate zone of Geneva. b) Annual irradiation on PV modules oriented between azimuth 80° – 280° and greater than 950 kWh/m^2 , visualization of tilt in 5° steps, azimuth in 1° steps.

2

azimuth 182° , which is around 10% larger than at horizontal irradiation. Between 35° – 0° tilt the irradiation is decreases again until horizontal irradiation.

2.3.3 Flat roofs and shading

On tilted roofs, the panel is considered to occupy only the size of the module itself. Unlike when using tilted roofs, the proposed approach takes into account the actual area A_{pv} occupied by the module on flat roofs. This is calculated as a function of the width of one module w_{pv} , the required minimum distance d^β between PV modules to prevent shading, and the relative tilt angle to the surface γ_{pv} . The distance between two rows of oriented modules is given by Equation 2.4. Thereby, h_{pv} is the module height and β is the design limiting angle that avoids shading. The design limiting angle corresponds to the lowest sun evaluation during solar noon that occurs within a year. Figure 2.3 illustrates this geometric correlation.

$$A_{pv}(\gamma_{pv}) = w_{pv} \cdot d = w_{pv} \cdot h_{pv} \cdot \frac{\sin(\gamma_{pv} + \beta)}{\sin(\beta)} \quad \forall \gamma_{pv} \in Y \quad (2.4)$$

The design limiting angle is not only used for placing the modules on the roof but also for simplification during the determination of incident irradiation. A common assumption is that there is no shading between modules if the placing of the modules respects the design limiting angle [85]. Simulations confirmed the hypothesis that the irradiation loss from direct irradiation is small, if the limiting angle is respected during placement. However, the diffuse component has a significant share on the losses and leads to a reduction for the tilt with maximum annual yield (e.g., -8° in

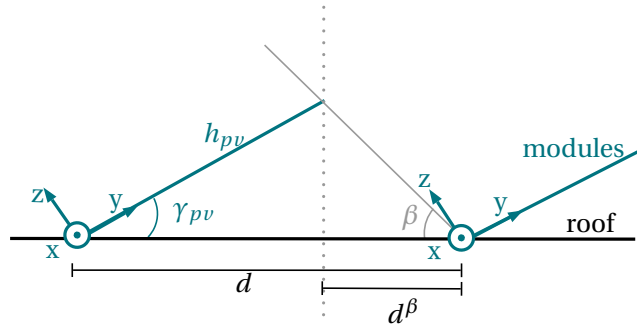


Figure 2.3 – Distance d between two modules (green) for a given module height h_{pv} , tilt angle γ_{pv} , and sun elevation/ liming angle β .

2

Geneva) [86].

This simplification is not needed when modeling the irradiation with the cumulative sky approach, as described in the previous section. The total irradiation from the partly shaded skydome is reduced by the patches that are not visible from the perspective of the PV module, i.e. that are below the limiting angle. The relative limiting angle is different for each skypatch, since the relative azimuth direction between patch and panel ($\alpha_{pt} - \alpha_{pv}$) varies and therewith the relative distance between the rows $d^{\beta,\alpha}$. Figure 2.4 visualizes this geometric relation and Equation 2.5 expresses the relative distance between the modules along the relative orientation of the patch.

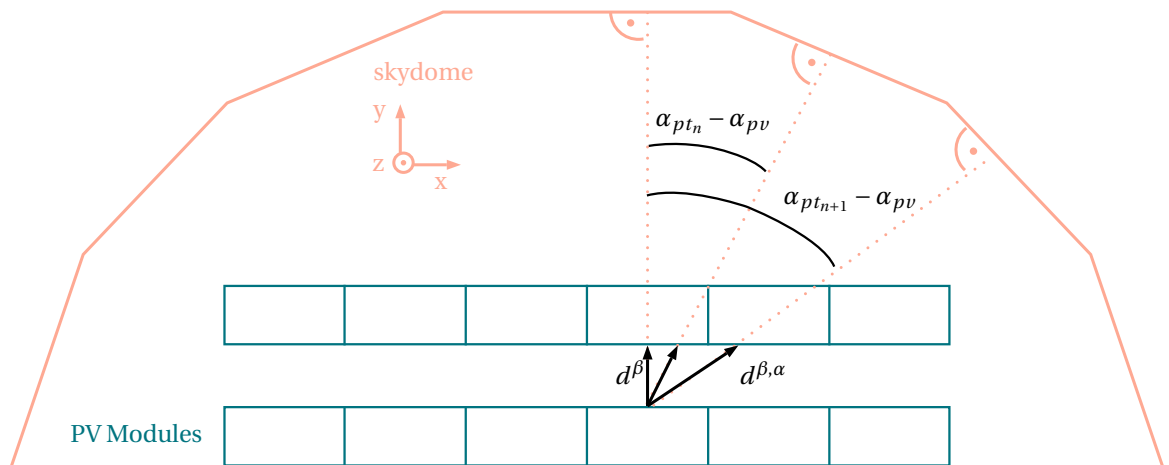


Figure 2.4 – Distance d between the modules for determining the inter-modular shading depending on the relative azimuth orientation $\alpha_{pt} - \alpha_{pv}$.

$$d^{\beta,\alpha} = \frac{d^\beta}{\cos(\alpha_{pt} - \alpha_{pv})} \stackrel{(2.4)}{=} \frac{\sin(\gamma_{pv}) \cdot h_{pv}}{\cos(\alpha_{pt} - \alpha_{pv}) \cdot \tan(\beta)} \\ \forall \beta \neq 0, \quad \forall \{pt \in S | \alpha_{pt} - \alpha_{pv} \neq \pm 90^\circ\} \quad (2.5)$$

2.3. Method

Distance $d^{\beta,\alpha}$ yields to the limiting angle β^α along the relative azimuth direction (Equation 2.6). The limiting angle β^α is greatest and equal to the design limiting angle β for the patch straight in front of the panel ($\alpha_{pt} = \alpha_{pv}$) and then decreases towards the boundaries of the light capture zone.

$$\tan(\beta^\alpha) = \frac{\sin(\gamma_{pv}) \cdot h_{pv}}{d^{\beta,\alpha}} = \cos(\alpha_{pt} - \alpha_{pv}) \cdot \tan(\beta)$$

$$\forall \alpha_{pv} \in A, \forall \gamma_{pv} \in Y, \quad \forall \{\alpha_{pt} | pt \in S\} \quad (2.6)$$

To determine the shaded irradiation, the irradiation from the one patch is piecewise linearized over the evaluation angle of the patch, which varies 12° , with ϵ_{pt} marking the central point (Equation 2.7). The shading factor of one patch $s_{pt} \in [0; 1]$ is equal to zero for completely shaded patches and 1 for completely unshaded patches.

$$s_{pt}(\beta) = \begin{cases} 0 & \epsilon_{pt} \leq \beta^\alpha - 6 \\ \frac{\epsilon_{pt} + 6 - \beta^\alpha}{12} & \beta^\alpha - 6 < \epsilon_{pt} < \beta^\alpha + 6 \\ 1 & \epsilon_{pt} \geq \beta^\alpha + 6 \end{cases} \quad \forall \{(\alpha_{pt}, \epsilon_{pt}) | pt \in S\} \quad (2.7)$$

Equation 2.8 gives the partly shaded irradiation in dependence of the chosen design limiting angle β .

$$irr_{pv}(\alpha_{pv}, \gamma_{pv}, \beta) = (-1) \cdot \sum_{pt=1}^S s_{pt}(\beta) \cdot irr_{pt}(\alpha_{pv}, \gamma_{pv})$$

$$\forall \alpha_{pv} \in A, \forall \gamma_{pv} \in Y \quad (2.8)$$

Figure 2.5 presents a visualization of the relative irradiation loss for different design limiting angles. Thereby, the unobscured skydome and the panel in the same orientation give the reference irradiation.

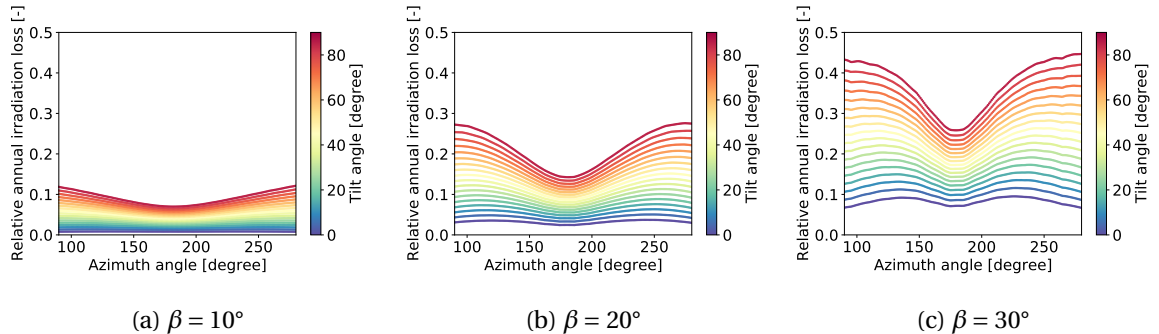


Figure 2.5 – Irradiation loss of PV panel shading for different design limiting angles β .

The design limiting angle has a significant impact on the received irradiation on the panel. Low

angles lead to much lower losses (max around 10% for $\beta = 10^\circ$) than do high angles (max around 45% for $\beta = 30^\circ$) but also require more surface area of the roof. The losses are less for south oriented panels, since the direct irradiation of the sun from this direction comes from higher elevation angles.

The proposed approach to model the irradiation losses includes both direct and anisotropic diffuse irradiation, with two simplifications: 1) all rows are considered to be partly shaded, even the front row, and 2) below β^α , the whole panel is receives no irradiation, although this is only true for the foot of the panel. The latter simplification implies irradiation losses even for very low tilt angles. As studies show that the electricity generated drastically drops off for partly shaded panels [86], this is considered a reasonable assumption.

2

2.3.4 Model integration PV Panel

The unit model of the PV panel is stated in Equations 2.9 to 2.13. The sizing value f_{pv} is integrated in the sizing equations (Equations 1.1) of each renewable energy hub at the building scale $b \in B$.

$$f_{b,pv} = \eta_{pv}^{ref} \cdot h_{pv} \cdot w_{pv} \cdot \sum_{r \in Ro} \sum_{o \in O} n_{b,pv,r,o} \quad \forall b \in B \quad (2.9)$$

$$A_{b,r} >= \sum_{o \in O} A_{pv}(\gamma_{pv}) \cdot n_{b,pv,r,o} \quad \forall b \in B \quad \forall r \in R \quad (2.10)$$

$$\dot{E}_{b,pv,p,t}^+ = h_{pv} \cdot w_{pv} \cdot \sum_{r \in Ro} \sum_{o \in O} n_{b,pv,r,o} \cdot \eta_{pv,o,p,t} \cdot irr_{pv,o,p,t} \quad (2.11)$$

$$\forall \{o = (\alpha_{pv}, \gamma_{pv}) \in O | \alpha_{pv} \in A, \forall \gamma_{pv} \in Y\}, \forall p \in P, \forall t \in T$$

The sizing value f_{pv} represents the total size of PV panels in kWp given by the total number of installed modules n_{pv} , the height h_{pv} and the width w_{pv} of one PV modules, and the reference efficiency in standard conditions η_{pv}^{ref} (Equation 2.9). The installation of panels is limited by the available roof area A_r , whereas A_{pv} is the space the modules occupy on the roof (Equation 2.10). A_{pv} is the same than the product $h_{pv} \cdot w_{pv}$ only for installation on facades, oriented roofs or horizontal panels. On flat roofs, inter-modular shading is considered, thus different rows of modules occupy a greater surface ($A_{pv} > h_{pv} \cdot w_{pv}$). The generated electricity (\dot{E}_{pv}^+) results from the sum over the electricity from each panel on every roof r and of each orientation o (Equation 2.11). The generated electricity is included in the energy balance of each building energy system (Equation 1.2a).

$$\eta_{pv,o,p,t} = \eta^{inv} \cdot [\eta_{pv}^{ref} - \delta_{pv} \cdot (T_{pv,o,p,t} - T_{pv}^{ref})] \quad (2.12)$$

$$T_{pv,o,p,t} = \frac{U_{pv} \cdot T_{p,t}^{ext}}{U_{pv} - \delta_{pv} \cdot irr_{pv,o,p,t}} + \frac{irr_{pv,o,p,t} \cdot (\nu_{pv} - \eta^{ref,pv} - \delta_{pv} \cdot T^{ref,pv})}{U_{pv} - \delta_{pv} \cdot irr_{pv,o,p,t}} \quad (2.13)$$

$$\forall \{\alpha_{pv} \in A, \forall \gamma_{pv} \in Y | (\alpha_{pv}, \gamma_{pv}) \in O\}, \forall b \in B, \forall p \in P, \forall t \in T$$

2.3. Method

Equations 2.12 and 2.13 describe the efficiency of the PV panel $\eta_{pv,c,p,t}$ as a function of the temperature of the panel. The PV module temperature is depending on the external temperature T^{ext} and the oriented irradiation density on the panel $irr_{pv,o}$ [22, 61]. The module heat transfer coefficient U , the absorption coefficient v , and the temperature coefficient δ_{var} are parameters specific to each PV panel. The performance in standard test conditions is given by the reference efficiency η^{ref} and the reference temperature T^{ref} equal to 298 K.

2.3.5 Case study

The proposed method is applied to a case study area in Switzerland. The case study area is the same than described in Chapter 1.2.6. The whole case study area consists of 40 buildings of different types. In the first part of the case study, the solar integration of one typical renewable energy hub is presented. The typical residential building has a heated area of 250 m^2 and a large available roof area consisting of four tilted and one flat surfaces (see Table 2.1).

Table 2.1 – Building parameters for a typical single-family house with large available roof surface.

Description	Value	Unit	Ref.
Energy reference area (ERA)	250	m^2	[44]
Domestic hot water demand	292	$1/\text{m}^2 \text{ yr}$	[31]
Solar Gains	18	$\text{kWh}/\text{m}^2 \text{ yr}$	[31]
Heat Gains	24	$\text{kWh}/\text{m}^2 \text{ yr}$	[31]
Design supply/return temperature	65/50	$^\circ\text{C}$	[23]
Heat transfer coefficient	2.09	$\text{W}/\text{m}^2 \text{ K}$	[23]
Heat capacity coefficient	120	$\text{Wh}/\text{m}^2 \text{ K}$	[31]
Annual Electricity demand	39.5	$\text{kWh}/\text{m}^2 \text{ yr}$	[87]
Surface	Azimuth	Tilt	Area
North-west roof	352°	48°	29.5 m^2
South roof	172°	27°	29.5 m^2
East roof	82°	47°	78.6 m^2
West roof	262°	47°	89.7 m^2
Flat roof	(-)	0°	41.8 m^2

For determination of the oriented shading losses between PV modules, the design limiting angle β is set to 20° , which represents the lowest sun evaluation during solar noon for Geneva in Switzerland, occurring on the 21st of December [88]. This was chosen as an acceptable trade-off between space requirements and shading losses. Shading losses are below 10% for tilt angles between the horizontal position and those leading to maximum electricity generation (see Figure 2.5b).

Typical input data is clustered according to Section 1.2.6. However, instead of electrical demand profiles from national norms, the uncontrollable load is derived from measurements, which are dis-aggregated at building level by Holweger et al.[87]. As these measurements show differences

from weekdays to weekends, this aspect is respected in the clustering algorithm.

2.4 Results and discussion

The result section aims at answering the main research question of this chapter *What is the impact of the orientation of PV panels on renewable energy hubs and the grid?* Thereby, different analyses are made, which are structured as follows. At first, the solar integration of individual renewable energy hubs is considered. Special focus is thereby given to the optimal orientation of the PV panels and the connected self-consumption (SC). Afterwards, the proposed approach of this chapter is compared to the state of the art in BES optimization, which assumes horizontal panels. The final part of the result section discusses the impact of PV panel orientation on the electricity grid.

2

2.4.1 PV panel integration in renewable energy hubs at the building scale

The optimal PV panel integration in renewable energy hubs is explored by applying a MOO framework. The results of the MOO for the reference building (Table 2.1) are shown in Figures 2.6 and 2.7. The capital expenses (CAPEX) and operational expenses (OPEX) for each non-dominated solution on the Pareto front are shown in Figure 2.6a and are divided by the ERA of the building to ease comparison. The CAPEX ranged from a minimum of 2.8 CHF/m²yr (Scenario 1) to 48 CHF/m²yr (Scenario 14), whereas the OPEX ranged from 1.9 to 24 CHF/m²yr. The scenario numbers (1–14) were defined as the points on the Pareto curve, ordered from the lowest to the highest CAPEX.

Although all scenarios were optimal from a Pareto perspective when looking at CAPEX and OPEX separately, the analysis of total expenses (TOTEX) told a different story. As shown in Figure 2.6d, the resulting TOTEX were similar in Scenarios 1 through 9 at around 27 CHF/m²yr (minimum TOTEX for Scenario 4–6 at 25 CHF/m²yr), whereas they increased rapidly in Scenarios 10–14, reaching a maximum of approximately 50 CHF/m²y. The increase in TOTEX in Scenarios 9–14 was due to the fast increase in CAPEX in these scenarios, mostly due to the decision to install batteries (first appearing in Scenario 10), which was not compensated by a commensurate reduction in OPEX. The reason for this trend can be seen in Figure 2.6c: in Scenarios 3 to 8, the OPEX were reduced by installing PV panels, hence reducing the electricity demand from the grid, while gradually increasing the electricity feed-in. As the PV capacity saturated, OPEX could be further reduced by increasing the SC, because of the price difference between buying electricity from the grid and selling it to the grid. This could be achieved by installing batteries, which allowed for a better match between demand and supply. From Scenario 9 to 14, both the electricity demand from the grid and feed-in decreased, meaning that the total amount of energy generated locally remained approximately constant, but it was used for fulfilling the demand rather than sold to the grid.

This can be also observed from the evolution of self-sufficiency (SS) and SC in Figure 2.6b. The SS gradually increased when the PV panels were installed, and continued increasing even as the PV

2.4. Results and discussion

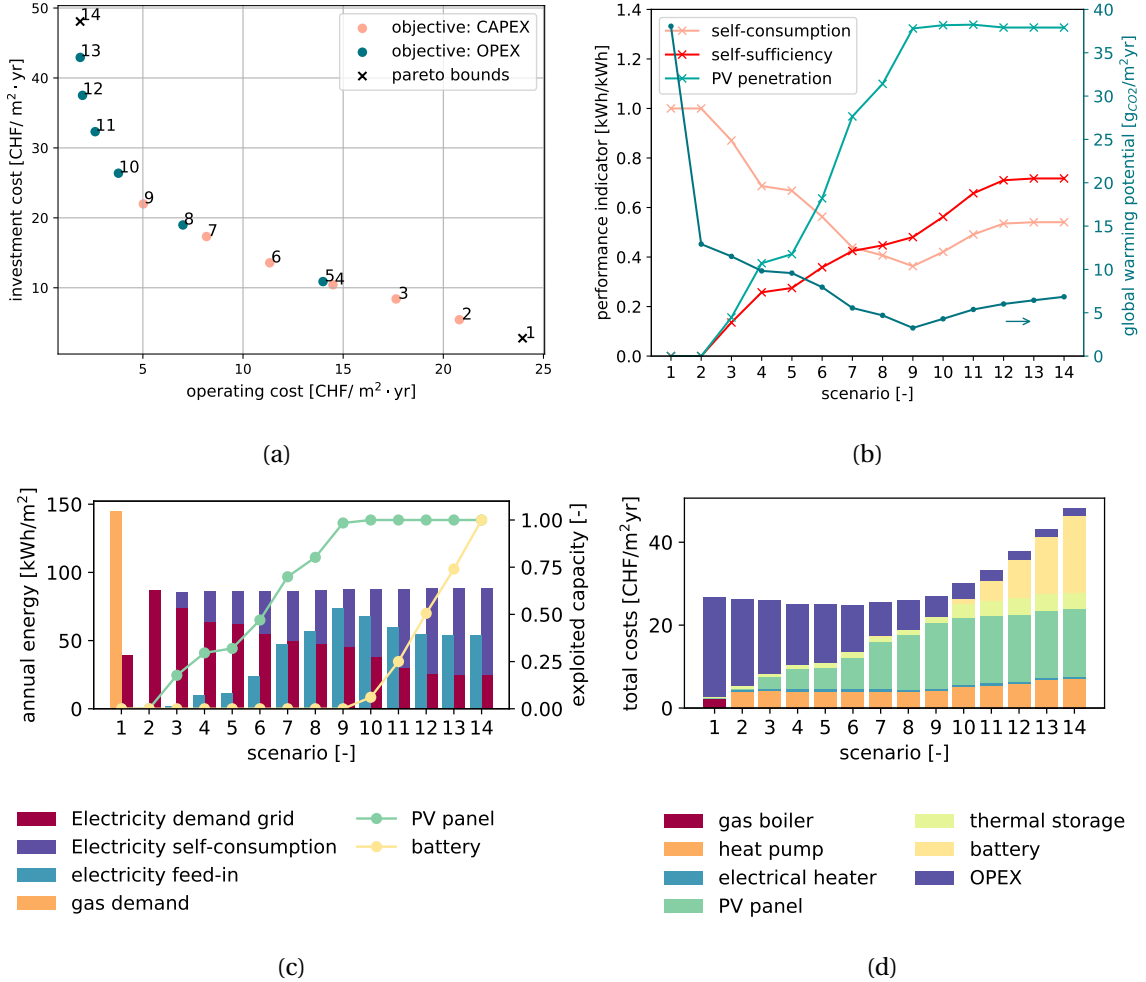


Figure 2.6 – Optimal integration of PV panels in renewable energy hubs. Results of MOO of one residential building: (a) definition of Scenarios on Pareto frontier for investment and operation costs, (b) performance indicator for each scenario, (c) usage of resources, and (d) distribution of total annual cost in identified energy system configurations.

penetration flattened, because of the use of batteries. On the other hand, the SC first decreased with increasing PV penetration (until Scenario 9), and then began increasing again as a result of the use of batteries.

Figure 2.6b also shows the performance of the Pareto-optimal solutions in terms of global warming potential (GWP). The main contribution to reduce the environmental impact of the system came from the use of heat pumps instead of gas boilers for heating, which reduced the GWP from approximately 37 to 13 gCO_{2,eq}/m²yr. The addition of PV panels provided a significant contribution to reducing CO₂ emissions, which reached a minimum of 3.2 gCO_{2,eq}/m²yr in Scenario 9. From then onward, the use of batteries had the opposite effect, because of the losses in the charge/discharge cycle and of the large GHG emissions connected to the battery production process.

Concerning other technologies installed, thermal energy storage was used in most scenarios. A relatively small thermal storage was installed in Scenarios 2–9; whereas in Scenarios 10–14 larger systems were installed, following the same principle as for the batteries.

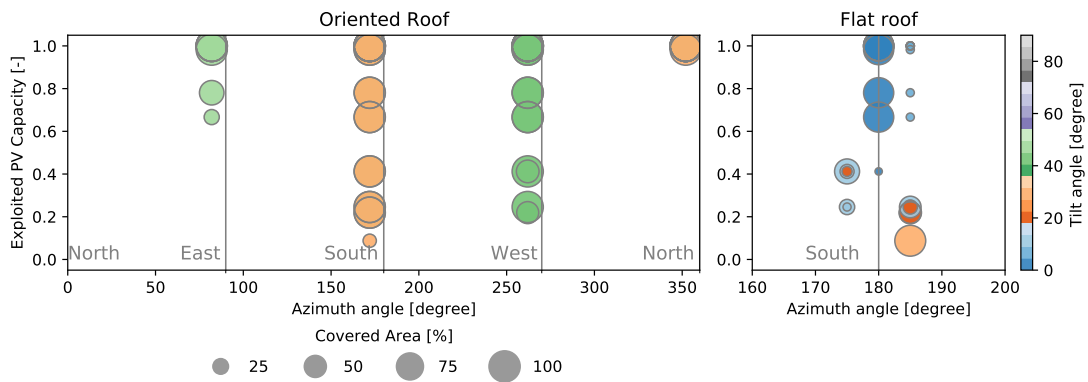


Figure 2.7 – Optimal distribution of PV installation for different roofs.

Additional information related to the installation of PV panels is provided in Figure 2.7. These results start providing insights related to the main topic of this chapter. For low installed PV capacity, panels were equipped on the flat and on the south-oriented roof. On the flat roof, the panels were positioned with a south orientation and with a 30°tilt, according to common practice. However, at even a small increase in the total installed PV capacity, the west-oriented roof was used over the east-oriented roof, and the azimuth and tilt of the panels installed on the flat roof changes. This was likely because west-oriented panels provided a better match between supply and demand than did east-oriented panels. Finally, in Scenario 14, the east facing and the north facing roofs were also covered with PV panels, whereas the panels placed on the flat roof were installed with 0°tilt angle to minimize shading effects between panels, hence allowed for the installation of more PV modules on the same roof area.

2.4.2 Optimal orientation and the role of self-consumption

One additional objective of this study was to determine the effect of the interaction between the hourly variation of the thermal and electrical demand, the energy system, and the choice of the surface where the solar panels are installed. The results shown in Figure 2.7 serve as an excellent starting point for this discussion. Although the south-facing rooftops were selected first, west-facing surfaces were chosen over east-facing surfaces. This was further explored in the case of a building with no tilted roofs: in this case, the optimizer had full freedom of choice in terms of orientation and tilt, rather than being forced to choose among a limited set of options, and can therefore provide more insight.

2.4. Results and discussion

These results are presented in Figure 2.8. Figure 2.8a refers to the reference pricing case of 0.24 CHF/kWh for electricity purchased from the grid and a feed-in tariffs of 0.08 CHF/kWh, whereas Figure 2.8b refers to the same case but with a 0 CHF/kWh feed-in price. As expected, given its highest yearly energy generation, south-oriented panels were preferred; however, at feed-in tariffs of 0 CHF/kWh, the panels were slightly oriented towards the west and had a higher tilt, especially in the cases with a lower total installed PV capacity.

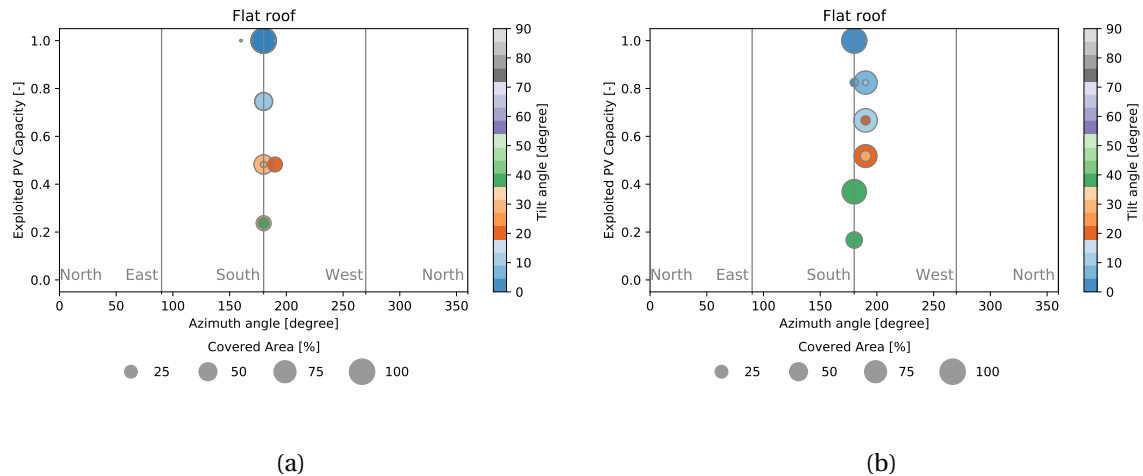


Figure 2.8 – Optimal PV orientation for different installed capacities on a flat roof: (a) cost optimal placement for an electricity price of 0.24 CHF/kWh and feed-in tariffs of 0.08 CHF/kWh, and (b) optimal placement for self consumption for an electricity price of 0.24 CHF/kWh and feed-in tariffs of 0 CHF/kWh.

In most residential buildings, the main energy demand is in the evening, when people are at home, and during the heating season in winter, when the sun is lower in the sky, thus explaining this orientation shift. However, this effect was minor, since the developed model included optimal scheduling. This leads to the conclusion that, although this effect did not seem to have a substantial influence on the overall performance, the common practice of installing PV panels with the azimuth and tilt that maximizes energy generation may not be the best choice, especially when the objective is to maximize self-consumption. This trend is only seen for scenarios where only parts of the roofs were covered with PV panels: when the whole roof is covered, the optimizer prioritized the maximization of the yearly generation, thus favoring azimuth and tilt angles that minimize shading among panels.

2.4.3 Comparison with flat roof assumption

This chapter aims to provide also an estimation of the error generated by assuming horizontal panels on the entire roof surface when attempting to estimate the PV potential from distributed generation. Although this assumption allows a simpler analysis and can rely on more limited set of information,

it also introduces error.

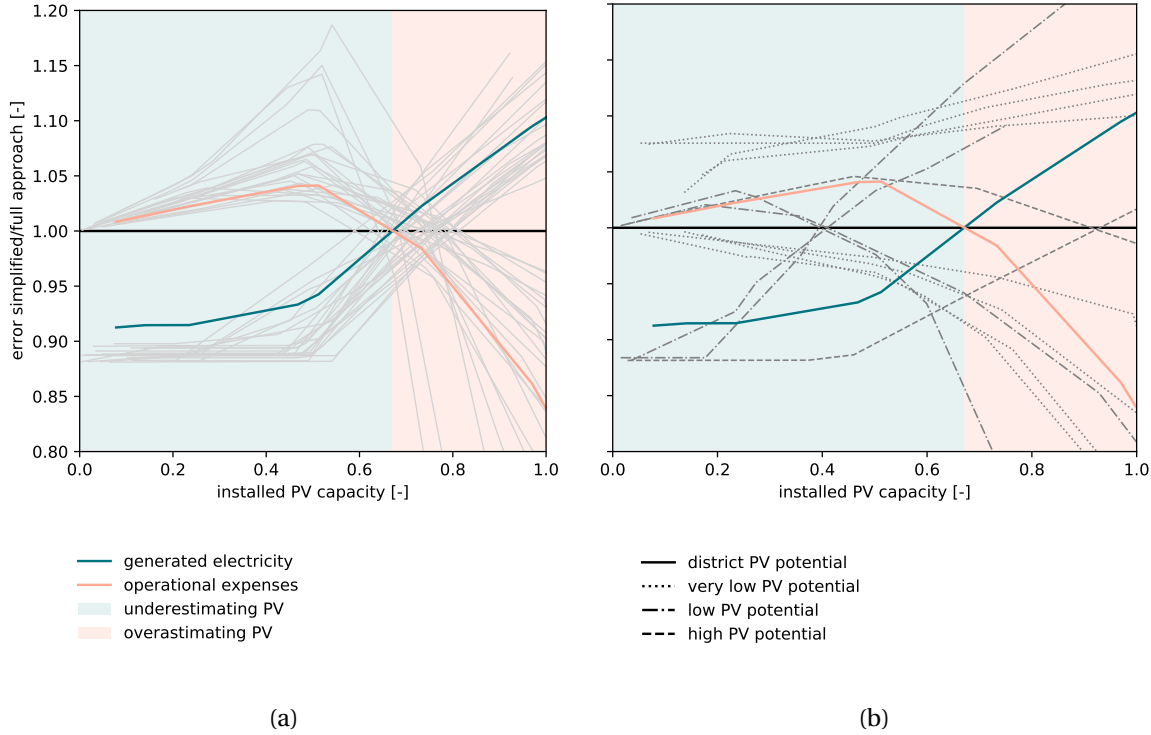


Figure 2.9 – Error caused by assuming horizontal PV panels to optimal PV orientation for a district (coloured lines) of 40 buildings (grey lines). Installed capacity = 100% when all available roofs are covered.; Buildings with (a) average behavior (b) outlier behavior.

The extent of the deviation between the "simplified" and "detailed" approaches for the 40 buildings with individual roofs and load profiles is shown in Figure 2.9a. The PV capacity being 100% was considered for the case that all available roof surfaces were occupied with PV modules. For low exploited PV capacity, the general trend was that the best surfaces were used, and, whenever possible, the tilt angle was selected to maximize the yearly energy generation. As a result, the simplified assumption of panels installed with zero azimuth and tilt caused an underestimation of the generated electricity, and a consequent overestimation of the overall operational expenses. As "worse" roofs were used, the error was reduced, until the error sign reverses; for high levels of PV penetration, as west-, east- and north-oriented roofs were exploited, the simplified flat panel assumption instead became an overestimation of the total capacity. While the error largely depended on the individual case, it generally ranged between -12% and +20% for the generated electricity, and -20% and +20% for the operational expenses.

Unlike the estimation of generated electricity, the error seen in the estimated operating expenses did not increase monotonically, but peaked at approximately 50% PV capacity. This can be explained by the difference in feed-in and electricity prices. The error in the estimation of the operational

2.4. Results and discussion

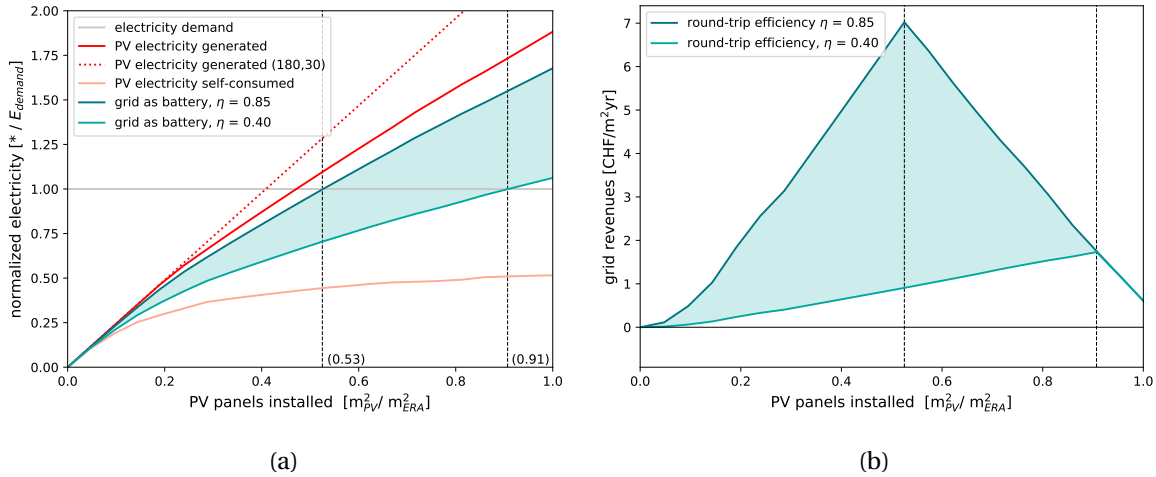
expenses was low in systems with low PV capacity. Here, SC was highest and could be maximized with the optimal scheduling of electrical loads. At some point, these scheduling measures were fully exploited in case of the simplified approach, all additional generated electricity was completely fed into the grid. In contrast, in the full approach "worse" roofs were used, which generated less electricity but led to a better match of demand and supply profiles. Hence, it led to further increase of SC, causing the peak of overestimating costs at 50% PV capacity. After this point, the limit of SC in the full approach was reached and the overproduction of electricity in the simplified approach was so high, that the revenues from the feed-in tariffs decreased the electricity bill drastically.

Whereas Figure 2.9a shows the behavior of "average" renewable energy hubs at the building scale, Figure 2.9b shows some outliers, i.e. renewable energy hubs that behaved remarkably differently from the rest. In the case of renewable energy hubs with very high PV potential, the simplified approach tended to always underestimate the potential. Renewable energy hubs with large, completely flat roofs are an example of this case: here, in almost all scenarios, the optimal placement involved using panels with a 30° tilt, which generated more energy than the flat case. On the other hand, when the PV potential of the renewable energy hub was very low, the electricity generated in the simplified approach was always overestimated; this can be the case of a house with a pitched roof facing east and west, where all available surfaces have a lower potential compared to a flat roof and, hence, the simplified approach tends to always overestimate the potential.

2.4.4 Impact on the grid

The main rationale for not following the common practice of installing PV panels with azimuth and tilt that maximize yearly energy generation is related to the benefits that this gives towards maximizing SC. A renewable energy hub is connected to the grid, maximizing SC helps to balance loads on the grid and thus avoids excessive swings in the use of centralized power generation units. This aspect can become crucial once renewable energy sources (especially uncontrollable ones, such as wind and solar power) take up a significant share of the national energy mix. Figure 2.10 allows getting a better understanding of this point, and of how it is connected to the matter of PV panels installation on top of roofs. Here, as demonstrated from the deviation between the energy generated by the optimal system (solid red line) installed on a real roof and the energy generated by a hypothetical system with all panels oriented south with a 30°angle (dashed red line), the error, that was generated by not considering the orientation of the PV panels, is apparent. With a ratio of surface area of installed PV panels to the heated surface of just under 50%, the yearly demand of the building could be satisfied locally.

However, this perspective considered the grid as a perfect energy storage system. As shown by the actual value of the PV electricity that was self-consumed, most of the generated electricity was sold to the grid, and then was purchased back when needed. The share of the demand that was satisfied



2

Figure 2.10 – a) The need of PV panels of one renewable energy hub at the building scale in Switzerland to reach self-sufficiency with re-imports. b) Revenues as a function of installed PV capacity and grid efficiency from the perspective of the grid. The grid buys electricity at a feed-in tariffs of 0.08 CHF/kWh and resells for electricity price 0.24 CHF/kWh.

with the energy generated from the PV panels increased with the PV surface installed; however, this share saturated at around 50% of the demand (Figure 2.10a).

From the point of view of each individual renewable energy hub, the grid can be seen as a battery that is able to absorb excess energy from distributed generation and sell it back when the demand exceeds the generation. There are several ways for the grid to fulfill this role: pumped hydroelectric storage is the most commonly used [89, 90], whereas the use of large battery systems is still limited to few cases, and other technologies (such as compressed air storage or hydrogen) are yet to reach market maturity. Based on this an estimation of the PV system size required for a reference residence to achieve a net zero balance between energy locally generated and consumed for different values of the average efficiency of the storage is shown in Figure 2.10a. This assumption had a dramatic influence on the surface required for energy balance: for a round-trip efficiency $\eta = 0.85$ (which would be the case of lithium-ion batteries), the overall surface required would only slightly increase from the $\eta = 1$ assumption. In that case, a equivalent of around half the ERA of PV panel installation was needed to be self-sufficient. If, however, a much lower round-trip efficiency was assumed ($\eta = 0.40$, which would be in the range of what can be expected when using hydrogen for energy storage), the surface of PV panels installed to reach self-sufficiency was almost doubled (0.91). This shows that large surfaces are needed in order to be self-sufficient of PV electricity alone. This study was based on a single family home, with huge available roof surfaces. It is unrealistic that buildings have available roof surfaces as large as their ERA at their disposal, especially in high-rise urban typologies.

The effects of the efficiency of the grid as storage for the grid operators can be observed in Figure

2.4. Results and discussion

2.10b based on the assumption of 24/8 ct/kWh for electricity purchased from/sold to the grid. When the round-trip efficiency η was high, most of the energy purchased from the renewable energy hubs was able to be sold back, and hence the profit was large. With a lower round-trip efficiency η , the profits decreased dramatically from the perspective of the grid. The grid revenue peaked at the point of SS of the renewable energy hub. At this point the share of generated electricity, which was sold to the grid but bought back at a later time was largest.

The common interest in efficient grid infrastructure is revealed by Figure 2.10 . From the perspective of the grid operator, profits could be higher as less energy was lost in the charge–discharge cycle, and these profits could then be used to reinvest into upgrading the grid itself, generating a positive, cyclic effect. From the perspective of the renewable energy hub, self-sufficiency could be achieved with a lower surface of PV panels installed (and, hence, with lower investment costs) and the supply was more secure, since there was 75% less traffic in the network (PV electricity generated = 1.75, with $\eta = 0.40$ at the point $0.91 m_{PV}^2 / m_{ERA}^2$).

2

The investigation of a different way to deal with the limitations of the grid is shown in Figure 2.11. One solution would be to increase the level of self-consumption. The effect of taking into account the effect of the grid-balance constraint on the installation decision of PV panels and on the preferred azimuth and tilt is shown in Figures 2.11a and 2.11b. Here, two alternative means are implemented in order to minimize the perturbations resulting from the exchange of renewable energy hubs with the superior network: limiting the amplitude of power variations compared with an average value (GM, Equation 1.30), or reducing ratio ϵ_{el} between the feed-in tariffs and electricity cost. Only one solution of the Pareto front is included here, i.e., that which minimizes the TOTEX.

The results of the first strategy are shown in Figure 2.11a. When no limitation was applied (left plot), almost all PV panels were installed facing south: with no limitation to the power exchanged with the grid, the optimizer selected the configuration that maximized energy generation. When a limited restriction was applied (GM = 3, center plot), there was a clear shift towards the west; even though the variation only referred to less than half of the installed PV capacity and for only 10°rotation,a clear trend was visible. This was confirmed when a stricter limitation on grid exchanges was imposed (GM = 1.5, right plot), where less than half of the panels were installed towards south and the average rotation towards the west was even higher. However, this had a relatively small effect on the SC, which only increased from 0.52 to 0.54.

The results of changing the relative price between energy purchased from and sold to the grid was shown in Figure 2.11b. The effect on the azimuth was less evident, but still present. However, a more distinct effect on the tilt angle was seen, which tended to increase (from 30°to 40°). Also, it appeared that the effect on the SC was higher in this case (it increased from 0.52 to 0.59), which might was related to the fact that for electrified heating systems, the electricity demand is highest during winter, where the sun is lower in the sky. Hence, by increasing the tilt angle, SC could be increased.

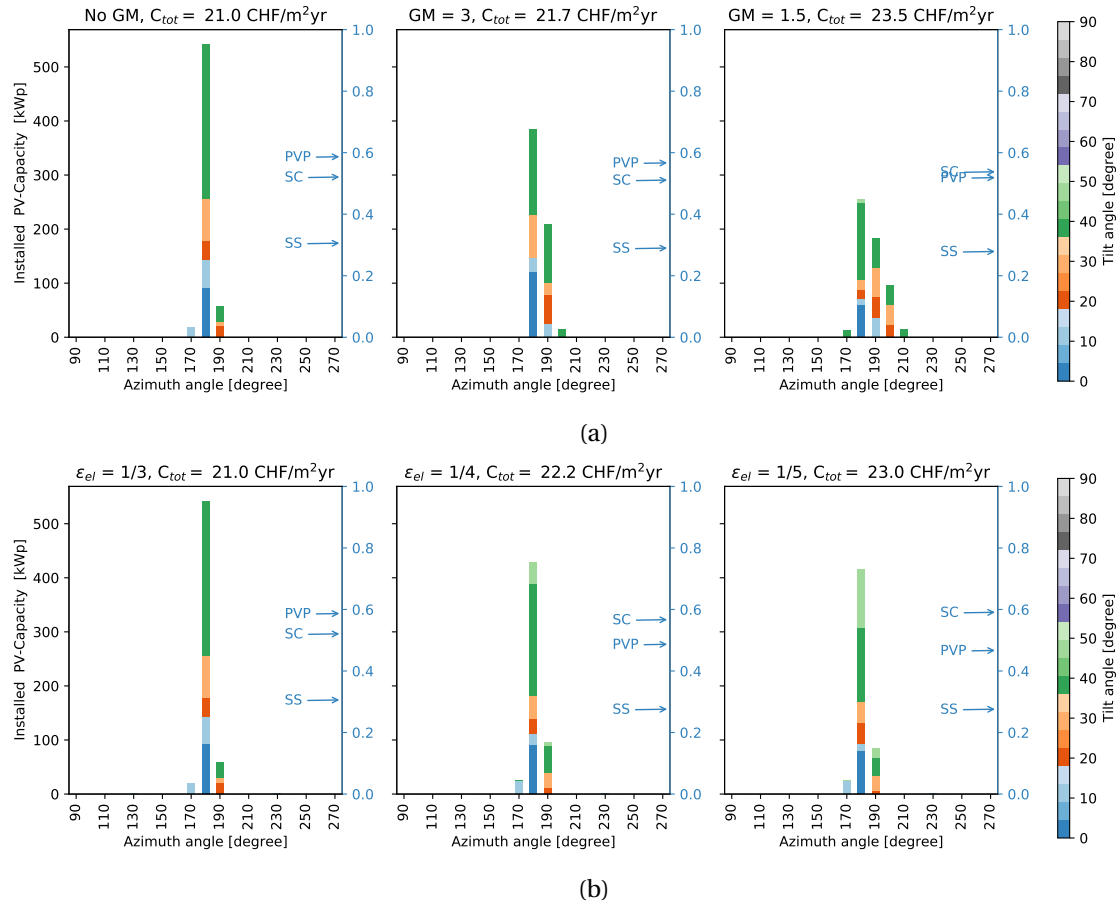


Figure 2.11 – Distribution of PV installation and orientation for total cost optimization of 40 buildings with individual load profiles. Assumption of flat roof with unconstrained orientation possibilities. a) Three different grid constraints. b) Three different electricity price shares ϵ_{el} = feed-in tariff/electricity price.

The analysis of a district with 40 buildings with individual roof orientation and demand profiles demonstrated that the best economic performance was achieved with around 40% rooftop occupancy, as shown in Figure 2.12. Even though the optimal orientation was impacted by the orientation of available surfaces, the previous trend of different policies can be confirmed in Figure 2.12a as well as in Figure 2.12b. Imposing a constraint on the maximum peak, resulted in a shift westwards, whereas changing the relation between electricity supply and feed in tariff has an impacted on the optimal tilt angle.

2.5. Conclusion

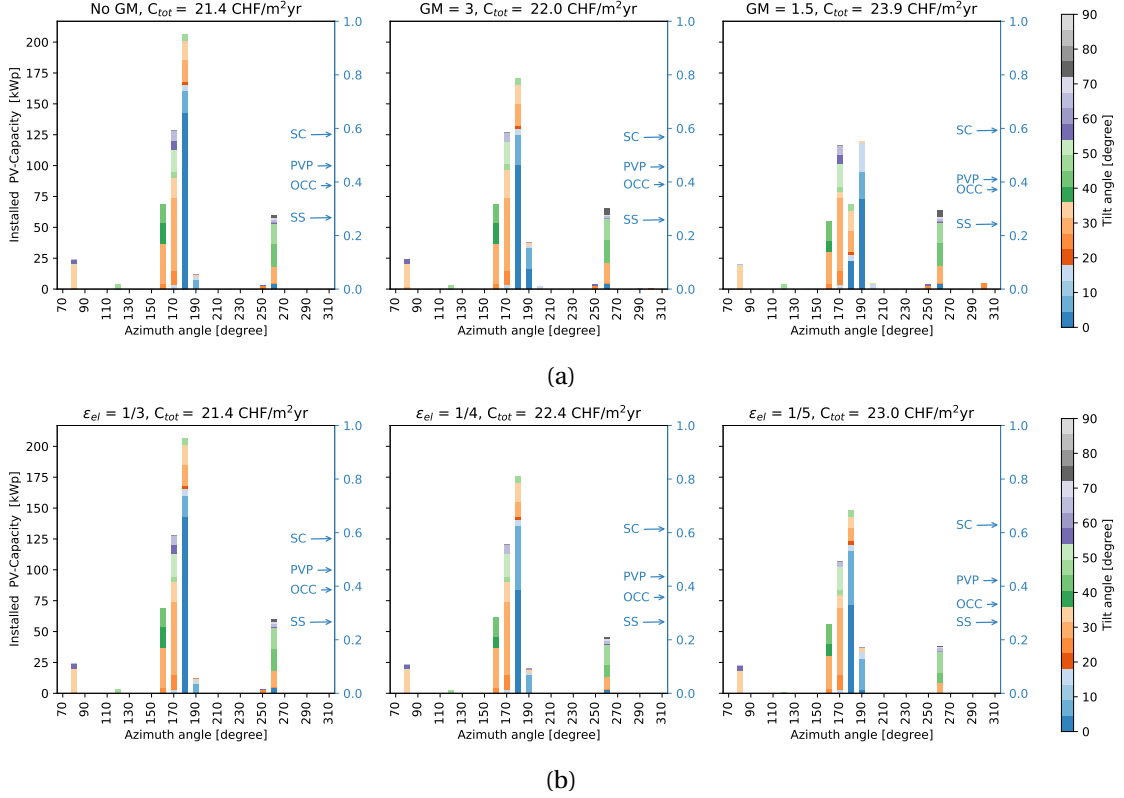


Figure 2.12 – Distribution of PV installation and orientation for total cost optimization of 40 buildings with individual load profiles and real roof orientations. Occupancy (OCC) of total available surfaces. a) Three different grid constraints. b) Three different electricity price shares ϵ_{el} = feed-in tariff/electricity price.

2.5 Conclusion

In this chapter, the influence of the orientation of PV panels on the design and performance of renewable energy hubs at the building scale was analyzed. Existing literature in the field of BES optimization has mainly considered horizontal PV modules and has based the decision of purchasing them on global irradiation without shadowing effects. This chapter therefore has aimed to estimate the influence of using different orientations, both from the perspective of the individual renewable energy hub and of the grid, and provide a methodology for selecting which roofs should be covered first. The results confirmed the validity of the common assumption of the favorability of south-oriented modules with an approximate tilt of 30°. However, this did not hold true when resources were available for more modules or when the focus shifted to a collection of buildings. To optimize (SC), the optimal orientation was further west and with higher tilt than the standard solution. To maximize the PV capacity on the roof, the use of horizontal panels maximized the usable roof area.

The most interesting results, however, were related to the interaction with the grid. For higher levels

of PV penetration, the role of the grid became crucial. Grid operators have the power to influence the quantity as well as the quality of grid exchange by acting in different directions:

Grid efficiency High grid efficiency was a common interest for both the building owner and the grid operator. With an 85% grid efficiency, a residential building would need around half of its heated surface in area of PV modules to be self sufficient. The point of SS also marked the maximum grid revenue at almost 7 CHF/ m²yr. A lower round-trip efficiency required more PV panels to achieve SS, generated a greater stress on the grid, and reduced annual grid revenues.

Feed-in The pricing of the electricity exchange with the grid influenced the feed-in to the grid. For lower feed-in prices (or higher demand prices), the most economic solution was to increase tilt angles and slightly lower the PV penetration. This increased SC for a constant level of SS.

Peak power Constraining the peak power of the grid exchange led to a variation in azimuth angles. By moving panels 20°westward and optimally scheduling the operation, the peak was reduced by 50% while total costs increase by 8.3%.

Even though the optimal orientation strategy was impacted by the orientation of available surfaces, the trend of different grid policies was confirmed by analyzing a 40-building district with individual roof orientation and demand profiles. Comparing the resulting optimally oriented and horizontally oriented panels indicated that the latter generated high error in the estimation of the PV performance. Assuming horizontal panels, caused an overestimation in operating costs by approximately 5% and a 10% underestimation in generated electricity for low PV surfaces. For greater PV surfaces installed, the trend was reversed, and the relative error could increase to up to 20%.

The need of PV panel installation in order to be self-sufficient with grid re-imports alone, was analyzed with a building with huge available roof surfaces. The area of the available roof was almost identical to the ERA, which was useful to study different limits and requirements. This high ratio between available roof surface and ERA is however not available for most buildings, especially not for high-rise urban typology. In these cases, the role of facades has to be considered. This aspect is further analyzed in the following Chapter 3.

Facades in interconnected renewable energy hubs

Overview

- Assessment of solar irradiation on facades including shadows from surroundings
- Analysis of district energy systems as a collection of renewable energy hubs at the building scale
- Analysis of the needs and limitations for integrating a high share of renewable energy in renewable energy hubs at the building scale
- Estimation of the amount of electricity generated from the energy hub that needs to be distributed or stored, and the related costs

The content of this chapter is published in [21].

As a main stakeholder, authorities often lack the appropriate tools to frame and encourage the transition, and monitor the impact of energy transition policies. Compared to existing literature in the field, the proposed approach combines an advanced modeling of the energy generation potential from photovoltaic (PV) panels with a detailed representation of the district energy systems, thus allowing an accurate representation of the interaction between the energy generation from PV and the rest of the renewable energy hub. The proposed approach was applied to a typical residential district in Switzerland. The results showed that the district can achieve carbon neutrality based on PV energy alone, but that this requires covering all the available district's rooftops, and part of the district's facades. Whereas facades are generally disregarded due to their lower generation potential, the results also concluded that facade-PV can be economically convenient for a wide range of electricity prices, including those currently used by the Swiss grid operators. Achieving self-sufficiency for the district was challenging: it could be achieved by covering approximately 42% to 100% of the available surface when the round-trip efficiency decreased from 100% to 50%. The results underlined the importance of storage for achieving self-sufficiency: even with 100% round-trip efficiency for the storage, very large capacities were required. However, energy demand reduction through renovation would allow for self-sufficiency to be reached with half of the PV and storage capacity required.

3.1 Introduction

Political authorities and other stakeholders in the energy value chain have the responsibility to implement energy transition pathways by increasing decentralized renewable energy generation. As a main stakeholder, authorities often lack the appropriate tools to frame and encourage the transition, and monitor the impact of energy transition policies. Network operators as well need appropriate frameworks and guidelines to implement the transition with a business perspective. The electrification of the building stock has the potential to lower local pollutant emissions and increase the energy system efficiency, especially when coupled with local renewable energy sources [7, 8]. In terms of small, decentralized renewable energy generation systems, roofs constitute the most obvious solution for the integration of PV generation in buildings [3]. However, while the recent decrease in PV systems' investment costs made rooftop PV a proven, cost-convenient choice in many parts of the world (even in the absence of subsidies [9]), today more than 90% of the solar potential on the top of roofs is still unexploited.

In urban environments, however, the limited available space for including locally generated renewable energy compared to the energy demand represents an additional challenge towards a complete decarbonization of the energy system. As a result of this challenge, together with the low cost of PV modules, research in recent years also investigated the role of facades in urban context.

3

3.1.1 State-of-the-art

Initial feasibility studies focused on a general estimation of the potential from PV facades, introducing the concept of vertically oriented surfaces [73]. These early studies, however, did not consider PV panels or shadow modeling, thus generally overestimating the PV generation potential. However, even when these aspects were taken into account, existing literature shows that the inclusion of PV panels from different oriented roofs and facades can be beneficial for matching electricity demand profiles. As a relevant example, Freitas et al. [91] showed the economic feasibility of facades for the case of two building blocks in Portugal and demonstrated that including facades has the effect of reducing the required storage size.

To expand the scope from single buildings to whole districts, 3D simulation software using ray tracing techniques like LiDAR in combination with geographic information systems (GIS) tools were developed [92–94] and commonly used to estimate solar potential on all surfaces in a district [78, 95, 96]. The use of these tools also allowed the inclusion of surrounding buildings in the model, a necessary condition to include the effect of shading on the potential of PV generation from facades. In addition, the *Sky view factor* is a commonly used indicator for determining the amount of diffuse irradiation on the surface [97, 98], whose use becomes even more relevant in the case of PV systems on facades.

3.1. Introduction

The solar potential on facades is, in general, lower than on roofs [99]. However, previous research suggested that facade PV can be crucial to achieve high levels of decarbonization and self-sufficiency in urban environments. Redweik et al. [92] showed that the combined PV potential on roofs and facades exceeds the non-baseload demand for a district located in Portugal and could furthermore contribute up to 75% of the total electricity demand. Also, Aguacil et al. [100] suggested to take PV installation on facades into account, especially for high-rise buildings. Li et al. [101] and Diez-Mediavilla et al. [102] even suggested that facades can be competitive with roof installations.

The potential for facades also strongly depends on the location. At lower latitudes (such as in the case of Portugal [92]) rooftop solar is economically superior to facades, as in the latter case the payback increased from 10 to 20 years. At higher altitudes, however, the situation can be different. Horn et al. [103], based on the results of a case-study application in Germany, suggested that the solar potential on facades can exceed that on roofs during the winter months, as a result of the sun being low in the sky. Clearly, the orientation of the surface also has a role in the performance of the system. As a relevant example, Pantic et al. [104] determined a 12-year carbon and a 10-year payback time of PV panels mounted on south-oriented facades in Serbia.

3

A comparative analysis of the state-of-the-art of research about the role of facades in urban energy systems is represented in Table 3.1. The analysis shows one of the main gaps in existing literature: most available studies only consider facade PV systems on their own, and do not explore the importance of their interaction with the rest of the building energy system (BES). These studies are usually conducted from the perspective of urban planners and architects, and are aimed at assessing the solar potential on the complete envelope in order to find the best concepts and designs.

Conversely, papers focusing on the design of the energy system of buildings, which include irradiation models, are generally focused on two aspects. The first is that irradiation models are required to assess the solar contribution to the heating and cooling demand [23]. The second is that irradiation models are also used for modeling the contribution of solar panels (both thermal and electricity) to BES [26, 38]. However, in most cases, these studies rely on the use of global irradiation to model the incoming solar radiation. This corresponds to assuming horizontal panels [60], a simplification that was shown to generate a relevant error (over-estimation or under-estimation, depending on the case) in the calculation of how much electricity is generated by PV panels [52].

Table 3.1 – Literature overview of solar irradiation modeling on buildings. ✓ = yes, aspect included, X = no, not included, S = simplified, N/A = not answered, PV = Photovoltaic Panels, BAT = Battery, BES = Building Energy System.

roofs	facades	shadow	PV	BAT	BES	focus	method	reference
✓	✓	X	X	X	X	surface	simulation	[73]
✓	✓	X	✓	X	X	surface	simulation	[105]
✓	✓	X	S	X	X	building	simulation	[102, 104, 106]
X	✓	✓	X	X	X	building	simulation	[99]
X	✓	✓	✓	X	X	building	simulation	[107]
X	✓	✓ [†]	✓	X	X	building	simulation	[108]
✓	✓	✓ [†]	✓	X	X	building	simulation	[109]
✓	✓	X	✓	X	S*	building	simulation	[110]
✓	X	X	✓	X	✓	building	simulation	[111]
✓	✓	N/A	✓	X	S*	building	simulation	[103]
✓	✓	✓	S	X	X	building	simulation	[112]
✓	✓	✓	✓	X	X	building	simulation	[101]
✓	✓	✓	✓	X	S*	building	simulation	[113]
✓	✓	✓	✓	✓	✓	building	simulation	[100]
✓	X	X	S	X	X	district	simulation	[114]
X	✓	✓	X	X	X	district	simulation	[98, 115]
✓	✓	✓	X	X	X	district	simulation	[79, 92, 93, 95]
✓	✓	✓	S	X	X	district	simulation	[116]
✓	X	✓	✓	X	X	district	simulation	[78]
✓	✓	✓	✓	X	X	district	simulation	[97]
✓	✓	✓	✓	X	X	building	genetic algorithm	[75]
✓	✓	✓	✓	✓	X	building	genetic algorithm	[91]
S ⁺	X	X	✓	X	✓	building	genetic algorithm	[26]
S ⁺	X	X	✓	✓	✓	building	optimization	[38]
S ⁺	X	X	✓	X	✓	district	optimization	[58, 117–119]
S ⁺	X	X	✓	✓	✓	district	optimization	[55, 120–123]
✓ [†]	X	✓ [†]	✓	✓	✓	district	optimization	[63]
✓	✓	✓	✓	✓	✓	district	optimization	this chapter

[†] Shadow aspect is included as measurement of the irradiation on actual surface. Shadow influence is not considered with the help of a replicable model.

* If the building energy system is considered simplified, its size is neither optimized nor designed and the operation is not optimally scheduled.

⁺ Roofs are simplified in the sense that they limit bounds for installation and are considered as being horizontal.

3.1.2 Gaps and contributions

Based on the aforementioned literature review, there is a gap in the academic literature related to the intersection of energy system design in buildings and the solar potential on facades. This chapter accordingly aims to investigate following research contributions and questions:

- What is the role and potential of facades in decentralized energy hubs?
 - Close the gap between architects assessing solar potential on building surfaces and engineers designing solar-based energy systems.
 - Integrate different PV panel orientation possibilities together with a shadow model from the surroundings in the optimization approach of renewable energy hubs.
 - What is the optimal investment strategy for PV systems in the district?
 - Investigate the needs and limitations for installing PV panels and what is thereby role of facades?
 - Estimate the amount of electricity generated from the district that, from the perspective of the electricity grid, needs to be distributed or stored, and the related costs.

Whereas it would be impossible to achieve general conclusions based on one single study, this chapter aims at suggesting a potential methodological approach to address this gap in the scientific literature, and presents the application to a specific case study in order to showcase the potential of the proposed approach.

3.2 Method

The aim of this chapter is to integrate PV modules on both roofs and facades in the optimal design and the scheduling of energy conversion and storage technologies. Furthermore, the aim is to investigate the response of a fully integrated renewable energy hub at the district level to the inclusion of high shares of solar energy.

In the proposed approach, renewable energy hubs interact with each other in two ways: 1) by contributing to the overall electricity balance of the district, both consuming and generating electricity, and 2) by shading neighboring building surfaces and roofs, thus influencing the actual potential for local solar generation. An overview about the proposed approach is provided in Figure 3.1.

To be able to take both the optimal integration at building level and the behavior of the whole district into account, a mixed-integer linear programming (MILP) framework is formulated, where unit sizes and installation decisions in each building are used as the main optimization variables. The approach is based on the general formulation of the renewable energy hub at the building scale, which can be then applied to different building types in a district. The model derives from the BES framework described in Chapter 1. Special attention is dedicated to the further development of the

oriented irradiation modeling proposed in Chapter 2, which is modified to include the modeling of shading effects between different buildings in the districts similar to the work of Schüler [124].

To clearly differentiate decision variables from input parameters, bold typeset is used to represent all decision variables. As all sets are predefined, normal and capital typeset is used. The main problem sets are: the set of buildings B and their allocated facades F , the set of available conversion and storage units U ; the different days of the year are represented by periods in the set P , to which hourly timesteps are allocated and contained in set T . The sets A and Y are used to express the orientation of the PV panels with azimuth and tilt angles, respectively.

3.2.1 Decentralized district energy system

The district is considered as a collection of renewable energy hubs at the building scale. Each renewable energy hub includes multiple unit technologies that can contribute to satisfy the different energy demands (Figure 3.1). Both the space heating (SH) and domestic hot water (DHW) demands can be fulfilled by a gas boiler, converting natural gas into thermal energy, or by heat pumps (HPs) and electrical heaters, both converting electricity to thermal energy. PV panels are also considered as energy conversion units, converting incoming solar irradiation to electricity. The system also includes storage technologies: thermal and electrical storage. For thermal storage, two different tanks are considered: one for SH and one for DHW. Electricity energy storage is considered in the form of lithium-ion batteries.

In the proposed models, buildings are differentiated not only based on their construction characteristics (surface, volume, roof type, etc.) but also by their usage, such as residential or industrial, and their renovation state. In addition to having an effect on the total yearly demand, these aspects also influence the hourly energy demand profiles, which in turn have a relevant effect on the overall energy balance of the district. Energy can be exchanged with the electricity grid in both directions, whereas hot water and natural gas can only be supplied by the grid to each building.

The MILP problem is defined with the minimization of the BES costs as the main problem objective. This involves the combination of two separate contributions: operating and capital expenses. As these two objectives are generally competing (solutions with high capital expenses (CAPEX) have low operational expenses (OPEX), and vice versa), the problem must be approached using a multi-objective optimization (MOO) approach. The MOO problem is implemented using the ϵ -constraint method, thus considering the OPEX as the main problem objective and solving different optimization problems where the CAPEX is constrained at incrementally increasing values. The same principle is then repeated after inverting the roles of the two objectives. The objectives are applied at building level and are detailed in Section 1.2.4.

In addition to the problem objectives, key performance indicators (KPIs) are defined to provide

3.2. Method

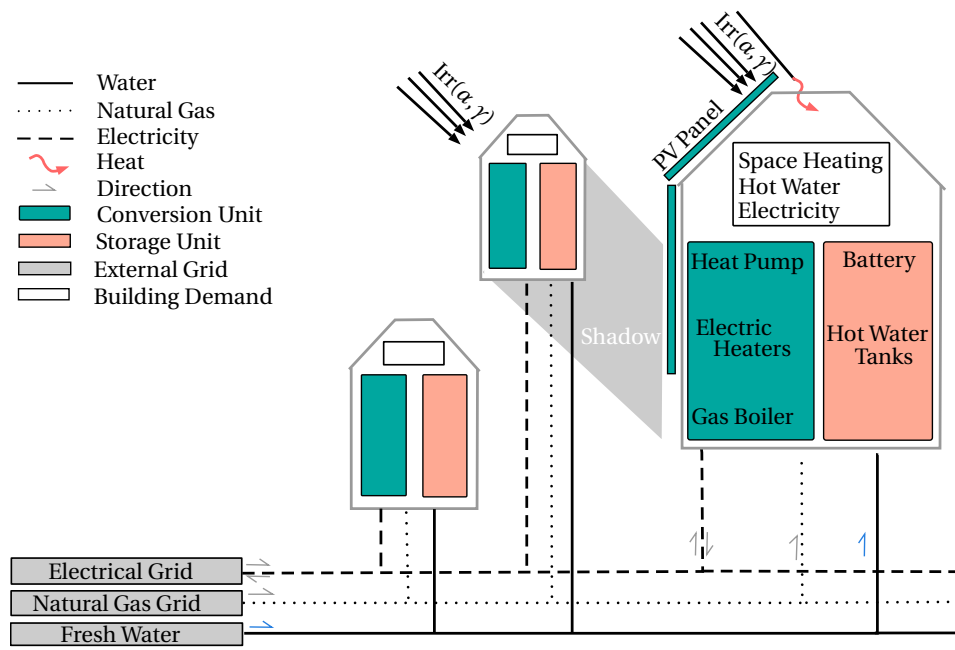


Figure 3.1 – Overview of a decentralized district energy system. Considered aspects in this chapter: photovoltaic panels on roofs and facades. Interconnection of renewable energy hubs via the grid, shading of buildings and solar gain from oriented irradiation irr .

3

additional information regarding the performance of the system. The KPIs are applied on the entire district and therefore have to be developed further with respect to Section 1.2.5. The possibility that electricity can be both generated and consumed in the district itself is accounted for and the load is balanced at the level of the district's transformer (Equation 3.1).

$$\dot{E}_{p,t}^{TR,+} - \dot{E}_{p,t}^{TR,-} = \sum_{b \in B} \dot{E}_{b,p,t}^{gr,+} - \sum_{b \in B} \dot{E}_{b,p,t}^{gr,-} \quad \forall p \in P \quad \forall t \in T \quad (3.1)$$

The electricity supply from the grid $E^{gr,+}$ and the feed-in electricity $E^{gr,-}$ of each building b are the result of the electricity balance of each renewable energy hub (Equation 1.2a). The sum of the interconnections of all renewable energy hubs in the district leads to the electricity exchange at the transformer $E^{TR,\pm}$. The electricity exchange at the transformer is accounted for in the KPIs. For readability, the following Equations 3.2 and 3.3 are expressed with annual values. The self-consumption (SC) and the self-sufficiency (SS) are KPIs used to evaluate the performance of the

system in terms of its interaction with the grid.

$$SC = \frac{(\sum_{b \in B} E_{b,pv}^+) - E^{TR,-}}{(\sum_{b \in B} E_{b,pv}^+)} \quad (3.2a)$$

$$SS = \frac{(\sum_{b \in B} E_{b,pv}^+) - E^{TR,-}}{(\sum_{b \in B} E_{b,pv}^+) - E^{TR,-} + E^{TR,+}} \quad (3.2b)$$

In Equation 3.2a, SC represents the share of the generated electricity from all PV panels E_{pv}^+ consumed within the district [37]. In Equation 3.2b, SS represents the ratio of the onsite generated electricity consumption to the total electricity demand [37].

The benefit for selling the generated electricity to the grid and for avoiding electricity import is measured by annual revenues (AR) [40]. In this chapter, electricity can only be generated by PV panels, hence their associated revenues are the only ones considered in the following Equation 3.3.

3

$$AR = (c^{el,+} \cdot SC + c^{el,-} \cdot (1 - SC)) \cdot \sum_{b \in B} E_{b,pv}^+ \quad (3.3)$$

Additional KPIs are used to evaluate how the system performs in terms of greenhouse gas (GHG) emissions, included here based on their CO₂ equivalence [3]. As shown in Equation 1.17, the total global warming potential (GWP) is divided into the share coming from the operation and the construction of the BES (see Section 1.2.5).

$$G^{op} = \sum_{p \in P} \sum_{t \in T} \left(g_{p,t}^{el} \cdot E_{p,t}^{TR,+} - g_{p,t}^{el} \cdot E_{p,t}^{TR,-} + g^{ng} \cdot \sum_{b \in B} \dot{H}_{b,p,t}^{gr,+} \right) \cdot d_p \cdot d_t \quad (3.4)$$

Equation 3.4 shows how the GWP from the system's operations is balanced at the transformer TR , where the volatile emission parameters $g_{p,t}$ are accounted for in the calculation of the GWP per kWh consumed electricity E [33] or natural gas H . The parameter d_t accounts for the duration of each timestep within a period and d_p for the frequency of each period within one year. In addition to the total GWP of the system, the carbon payback time (CPT) is used as an additional KPI of the system based on Equation 1.38 in Section 1.2.5.

3.2.2 Expansion of the validity range for PV installations

In this chapter, installation of PV panels are allowed on the full envelope of the buildings. Therefore, the validity range for PV installations has to be extended in comparison to the previous work in Chapter 2. Figure 3.2 demonstrates why at least two intervals for the MILP modeling of PV panels

3.2. Method

are required.

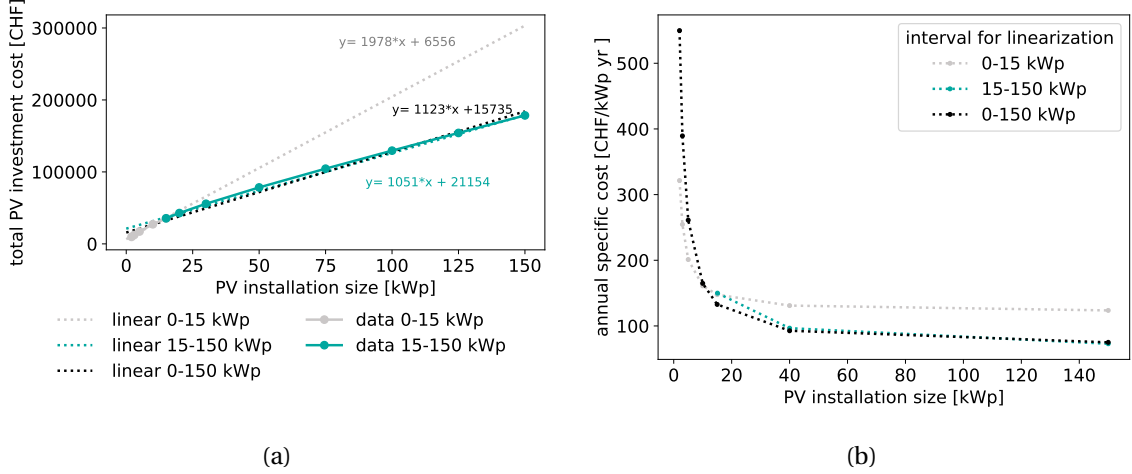


Figure 3.2 – Visualization of the need for piece-wise linearization of the cost function for PV panels. a) Linearization of different validity ranges, data derived from [125]. b) Annual specific cost of identified linearizations.

To simply extend the validity range for the identified cost function for installation between 0-15 kWp, leads to an overestimation of costs for a project with huge PV installations (Figure 3.2a). Whereas one linearization for the interval 0-150 kWp would penalize, small, mostly roof, PV installations (Figure 3.2b). To overcome this issue, the cost function (former Equation 1.16b) is piece-wise linearized for the PV panels (Equation 3.5).

$$C_b^{inv,u} = \sum_{l \in L} b_{b,u,l} \cdot (i_{b,u,l}^{c1} \cdot y_{b,u,l} + i_{b,u,l}^{c2} \cdot f_{b,u,l}) \quad \forall b \in B, \quad u = p v \quad (3.5)$$

The decision to purchase PV panels is represented by the binary variable y , whereas the continuous variable f represents the unit size. The parameters i^{c1} and i^{c2} are the results of the linearization of the unit cost function with bare module b in each linearization interval l . Additionally, the sizing constraints (Equation 3.6) are added to the former sizing constraints from Equations 1.1.

$$y_{b,u,l} \cdot F_{u,l}^{min} \leq f_{b,u,l} \leq y_{b,u,l} \cdot F_{u,l}^{max} \quad (3.6a)$$

$$F_{u,l=0}^{min} = F_u^{min} \quad (3.6b)$$

$$F_{u,l=n}^{min} = F_u^{max} \quad (3.6c)$$

$$\forall l \in L \quad \forall b \in B \quad \forall u = p v$$

The upper and lower bounds (F^{min}, F^{max}) for unit installations are necessary for identifying the validity range of the linearization [29]. The lowest bound F^{min} has to be equal to the lower bound

of the first linearization interval (Equation 3.6b). The end of the overall validity range is defined by parameter F^{max} of the last considered interval (Equation 3.6c)

$$y_{b,u} = \sum_{l \in L} y_{b,u,l} \quad (3.7a)$$

$$f_{b,u} = \sum_{l \in L} f_{b,u,l} \quad (3.7b)$$

$$\forall l \in L \quad \forall b \in B \quad \forall u = PV$$

Equation 3.7a ensures that only one interval l can be activated. The unit size, which is chosen, is equal to the total installed size (Equation 3.7b) .

3.2.3 Solar irradiation and shading among buildings

The hourly irradiation is modeled using the anisotropic irradiation model which was first proposed by [126] and later improved for all sky conditions [84]. The skydome descritization [83] is applied using the Ladybug plug-in of the Grasshopper suite [127] to include the oriented irradiation into a MILP formulation. For more information about modeling oriented irradiation in MILP problems, the reader should refer to Chapter 2.3. In the remaining part of this section, the focus is on the inclusion of facades, the main element of novelty in this chapter. Compared to roofs, the direct solar irradiation on facades highly depends on shading from neighboring buildings, making it necessary to include a detailed shadow modeling. The shadow modeling employed in this study only includes the shadow from surrounding buildings, not from other obstacles (such as trees). Figure 3.3 visualizes an exemplary geometric relation between two buildings.

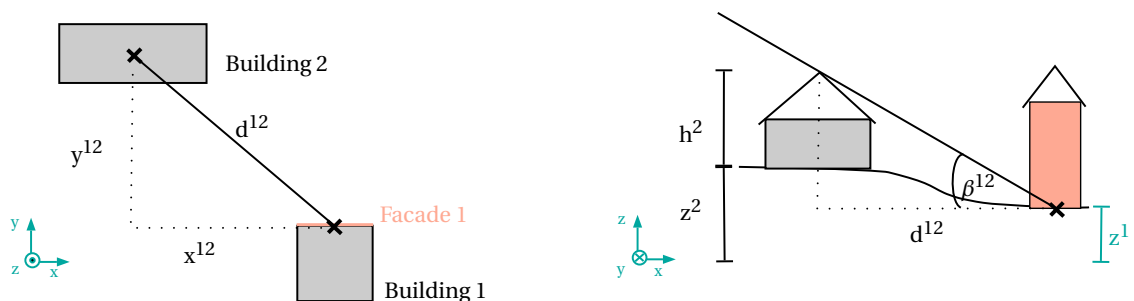


Figure 3.3 – Exemplary visualization of the geometry for Facade 1, with distance d^{12} to Building 2 and the sky-limiting angle β .

The positions of buildings and facades are given in x,y z coordinates, where y points to the north and x to the east. The coordinate z is the elevation. The assumption is that the shortest distance is between the center point of the facades and the center point of the building (Figure 3.3).

3.2. Method

$$x_{f,b} = |x_b - x_f| \quad (3.8a)$$

$$y_{f,b} = |y_b - y_f| \quad (3.8b)$$

$$d_{f,b} = \sqrt{(y_{f,b})^2 + (x_{f,b})^2} \quad \forall f \in F, b \in B \quad (3.8c)$$

Equations 3.8 show how the distance between buildings b and facades f in x and y coordinates is calculated. The sky-limiting angle β represents the lowest elevation angle from which irradiation reaches the facades (Figure 3.3).

$$\tan(\beta_{f,b}) = \frac{h_b + z_b - z_f}{d_{f,b}} \quad \forall f \in F, b \in B \quad (3.9)$$

In Equation 3.9, the reference point for the sky-limiting angle is the bottom of each facade (z_f). Based on this assumption, the effect of the building's height on the electricity yield is only based on its role in the calculation of the total available surface (higher buildings have a larger facade surface available). A building's height only influences the shading of other buildings' solar generation potential, but not of its own. This is considered a conservative assumption in order to not overestimate the energy generated by PV panels installed on facades. The facades of high-rise buildings is divided into several parts, applying the proposed approach. The sky direction is expressed by the azimuth angle α , which is 0° for north and 180° for south. Figure 3.4 shows the different azimuth angles of the facades, surrounded buildings and skydome patches.

3

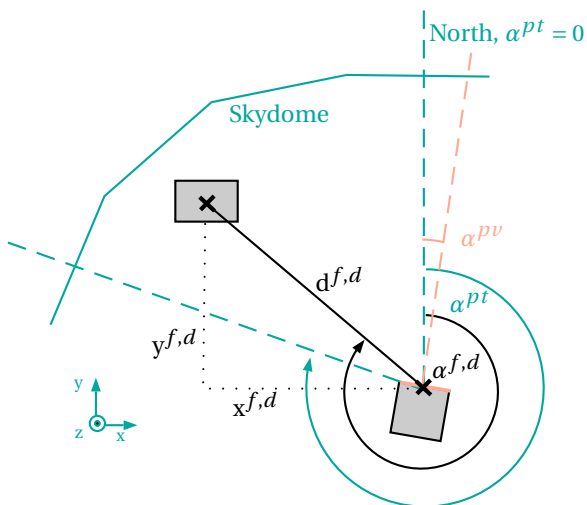


Figure 3.4 – Outline sketch of different azimuth angles. The azimuth orientation of the facades are identical to possible PV modules α_{PV} . $\alpha_{f,b}$: azimuth direction of surrounding buildings, α_{pt} : azimuth direction of each patch of the skydome.

Equation 3.10 shows how the azimuth position of building b is calculated. Knowing the signs of both catheti makes it possible to assess the correct quadrant for azimuth angle $\alpha_{f,b} \in [0^\circ, 360^\circ]$.

$$\alpha_{f,b} = \arctan\left(\frac{x_b - x_f}{y_b - y_f}\right) \quad \forall f \in F, b \in B \quad (3.10)$$

As a building is receiving irradiation from all patches of the skydome ($pt \in S$), the sky-limiting angle β needs to be calculated for all sky directions.

$$\tan(\beta_{f,b,\alpha}) = \frac{h_b + z_b - z_f}{d_{f,b}} \cdot \cos(\Delta\alpha) = \tan(\beta_{f,b}) \cdot \cos(\alpha_{f,b} - \alpha_{pt}) \quad \forall f \in F, b \in B, \forall pt \in S \quad (3.11)$$

In Equation 3.11, the sky-limiting angle β is greatest in the azimuth direction $\alpha_{f,b}$ of the building causing the shadow. Finally, the highest sky-limiting angle $\beta_{f,\alpha}$ in each azimuth direction α_{pt} of the skydome is selected among all surrounding buildings for each facade f (Equation 3.12).

3

$$\beta_{f,\alpha} = \max\{\beta_{f,b,\alpha} : b \in B\} \quad \forall f \in F, \alpha_{pt} | pt \in S \quad (3.12)$$

The sky-limiting angle in each azimuth direction is then used to determine the shaded irradiation. Thereby, the method is similar to the calculation of inter-modular shading of PV modules on flat roofs, described in Chapter 2.3.

$$s_{f,pt} = \begin{cases} 0 & \epsilon_{pt} \leq \beta_{f,\alpha} \\ \frac{\epsilon_{pt} + 6 - \beta_{f,\alpha}}{12} & \beta_{f,\alpha} - 6 < \epsilon_{pt} < \beta_{f,\alpha} + 6 \\ 1 & \epsilon_{pt} \geq \beta_{f,\alpha} + 6 \end{cases} \quad \forall f \in F, (\alpha_{pt}, \epsilon_{pt}) | pt \in S \quad (3.13)$$

The skydome is piece-wise linearized over the evaluation angle of one patch, which varies 12° , with ϵ_{pt} marking the central point of each patch (Equation 3.13). The resulting shading factor of one patch $s_{pt} \in [0; 1]$ is equal to zero for completely shaded patches, 1 for completely unshaded patches.

$$irr_{f,pv}(\alpha_{pv}, \gamma_{pv}) = (-1) \cdot \sum_{pt \in S} s_{f,pt} \cdot irr_{pt}(\alpha_{pv}, \gamma_{pv}) \quad \forall \alpha_{pv} \in A, \forall \gamma_{pv} \in Y \quad (3.14)$$

Equation 3.14 shows how the irradiation on facades is calculated when taking into account shading from neighboring buildings. As possible PV panels can only have the same orientation of the facades they are installed on, the azimuth and tilt orientation of the facades are equivalent to the

orientation of the PV panel. In contrast to the azimuth angle, tilt angle of the facades is always the same $\gamma_{PV} = 90^\circ$. The irradiation of each oriented patch of the skydome irr_{pt} is transferred to the perpendicular irradiation, which is received on the PV panels. This is achieved using the principle of a two-stage rotation in a three-dimensional space, which is treated in detail in Chapter 2.3.

3.2.4 Solar heat gains

The heat gains in each building are partly a result of solar irradiation. Common practice is to use a fixed share, which describes how much of the global irradiation is converted to heat gain (Equation 1.12). This approach can be improved with the oriented irradiation and the detailed knowledge of the geometry and the shadow on the buildings' envelope (Equation 3.15).

$$\dot{Q}_{b,p,t}^{irr} = \sum_{f \in F} \frac{A^g}{A_{f,b}} \cdot f^s \cdot g^{glass} \cdot irr_{f,p,t}(\alpha_f, \gamma_f) \quad \forall b \in B \quad \forall p \in P \quad \forall t \in T \quad (3.15)$$

Perez [128] details typical ratios of glass-to-facades surface A^g/A_f for each building type (Equation 3.15). The g-values measures the amount of solar irradiation which is transferred to heat. It is assumed that shading devices are used for irradiation greater than 200 W/m^2 [128]. f^s is a constant, 0.9, accounting for dirt and non-perpendicular irradiation on the windows [31]. The solar irradiation on the facades irr_f depends on the facade's azimuth orientation α_f and the tilt angle γ and is a result of previous Section 3.2.3.

3.2.5 Data-driven approach

The data layers of Table 3.2 are used to represent multiple configurations of decentralized energy demand and generation. Except for the grid topology and measurement [87], the approach uses Open Government Data (OGD) including the climatic conditions, building database [45] with roof and facade geometries [129, 130], energy demand standards [31, 131] and statistical values [23].

Table 3.2 – List of necessary data layers.

Type	Data	Description
Environment	Weather data	Temperature and solar irradiation [48, 132]
Land registry	Cadastre	Footprint area [44, 133]
Buildings	Official Buildings Registry	Usage, construction/renovation date, heating system, height, number of floors, reference energy area [44, 45]
	3D model	3D surfaces [129]
	Solar roof and facade	2D surface area and orientation [130, 134]
	Energy statistics and standards	Overall heat transfer coefficient, heat capacity, people presence, electrical loads, internal and external gain [31, 131]
Grid	Grid topology	Location and parameters of transformer, lines and injection points [135]
	Load measurements	Hourly load aggregated at the transformer [87, 135]

3.2.6 Case study area

The method is demonstrated on a typical, central European, peri-urban, residential area comprising 31 buildings, mostly single and multi-family houses (Figure 3.5a). The buildings considered are all connected to the same measured transformer, the other buildings of the district being used solely for their shadowing effect. Figure 3.5b shows that, whereas the largest share of the PV generation potential lies in the building roofs, facades also have a significant potential. As expected, south-oriented facades have the largest potential, followed by east- and west-oriented facades. It is interesting to notice that the specific solar potential of the most promising south-oriented facades is higher than that of the least promising roofs. The large amount of annual input profiles requires clustering of the solar irradiation and the external temperature. The k-medoids clustering, commonly applied to combined heat and power systems [136] allows for the identification of 10 typical days and 2 extreme periods. While detailed information is available in the appendix, Table 3.3 provides an overview of the main building-related parameters. In all buildings the desired indoor temperature is set to 20 °C and the hotwater is supplied at 60 °C.

3.2. Method

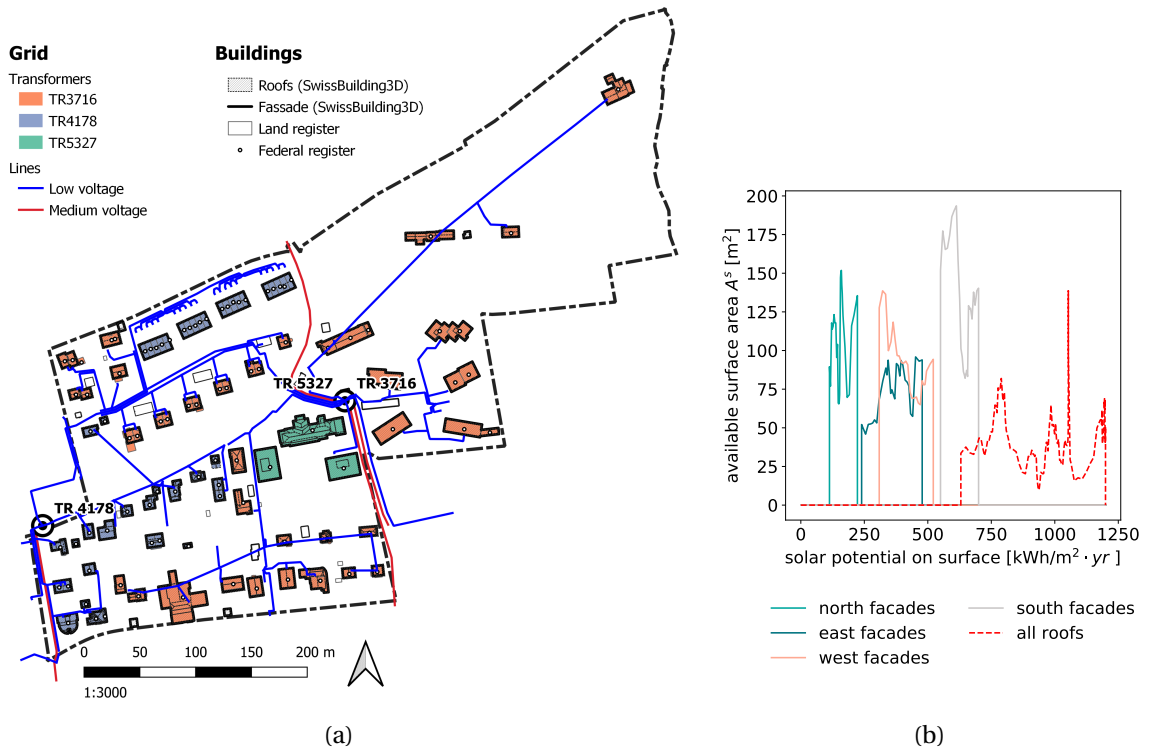


Figure 3.5 – Details of the case study area. a) Map of the area, a typical central European peri-urban residential area. b) Solar PV potential on roof and facade as a function of the orientation.

Table 3.3 – Overview input data for 31 buildings. All buildings are connected to the same low-voltage grid.

		Multi family house	Multi family house	Single family house	
Building type ⁺		I	I	II	
Building category ⁺	existing		standard		
Number of buildings	11	2	18		
Total net surface	A^{net}	9200	1100	5600	m^2
Total energy ref. area	A^{era}	11500	1400	7000	m^2
Total roof area*	A^s	4200	560	4400	m^2
Total facade area*	A^s	7700	870	5900	m^2
Annual electricity demand [†]	E^B	37 ± 17	50 ± 21	60 ± 60	$\text{kWh}/\text{m}^2_{net}$
Annual hot water demand [†]	Q^{dhw}	25 ± 0	25 ± 0	19 ± 0	$\text{kWh}/\text{m}^2_{net}$
Annual internal heat gain [†]	Q^{int}	30 ± 2	32 ± 0	29 ± 2	$\text{kWh}/\text{m}^2_{net}$
Solar heat gain [†]	Q^{irr}	22 ± 6	20 ± 3	31 ± 10	$\text{kWh}/\text{m}^2_{era}$
Design supply temperature	T_0^s	65	41.5	65	$^\circ\text{C}$
Design return temperature	T_0^r	50	33.9	50	$^\circ\text{C}$
Heat transfer factor [†]	U	1.74 ± 0.24	0.83 ± 0	1.84 ± 0.21	$\text{W}/(\text{m}^2_{era} \text{ K})$
Heat capacity factor [†]	C	118 ± 5	120 ± 0	120 ± 0	$\text{Wh}/(\text{m}^2_{era} \text{ K})$

⁺ according Swiss standard norm [31]

* Area available for PV installation. Details available in [82].

[†] Average values \pm standard deviation. Detailed building data is available in the appendix.

3.3 Results and discussion

The role of PV integration in decentralized energy systems is addressed in this section. The optimal integration strategy of PV panels is analyzed and the need of facades in order for the district to become carbon neutral and self-sufficient is highlighted. Thereby, economical feasibility of PV installations is analyzed and required storage capacity are then further detailed.

3.3.1 What is the potential of energy generation from PV in the district?

The results of the optimization confirmed what was observed about the per-surface generation potential. The conclusions resulting from the analysis of the potential from installing PV on facades were different depending on what perspective was being considered. The general trend, as expected from what is shown in Figure 3.5b, was that rooftop-PV had a much better performance compared to facade-installed PV, which is clearly shown by the fact that panels were first installed on roofs (Figure 3.6a). The comparison of Figure 3.6a and 3.6b shows clearly the reason: in cost intensive solutions, the cost for facades dominated the total PV-related investment, while it still provided less than half of the total energy generated. However, looking at the same figures from another perspective, facades had the potential to increase the total energy generation from PV by approximately 97%. While they might not represent the most cost-efficient solution, they certainly can play an important role in improving the SS of the district.

3.3. Results and discussion

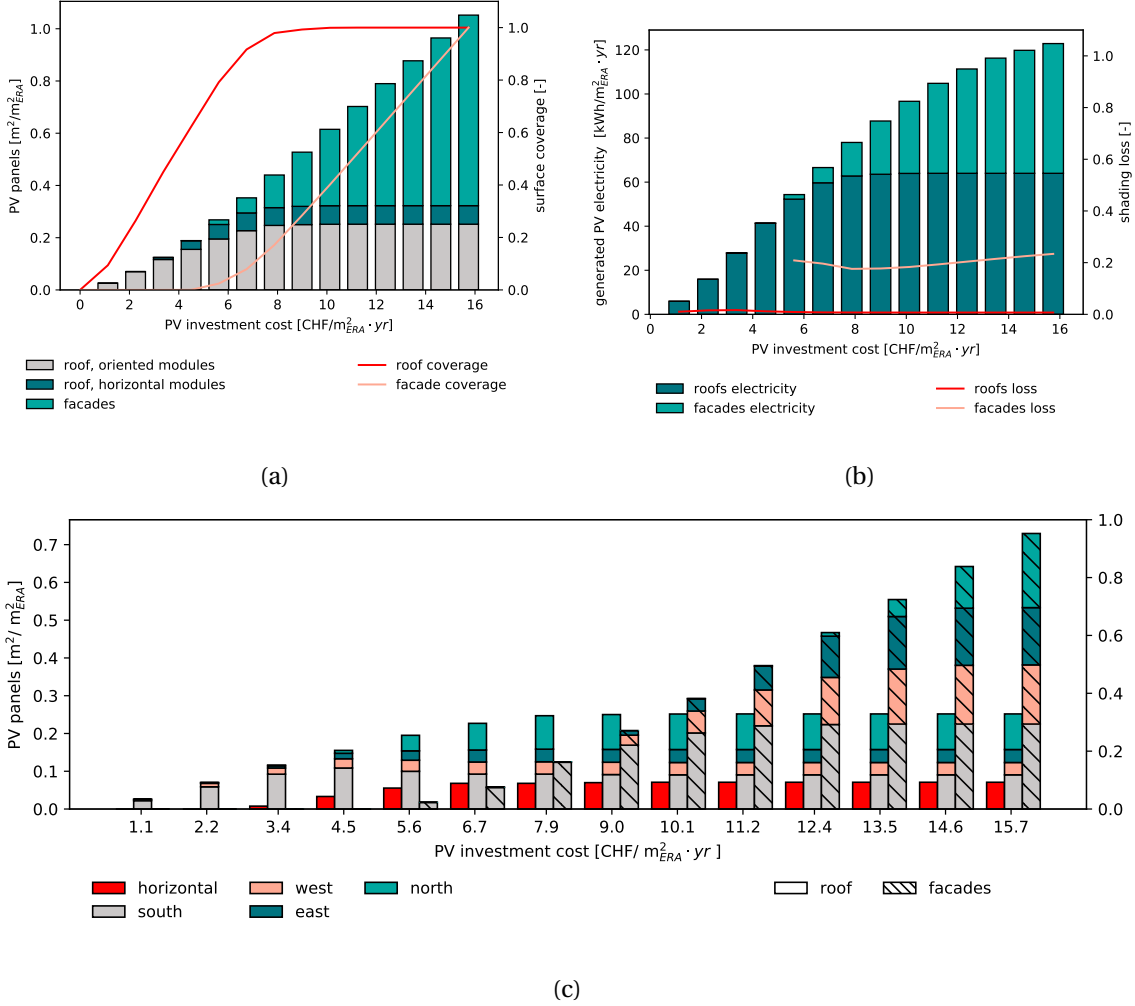


Figure 3.6 – Economically best PV installation for 31 residential buildings, normalized to total energy reference area in the district. a) Area of installed modules sorted by orientation type, PV modules with tilt = 0°are horizontal, tilt angles = 90°are facades, oriented modules summarize all other tilt angles. b) Annual generated electricity and shading losses depending on surface type. c) Orientation of economically best PV installation.

Looking more in detail at the surfaces where PV panels were installed depending on the optimization scenario, it can be noticed that some of the vertical surfaces were used even when roofs were not fully exploited yet. This is a consequence of two factors: first, the fact that (as shown in Figure 3.5b) some facades had a higher specific PV generation potential than some roofs, as in the case of south-oriented facades compared to tilted, north-oriented roofs; second, the fact that the CAPEX-constraint was not enforced at district level, but at building level. This implies that when at district level there might still be 10% of roofs available, this might not be true at building level, where the optimizer is then "forced" to start using facades instead.

3.3.2 Are PV installations on facades needed to become carbon neutral?

The results of the optimization for a list of Pareto-optimal solutions is shown in Figure 3.7. More specifically, Figure 3.7a shows that the district could become approximately carbon-neutral already for a overall investment cost (approx. 12 CHF/m²yr). This result was achieved also thanks to a significant contribution of energy generated from the PV panels installed on facades, which contributed to approximately 40% of the total PV surface installed, or 60% of the available facade area, corresponding to PV deployment on all well-oriented facades.

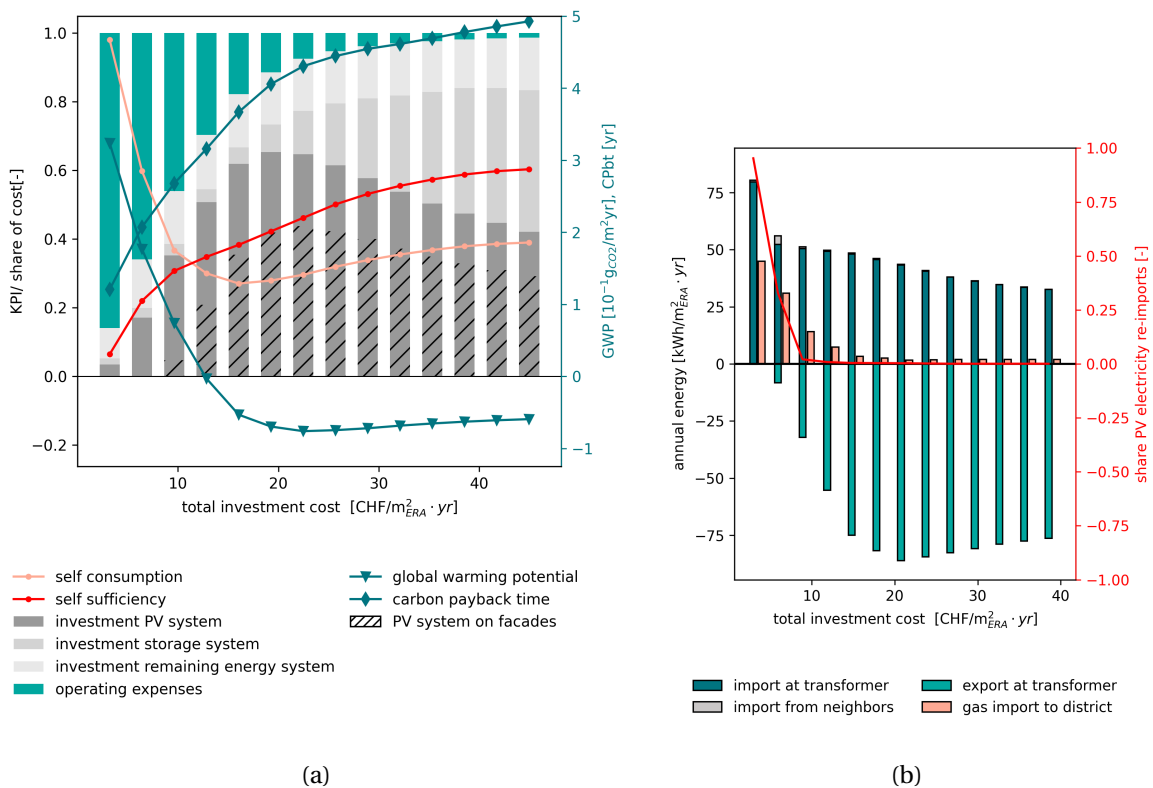


Figure 3.7 – Results of the MOO of 31 buildings in one low–voltage grid, normalized to total energy reference area in the district. a) performance indicators and cost distribution of identified energy systems b) electricity exchange and gas imports for the district.

Further increasing the allowed CAPEX only led to a limited improvement in terms of total GWP of the solution, that capped at a total CAPEX of approximately 20 CHF/m²yr. Beyond this limit, the overall GWP of the solution actually worsened: the increase in PV surface installed was compensated by the lower specific generation of PV panels installed on facades, and on the increasing battery capacity, which had little contribution to the overall energy balance, but increased costs and GWP potential. As current tariffs (electricity cost = 20ct/kWh and feed-in price = 8 ct/kWh) favor self-consuming locally generated energy over selling it to the grid, solutions with an increased CAPEX bound tended to shift towards the increase of battery capacity as to reduce energy exchanges with the grid. This

3.3. Results and discussion

is shown clearly in Fig 3.7b: moving towards high-CAPEX solutions, the imports and exports at the district transformer decreased. At the same time the energy locally generated increased only marginally, while the focus was shifted towards using it locally to maximize revenues.

3.3.3 How much electricity can be generated locally and cost-efficiently?

The results presented in Figure 3.7 represent Pareto-optimal solutions for the two competing objectives of minimizing OPEX and CAPEX. However, the choice of the individual prosumer will be influenced by the profitability of the investment, which is a result of the combined effects of CAPEX and OPEX. Policy makers and grid operators might be interested in knowing how different energy prices can influence the profitability of a PV investment, and hence the amount of PV installed and of resulting electricity generated. From the prosumer perspective, this translates into the question "how many PV panels can I install if I aim for the investment to pay back by the end of the PV panels' lifetime?". From the policymaker perspective, the question instead is "how should tariffs be set in order to achieve the desired electricity generation from PV panels?". The extent to which facade solutions are cost efficient depended on the installed surface, as shown in Figure 3.8. The Point A represents the surface of installed PV panels for which lifetime revenues and investment are equal. This showed that with current tariffs large surfaces of facades could be covered with PV panels, while still achieving a positive economic performance. This was strongly influenced by the choice of tariffs by the system operator.

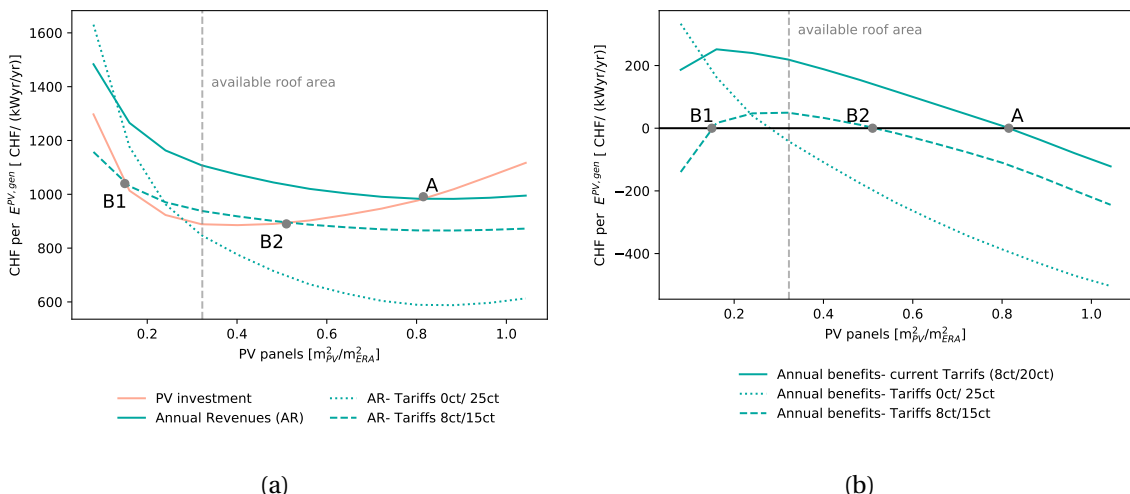


Figure 3.8 – a) PV investment per generated PV electricity $E^{PV,gen}$ and implicit revenues for different feed-in/demand prices. Economic point: investment in PV and connected revenues are balanced. Point A - current tariffs (8ct Feed-in, 20 ct demand price); points B1 and B2- exemplary tariffs with two break-even points. b) Annual benefits, which are the annual revenues subtracted by the PV investment.

At current tariffs (0.20/0.08 CHF/kWh) large facade surfaces could be covered with PV panels in

conditions where lifetime revenues were larger than the investment cost. Lowering the purchase price (e.g. 0.15/0.08 CHF/kWh) tended to worsen the economic performance in the whole surface range, as it affected the portion of the generated electricity that is self-consumed. In this case, according to the optimization's results, there was a limited window where PV was convenient: for installed surfaces below Point B1 (Figure 3.8) the fixed component of the investment was predominant. For installed surfaces higher than B2 the combination of two factors made these solutions economically unfavourable. First, new PV panels were installed on surfaces that generated less electricity per unit of surface installed. Second, every new panel mostly contributed to the annual revenues with electricity that is sold to the grid (and not self-consumed) in which, less is paid to the prosumer. Finally, the effect of decreasing feed-in tariffs to 0 CHF/kWh was shown by the dotted line. In this case, facades should be discarded: only self-consumed electricity mattered, so the most economically convenient choice was to install only a few panels and only on roofs.

3

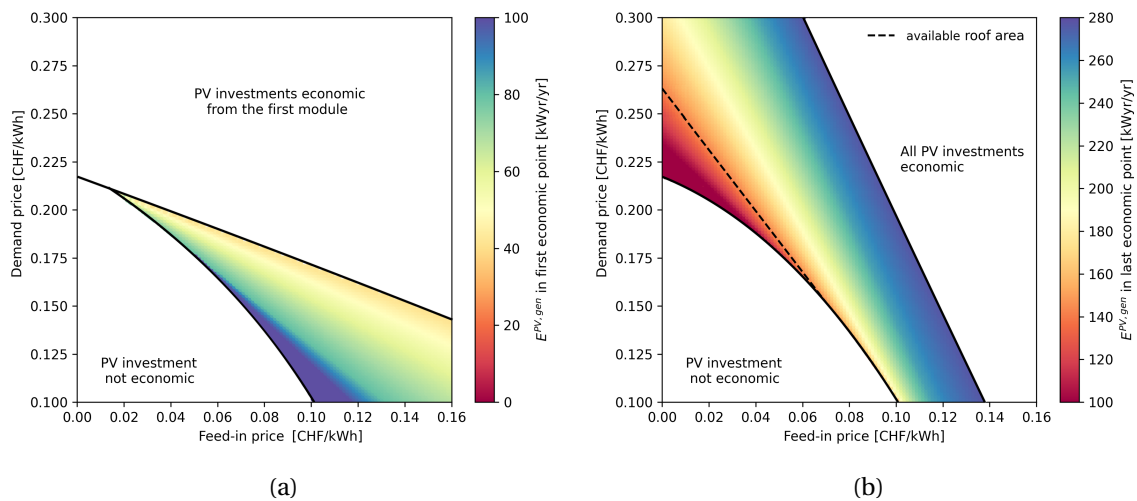


Figure 3.9 – Variation of the PV yearly generation to achieve break-even as a function of feed-in and demand prices. a) first break-even point (B1) b) last break-even point (B2 or A) in Figure 3.8.

Evidently, the location of the economic break-even point depended on a combination of the two tariffs. This can be seen more clearly in Figure 3.9, where Subfigure 3.9a shows the position of point B1 (lowest installed surface that makes the installation of PV panels economically favourable). Moving towards the upper white area would substantially mean eliminating the entry barrier to new producers, especially smaller ones. This can be achieved by a combination of feed-in and purchase tariffs. It is however more interesting to look at the position of point B2 (highest economically favorable surface) in Figure 3.9b. This figure shows the importance of increasing feed-in prices if the objective is to maximize generation. For instance, even at today's demand price, increasing the purchase price from 0.08 CHF/kWh to 0.10 CHF/kWh would theoretically make all roof and facade surfaces economically convenient. The results also show the extent of the variation. The average annual electricity generation from installed PV ranged between 100 and 280 kWyr/yr, showing that

3.3. Results and discussion

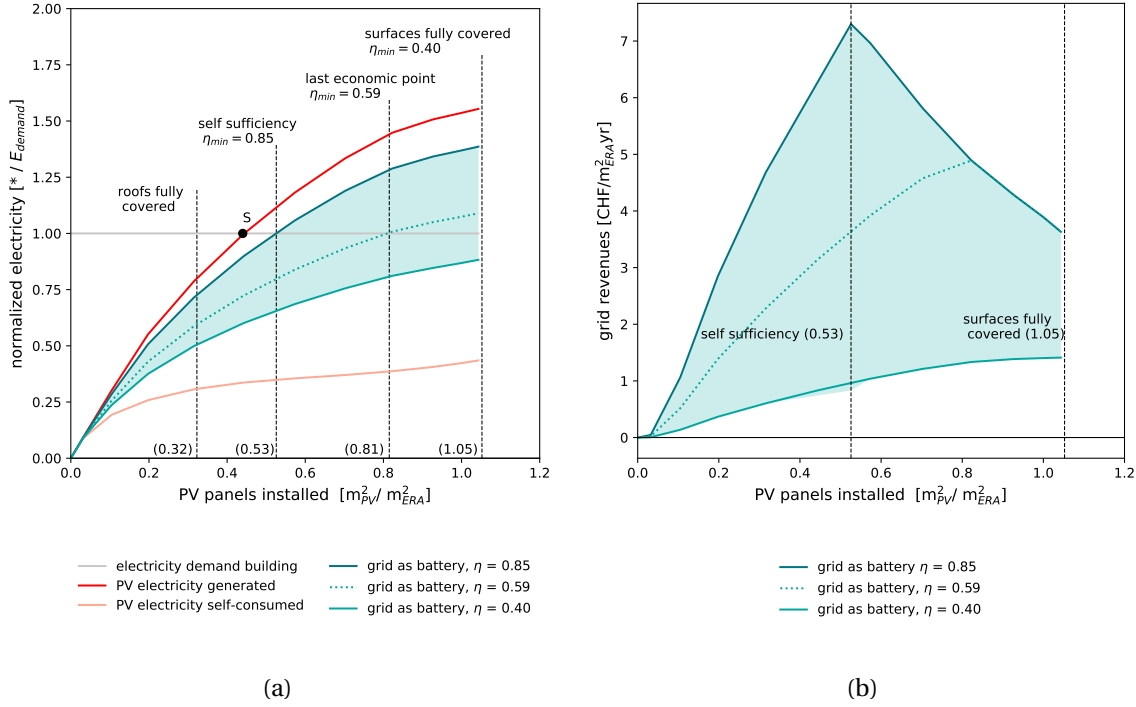
appropriately choosing electricity tariffs could lead to an increase of almost 200% of the yearly energy generated by PV panels in the district. In Figure 3.9, the dashed line represents the tipping point between the end of the roof surface available and the start of using facade surfaces. As it can be seen, even with today's energy prices, facades (at least the ones with the highest solar irradiation) could be used for PV generation profitably. Understandably, increasing demand and feed-in prices both play in favor of an increased profitability of facade surfaces. As mentioned above, at (0.20/0.10 CHF/kWh) tariffs, also north-oriented facades became potentially valid for PV panel installation from an economic perspective.

3.3.4 How much PV is needed to achieve self-sufficiency?

In previous results, it was shown that the district can achieve carbon neutrality relatively easily and with current tariffs most facades are economically feasible. But how much PV is actually needed to cover the electricity demand at all times? In fact, not all generated energy is used locally. As shown in Figure 3.7a , the SC was below 60% for all scenarios, while a significant part of the generated energy was sold to the grid and was later purchased back, thus using the grid as electricity storage. Including re-imports in the definition of SS and assuming that the grid-as-storage works with 100% round-trip efficiency led to the minimum required area of PV per energy reference area (ERA) = 0.44 (point S) to achieve self-sufficiency. Depending on the efficiency that was assumed for the grid-as-storage, the amount of surface covered by panels increased.

If the storage is assumed to be lithium-ion batteries (which would be the most likely case for district-level storage, connected to the same low-voltage grid as the district), it is possible to assume a relatively high round-trip efficiency for the grid-as-storage. In Figure 3.10 a the line for $\eta = 0.85$ can be used as reference, showing that in this case the PV surface needs to be increased only marginally. Another relevant point in Figure 3.10 is represented by the "last economic point", that is the largest amount of PV panels that can be installed with the expectation of recovering the investment within the panels' lifetime with current tariffs. The efficiency of the grid-as-storage that allows SS in this point was approximately 0.59. Incidentally, this is quite similar to the round-trip efficiency of pumped hydro storage (PHS), today the most common way of doing grid-level storage in Switzerland. Further insights about storage systems for electricity are available at [137, 138]. Finally, the case of $\eta = 0.40$ is shown in Figure 3.10, a relatively optimistic example of round-trip efficiency of power-to-gas storage systems. In this case, the results showed that the available surface was simply not sufficient, and even covering all roofs and facades with PV panels would not allow to reach SS of the district. The actual minimum efficiency that needed to be achieved by the selected combination of storage technologies to achieve SS was $\eta = 0.50$.

Figure 3.10b shows the perspective of the grid operator, when looking at the importance of the efficiency of the grid-as-storage. Grid revenues are obtained from the difference between feed-



3

(a)

(b)

Figure 3.10 – a) The need of PV panels of 31 buildings balanced at the transformer to reach self-sufficiency (SS) with re-import for different round-trip efficiencies η . Point S: full SS with ideal storage ($\eta = 100\%$) in place. b) Revenues as a function of installed PV capacity and grid efficiency from the perspective of the grid. The grid buys electricity at a feed-in tariffs of 0.08 CHF/kWh and resells for electricity price 0.20 CHF/kWh

in and purchase electricity prices, but also depend on the amount of energy that is lost in the irreversibilities of the storage charge/discharge process. The results show that the grid could have positive income even with low storage efficiency. However, the clear interest in working with high round-trip efficiency was also demonstrated from the perspective of the grid. The highest grid revenues were achieved at the point of complete SS. When the PV capacity was exceeding the need, the district did not need to purchase extra electricity but continued to sell surplus electricity, hence the grid revenues only decreased.

3.3.5 How much energy storage is needed to achieve self sufficiency?

The results shown in the previous sections highlight the fact that the district required a relevant amount of storage in order to become self-sufficient, in addition to the thermal and electricity storage systems installed in individual buildings. The actual amount of district storage required is shown in Figure 3.11b, relative to the total amount of energy locally generated by PV panels. The results show that the storage capacity required in the case of ideal storage (100% round-trip efficiency) to achieve SS was prohibitive: more than 35 kWh/m².

3.3. Results and discussion

There are different ways to decrease the need of storage. One is to increase the energy conversion efficiency (e.g. a district heating network using CO₂ HPs [7]), another possibility is to decrease the demand by retrofitting the buildings [139]. The results of this analysis are shown in Figure 3.11a. Three main scenarios are addressed:

- baseline scenario (air-source HP, actual building stock) referring to the results shown in the previous part of this section;
- improved HP case, where high-efficiency HPs using a CO₂ network as cold source; The annual coefficient of performance (COP) for the HPs in the district increased from 3.25- 3.9 to 4.1 - 4.5 by switching from ambient air to CO₂. The value depended on different operation strategies in Pareto-optimal solutions.
- renovated building stock case, with standard HPs but with isolated buildings (achieved with assumed heat transfer factor $U = 0.8 \text{ W}/(\text{m}^2\text{K})$ and design return/supply temperatures $T_0^{r/s} = 41.5/ 33.9^\circ\text{C}$ [23]);

The results show, as expected, that increasing the efficiency of the building stock, a very expensive measure [139], was the most efficient solution to decrease the amount of district-level storage required to achieve SS. For all three scenarios the maximum storage time, that is the longest time of a positive state of charge, was several months, meaning that seasonal storage was required.

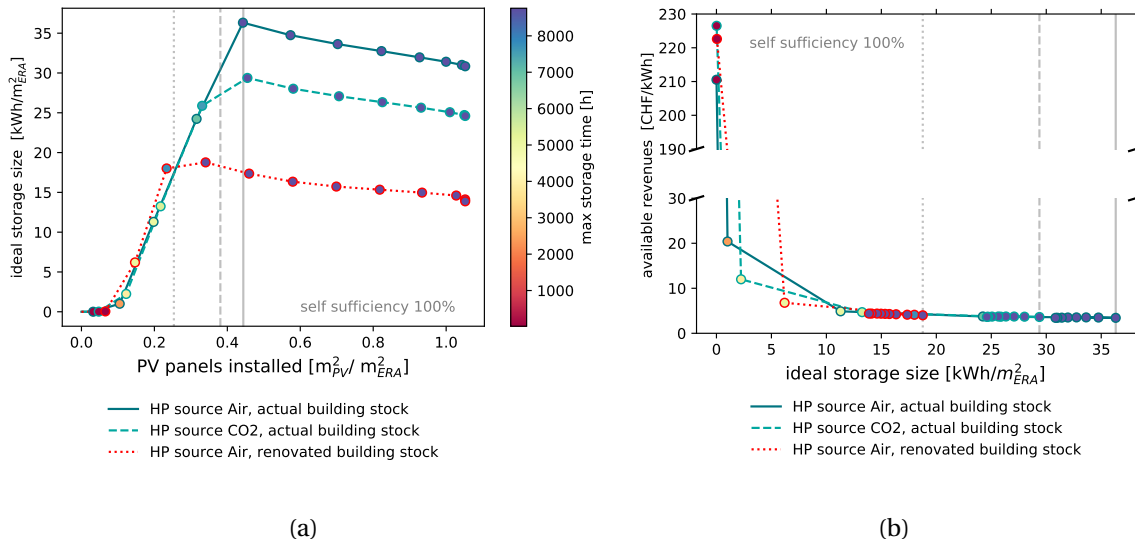


Figure 3.11 – Key identifiers of a storage system with round-trip efficiency $\eta= 100\%$ (equivalent to point S in Figure 3.10a) to store surplus PV electricity for different efficiency strategies. a) Required storage size and time. b) Directly available price form buying at feed-in tariff of 0.08 CHF/kWh and selling at for electricity price 0.20 CHF/kWh

Regardless of the type of retrofitting solution, is this much storage in the system affordable? Grid operators recur to a variety of means to store energy (from existing PHS to simply balancing the grid

with centralized power generation). However, the capacity of the medium–voltage grid is limited to host high level of PV penetration in the low–voltage grid [140]. It can be worth answering this question by looking at how much money would be directly available in the district by using the revenues generated by the different demand/feed-in electricity prices. The results of this analysis are shown in Figure 3.11b. Only the scenario with very limited PV panels installed generated notable revenues. In this case, the storage had multiple annual cycles and generated more revenues.

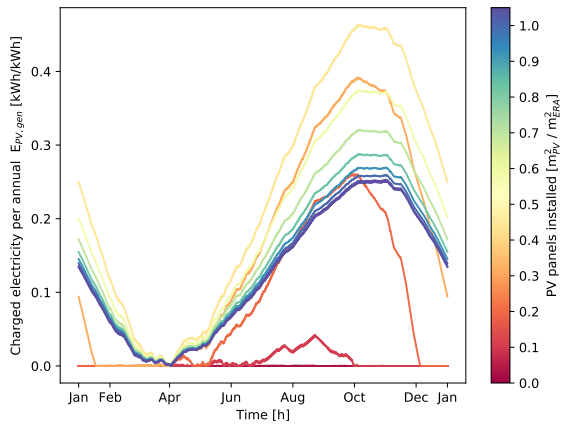


Figure 3.12 – State of charge of a storage system aiming at self-sufficiency for different levels of PV penetration.

The reason behind the sharp increase in required storage size when the PV surface installed increases can be seen in Figure 3.12. At the low range, storage was only used for daily balancing purposes, thus requiring a very limited amount of storage size. In Figure 3.12, the first line appears flat, as the required daily storage capacity was low. At higher PV surfaces installed, achieving SS requires seasonal storage. All solutions where the ratio between PV installed surface and heated surface is above approximately 20% show a demand for seasonal storage. The state of charge of the storage peaks in the end of the summer, and then gradually decreases during the winter.

3.4 Conclusion

This chapter aimed at investigating the potential of facades in interconnected renewable energy hubs. Thereby to analyse the requirements to achieving carbon neutrality and SS, by using a combination of PV electricity generation and different energy conversion units. The problem was addressed with a decentralized design strategy of a residential district, which considered a collection of renewable energy hubs at the building scale. The OPEX and CAPEX of the system were considered competing objectives, and the installed sizes and operating load of the different energy conversion units (including PV panels and batteries) as main optimization variables.

Compared to existing literature in the field, the proposed approach combines an advanced modeling

3.4. Conclusion

of the energy generation potential from PV panels with a detailed representation of the district energy systems, down to the system of each individual building, thus allowing an accurate representation of the interaction between the energy generation from PV and the rest of the system. The proposed approach was applied to a typical, central European, residential district located in Switzerland, in the proximity of the metropolitan area of Geneva. The results of the application of the proposed method are summarized in Table 3.4.

Table 3.4 – Overview of identified solutions for a future decentralized district. Self-sufficiency (SS), round-trip efficiency η of the electric storage system.

solutions	PV coverage			
	A_{PV}/A_{ERA}	roof	facade	total
full PV roof coverage, SS= 75%	0.32	100.0%	0.0%	30.5%
full SS, $\eta=100\%$	0.44	100.0%	16.4%	41.9%
full SS, $\eta=85\%$	0.53	100.0%	28.8%	50.5%
carbon-neutrality	0.62	100.0%	41.0%	59.0%
full SS, $\eta=59\%$	0.81	100.0%	67.1%	77.1%
full PV coverage, SS with $\eta=50\%$	1.05	100.0%	100.0%	100.0%
full SS solutions with $\eta = 100\%$	storage capacity		PV coverage	
Air HP	35.0 kWh/m²_{ERA}		41.9%	
CO ₂ HP	29.0 kWh/m ² _{ERA}	(-17.1%)	36.2%	(-13.6%)
Building envelope renovation	18.8 kWh/m ² _{ERA}	(-46.3%)	23.8%	(-43.2%)

3

Facade PV specific energy potential Facades had a high theoretical potential, based on their surface compared to roofs: the total facade surface in the district summed to about twice as much than that of rooftops. However, the less optimal orientation towards the sun and the shading among buildings had the effect of significantly worsening their electricity generation potential. Overall, however, the installation of PV panels on facades had the potential of increasing the total energy generated by approximately 97%.

PV placement order The results of the multi-objective optimization showed that, as expected, PV panels were prioritized on roofs (first horizontal, then south-west-east-north) and only then on facades (south, west/east, north). This was clearly due to the higher specific energy generation potential of roofs compared to facades. The moment of the day when solar power is generated counted only to a smaller extent.

Solar-driven district carbon neutrality Facades could play an important role in the energy systems of districts. The results of the multi-objective optimization showed that it was relatively cost-efficient to achieve carbon neutrality, but that this was only possible if PV panels were also installed on facades, based on the current energy conversion units and building stock. Further additions of PV panels and batteries allowed for the reduction of operating costs but

had little effect a further reduction of the total GWP of the energy system.

Economic convenience of facade PV Facades were costly, and less cost-efficient compared to rooftop solar. However, the results of the analysis of the influence of electricity prices (both for purchasing electricity from the grid and feed-in) showed that there were many combinations of tariffs that make facades economically convenient over their lifetime. These results thus highlighted the influence that electricity prices have on the maximum PV surface that can be covered while still being economically viable. Current tariffs would allow up to 80% of the total available surface to be covered.

Achieving district self-sufficiency Reaching SS based on PV electricity alone requires the installation of storage systems. Depending on the assumption for the round-trip efficiency of the grid considered as a storage unit, it was more or less challenging to achieve SS for the district. SS could be achieved by covering from approx. 40% to 100% of the available surface when the round-trip efficiency decreased from 100% to 50%.

Storage requirements The results underlined the importance of storage for achieving SS, and the fact that even when assuming a 100% round-trip efficiency for the storage, very large storage capacities were required. The results also showed that the grid revenues generated by the difference between retail and feed-in prices were not sufficient to pay for the storage that is required to make the district self-sufficient, suggesting that public funding would be crucial for supporting these developments. This was true already at relatively low installed PV capacity ($A_{PV}/A_{ERA} = 0.2$), when storage started to be required for seasonal instead of daily storage, thus increased dramatically the required capacity and storage time.

The role of building renovation Of the solutions tested in this study, building renovation, with its important effect of energy demand reduction, was identified as the most promising in synergy with PV generation. This is because building renovation allowed for the reduction of both the required installed PV and storage capacity to achieve SS by half.

Computational reduction for centralized energy systems

Overview

- Two methods to reduce computational effort for complex energy systems
- First method: time-series aggregation (TSA), with simultaneous detection of outliers
- Second method: decomposition algorithm for multi-objective optimization of district energy systems
- Runtime reduction for calculating districts on the scale of low-voltage grids

The content of the first part of this chapter is published in [141, 142]. The second part is submitted to [143] (in Review).

Optimal design and scheduling of energy systems with a high share of renewables is a complex and computationally demanding task. The mismatch of supply and demand of energy requires the consideration of timeseries with a granularity of a few minutes, which is in contrast to the lifetime of the system of multiple decades. This chapter proposes two algorithms for systematically reducing computational efforts of district energy system (DES). The first algorithm reduces the input data by exploiting the two-stage nature of the optimal design and planning of the system and sequentially performing k-medoids clustering. Unlike the state-of-the-art, the influence of different numbers of typical periods is not examined on the quality of the clustering algorithm but on the objective function and the integer decisions. The solution time of the multi-objective optimization (MOO) could be reduced by approximately 90%, while diverting less than 2% on Pareto-optimal solutions. However, the comparison of two case studies with different levels of complexity demonstrated that this method was not reducing the computational effort sufficiently enough. Therefore, a second algorithm is proposed, which is a Dantzig–Wolfe decomposition. Contribution to the state-of-the-art is a formulation for multi-objective optimization, which also allows an improvement of the initialization of the algorithm. The method is validated with the compact model formulation of the same problem. Results show that the decomposition method diverted less than 0.02% but reduced the solution time sufficiently in order to calculate whole low-voltage distribution grids.

4.1 Introduction

The energy sector is currently facing multiple transforming forces. In the context of rising concerns for anthropogenic CO₂ emissions, the integration of renewable energy sources is becoming an increasingly widespread solution for reducing the carbon footprint of energy systems [144]. The optimal integration of renewable resources in energy systems is a complex task, as both aspects, optimal scheduling of operation as well as strategic planning of system design, have to be considered side by side. Energy system optimization using mixed-integer linear programming (MILP), where an integer represents the decision for or against installing a technology, is a widely adapted framework. The mismatch of availability of renewable energy sources and demand of energy requires the consideration of time-series data with a resolution of a few minutes, which is in contrast to the lifetime of the system of multiple decades. The challenge of the inclusion of unit decisions, a project horizon of several decades as well as hourly time-series results in not only the need of a large amount of data. It also leads to extensive computational problems.

To make the problem computationally tractable, simplifications have to be either made in the spatio-temporal dimension, that is reducing input data, or in techno-economic dimension [46]. Latter corresponds to the reduction of complexity of the modeling framework itself. This chapter considers both aspects. In the first part, a novel time-series aggregation method is introduced to systematically reduce input data. In the second part the Dantzig-Wolfe decomposition approach is applied, which splits the complex problem into several pieces. Hence, it reduces the complexity of each single problem.

4.2 Time-series aggregation

This section proposes an algorithm for systematically reducing the input data and therefore the computational effort for solving MILP of energy systems. Before the method is detailed, an overview of the state-of-the-art is provided. The section finishes with a demonstration of the algorithm on two case studies with different complexities.

4.2.1 State-of-the-art

The aggregation of time-series to typical periods is specifically popular, as patterns occur naturally in the supply and demand of energy, which arise in the time dimension through hourly, daily and seasonal cycles. A recent comprehensive review by Hoffman et al. [46] analyzed TSA methods for modeling energy systems applied in 130 different publications. Schütz et al. [47] compared different aggregation methods for the selection of typical demand days, such as k-means, k-medians, k-centers, k-medoids, seasonal and monthly based classifications. Hoffman et al. and Schütz et al. [46, 47] showed that the more intuitive aggregation methods of seasons or months led to signifi-

4.2. Time-series aggregation

cantly larger errors than machine learning methods for the same computation time. Algorithms within the latter category performed similarly well, although k-medoids were the most reliable for approximating costs.

The first challenge of aggregation of time-series is usually to identify the optimal number of typical periods. State-of-the-art approaches in modeling complex energy systems almost exclusively based their decision on key performance indicators (KPIs) of the clustering algorithm itself, e.e., the sum of squared errors (SSE), root mean square deviation (RMSD), mean average percentage error (MAPE) or silhouette index for defining the length and amount of typical periods [22, 145, 146]. However, this procedure dis not provide sufficient guarantee of aggregation quality with respect to application to the energy system optimization. This procedure considered neither the influence on its optimal objective value, nor the unit choices. Therefore, Brodrick et al. [147] considered the change of unit decision while increasing the amount of typical periods next to the SSE of the k-means algorithm. Schütz et al. [47] showed that the typically applied assessment of the aggregation by using SSE was not sufficiently suitable for energy system synthesis problems. Therefore, Bahl et al. [148] developed a systematic method for bounding the error of the aggregation in the objective function. This has laid the foundation for a rigorous formulation of time-series relaxation and aggregation comprising a method for effectively including seasonal storage [149, 150]. The mathematically rigorous formulation [149] creates an upper and lower bound of the objective function and iterates the procedure by increasing the resolution of TSA until an optimal gap criterion is met.

As a final step, extreme periods are added to the aggregated time-series [145]. These extreme periods serve as protection or guarantee that the energy system can still provide the required services in these extreme situations. Therefore, extreme periods were often given by national regulations and were added in a post-processing step and were not further analyzed [38, 146, 151].

4.2.2 Gaps and contributions

Previous review of the state-of-the-art allows concludes that machine learning algorithms for data reduction techniques are not very well integrated in the optimization technique of complex energy systems. Thus, a new iterative procedure of TSA is proposed, which evaluates the influence of the clustering algorithm on the objective function as well as on integer variables.

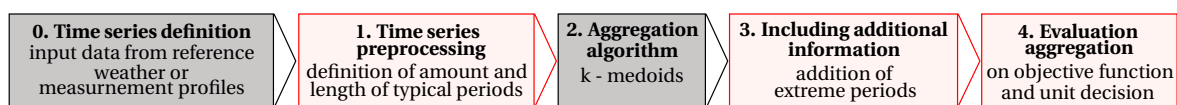


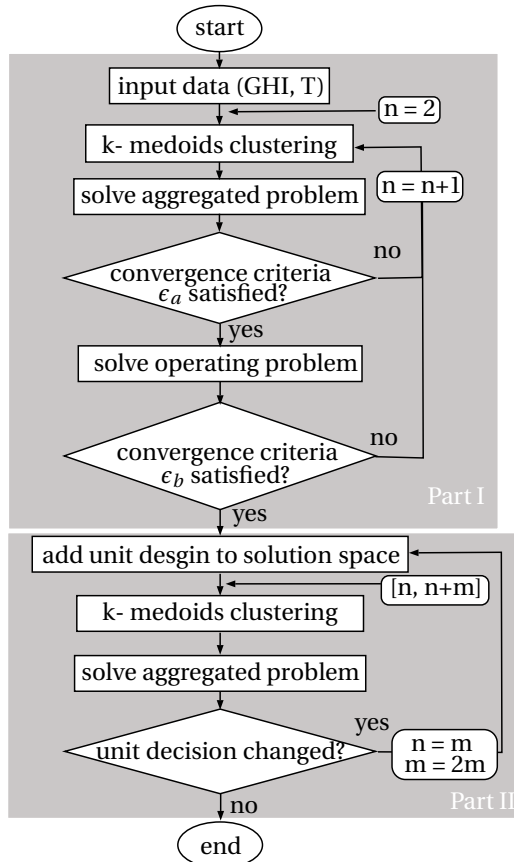
Figure 4.1 – Procedure of TSA with steps discussed in this chapter highlighted in red

An overview of the usual steps involved in TSA is provided in Figure 4.1. In the figure, the steps, which

are modified in comparison to the current state-of-the-art, are highlighted. Recent work identified the k-medoids algorithm as the most reliable for economic evaluation of energy systems [46, 47]. Hence, the k-medoids algorithm is chosen as the aggregation method in step 2 (see Figure 4.1). Another challenge is TSA for complex energy systems is in general overlooked: the role of extreme periods. The extreme periods have an influence on the installed capacity of energy technologies. This chapter additionally investigates the role of outliers, which serve as extreme situations for the energy system. In this chapter, the aggregated problem (AP) is the energy system optimization based on typical periods, whereas the operating problem (OP) is the optimization of only the operation, with fixed unit decisions, on a full time-series.

4.2.3 Method

An overview of the proposed algorithm is displayed in Figure 4.2. It consists of two parts; of which the first focuses on the objective function evaluation, whereas the second evaluates the integer decision variables.



Algorithm part 1 The first part is characterized by an iterative process with two separate convergence criteria on the value of the objective function. With every iteration the percentage change between the solution of the aggregated problem (AP) based on k-medoid clustering between n and $n-1$ clusters is calculated. Only when the first convergence criterion, $|\epsilon_a| \geq \frac{AP_n - AP_{n-1}}{AP_n}$, is met, the operating problem (OP) on the full time-series but with fixed unit sizes is solved. Subsequently, the second convergence criterion $|\epsilon_b| \geq \frac{OP_n - AP_n}{AP_n}$ is evaluated. The iteration continues with the calculation of both problems until the second criterion is also valid. Finally, the sizing and selection variables are added as a result to the solution space.

Algorithm part 2 The second part is initiated with the first element, characterized by n clusters in the solution space. The purpose of the second part is to compare the integer decisions and possibly add new elements to the solution space that provide different unit choices, but have a similar value of the objective function. Therefore, the AP is calculated with

Figure 4.2 – Overview of the iterative procedure for systematic input data reduction

$n + m$ steps. If the unit decisions remain unchanged, the TSA is terminated with n typical periods.

The following list details the definition and a possible choice of tuning parameters:

- Convergence criterion $|\epsilon_a| \geq \frac{AP_n - AP_{n-1}}{AP_n}$: Variation between the solution of the aggregated problem between n and $n-1$ clusters;
- Convergence criterion $|\epsilon_b| \geq \frac{OP_n - AP_n}{AP_n}$: Variation between the solution of the aggregated problem of n clusters and the non-aggregated operating problem with fixed unit decisions from the aggregated synthesis;
- Number of additional iterations comparing unit decisions m .

Outlier detection Similar to the method developed by Liu et al. [152], outliers are detected during the process of clustering. The procedure is as follows:

1. Clustering of the data set
2. Calculation of the Euclidian distance from all periods to their centroid
3. Removal of o outlier periods with the largest distance to their centroid from the data set
4. Repetition of steps 1-3 until centroids do not change anymore.

The detected number of o outliers are added as individually occurring typical periods to the optimization problem. In contrast, demand peaks remain as extreme periods. As the current standard in the optimization of energy systems, presented by Stadler,[22], one cold weather and one hot weather period is added, both consisting of one single timestep.

4

4.2.4 Case study

Two case studies with different levels of complexity demonstrate the usefulness of proposed procedure. The first case study is a typical Swiss building located in the climatic zone of Geneva. The building is a residential, single-family home with 2 floors and in total 250 m^2 energy reference area (ERA), built around 1950. The considered energy demands are: electricity demand, thermal demand for space heating and hot water. The optimization is formulated as a MILP problem with the aim of finding the optimal sizing and operation among nine energy conversion and storage technologies. For further insights on the modeling approach of the building energy system (BES), the reader is referred to Chapter 1. Potential installation of photovoltaic (PV) panels are assumed to be horizontally oriented. Over a full time-series of one year, this case study leads to over 830 thousand constraints and 780 thousand variables, among which are almost 9000 binaries.

The second case study includes the same building plus the 4 neighboring buildings, all residential buildings, among which one multi-family home and 3 additional single family homes built between 1950-2000. Additionally, all allocated roof surfaces are considered for possible PV panel installations,

leading to 24 different roofs and their orientations to choose from. The modeling approach for orienting PV panels is reported in Chapter 2. The second case study, for a full time-series of one year, sums up to over 4.1 million constraints, almost 4 million variables among which are almost 44000 binaries.

The tuning parameters of the algorithm are set to be $\epsilon_a = 5\%$, $\epsilon_b = 5\%$ and $m = 3$. The k-medoids clustering with the R package *wcKMedoids* is performed for aggregating one typical year [48]. The problem is formulated in AMPL and solved with CPLEX 12.9.0.0 on a local machine with the following processor details: Intel(R) Core (TM) i7-8559U CPU @ 2.70GHz. The relative tolerance between the relaxed linear problem and the best integer solution is set to $\text{mipgap} = 5e-7$. The remaining CPLEX settings are equal to the default settings reported in [153].

4.2.5 Results and discussion

In a pre-processing step, global irradiation (GHI) and the external temperature (T) are clustered to different numbers of k-medoids. The length of one typical period is chosen to be 24h. Figure 4.3 displays the quality of the aggregation. The common procedure for selecting the amount of typical periods is to define a slope threshold of the KPIs. A slope threshold of 10% would lead to around 10 typical periods. Thus, the result of the proposed TSA is compared to 10 typical periods in the following.

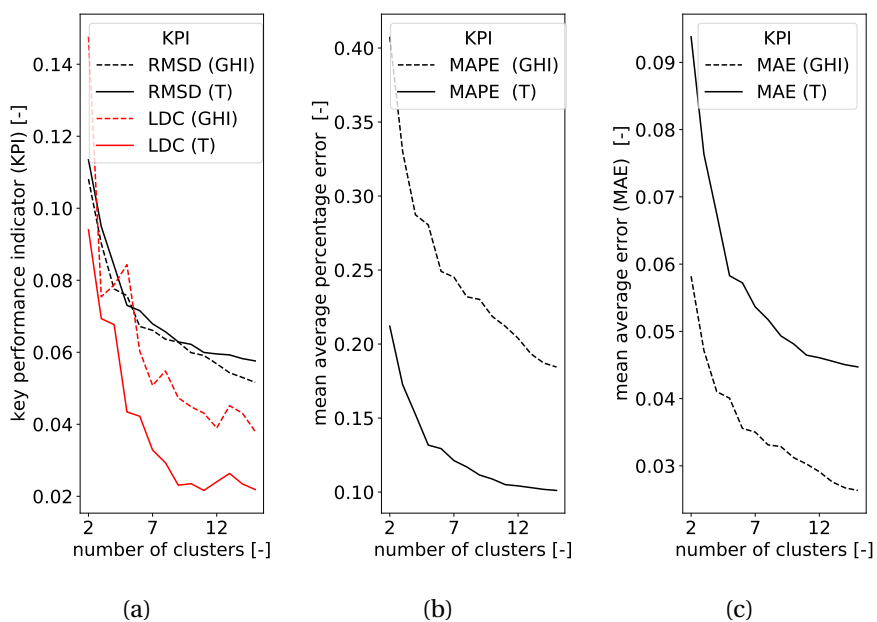


Figure 4.3 – Key performance indicators (KPIs) of the k-medoids clustering of global irradiation (GHI) and the external temperature (T). a) Root mean square deviation (RMSD) and difference on the load duration curve (LDC) b) Mean average percentage error (MAPE) c) Mean average error (MAE).

4.2. Time-series aggregation

Algorithm part 1 First, the AP with an increasing number of clusters is solved. The objective function is total expenses (TOTEX), which is equally weighting the two conflicting objectives, operational expenses (OPEX) and capital expenses (CAPEX), of the MOO. Figure 4.4 demonstrates Part 1 of the proposed algorithm for the first case study, about one typical residential building.

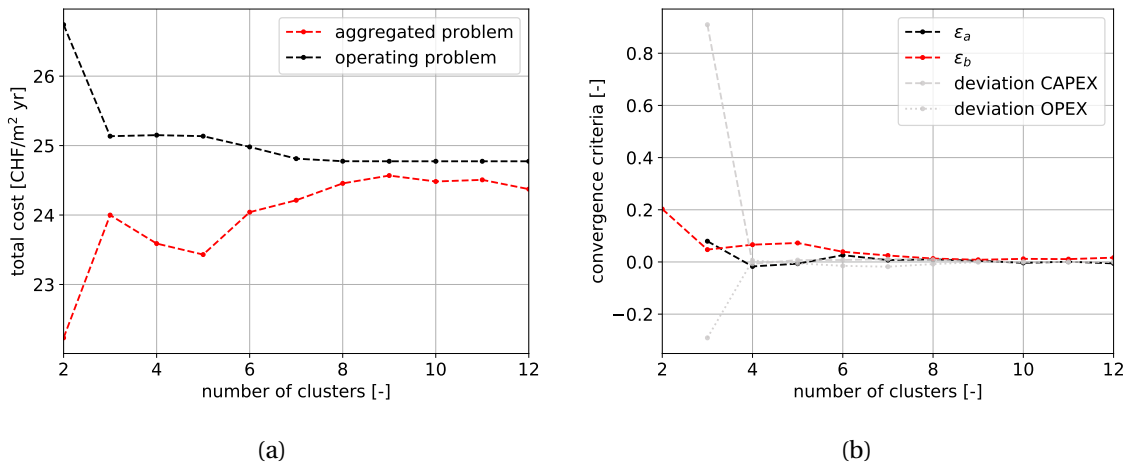


Figure 4.4 – Demonstration of Part 1 of the TSA algorithm, case study with one building and TOTEX objective. Impact of a different number of clusters on a) the objective function b) the convergence criteria ϵ_a and ϵ_b , as well as deviation of CAPEX and OPEX to $n - 1$ clusters.

The algorithm started with two clusters. To be able to observe the relative change of the objective function, the AP was immediately solved for three typical periods. Already, after three clusters the convergence criterion ϵ_a was approximately 5%. The unit decisions were fixed and OP on the full time-series was solved. The second convergence criterion ϵ_b was also below 5% and therefore three typical periods were chosen as result of Part 1. For demonstration purposes, the AP and OP on the full time-series was solved up to 12 typical days. After seven typical days, the difference of the objective functions, which is the second convergence criterion, remained below 1%.

Figure 4.5 visualizes the demonstration of Part 1 of the algorithm for the second and more complex case study.

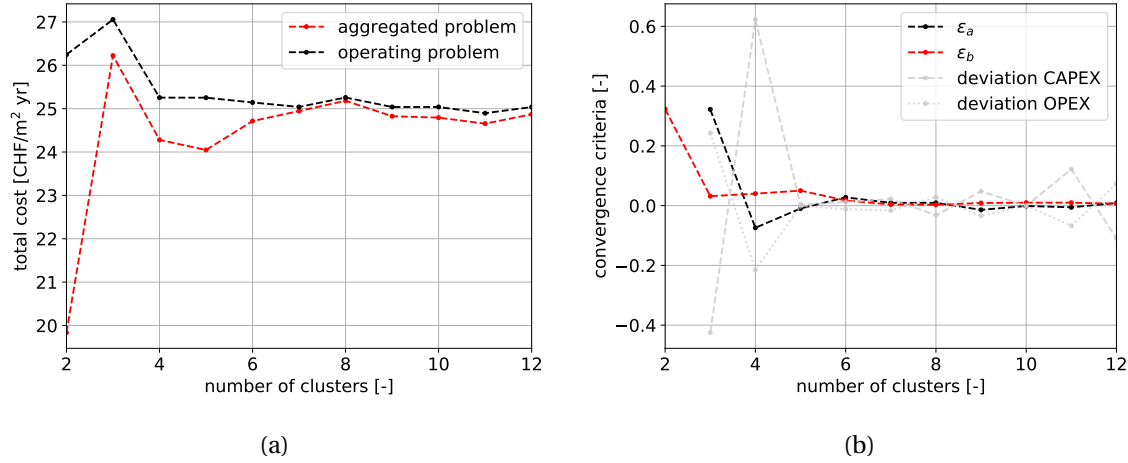


Figure 4.5 – Demonstration of Part 1 of the algorithm, case study with five buildings and TOTEX objective. Impact of a different number of clusters on a) the objective function b) the convergence criteria ϵ_a and ϵ_b , as well as deviation of CAPEX and OPEX to $n - 1$ clusters.

4

For three clusters the first convergence criteria ϵ_a was over 30% and not satisfactory. Thus, one additional cluster was added. For four clusters ϵ_a was reaching 5%. Hence, the OP was solved, which led to $\epsilon_b = 4\%$. For the second case study, four typical days seemed appropriate for initiating the second part of the algorithm.

Algorithm part 2 The aim of Part 2 of the algorithm is to confirm that the unit decisions are sufficiently taken with the detected number of typical periods (see Figure 4.2). Figure 4.6 shows the unit decisions, which are taken for different number of clusters.

For the first case study (Figure 4.6a), an heat pump in combination with an electrical heater and thermal storage tanks was detected as the most economical decision for two clusters. For three clusters, PV modules were additionally installed. This configuration stayed the same for all further investigated number of clusters. Therefore, the three typical periods could be confirmed and further used during MOO. Figure 4.6b visualizes Part 2 of the algorithm for the more complex case study of 5 residential buildings with individual roof orientation. For the suggested number of four clusters, the unit decisions were heat pumps, additional electrical heaters for peak loads, thermal storage tanks and PV panels. These decisions stayed the same for the observation period of $m = 3$ and the TSA could be ended with four typical periods for the second case study.

Multi-criteria decision making The overall goal is to propose a TSA method, which is usable not for only a single run of one objective, but which can be used for all further investigations in the MOO domain. Therefore, this section is presenting the performance of the demonstrated TSA in context

4.2. Time-series aggregation

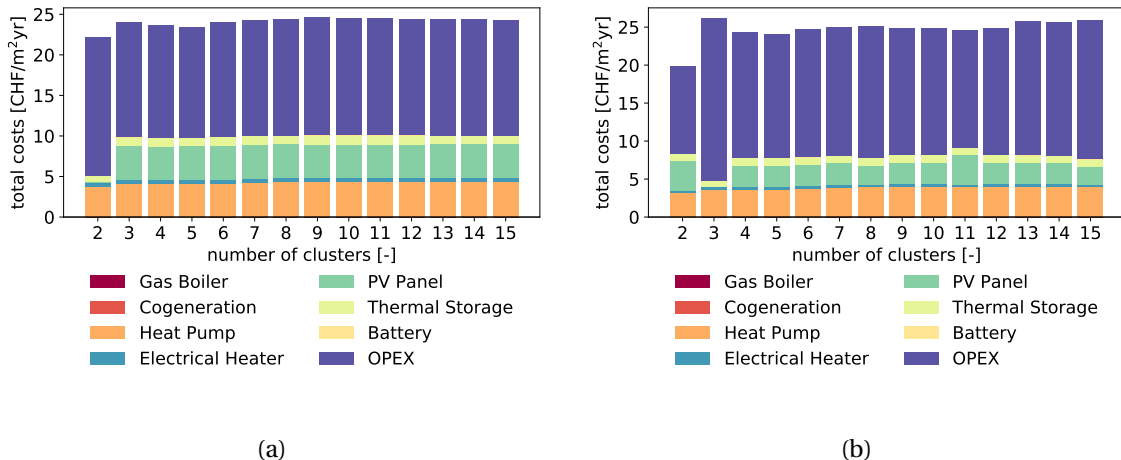


Figure 4.6 – Overview of unit decisions for the aggregated problem (AP) with different number of typical periods for minimizing TOTEX. a) Case study with 1 residential building. b) Case study with 5 residential buildings. Total costs are normalized by the ERA.

with the MOO of case study 1. Figure 4.7 compares the Pareto frontiers of aggregated problems to their corresponding, not aggregated, problem, which is the operating problem on a full time-series. Additionally, the difference of two APs is analyzed; The result of the proposed TSA method (three typical periods) is contrasted with the result of state-of-the-art approach (10 typical periods).

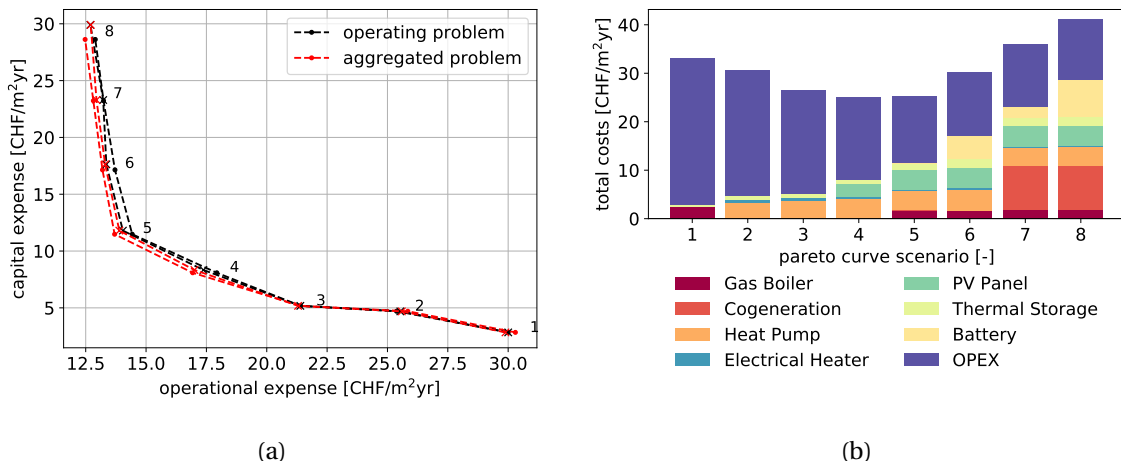


Figure 4.7 – Multi-objective optimization of one the energy system for one building. a) CAPEX - OPEX Pareto frontier; Aggregated problem (AP) with 10 typical periods (x) and 3 typical periods (•). b) Unit choices along Pareto frontier scenarios.

The CAPEX ranged from approximately 3 CHF/m² (Scenario 1) to almost 30 CHF/m² (Scenario 8). The unit decision of Scenario 1 was based on natural gas, only using a gas boiler and small thermal storage tanks. For this Scenario, the AP and its linked OP was almost identical on the Pareto frontier (Figure 4.7a). In contrast, the unit decision for Scenario 8 was more diverse and included

renewable energy sources such as PV panels and a heat pump but also thermal and electrical storage systems (Figure 4.7b). The performance of these units were all depending on the weather data or, in terms of the storage, the optimal scheduling within one typical period. Nevertheless, comparing the OPEX of the AP and the linked OP showed a deviation by only 3%. The difference among the AP with three typical periods and with 10 typical periods was less than 2%. Also in this comparison, the maximum difference was occurring in higher investment scenarios, which was based more on renewable energy sources.

The role of outliers K-medoids clustering is a method, which is itself robust to outliers. Therefore, the centroid is not changing during the detection of outliers. Nevertheless, seven outliers have been identified and added to the typical periods. Figure 4.8 demonstrates the impact of outliers on the MOO of the energy system.

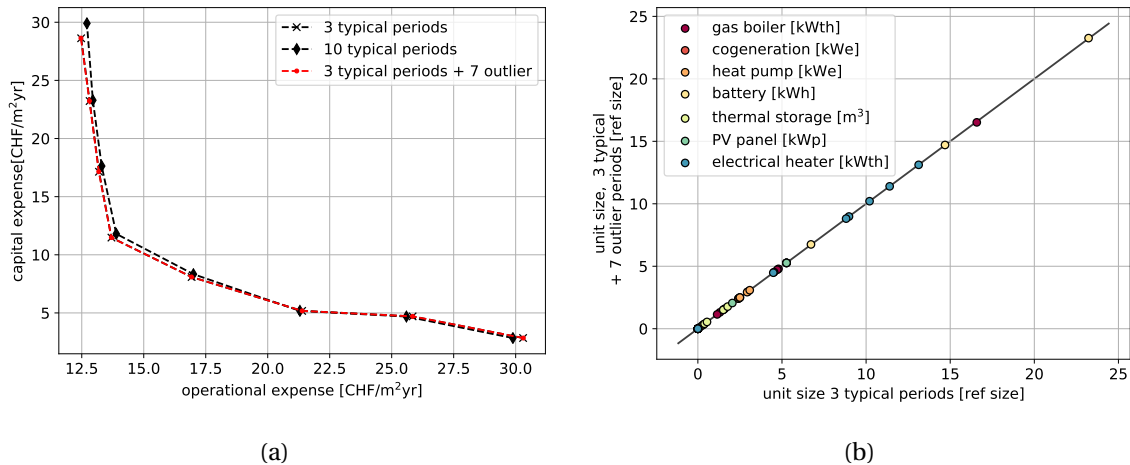


Figure 4.8 – Comparison of multi objective optimization with and without detected outliers. a) CAPEX- OPEX Pareto frontier b) Parity plot of all unit decisions along the Pareto frontier.

Along the Pareto frontier, identical unit decisions were taken and the Pareto frontier with and without seven outliers were identical. Outliers did not seem to have influence on the techno-economic assessment of the energy systems. However, Figure 4.9 shows an important impact of outliers.

Figure 4.9 visualizes the electricity exchange with the local distribution grid for both a low-investment and a high-investment scenario. The difference between these scenarios was not only related to costs, but furthermore to the increased share of renewable energy sources and the installed storage capacity. Both latter aspects led to reduced grid exchange. Outliers revealed electricity peaks of the grid exchange, which were higher than during typical periods. Hence, outliers may not be relevant for the thermal energy side of the system nor the unit decisions. But in future energy systems with a high share of renewable energy sources, they might need to be considered for a secure integration of decentralized energy systems.

4.2. Time-series aggregation

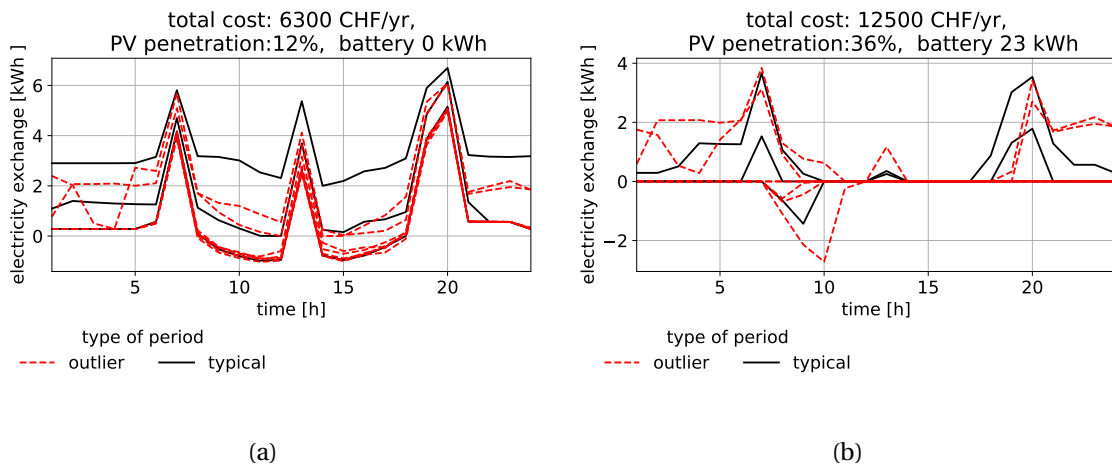


Figure 4.9 – The role of outliers on the electricity exchange for energy system designs with a) a lower investment and b) higher investment and greater share of renewable energy integration.

Solution time The computational effort of the proposed approach is shown in Figure 4.10.

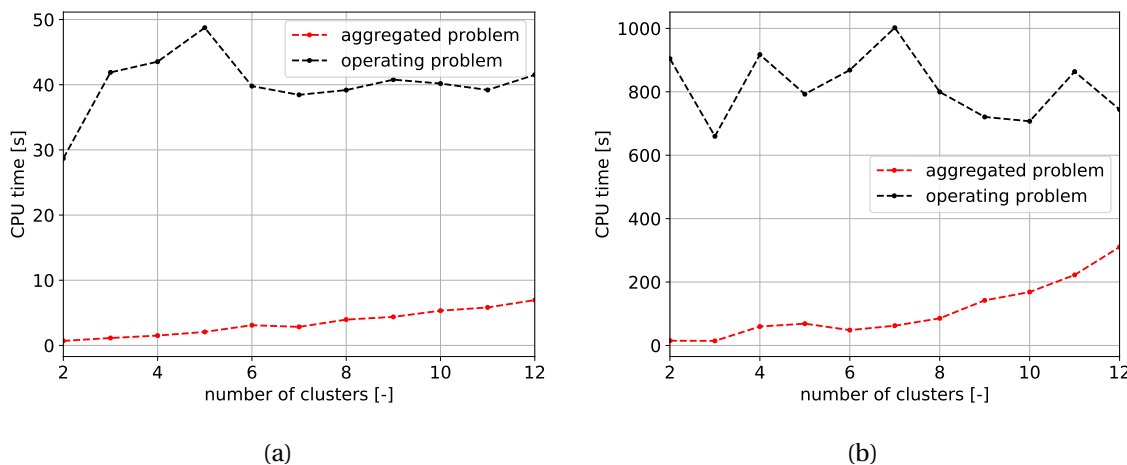


Figure 4.10 – Computation time of aggregated time-series including unit decisions (red line) and the operation problem of the full time-series, without unit decision (black line) a) Case study 1 (one building) b) Case study 2 (five buildings).

Applying the method proposed by Bahl et al. [151], the solution of the AP took seconds or up to a few minutes, whereas the solution of OP consistently took about four times longer. Due to a simple elimination of time consuming computing steps, the proposed framework reached lower total computational times. Table 4.1 summarizes the CPU time for the TSA as well as for the application during the presented MOO and compares it to the respective state-of-the-art.

The proposed method for TSA was reducing the CPU time by 40% and even for 61% for the more

Table 4.1 – Difference (Diff.) of the CPU time of the proposed approach to the state-of-the-art.

		Case study 1		Case study 2	
		CPU time [s]	Diff. [%]	CPU time [s]	Diff. [%]
TSA	state-of-the-art [151]	72	100	2570	100
	proposed approach	43	60	1000	39
MOO	state-of-the-art [22]	96	100	2870	100
	proposed approach	9	9	380	13

complex case study 2. This demonstrates the benefit of the method particularly for complex energy systems. Furthermore, the proposed approach led to a significantly lower number of required typical periods than what was reported in the state-of-the-art procedure. Using the k-means aggregation method on the annual heating demand, Fazlollahi [146] identified 13 typical days, whereas k-medoids clustering of the weather data revealed eight typical days for Stadler [22]. The proposed TSA algorithm detected three and four typical periods for Case study 1 and Case study 2, respectively. This reduction of the required typical periods led to a decreased CPU time of around 90% for the application to MOO. However, even when applying the proposed TSA, the run-time increased by over a factor 40 due the increase in complexity between the case studies.

4

4.2.6 Main findings

This chapter proposes a novel method for TSA of complex energy systems. Compared to state-of-the-art approaches in this field the CPU time was reduced by 40% in the presented case studies. This was achieved by using two convergence criteria, which avoided the computationally intensive computation of the OP at each iteration step. An additional innovation is to take unit decisions into account, which allows for the application of the TSA method to MOO problems.

In contrast to comparable work in MOO of energy systems, the selection of the appropriate number of typical days is not based on KPIs evaluating the underlying machine learning algorithm. Hence, the presented TSA method allowed for a significant reduction in the runtime, by more than 90%, while diverting less than 2% on optimal solutions. The impact of the TSA on optimal solutions was greater, the more renewable energy technologies were included in the system. For systems with a high share of renewables, outliers revealed electrical peaks, which were greater than during typical periods. Outliers were however neither impacting the thermal energy side nor economic evaluation of presented MOO problems. One possible extension of this work is to analyze the impact of the tuning parameter of the proposed TSA method. Additionally, the usage of one typical year to represent a project horizon can be questioned. This includes the challenge of predicting changing weather, which is subject to climate change. The comparison of the solution time between the two case studies shows that the runtime increased by a factor of 40 by adding only four buildings. Calculating an entire district, which consists of 30 or more buildings seems computationally not

4.2. Time-series aggregation

affordable, even with the proposed TSA. The problem needs to be decomposed to reduce solution time even further. The decomposition is addressed in the next Section 4.3.

4.3 Decomposition algorithm

This section proposes a reduction of complexity in order to overcome the runtime issue of MILP energy system models. In contrast to reducing input data, this section details a decomposition strategy of the model formulation. Before the method is detailed, an overview of the state-of-the-art is provided. The section finishes by the validation of the decomposition approach. The application of the method is then demonstrated in Chapter 5.

4.3.1 State-of-the-art

The options for reducing the complexity of renewable energy hubs at the district scale, which are referred to as DESs optimization models in this chapter, can be divided into four categories: 1) aggregation of buildings 2) pre-selection of equipment 3) heuristic methods, including the bi-level decomposition 4) all other decomposition methods. All four categories are detailed in the following with the goal to identify the best method to simultaneously design and schedule DESs.

One option to overcome runtime issues is to consider a top-down approach, which is based on aggregated economic and socio-demographic indicators and was demonstrated by Li et al. [154]. This approach was a convenient way to estimate the energy consumption of large urban areas and usually used for energy policies [154]. The top-down approach had a low spatial resolution and the energy needs were often assumed to be supplied by centralized units. An alternative was applied by Stadler [22]; the reduction of the spatial resolutions and aggregate typical buildings. Whereas it effectively decreased the computation time, it oversimplified the problem and rendered the individual BES design impossible. Neglecting for example individual roof surfaces for the installation of PV panels led to an error which ranges from -12% to +20% for the generated electricity [52]. Therefore, this approach is not suitable for distributed energy systems that require a low-level detailed formulation.

Another option is to pre-select equipment, and hence reduce the complexity. In the context of DES, the distributed equipment was usually pre-selected in the literature. The resulting load curves were fixed as in the work of Lu et al. [155] or fixed and aggregated by Ma et al. [55]. The demonstrated benefit was that it allowed a detailed focus on the network, to optimize control strategies or design centralized plants. This strategy however neglected the optimal design and operation of distributed units. Another form of pre-selection is applied in two-stage approaches, which leverages on the two-level character between design and operation variables of the MILP framework. Wakui et al. [156] designed the units in the energy system in the first stage, which were then fixed in the second step. The second step is to optimize the operation of the network.

Heuristic methods are commonly used to solve large-scale problems which include renewable energies [157]. The advantage is that they allow a simultaneous optimization of design and operation.

4.3. Decomposition algorithm

A generic algorithm was identified as a robust method for solving MOO problems of complex thermal power plants by Wang et al. [158]. The disadvantage of heuristic methods is, that they are not guarantee to find the global optimum and the convergence time remains elevated [159].

Decomposition methods are seen as the best candidates to handle the increasing complexity of energy system models. A good overview about mathematical decomposition methods was provided by Grossmann [160]. The main and most common approaches are bi-level, Benders, Lagrangean decomposition and the rolling horizon strategy [160]. In a bi-level decomposition, the optimization of decision variables is split into two problems, the upper and lower level. At each level, only one part of the variables are optimized, while the other part is fixed as parameter. The advantage is the reduction of the problem size at each level. However, the lack of optimization coordination between the two levels resulted in the same drawbacks as the heuristic methods [159]. The difference between Benders and Lagrangean is that the former treats linking variables and the latter linking constraints. The problem would be fast to solve without these linking terms. Hence, the master problem (MP) in these decomposition problems handles the linking terms and the subproblems (SPs) are the independent sub-parts of the original problem. The advantages of these methods are the convergence guarantee and speed, and the ease to scale up the optimization problem with the parallelization of the SPs [161]. The drawback of the Benders decomposition is the inability to handle integer variables in the SPs [162]. The proposed solutions overcame the issue for a limited amount of integers [163], but remained insufficient for the optimization of DES.

Ondock et al. [164] applied the Lagrangean method to simultaneously design and operate a combined heat and power (CHP) plant in a residential district. For the application in distributed energy systems, the Lagrangean decomposition was further developed into the alternating direction method of multipliers (ADMM) and the Dantzig–Wolfe decomposition [165]. The ADMM is an extended version of the augmented Lagrangean method, solving optimization problems that can be split into two main objective functions. The shared decision variables are duplicated and linked with an equality constraint. The advantages are the convergence guarantee and speed [166, 167]. However, the number of splits, which can be performed is limited to two [168]. Additionally, the ADMM was outperformed by the Dantzig–Wolfe decomposition [169].

In the Dantzig–Wolfe decomposition, the linking constraints are not limited to the objective function and are forming the MP. The independent SPs are generating the decision space for the MP in an iterative process. This method allows for the individual design and scheduling of distributed and centralized energy units, and overcomes the scalability issue of the ADMM [161]. Also, the Dantzig–Wolfe decomposition is intentionally designed for linear problems. However, Schütz et al. [122] demonstrated that integers in SPs led to near optimal solutions, diverting less than 1.8% in calculations with a MIP gap of 1%.

Also, the rolling–horizon strategy deals with linking constraints. In contrast to constraints related to Lagrangean methods, these linking constraints are generated by the decomposition strategy itself. The idea is to divide the project horizon into smaller periods, for which the problem is solved

individually [170]. Linking constraints connect the different considered time-periods. The strength of this approach is to efficiently solve scheduling problem of networks under uncertainty, as demonstrated by Kopanos et al. [170] and Silvente et al. [171]. The simultaneous design of distributed and centralized energy systems was not focus in their work applying this method.

4.3.2 Gaps and contributions

The main limitations of previously discussed options to reduce solution time are summarized in Table 4.2. None of the presented options are sufficient in order to integrate the optimal design and operation of decentralized buildings in DES. The option that allows for the consideration of simultaneous optimization at both the building and the district level are the heuristic methods. They, however, do not guarantee a global optimum and additionally are leading to an increased runtime [159].

Table 4.2 – Limitation of decomposition approaches (SP: sub-problem).

simplification	approach	limitation	source
aggregation	top-down approach, aggregated buildings	oversimplification, no interaction in network	[154]
pre-selection	fixed and/or aggregated loads, pre-selected units	no optimal design of decentralized units	
heuristic search	genetic algorithm, bi-level decomposition	no guarantee for global optimum, increased runtime	[159]
decomposition	Benders	limited handling of integer in SPs	[162]
	ADMM	maximum two SPs possible	[168]

The most promising option is the Dantzig–Wolfe algorithm, as it allows the individual consideration of BESs as well the optimization of the whole DES. Thereby, applications reported low CPU time, the advantage to use parallel optimization, and the ability to increase the scope as the number of SPs are not limited [161]. The approach was first introduced by G.B. Dantzig and P. Wolfe in 1959 [172]. In recent years this method has become popular for solving complex optimization problems in a variety of fields such as bio-refining [173], oil refining [174] or model predictive control of chemical processes [175]. Finally, Harb et al. [176] applied the Dantzig–Wolfe decomposition for optimal scheduling of district heating networks. This method was further developed by Schütz et al. [122] to not only optimize the operation but also the design of DESs, but their study did not include MOO. The objective of the following section is to apply and validate the Dantzig–Wolfe decomposition to complex, distributed energy systems. An additional contribution is to develop a MOO framework for the Dantzig–Wolfe decomposition of energy systems.

4.3.3 General structure

Similar to other decomposition strategies, the problem is split into a MP and several SPs, when performing the Dantzig–Wolfe decomposition. The master problem is a reformulation of the original problem, whereas the subproblems are independent parts within the original problem. The independent SPs are usually linked with only a few constraints to the overall problem. Thus, inde-

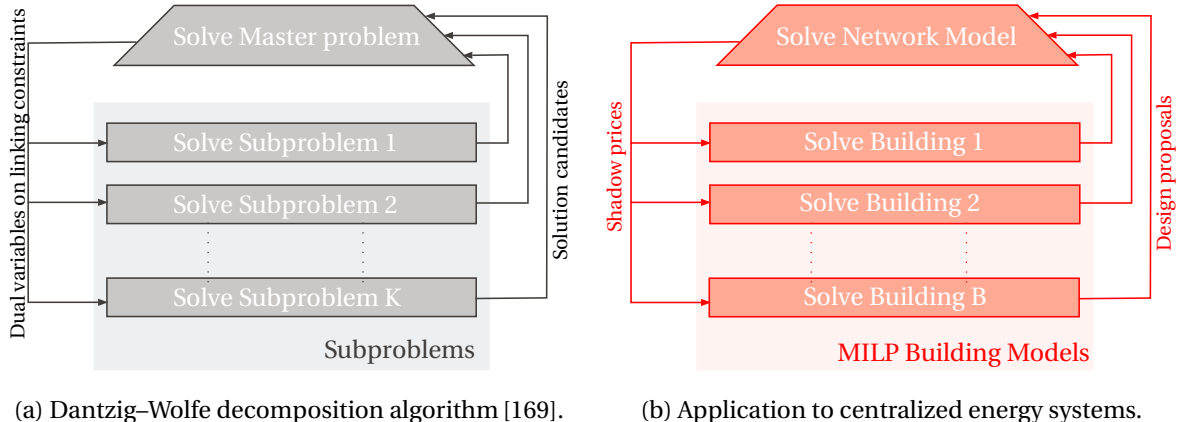


Figure 4.11 – Translation of the Dantzig–Wolfe decomposition principle to the design and operation optimization of centralized energy systems.

pendent subblocks and their linking constraints need to be identified in the compact formulation in a first step. In the case of district energy systems, that translates to BESs as subblocks and network balances as their linking constraints (Figure 4.11). In a second step, the SPs are substituted in the MP by a linear combination of their extreme points. The Minkowski’s representation theorem states that a bounded problem is identical, when only described with its extreme points [161]. In the Dantzig–Wolfe method, this behavior is exploited for moving all constraints and variables to the SPs, leaving only the linking constraints and the linear combination of extreme points in the MP. For the application to district energy systems, this translates in the network model as MP, which considers different optimal solutions from the SPs (Figure 4.11b). The connection of the MP to the SPs is established in two ways: SPs send their optimal design proposals to the MP, whereas the MP sends price signals to the SPs. The price signals resemble incentives to change the operation and design of the SPs.

The advantage of this method is that it exploits the natural structure of a district energy system and single buildings can be included with their own characteristics. Furthermore, this structure conveniently leaves the decentralized problems untouched, only the objective functions have to be adjusted in order to become SPs and be linked to the MP. The application of the Dantzig–Wolfe Algorithm to the case of district energy systems is summarized in Table 4.3. The main parts are detailed in the following.

Table 4.3 – Dantzig–Wolfe Algorithm and the corresponding part in the decomposition of district energy systems. Interpretation of dual values depends on the corresponding constraints.

Dantzig–Wolfe algorithm	application district energy systems
master problem (MP)	network model
linking constraints	network constraints
independent subproblems (SPs)	building energy system (BES) models
solution candidates	design proposal BES
dual values of linking constraints	e.g., microgrid tariff or investment sensitivity

Master problem The MP constitutes all aspects which are connecting or linking the SPs. Thus, in the application of centralized planning of a DES, the MP contains all network-related equations, such as the electricity grid, and centralized units or constraints. The overall aim of the MP is to coordinate the exchange from the district to the next level of the grid and to decide for or against design proposals within the district. The design proposals are both investment decisions of technologies and the schedule how the SPs exchange electricity within the district network.

In the following, the MP is detailed with all its equations. The main sets remain unchanged, all timesteps are allocated to set T of each typical period P, and all buildings are contained in set B of the district. The Dantzig–Wolfe Decomposition is an iterative algorithm, the set I keeps track of all iterations. Dual variables, which are important in the algorithm, are linked to their specific equation with the expression $\curvearrowright []$ and addressed later in this section.

$$0 \leq \lambda_{i,b} \leq 1 \quad \forall i \in I, \quad \forall b \in B \quad (4.1a)$$

$$\sum_{i \in I} \lambda_{i,b} = 1 \quad \forall b \in B \quad \curvearrowright [\mu_b] \quad (4.1b)$$

The new decision variable of the MP is λ , which decides for ($\lambda = 1$) or against proposals ($\lambda = 0$). The optimal solution of the whole district is a linear combination of these extreme points [161]. Convexity Equations 4.1a and 4.1b ensure that a proposal can be chosen maximally once and the linear combination of all selected proposals does not exceed one. The dual variable associated to Equation 4.1b is μ .

$$\sum_{i \in I} \sum_{b \in B} \lambda_{i,b} \cdot (\dot{E}_{i,b,p,t}^{gr,+} - \dot{E}_{i,b,p,t}^{gr,-}) \cdot d_p \cdot d_t = E_{p,t}^{TR,+} - E_{p,t}^{TR,-} \quad \forall p \in P, \quad \forall t \in T \quad \curvearrowright [\pi_{p,t}] \quad (4.2)$$

The main linking constraint is the electricity balance at the transformer TR of the district (Equation 4.2). The MP receives the grid exchange $E^{gr,\pm}$ from each building b in each iteration i , and balances the load at the transformer level. The associated dual variable of the network constraint is π . As π is in dependence of each typical period p and each timestep t , the frequency d_p of the

4.3. Decomposition algorithm

period and timestep duration d_t have to be considered already in the electricity the balance. In this way, π and electricity exchange at the transformer $E^{TR,\pm}$ are considered with their annual impact.

$$C^{el} = \sum_{p \in P} \sum_{t \in T} \left(c_{p,t}^{el,+} \cdot E_{p,t}^{TR,+} - c_{p,t}^{el,-} \cdot E_{p,t}^{TR,-} \right) \quad (4.3)$$

The annual cost for electricity C^{el} of the district is calculated by using Equation 4.3. The costs are associated with the total electricity purchase of the system $E^{gr,+}$ and the purchase price $c^{el,+}$ as well as the feed-in revenues $c^{el,-} \cdot E^{gr,-}$.

$$G^{el} = \sum_{p \in P} \sum_{t \in T} \left(g_{p,t}^{el} \cdot E_{p,t}^{TR,+} - g_{p,t}^{el} \cdot E_{p,t}^{TR,-} \right) \quad (4.4)$$

Similar to the annual cost of electricity, the annual global warming potential (GWP) associated with the electricity consumption is calculated in Equation 4.4. The impact of the electricity g is the same for the demand and the feed-in, as the feed-in electricity is consumed elsewhere in the distribution grid and avoids the generation at the current grid-mix.

4

$$C^{op} = C^{el} + \sum_{i \in I} \sum_{b \in B} \lambda_{i,b} \cdot C_{i,b}^{gas} \quad (4.5a)$$

$$C^{cap} = \sum_{i \in I} \sum_{b \in B} \lambda_{i,b} \cdot C_{i,b}^{cap} \quad (4.5b)$$

$$C^{tot} = C^{cap} + C^{op} \quad (4.5c)$$

$$G^{tot} = G^{el} + \sum_{i \in I} \sum_{b \in B} \lambda_{i,b} \cdot \left(G_{i,b}^{gas} + G_{i,b}^{bes} \right) \quad (4.5d)$$

The possible objectives of the MP are presented in Equations 4.5. Similar to the objectives of decentralized systems, objectives can be the OPEX (Equation 4.5a), the CAPEX (Equation 4.5b), the TOTEX (Equation 4.5c) or the GWP (Equation 4.5d). Input parameters coming from the design proposals of the SPs are the costs and GWP of each building energy system (C^{cap} and G^{bes} , respectively) and the operational expenses and the GWP connected to the purchase of natural gas (C^{gas} and G^{gas}) .

Dual variables The Dantzig–Wolfe decomposition leverages the duality concept of the problem. The dual problem is a twin problem to the original or primal problem. If duality applies and both problems are feasible, the objective value of the primal and the dual problem are identical. The two problems are inverted and (1) a minimization in the primal problem is a maximization in the dual problem and vice versa, (2) variables in the primal problem become constraints in the dual problem and each primal constraint a dual variable [161].

Table 4.4 – Example of a primal and a corresponding dual problem. The parameters of the problem are given in A as an $m \times n$ matrix, a vector $b \in \mathbb{R}_+^m$ and a vector $c \in \mathbb{R}_+^n$.

	primal problem	dual problem
objective function	$\min c' \cdot \mathbf{x}$	$\max b' \cdot \mathbf{y}$
constraints	s.t. $A \cdot \mathbf{x} \geq b \rightsquigarrow [y]$	s.t. $A' \cdot \mathbf{y} \leq c \rightsquigarrow [x]$
variables	$\mathbf{x} \in \mathbb{R}_+^n$	$\mathbf{y} \in \mathbb{R}_+^m$
dual variables	$[y] \in \mathbb{R}_+^m$	$[x] \in \mathbb{R}_+^n$

There are many additional interesting correlations between the primal and its dual problem, an exemplary pair is shown in Table 4.4. The correlations of particular interest in the Dantzig–Wolfe decomposition are the dual variables of the primal linking constraints. The dual values can be interpreted as Lagrange multipliers, which are applied to the primal constraints, and also called shadow prices or marginal values [177]. Dual variables measure the sensitivity of constraints with respect to the optimal objective function of the primal problem [177].

In the example in Table 4.4, the dual variable y indicates the sensitivity of the objective value to the right side of the primal constraints b . In other words, y expresses how much the objective function would improve by relaxing bound b . In the minimization of the exemplary primal problem, relaxing bound b means to decrease the value b , so x might take a smaller value, which would improve the objective function. The dual variables in the Dantzig–Wolfe decomposition are used as communication between the MP and the SPs. They signal each SP, how the overall objective value of the MP would improve, if they change their contribution to a specific linking constraint.

$$[\mu_b] = \frac{\Delta \text{obj}}{\Delta (\sum_{i \in I} \lambda_{i,b})} \quad \forall b \in B \quad (4.6)$$

The dual variable $[\mu]$ corresponds to Equation 4.1b and has the same physical unit as the objective function. As Equation 4.1b is valid for each building b , each constraint translates to a dual variable, which is specific to each building b and indicates how the network objective value changes if the SP modifies its design proposal (Equation 4.6).

$$[\pi_{p,t}] = \frac{\Delta \text{obj}}{\Delta (E_{p,t}^{TR,+} - E_{p,t}^{TR,-})} \quad \forall p \in P, \quad \forall t \in T \quad (4.7)$$

The dual variable $[\pi]$ in Equation 4.7 is related to the electricity balance at the transformer (Equation 4.2). It indicates how much the overall objective function changes if the electricity exchange of the whole district varies in that specific timestep t in period p . If the objective function of the MP is related to OPEX, the variable $[\pi]$ can be interpreted as electricity price (currency / kWh) within the

4.3. Decomposition algorithm

network. In this case, the lower bound of $[\pi]$ is the feed-in tariff and the upper bound is the retail tariff. For example, in times of net-import at the transformer, the district purchases electricity for the retail tariff. Additional electricity would need to be purchased for the retail tariff. In contrast, if a building is consuming less (or even is feeding in) electricity, it would, overall, save the amount corresponding to the retail tariff.

Subproblem One major advantage of the Dantzig–Wolfe decomposition is that the BES can remain individual and unchanged with respect to decentralized energy systems. The only adjustments required in order to include them in the centralized formulation of the decomposition are related to their objective functions, all other functions remain unchanged. The basis of the BES is described in Chapter 1.2, individual orientation of the roof surfaces are detailed in Chapter 2.3 and shadow casting among buildings and solar integration can be considered according to Chapter 3.2. In the following the modified objective functions, previously described in Section 1.2.4, are detailed.

$$\text{obj}_b = \min(C_b^{op} - \mu_b) \quad \forall b \in B \quad (4.8a)$$

$$C_b^{op} = \sum_{p \in P} \sum_{t \in T} \left(\pi_{p,t} \cdot \dot{E}_{b,p,t}^{gr,+} - \pi_{p,t} \cdot \dot{E}_{b,p,t}^{gr,-} + c_{p,t}^{ng,+} \cdot \dot{H}_{b,p,t}^{gr,+} \right) \cdot d_t \cdot d_p \quad \forall b \in B \quad (4.8b)$$

4

The dual variables π replace the electricity tariffs in the calculation of operational costs C^{op} (Equation 4.8b). The objective function for each SP (Equation 4.8a) are the OPEX subtracted the dual variable μ , which is also called the reduced cost of operation. The SP can still improve the overall objective of the MP, if the objective value is negative. In contrast, the SP is not able to propose a solution to further improve the objective value of the MP in case of a positive value [161].

$$\text{obj}_b = \min(C_b^{cap} - \mu_b) \quad \forall b \in B \quad (4.9)$$

The only change, which is necessary to minimize capital expenses C^{cap} , is to formulate the latter as the reduced cost of investment with the help of the dual variable μ . The capital expenses are calculated in Equation 1.16a. As the linking constraint of the electricity grid plays no role in this investigation, a problem with Equation 4.9 as the objective is independent from the dual variable π .

$$\text{obj}_b = \min(C_b^{op} + C_b^{cap} - \mu_b) \quad \forall b \in B \quad (4.10)$$

The reduced cost of total expenses is detailed in Equation 4.10. The incentive to change the operation schedule is accounted for with the dual variable π in the operational costs C^{op} , which are calculated according to Equation 4.8b.

$$\text{obj}_b = \min(\mathbf{G}_b^{op} + \mathbf{G}_b^{bes} - \mu_b) \quad \forall b \in \mathcal{B} \quad (4.11a)$$

$$\mathbf{G}_b^{op} = \sum_{p \in \mathcal{P}} \sum_{t \in \mathcal{T}} \left(\pi_{p,t} \cdot \dot{\mathbf{E}}_{b,p,t}^{gr,+} - \pi_{p,t} \cdot \dot{\mathbf{E}}_{b,p,t}^{gr,-} + g^{ng} \cdot \dot{\mathbf{H}}_{b,p,t}^{gr,+} \right) \cdot d_t \cdot d_p \quad \forall b \in \mathcal{B} \quad (4.11b)$$

The optimization of the total GWP of the system, is in principle very similar to the TOTEX minimization. The dual variable π accounts for the price, this time in terms of environmental impact per unit of consumed electricity (kg_{CO₂eq}/kWh). The operational GWP G^{op} balances the environmental impacts from the electricity exchange $E^{gr,+/-}$ and the natural gas consumption $H^{gr,+}$ (Equation 4.11b). The Objective Function 4.11a is the sum of all contributions to the total GWP, resulting from operation G^{op} and construction G^{bes} of the BES (Equation 1.20). It is reduced by the incentive to change the system proposal μ .

Multi-objective optimization Multi-objective optimization is, in general, necessary if two, or more, conflicting objective functions have to be considered. It is also possible to detect pathways to reach an ultimate goal. For example, in order to reduce the total GWP, the TOTEX - GWP Pareto frontier reveals actions, which should be considered first. Furthermore, the MOO results in a schedule for how to reach the best environmentally friendly system with incrementally increasing costs. The MOO of compact models is an algorithm, which is using epsilon constrains to generate a Pareto frontier. While the first objective is optimized, epsilon constrains serve as incrementally increasing upper bound of the second objective function. Afterwards, the position of the first and second objective is inverted. For the Dantzig–Wolfe decomposition, the epsilon constraint translates into a linking constraint, which is impacts the whole network.

Table 4.5 – Adjustments for MOO with Dantzig–Wolfe Algorithm. Example of the CAPEX - OPEX Pareto frontier, using ϵ constraints. Objective of the MP remains unchanged, one additional linking constraint, ϵ - constraint, is added to the MP and its dual variable is included in the objective function of the SPs.

	OPEX minimization CAPEX constrained	CAPEX minimization OPEX constrained
Objective MP	$\min(\mathbf{C}^{op})$	$\min(\mathbf{C}^{cap})$
ϵ - constraint MP	$\mathbf{C}^{cap} \leq \epsilon^{cap} \cdot A^{tot} \quad \sim [\beta^{cap}]$	$\mathbf{C}^{op} \leq \epsilon^{op} \cdot A^{tot} \quad \sim [\beta^{op}]$
Dual variable	$[\beta^{cap}] = \frac{\Delta \text{obj}}{\Delta \epsilon^{cap} \cdot A^{tot}} = \frac{\Delta \mathbf{C}^{op}}{\Delta \epsilon^{cap} \cdot A^{tot}}$	$[\beta^{op}] = \frac{\Delta \text{obj}}{\Delta \epsilon^{op} \cdot A^{tot}} = \frac{\Delta \mathbf{C}^{cap}}{\Delta \epsilon^{op} \cdot A^{tot}}$
Objective SPs	$\min(\mathbf{C}_b^{op} + \beta^{cap} \cdot \mathbf{C}_b^{cap} - \mu_b) \quad \forall b \in \mathcal{B}$	$\min(\beta^{op} \cdot \mathbf{C}_b^{op} + \mathbf{C}_b^{cap} - \mu_b) \quad \forall b \in \mathcal{B}$

Table 4.5 provides an overview about the changes, which are necessary for generating the OPEX - CAPEX Pareto frontier. The objective function of the MP needs no adjustments. The ϵ - constraint

4.3. Decomposition algorithm

is added to the MP. Its connected dual variable β , which indicates how much the overall objective value of the MP improves, in case the the respective ϵ limit is relaxed. The dual variable β is inserted in the corresponding objective function of the SPs, where it serves as weight between the conflicting objectives. Figure 4.12 visualizes the role of the dual variable β . The dual variable gives the gradient of

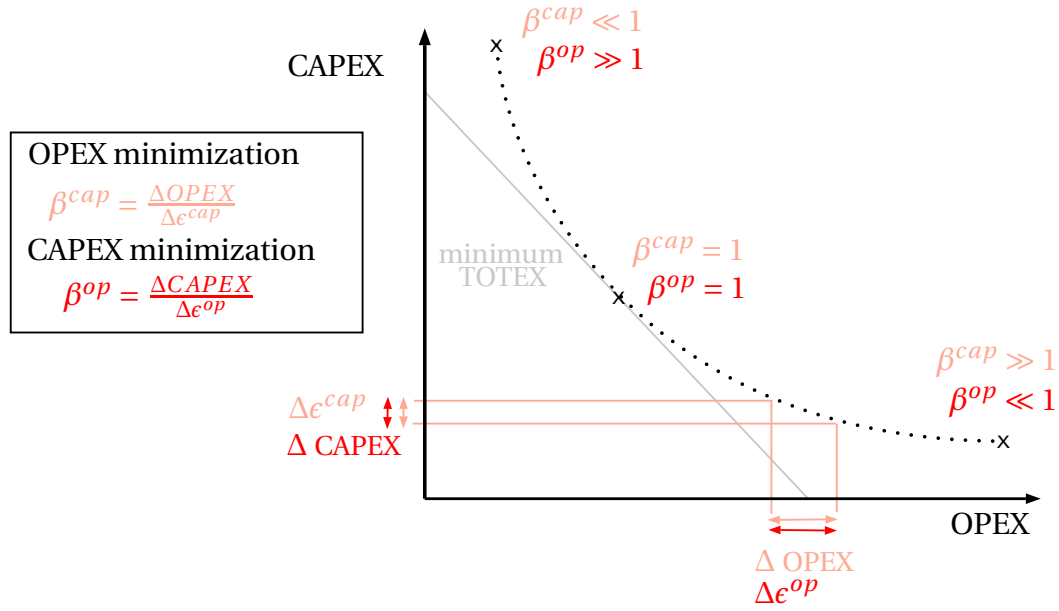


Figure 4.12 – The role of the dual variable β , when applying the Dantzig–Wolfe algorithm for MOO. Example of CAPEX- OPEX Pareto frontier [currency/m²], dual variable β to communicate ϵ constraint to subproblems, see Table 4.5.

4

the Pareto frontier itself. The more β increases, the more importance is given to the second objective. Near the bounds of the Pareto frontier, one objective function has steep change, whereas other the objective function changes slowly. For example, the minimum of CAPEX, is the maximum of OPEX. The relaxation of the constraint on CAPEX (expressed by β^{cap}) allows for a drastic improvement of OPEX. Therefore, β^{cap} takes a much bigger value than 1. The contrast is β^{op} , increasing the OPEX even more would not lead to a further reduction in the CAPEX. Therefore β^{op} takes a small value, close to 0. In the middle of the curve, the objective of the SP becomes an unweighted sum of both conflicting objectives, CAPEX and OPEX, both related dual variables are $\beta = 1$, which results in a TOTEX optimization.

4.3.4 Algorithm

The Dantzig–Wolfe decomposition is an algorithm, where the set of possible choices in the MP is increasing each iteration. The options increase at each iteration, until the best possible combination is detected and the algorithm stopped. The complete algorithm is visualized in Figure 4.13.

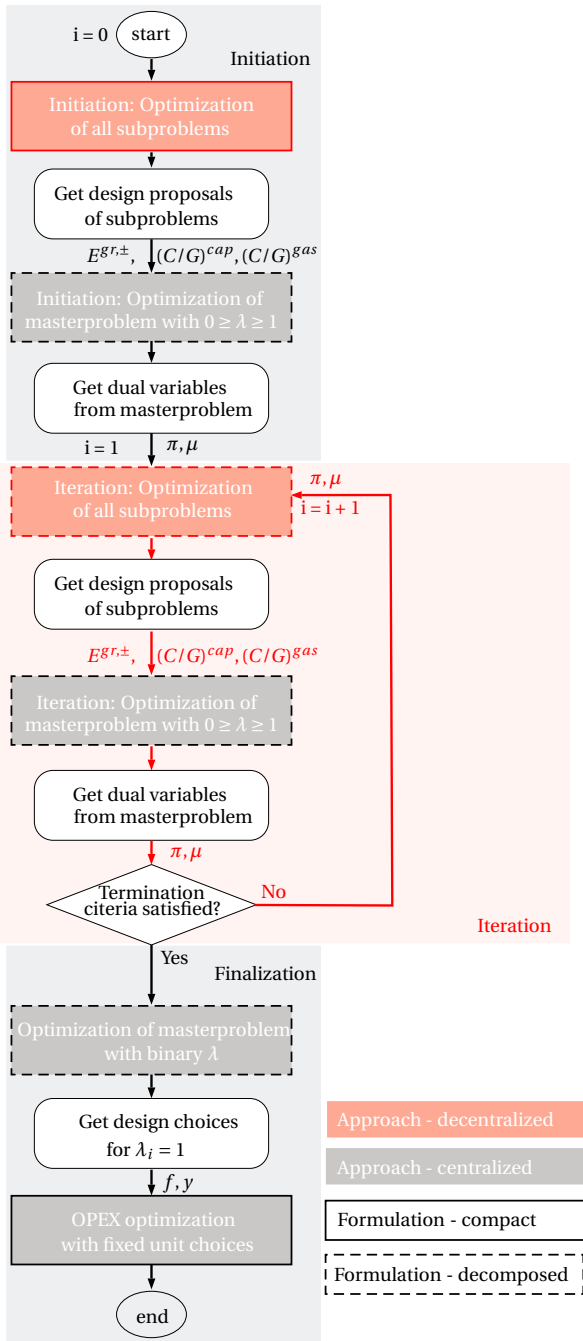


Figure 4.13 – Dantzig–Wolfe decomposition algorithm. Design proposals: $E^{gr,\pm}$ - electricity exchange schedule with the grid, C^{cap} - capital costs of each building energy system, C^{gas} - cost for the purchase of natural gas. Dual variables: π - incentive to change the electricity schedule, μ - incentive to change the design proposal. Decision variable: λ -proposal decision variable of the MP/network, f, y -decision variable for energy system technologies.

There are two different approaches possible in order to optimize a district energy system. The first approach is to optimize each building individually and one after the other. In this way, the approach is decentralized. In contrast, the approach is centralized when the district is optimized by considering all buildings at once and balancing the operation at the transformer of the low-voltage grid. The whole optimization algorithm can be separated in three main parts, the initiation, the iteration and the finalization, each part is further discussed in the following paragraphs.

Initiation The goal of the initiation is to detect the first values of the dual variables. There are two different initiation strategies implemented, which differentiate in the objective function of the first step. The initiation of the iterative process is a decentralized and compact optimization of all buildings in the district. The first strategy is to use the same objective function for each building than for the district optimization, e.g., if the TOTEX of the district has to be optimized, the initiation optimizes the TOTEX of all decentralized energy systems individually according to Equation 1.17. The second initiation strategy is to use the objective function, which is implemented for MOO and initialize β to generate 3 different solutions (see Table 4.5). This latter strategy has to be used to initialize the MOO. Thereby, the dual variable β is initialized with 50, 1, and 0.1 to mark the characteristic points of the Pareto frontier (see Figure 4.12). In that way, infeasibilities, which are resulting from the constraint

of the second objective, are avoided. The limit on the second objective is imposed on the district as a whole but might be infeasible for single SPs. The second strategy can also be used to initialize single-objective optimization. For example, in case of a TOTEX optimization, β can be initialized with the values 0.8, 1 and 1.1. The result is communicated as first design proposals to the MP. The MP is optimized with continuous variables λ , which is also called the relaxed MP optimization. The λ variables select design proposals for each SP. The dual variables are calculated from the result of the MP.

Iteration The iteration process is, in principle, what is described in Figure 4.11. The dual variables are sent to the SPs as incentive to change their proposals. All SPs are optimized, with the dual variables on linking constraints and modified objective functions (Equations 4.8, 4.9, 4.10, 4.11 or as in Table 4.5). The new design proposals of each SP are added to the pool of design proposals to the MP. The design proposals are electricity exchange schedules with the grid $E^{gr,\pm}$, the related costs, as well as GWP of investment decisions (C^{cap} and G^{bes}) and of purchasing and consuming natural gas (C^{gas} and G^{gas}). Afterwards, the relaxed optimization of the MP is executed and dual variables are calculated with the results. As long as no termination criterion is fulfilled, the dual variables are sent to the SPs and a new iteration circle starts.

Termination criteria Four termination criteria are implemented. In order to check the optimality, the reduced cost of each SP is calculated based on their last optimal solution but with the updated dual variables. The case of the reduced costs of every SPs being greater or equal to zero, translates into the fact that no building energy system can improve the overall objective any further by changing their design proposal. Thus, the optimum is found and the algorithm terminated [161].

The remaining three termination criteria are implemented for security reasons, to terminate the process without an optimal solution. The iterative algorithm is terminated in case:

- the total CPU time reaches a predefined limit.
- the total number of iterations reaches a predefined limit. Schütz et al. [122] uses 10 iterations as Sokoler et al. [169] demonstrated a few are enough.
- the last n iterations did not lead to a significant improve of the overall objective function.

Finalization When one termination criterion is satisfied, the iteration breaks and the algorithm enters its final stage. The MP is executed one more time, this time with binary decision variables $\lambda_i \in \{0; 1\}$. This step is necessary to choose discrete the integer decision of the SPs. The integrality constraints are already respected in the SPs, this final step also respects them in the MP [122]. The decision for a design proposal is returned, for which the unit choices are transferred to the centralized and compact formulation of the district. This last step is not necessary and is optional.

It does not change the value of the detected optimum, nor the electricity exchange schedule. It is used to post-calculate KPIs describing the whole district. In case of MOO, each Pareto point is one execution of the algorithm visualized in Figure 4.13 . All detected proposals are kept between the points and are sent to each optimization of the MP. After the first execution of the algorithm, they are also used to initialize the iteration.

4.3.5 Case study

The decomposition algorithm is applied to optimize the same district, which is reported in Chapter 3.2.6. All buildings are residential buildings, a mix between single- and multi-family houses. The district is located in the climatic zone of Geneva, Switzerland, weather data is clustered to ten typical days as described in Chapter 1.2.6. All 31 buildings are connected to the same low-voltage transformer of the electricity distribution grid. Each building energy system is modeled according to Chapter 1. The space heating and domestic hot water demand can be supplied by a gas boiler, a heat pump or two electrical heaters, one for each thermal demand. Electricity can be generated from PV Panels on the roofs of the building. All roof surfaces of the district are integrated with their individual orientation as described in Chapter 2. Batteries and two water tanks, one for each thermal demand, can serve as energy storage. The validation of the algorithm is achieved by the comparison to the same problem, which is not decomposed. As it is computationally impossible to calculate the whole district without applying the decomposition algorithm, a maximum of nine buildings are considered in the district. The four termination criteria are set to 1) a maximum of 9 iterations 2) maximum runtime of 20 minutes 3) not more improvement than 0.005% during the last 5 iterations and 4) the reduced costs of all SPs are greater or equal to 0. The problem is formulated in AMPL Version 20210220 and solved with CPLEX 20.1.0.0 on a local machine with following processor details: Intel(R) Core(TM) i7-9700K CPU @ 3.60 GHz. The relative tolerance between the relaxed linear problem and best integer solution is set to $mipgap=5e-7$. The remaining CPLEX settings are equal to the default settings reported in [153].

4.3.6 Results and discussion

The goal of the results section is, to demonstrate how the decomposition algorithm works and to validate it. The validation is carried out by comparing the result of the decomposed optimization to the corresponding result of the compact formulation. The compact model is the same optimization problem, however not decomposed. Hence, it has another solving strategy but it should ideally result in the same outcome.

Initiation and finalization In an iterative process, the initiation or the quality of the first guess impacts the number of iterations needed to find the optimal solution. Figure 4.14 shows the influence of different initialization strategies on the example of a single-objective optimization (SOO).

4.3. Decomposition algorithm

Additionally, it presents from which iteration the proposal is chosen in the final execution of the binary MP. The first initialization strategy is to use the same objective for each SP than for the MP.

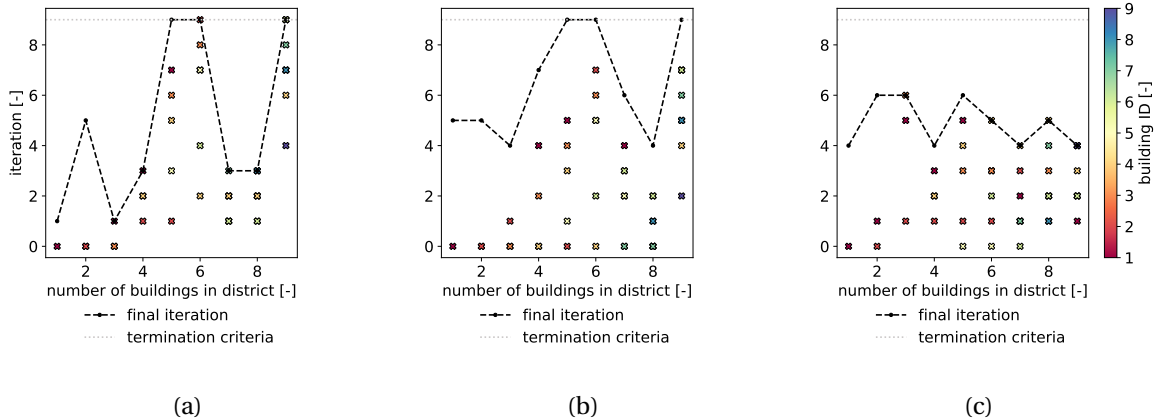
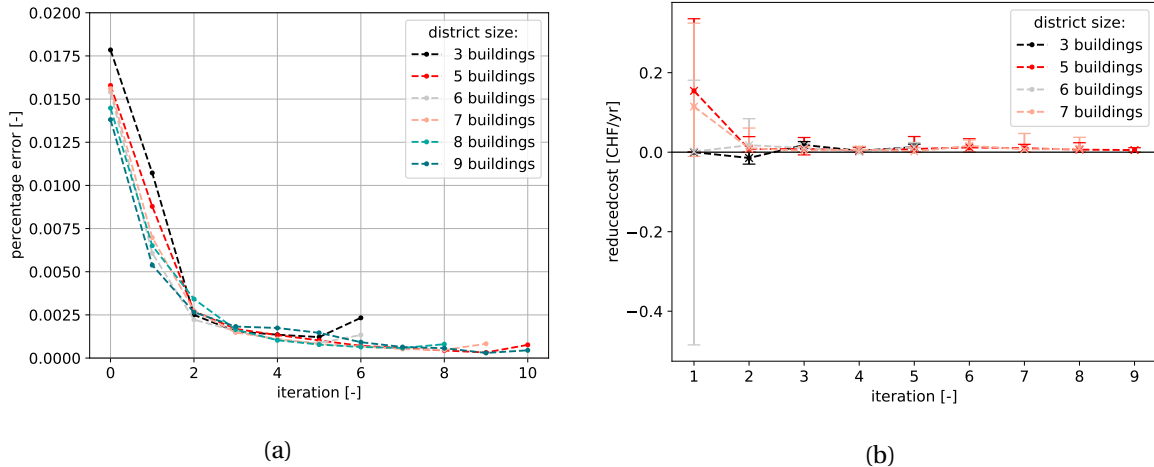


Figure 4.14 – Impact of different strategies on the termination of the iteration. The crosses visualize from which iteration the final design proposal is chosen. a) First initiation strategy with one single solution from each SP. b) Additional criterion: minimum iterations 4 b) Initialization with 2 additional near optimal solutions.

The result is visualized in Figure 4.14a. For a district size of five, six and nine buildings, the maximum number of iterations (=9) was reached and the algorithm was terminated. In contrast, the district size of three buildings was terminated after one iteration. The algorithm might have been terminated too early if the reduced costs were calculated based on too less design proposals. In that case, the number of design proposals do not allow for the capture the decision space and to sufficiently calculate the dual problem. An extreme example is the case of one point, the optimum of one point is the point itself. This problem exists only in the first iterations and only for small district sizes. The first try to overcome this issue is to not only include a maximum but also a minimum of required iterations. The case of an implemented minimum of four iterations is presented by Figure 4.14b. This method increased the solution time of the algorithm. For not one analyzed district, a solution was chosen from their final iterations. Hence, a minimum of the number of iterations addressed the problem of too little design proposals, but also increased the solution time with unnecessary iterations. The second initialization strategy is to use the objective function of the MOO (Table 4.5) and to initialize the dual variable β with three different values. Afterwards, all three design proposals are sent to the first optimization of the MP (see Figure 4.13). Figure 4.14c confirms that this strategy was overcoming the issue of termination after the first iteration. Furthermore, it demonstrates how an improved initiation strategy was improving the entire algorithm. The iteration was terminated after a maximal six iterations and no optimization reached the maximum allowed nine iterations.

Convergence Several TOTEX optimization problems with different sizes, which means with different numbers of buildings connected to the district, are compared. Figure 4.15 shows the convergence of the iterative decomposition process. The percentage error of the objective function at different iteration steps is visualized in Figure 4.15a. The termination criteria for optimality is shown in Figure 4.15b.



4

Figure 4.15 – Convergence of the Dantzig–Wolfe decomposition. a) Percentage error of the objective function with respect to the corresponding compact model for each iteration. b) Average reduced cost normalized to the total energetic reference area of the district, error bars show the min/max value of the reduced cost occurring in the district at each iteration.

At each iteration, the current objective function is compared to the final objective function of the corresponding compact formulation (Figure 4.15a). The initialization was already close to the optimum with less than 2% divergence. It can be observed that, the bigger the problem size, the smaller the error in the first iterations. In general, the error dropped below 0.25% already in the first two iterations. The algorithm was terminated after between five and nine iterations, which was the maximum of allowed iterations, hence a termination criterion. In Figure 4.15a, one additional iteration is added for each optimization to visualize the impact of the finalization. During the finalization, the MP is executed one more time with binary and non-continuous variables. This introduced an error which is neglectfully small and decreased with an increase of the problem size. Figure 4.15b shows the reduced costs at each iteration step. The reduced costs are the modified objective functions of the SPs and therefore individual for each building. In this example, the reduced costs associated with TOTEX are considered (Equation 4.10). The average reduced costs are visualized with error bars resembling the minimum and maximum occurring value within the district. When all values were positive, the criterion for optimality was fulfilled and the iteration was terminated.

4.3. Decomposition algorithm

Validation The motivation to use a decomposition algorithm is to ease computational effort while keeping the optimality and accuracy of the solution. Figure 4.16 shows the solution time of the compact formulation in comparison with the corresponding decomposed problem. The

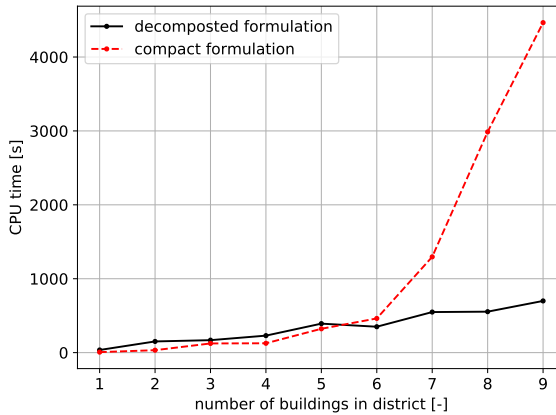


Figure 4.16 – Comparison of the computational effort with and without decomposition of the problem.

4

solution time of the compact formulation followed an exponential trend, whereas the effort of the decomposed formulation increased linearly (Figure 4.16). Minor variations of the CPU time from the linear trend line are explained by the different number of iterations needed to terminate the algorithm. To consider a whole low-voltage grid, several dozen buildings need to be included in the analysis. The exponential trend prognoses, that this scale is computationally untraceable for a compact formulation of the problem. However, the decomposition has the potential to overcome this issue due to the presented linear trend of the CPU. At the same time, the value of the objective functions were almost identical (Figure 4.17).

Figure 4.17a visualizes the result of the TOTEX optimization for different districts sizes. The course of the presented result was individual to the district size, as it was depending on the included buildings. It ranged between 18 CHF/m²/yr and 22 CHF/m²/yr. Thereby, the value of the decomposed and the compact formulation was identical. The result of the MOO of CAPEX and OPEX for a district, which contains eleven buildings, is shown in Figure 4.17b. The decomposition could be validated, and the frontier itself was well detected. In addition to the value of the objective, the decisions taken by the solver are a matter of interest in MILP optimization problems. In the case of optimizing energy systems, the decisions are the choice to purchase and install a unit. Figure 4.18 presents the number of required iterations before the algorithm is terminated (Figure 4.18a) as well as an comparison of unit decisions (Figure 4.18b).

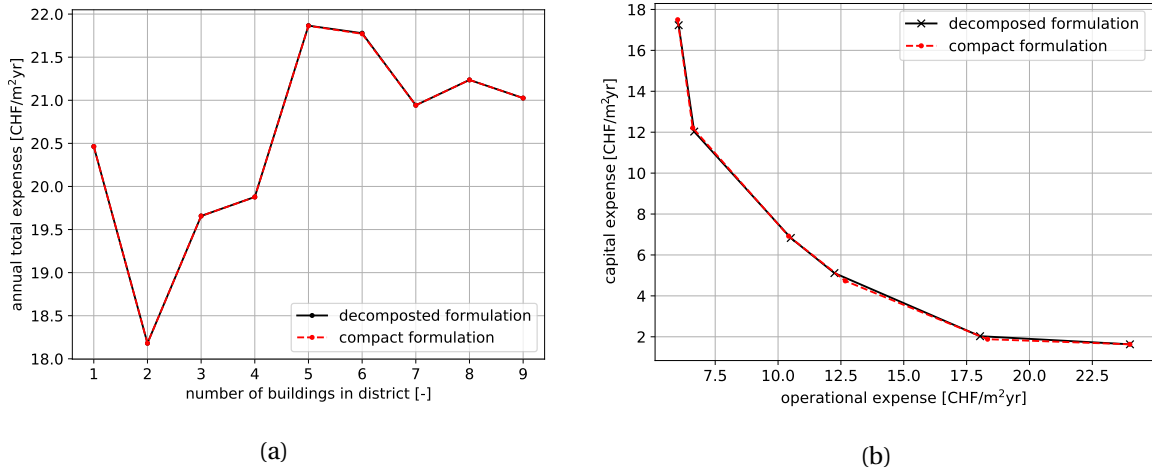


Figure 4.17 – Comparison of the objective function for the compact and decomposed formulation. a) Single objective TOTEX b) CAPEX - OPEX Pareto frontier of the MOO for a district size of 11 buildings.

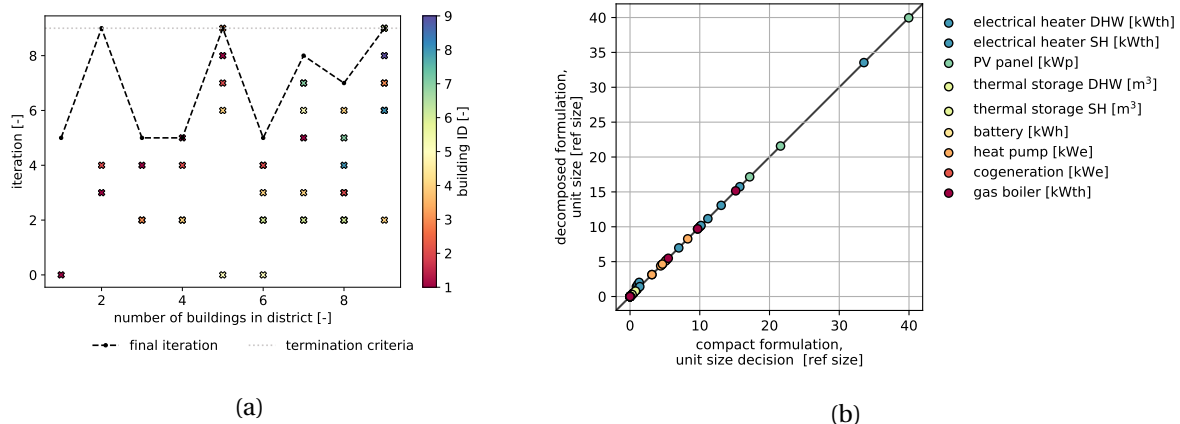


Figure 4.18 – a) Required iterations in the decomposed formulation for different district sizes. The crosses show from which iteration the design proposal for a building is chosen at the finalization stage. b) Comparison of the unit sizes for a district of nine buildings between compact and decomposed formulation.

Figure 4.18a shows that for the district size of six buildings, only five iterations were needed. In contrast, the optimization problem with nine buildings was terminated at one security termination criteria, the maximal allowed nine iterations. Although the process was not stopped because of the optimality criterion, Figure 4.15a shows that the difference to the optimum was less than 0.1 %. Furthermore, the installed unit sizes for the district size of nine buildings are compared for both formulations in Figure 4.18b. The comparison allows for the conclusion that almost identical unit decisions were taken. Therefore, it can be confirmed that the termination with the security indicator still leads to acceptable results. Figure 4.18a additionally presents from which iteration the proposal

4.3. Decomposition algorithm

was chosen in the final execution of the binary MP. In small district sizes, more iterations than necessary were executed. For a district size of two buildings, the algorithm reached the maximum number of nine iterations, however chose the design proposal from iteration four and three. For a higher number of included buildings, this behavior was not observed.

Dual variables Different dual variables are used in the decomposition, one for each linking constraint. The dual variable μ is linked to the objective function and is individual for each SP (compare Equation 4.6). It is a constant value, which is subtracted from the objectives of the SPs and used to assess the termination criterion. The related criterion are the reduced cost, which are presented in Figure 4.15b. However, a constant parameter value, which is subtracted from a minimization problem, has no impact on the result of the optimization.

The dual variable π is linked to the electricity exchange and is used to communicate price signals between the MP and the SPs in order to change the operation schedule (compare Equation 4.7). Figure 4.19 presents the dual variable for optimizing OPEX on one typical day in winter (Figure 4.19a) and one in summer (Figure 4.19b).

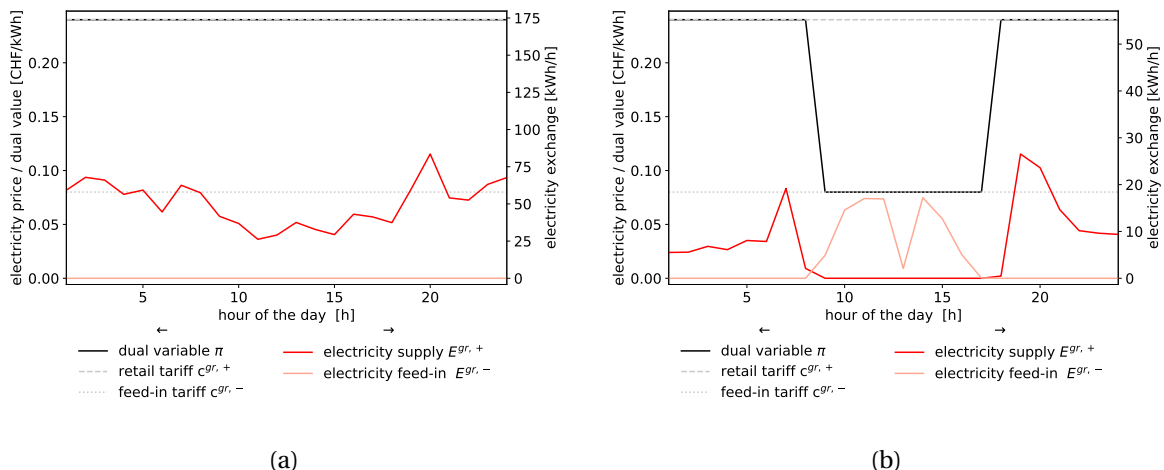


Figure 4.19 – Dual variable π and electricity exchange of a district on a typical a) winter period and b) summer period.

The district was a net-importer during the whole winter period (Figure 4.19a). There was only electricity demand and no feed-in from the district. If the SP can change its operation schedule and save, for example 1 kWh of electricity, the total objective function is reduced by the cost of that 1 kWh of electricity. Since it would need to be imported, the related costs which can be saved is the retail tariff. Therefore, the dual variable took the retail tariff for the whole winter period. In contrast, Figure 4.19b shows the situation in case there is surplus electricity, which is exported from the district. During mid-day, the electricity from the installed PV panels were exported. In that time, the 1 kWh of electricity from the previous example costed only the amount of the feed-in

tariff. Therefore the dual variable π took the feed-in tariff. Before and after the period of feed-in, the situation was the same as during the winter day and the district was a net-importer. Hence, the dual variable π took the retail tariff.

The last dual variable, which is introduced in this chapter is the dual variable β . The dual variable β is associated to the constraint on the second objective function during MOO (compare Table 4.5). This constraint is valid for the whole district, hence a linking constraint. Figure 4.20 displays the result of a MOO of eight buildings.

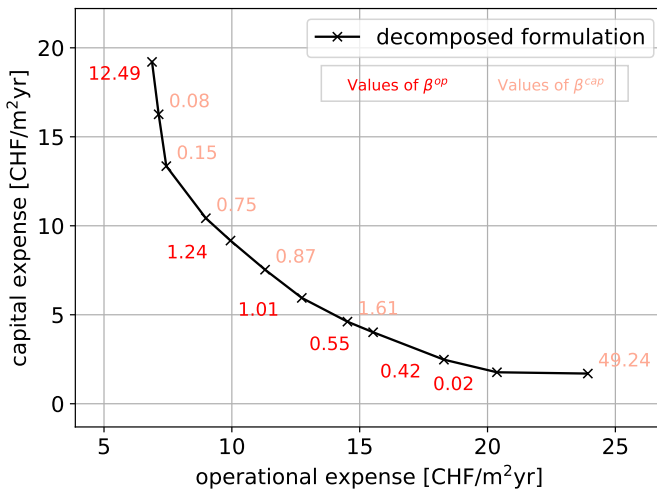


Figure 4.20 – Dual variable β during the MOO of a district with eight buildings. β is dimensionless (see Figure 4.12).

The stricter the limit on the second objective, the greater the possible improvement on the first objective by loosening this limit. The greater the sensitivity on the objective, the greater the related dual variable. Hence, β was greatest close to the minimum of the second objective. For example, CAPEX was the first objective and OPEX was the second objective. An OPEX limit of around 7 CHF/m²yr led to β^{op} around 12. (Figure 4.20). This means, relaxing the ϵ -limit of the OPEX by 1 unit, the CAPEX could have improved by 12 units. Close to the CAPEX optimum, the situation was the reverse. A relaxation of the OPEX constraint could not significantly improve CAPEX and therefore β took small values like 0.02 (Figure 4.20).

4.3.7 Main findings

In the second part of this chapter, the Dantzig–Wolfe decomposition approach is applied to the case of district energy system optimization. This decomposition approach allows for the splitting of the original, compact formulation into several smaller parts and thereby reduces the overall runtime. The approach is similar to the method described by Schütz et al. [122]. Contribution to

4.3. Decomposition algorithm

the state-of-the-art is the implementation of the Dantzig–Wolfe method to MOO of DES. In a first step, the different parts of the decomposition algorithm are identified: the MP which contains the network model and its linking constraints and the SPs, which are the individual BESs within the district. Dual variables serve as communication between the MP and the related SPs. In a second step, the MOO is implemented. The usual procedure of generating Pareto frontiers with the help of ϵ -constraints of the second objective [178] translates into one additional linking constraint and one additional dual variable. The dual variable related to the MOO also allowed for the improvement of the initialization strategy of the algorithm itself. The decomposition approach is validated with the related compact formulation of the same problem. The results showed an error less than 0.02 % on the objective function and identical unit decisions. The computational effort of the decomposition followed a linear trend when adding buildings to the district, whereas the solution time of the compact formulation increased exponentially. Therefore, the presented decomposition has the potential to ease the computational effort sufficiently in order to calculate whole low-voltage electricity grids with several dozen buildings connected. The centralized optimization of renewable energy hubs of low-voltage electricity grids are further analyzed in the following chapter.

Renewable energy hubs at the district scale

Overview

- ▶ Application of the centralized design strategy to several dozen buildings connected to the same low-voltage grid
- ▶ Comparison of the centralized and decentralized design strategies, methods proposed in Chapters 4 and 3, respectively
- ▶ Analysis of the needs, limitations, and solutions for integrating a high share of renewable energy in in renewable energy hubs at the district scale

The content of this chapter is submitted partly to [143] (in Review).

Integrating renewable energy technologies in district energy systems is a common interest in order to meet the challenges associated with the energy transition. The optimal planning of these renewable energy hubs at the district scale is a computationally intensive task, as each building in the district has its own energy system installed that exchanges resources with the community. In this chapter, the proposed and previously validated Dantzig–Wolfe decomposition is applied to ease computational efforts. The resulting centralized design strategy was then compared with the decentralized design strategy, where each building is optimized sequentially. Both methods were applied to a typical peri-urban district in the area of Geneva, Switzerland. Results show that the coordinated investment and operation strategy of the centralized approach allows a higher electrification of the system, leading to an increase of photovoltaic penetration (PVP) by 40%, to $PVP = 0.6$. This reduced the total global warming potential by 20% for the same total expenses. The centralized investment strategy differed most from the decentralized strategy for photovoltaic (PV) panels; using the centralized strategy, a wide range of PV installation on less-optimal surfaces became economically interesting. Economically feasible self-sufficiency was achieved by installing 0.39 to 0.98 m^2 PV panels per energetic reference area, when the round-trip efficiency of the storage systems decreased from 100% to 45%. For the examined district to become carbon neutral using only solar energy, 73% of available surfaces must be covered with PV panels; refurbishing the building stock can reduce this value by 55%. The most economically convenient solution to overcome transformer limitations were district storage for peak shaving and photovoltaic curtailment. The cost increase were around 600 CHF per kWyr annual capacity shortage, regardless of the considered district energy system.

5.1 Introduction

Efforts to decentralize the energy system in the context of the energy transition require optimally integrated distributed energy systems in a network infrastructure. Distributed energy systems, such as single buildings in a district, do not only require energy in the form of electricity or heat but also generate and feed into the network. Planning the optimal integration of renewable energy technologies is a complex and multi-layered task that requires the analysis of the impact of their integration on the network, the interaction between buildings, and the design and scheduling of energy system itself. These different aspects and perspectives are discussed in this chapter. First, an overview of the state-of-art of modeling of district energy systems is provided. A concise methodology section is then presented in Section 5.2; this chapter focuses on the application of the methods developed in previous chapters. The methods are then applied to a residential urban district comprising over 30 buildings and is detailed in the results provided in Section 5.3.

5.1.1 State-of-the-art

District energy systems are commonly optimized using a mixed-integer linear programming (MILP) framework. MILP optimization was used in all contributions listed in Table 5.1, except for those by Fazollahi [179], who employed a mixed-integer non-linear framework. Generally, the integer variables are used to model part-load stages of technologies or the decision to choose equipment. The volatile nature of renewable energy technologies and the dependence of the energy demand on ambient weather requires the consideration of annual time-series. The resulting modeling frameworks are computationally untraceable optimization models [180]. Therefore, it is current standard to perform time-series aggregation (TSA), which clusters annual profiles to typical periods [46]. TSA was applied in all presented contributions in Table 5.1. When the only simplification made to the model was the aggregation of time-steps, very few periods were used, generally representing one for each season [117, 123, 181]. Researchers performing comprehensive reviews regarding TSA have concluded that seasonal averages lead to considerably higher errors than machine-learning techniques, such as k-medoids clustering [46, 47]. Furthermore, as demonstrated in Chapter 3, applying only TSA cannot overcome computational issues on large-scale applications. Therefore, the model complexity must be reduced further by either reducing the problem size or decomposing the solution strategies.

One option is to pre-calculate building scenarios and optimize the selection of these scenarios at the district level. Pickering et al. [182] applied this strategy on two case studies containing 12 and 17 buildings, respectively. The first case study considered a district with cooling demand but no heating demand in India, whereas the second case study had the reverse situation in the UK [182]. The method employed for aggregating scenarios did not allow building interaction to be considered. Therefore, their results indicated that district energy system solutions were not

5.1. Introduction

Table 5.1 – Literature review on the optimization of urban energy system problems.

simplification	approach	focus (buildings)	MOO	source
aggregation [†]	temporal	district (5)	✗	[181]
	temporal	district (10)	✗	[117]
	temporal	district (35)	✗	[123]
	scenarios	district (16)	✗	[182]
	spatial	country (5–800)	✗	[183]
	spatial	district (4)	✗	[119]
	spatial	district (3)	✓	[22]
pre-selection	fixed loads	grid ⁺	✗	[155, 184]
	aggregated loads	grid ⁺	✗	[55, 185]
	two-stage	district (4)	✓	[156]
heuristic	bi-level	city (13)*	✓	[179]
	bi-level	district (20)	✓	[186]
	bi-level	district (5)	✓	[118]
decomposition	Rolling horizon	district (30)	✗	[171]
	Benders	grid ⁺	✗	[187]
	ADMM	grid ⁺	✗	[188–190]
	Dantzig–Wolfe	district (3–100)	✗	[122]
	Dantzig–Wolfe	district (31)	✓	this work

[†] all of presented approaches use time series aggregation, explicitly presented use it exclusively

* buildings are aggregated to 13 districts

⁺ focus is the grid, without designing or controlling decentralized loads

economic feasible and individual building systems should be preferred [182]. Stadler [22] also used this method to assess the energetic impact of the building stock of Switzerland. The entire building stock was presented using three building types and nine different renovation stages; pre-calculated scenarios of each building type were then aggregated to analyze the national system. These scenarios were developed using an MILP optimization framework that considers one building at a time. Stadler [22] furthermore demonstrated a multi-building example, in which one rural and one urban case study was analyzed with 13 and 5 buildings, respectively. The buildings in both case studies were aggregated to three buildings, which similarly made it impossible to assess the interconnection of buildings. This simplification was then furthered by aggregating the distributed loads of the entire district, resulting in a purely centralized energy system design [55]. Similarly, Liu et al. [184] and Lu et al. [155] presented a detailed focus on network modeling and design for both a district heating network and electricity grid. However, their work was not focused on the design of the building energy systems (BESs); rather, the distributed loads were integrated on network nodes,

and the layout of the two grids was designed and optimized.

Unlike these methods, decomposition allows both decentralized and centralized equipment designs to be considered while focusing on the operation of the network. A popular method to investigate this is bi-level decomposition. Fazlollahi [179] aggregated buildings to districts and then applied bi-level decomposition to optimize the energy system of Geneva, Switzerland. The bi-level decomposition of five buildings in a district with integrated grid constraints demonstrated the potential of a coordinated equipment design and scheduling [57]. Grid operation scheduling allowed a higher share of renewables to be integrated, thereby decreasing the global warming potential by 40% [57]. However, the bi-level method is a heuristic approach with no guarantee that the global optimum will be found [159]. Furthermore, this solution strategy still had an increased runtime. Morvaj et al. [118] reported a runtime between 12–30h for a single-objective optimization (SOO) of five buildings. Therefore, deterministic decomposition approaches, such as the alternating direction method of multipliers (ADMM) have gained popularity [188–190]. However, the ADMM can only be applied to two subproblems (SPs) [168]; researchers have thus used this technique to consider the control of microgrids, not the design of distributed energy systems [188–190]. Furthermore, the ADMM is outperformed by the Dantzig–Wolfe method [169], which was applied by Schütz et al. [47] to optimize over 100 residential buildings. Their result demonstrated the potential of a coordinated optimization approach and reduced the total expenses (TOTEX) by 4% and the global warming potential (GWP) by 23.7%.

5.1.2 Gaps and contributions

5

A review of the literature in the field of the coordinated design and operational scheduling of district energy systems reveals that the computational effort remains a major hurdle. Even after aggregating four buildings, Yang et al. reported [119] a runtime of 5 h 48 min. Applying decomposition strategies, Wakui et al. [191] reported a runtime of 2–55.5 h for a single optimization of 5–100 buildings. Schütz et al. [122] required 2.6 h for the single optimization of 10 buildings. Prior researchers have either oversimplified the model or considered only the grid operation; further, researchers performing a multi-objective optimization (MOO) have only considered heuristic approaches. In this chapter, therefore, a centralized, deterministic MOO strategy of all buildings connected to the same low-voltage grid is proposed to address the following questions:

- What is the benefit of considering renewable energy hubs at the district scale, which comprises a centralized, coordinated scheduling and investment approach?
- How do different design strategies influence the integration of renewable energy technologies in the district?
- What are the needs and limitations to become self-sufficient or carbon neutral in the district?
- How can the detected limitations be overcome?

5.2 Method

To highlight the benefits of a coordinated design of distributed energy systems, two possible design strategies of a renewable energy hub are compared in this section. On one side, the design strategy is decentralized, on the other, centralized., as presented in chapters 3 and 4, respectively. Because the focus here is on the application and comparison of the developed methods, only the necessary changes to the previously presented method are discussed.

Decentralized design strategy In the decentralized design strategy, MOO of BESSs are considered with the perspective of individual buildings and preformed sequentially. The district is modeled as a collection of renewable energy hubs at the building scale. Once the optimal design and operation is identified, the electrical loads are balanced within the district. This design strategy is identical to the one proposed and described in Chapter 3.

Centralized design strategy In the centralized design strategy, the distributed energy systems within the district are designed and operated according to a common, central objective. Decisions regarding investment and operations are taken with respect to the community, not individuals. This strategy is to consider one renewable energy hub at the district scale. The decomposition method developed and described in Chapter 4 was applied to overcome runtime issues for in centralized design strategy.

5.2.1 Key performance indicators

Regardless of the design strategy, two perspectives must be considered when describing the results of the design and operation of an renewable energy hub: that of the perspective of the building owners and of the community. The difference between these two perspectives can be characterized by what is generated and consumed in the district itself, also called the effect of pooling. For example, if a building imports electricity produced by a neighbor, this electricity for accounted in building's perspective but is not recognizable at transformer level.

The key performance indicators (KPIs) that are considered in this chapter and are not influenced by the different perspectives are the annual revenues (AR) (Equation 1.33) and photovoltaic curtailment (PVC) (Equation 1.29). The KPIs that are impacted by the two perspectives are further detailed using the general notation, where bold typesetting indicates variables and normal typesetting indicates parameters. In the centralized strategy, this classification changes during the decomposition algorithm, as detailed in Chapter 4.

Building perspective Here, each BES is analyzed independently from the network. BESs were defined in more detail in Chapter 1. In this chapter, the building perspective is analyzed by aggregating building-specific values.

$$E^{gr,\pm} = \sum_{b \in B} \sum_{p \in P} \sum_{t \in T} \dot{E}_{b,p,t}^{gr,\pm} \cdot d_t \cdot d_p \quad (5.1)$$

The electricity E imports (superscript +) and exports (superscript -) in the district can be represented by the sum of the exchanges over all buildings in the district (Equation 5.1).

The annual operational expenses (OPEX) are the costs related to the interaction with the local electricity and natural gas grids. From the building perspective, these expenses are the sum of all yearly bills that building residents receive for consuming electricity E or natural gas H .

$$C^{op} = \sum_{b \in B} \sum_{p \in P} \sum_{t \in T} \left(c_{p,t}^{el,+} \cdot \dot{E}_{b,p,t}^{gr,+} - c_{p,t}^{el,-} \cdot \dot{E}_{b,p,t}^{gr,-} + c_{p,t}^{ng,+} \cdot \dot{H}_{b,p,t}^{gr,+} \right) \cdot d_t \cdot d_p \quad (5.2)$$

In Equation 5.2, the annual expenses on the level of single buildings (Equation 1.15) are summed over all buildings b in the district. Thereby, the electricity exchange $\dot{E}^{gr,\pm}$ from the buildings to the district is considered. The electricity exchange at the local transformer does not influence the OPEX when this KPI is analyzed from the perspective of the buildings.

5

Community/Transformer perspective The community perspective considers the district as a whole. In contrast to the building perspective, exchanges between buildings in the district are not specifically evaluated; rather, the focus is on exchanges between the community and the outside world. The only resource that can be both imported and exported is electricity. Therefore, this perspective is also called the transformer perspective.

$$\dot{E}_{p,t}^{TR,+} - \dot{E}_{p,t}^{TR,-} = \sum_{b \in B} \dot{E}_{b,p,t}^{gr,+} - \sum_{b \in B} \dot{E}_{b,p,t}^{gr,-} \quad \forall p \in P \quad \forall t \in T \quad (5.3)$$

The electricity exchange from each building is balanced at the transformer TR (Equation 5.3).

$$C^{op} = \sum_{p \in P} \sum_{t \in T} \left(c_{p,t}^{el,+} \cdot \dot{E}_{p,t}^{TR,+} - c_{p,t}^{el,-} \cdot \dot{E}_{p,t}^{TR,-} + \sum_{b \in B} c_{p,t}^{ng,+} \cdot \dot{H}_{b,p,t}^{gr,+} \right) \cdot d_t \cdot d_p \quad (5.4)$$

The annual OPEX from the perspective of the community includes pooling. Fees for using the community network are not considered. Hence, only the electricity exchange at the transformer is

5.2. Method

accounted in the annual expenses (Equation 5.4).

$$\psi = \frac{\sum_{p \in P} \sum_{t \in T} \left(\left(\sum_{b \in B} \dot{E}_{b,p,t}^{gr,-} \right) - \dot{E}_{p,t}^{TR,-} \right) \cdot d_p \cdot d_t}{\sum_{b \in B} \sum_{p \in P} \sum_{t \in T} \dot{E}_{b,p,t}^{gr,-} \cdot d_p \cdot d_t} \quad (5.5)$$

However, the exchanges between the buildings and the grid are acknowledged in the share of electricity re-imports ψ (Equation 5.5), which represents the share of electricity that is exported by buildings ($\dot{E}_b^{gr,-}$) and then re-imported by neighbors. Thus, this electricity stays within the district, is not exported at transformer TR , and is used to cover a part of the electricity demand. Hence, the high share of re-import decreases the demand at the transformer, which reduces the OPEX of the district. The share of re-imports is a KPI that can be used to measure how well the generated electricity is used within the district. A related KPI is the self-consumption (SC), which represents the share of the total generated electricity that is consumed by the renewable energy hub, and can be expressed as [37] (Equation 5.6).

$$SC = \frac{E_{chp}^+ + E_{pv}^+ - E^{TR,-}}{E_{chp}^+ + E_{pv}^+} \quad (5.6)$$

Here and Equations 5.7 and 5.8, annual values are used to increase readability. In studied the district, electricity can be generated by PV panels and combined heat and power (CHP) units.

$$SS = \frac{E_{chp}^+ + E_{pv}^+ - E^{TR,-}}{E_{chp}^+ + E_{pv}^+ - E^{TR,-} + E^{TR,+}} \quad (5.7)$$

Self-sufficiency (SS) is the share of electricity demand that is covered by onsite generated electricity [37] (Equation 5.7).

$$PVP = \frac{E_{pv}^{gen}}{E_{pv}^+ - E^{TR,-} + E^{TR,+}} \quad (5.8)$$

The PVP indicates how much of the total electricity demand of the district could be covered by generated electricity from photovoltaic panels (Equation 5.8). In the value for PVP, electricity is evaluated that can potentially be generated by installed PV panels (E_{pv}^{gen}). The difference to the

actually generated electricity E_{pv}^+ is the curtailed electricity (Equation 1.29).

$$G^{tot} = G^{bes} + \sum_{p \in P} \sum_{t \in T} \left(g_{p,t}^{el,TR} \left(\dot{E}_{p,t}^{TR,+} - \dot{E}_{b,p,t}^{TR,-} \right) + \sum_{b \in B} g_{p,t}^{ng} \cdot \dot{H}_{b,p,t}^{gr,+} \right) \cdot d_p \cdot d_t \quad (5.9)$$

The total GWP is calculated using to Equation 5.9. The period and time-dependent parameters $g_{p,t}$ account for the GWP per kWh of consumed electricity at the transformer [33]. The GWP of the energy system G^{bes} is calculated according to Equation 1.18. Thereby, the centralized district units, detailed in the following section, are included.

5.2.2 Centralized units

The centralized design strategy enables the optimal sizing and scheduling of central district units. In this chapter, the considered district storage system uses a centralized lithium battery and was modeled according to the framework, described by Stadler [22]. This modeling framework includes the constant discharge and charge efficiency (0.9), battery efficiency (0.99), and limits for the state of charge (0.2–0.8). The cost of the batteries (441 CHF/kWh) were modeled according to the review of cost projections for utility-scale lithium-ion batteries, presented by Cole et al. [192].

$$\dot{E}_{p,t}^{TR,+} - \dot{E}_{p,t}^{TR,-} = \sum_{b \in B} \dot{E}_{b,p,t}^{gr,+} - \sum_{b \in B} \dot{E}_{b,p,t}^{gr,-} + \dot{E}_{p,t}^{bat,-} - \dot{E}_{p,t}^{bat,+} \quad \forall p \in P \quad \forall t \in T \quad (5.10)$$

5

The difference to the storage systems, which are included in BESs, is that the unit is allocated to the district level. The electricity charge and discharge from the central battery $E^{bat,\pm}$ is included in the electricity balance of the district (Equation 5.10) rather than the energy balance of the buildings (Equation 1.2).

$$C^{cap} = \frac{i(1+i)}{(1+i)^n - 1} \cdot \left(C^{inv,bat} + C^{rep,bat} \right) + \sum_{b \in B} C_b^{cap} \quad (5.11)$$

The capital cost of the battery is accounted for at the community level (Equation 5.11). All other modeling constraints concerning the unit sizing or the energy storage system remained unchanged with respect to the method that was detailed in Chapter 1.

5.2.3 Centralized constraints

A centralized design strategy enables the usage of centralized constraints and limitations. Here, the maximum capacity of the local low-voltage transformer is considered. The electricity export and the

5.2. Method

import is constrained within the feasibility range of the transformer (Equation 5.12).

$$\dot{E}_{p,t}^{TR,\pm} \leq \dot{E}_{p,t}^{TR,max} \quad \forall p \in P \quad \forall t \in T \quad (5.12)$$

The centralized constraint (Equation 5.12), a linking constraint included in the master problem (MP) of the decomposition, can cause infeasibilities in the initiation of the decomposition algorithm. The MP is initialized by design proposals from the SPs. First design proposals, which are sent to the MP of the decomposition, do not necessarily respect the centralized constraints. As a result, the MP is unable to choose design proposals within the limit of the constraints.

$$GU^\pm = \frac{\dot{E}_{p,t}^{TR,max}}{\max_{p,t} \left(\sum_{b \in B} \dot{E}_{b,p,t}^{B,-} \right)} \quad (5.13)$$

To overcome this issue, the equivalent grid usage (GU) (Equation 1.28) is calculated as the ratio of the transformer capacity to the maximum occurring uncontrollable load of the buildings E^B (Equation 5.13).

$$\dot{E}_{b,p,t}^{gr,\pm} \leq GU^\pm \cdot \max_{p,t} \left(\dot{E}_{b,p,t}^{B,-} \right) \quad \forall b \in B \quad \forall p \in P \quad \forall t \in T \quad (5.14)$$

The SPs of the decomposition are the optimization of individual BESs. Hence, the grid usage is included in the SP formulation of each building (Equation 5.14). This constraint is only needed during algorithm initiation and can be dropped during the iterative process.

5.2.4 Case study

The proposed method was then applied to the same case study as detailed in Chapter 3 for the decentralized design strategy to demonstrate the potential of the centralized design strategy. This case study district is a typical peri-urban European district located in the metropolitan area of Geneva, Switzerland. All 31 buildings considered, are connected to the same low-voltage transformer. Further details about the case study are provided in Section 3.2.6.

5.3 Results

The benefits of a centralized district energy design, while focusing thereby on the grid-aware integration of solar energy, are highlighted in this section. First, the centralized design strategy, in which the renewable energy hub is optimized from the perspective of the entire community is compared with the decentralized design strategy, in which optimal solutions are considered from the perspective of each building individually and then afterwards balanced at transformer level in an aggregation step. The centralized optimization strategy is then further analyzed to reveal the optimal integration of renewable energy technologies. Thereby, the influence on the electrical grid and required storage capacities are also analyzed.

5.3.1 What is the potential of a centralized design strategy?

Given that the optimization problems created by the centralized design strategy are more complex and therefore computationally more expensive to solve, the potential of a centralized optimization strategy is highlighted in this section.

Multi-objective optimization MOO using both optimization strategies demonstrated minimum annual capital expenses (CAPEX) of approximately 1.4 CHF per energy reference area (ERA), as shown in Figure 5.1.

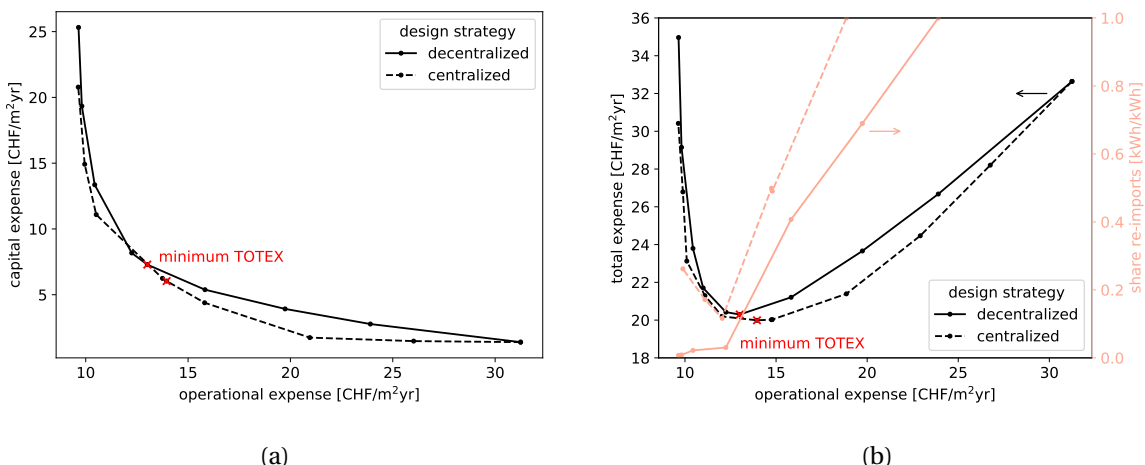


Figure 5.1 – Multi-objective optimization (MOO) of a residential district with 31 buildings. a) Comparison of the CAPEX–OPEX Pareto curve resulting from the decentralized and centralized optimization strategies. Minimum total expenses (TOTEX) marked on both curves. b) TOTEX and share of re-imports of generated electricity for increasing OPEX.

This is because there are no centralized or interacting units between buildings in the solution with lowest CAPEX. As a result, that the cheapest investment for each building is also the cheapest

5.3. Results

investment for the community. The energy system with a minimum CAPEX uses natural gas boilers in each building that are not connected to the electricity grid or a district heating network and thus can be operated independently. Increasing the investment in the energy system clarifies the difference between the two strategies. Using the centralized strategy, a 5% increase in the CAPEX allowed for a 30% decrease in the OPEX. In contrast, the decentralized design strategy required an increase in the CAPEX by more than 180% (from 1.4 CHF/m² to 4 CHF/m²) for the same reduction in the OPEX. This difference decreased between the two strategies when further reducing the OPEX; lowering the OPEX requires less dependency on purchasing resources from the grid but requires the installation of CAPEX-intensive equipment (i.e., local heat and electricity generation and storage systems). Therefore, these systems are more independent. This was observed for each building as well as for the community as long as there are no centralized units or requirements. Therefore, the resulting low-OPEX scenarios were similar using both strategies. However, the centralized strategy remained non-dominated in each scenario along the Pareto curve (Fig. 5.1a). This behavior can be explained in part by how generated electricity is used in both strategies (Figure 5.1b). The annual OPEX ranged from 30 to 10 CHF per ERA. Initial reductions in the OPEX were characterized by switching from natural gas resources to electricity, followed by the integration of renewable energy sources, and finally by the installation of electricity storage systems (i.e., batteries). The centralized design strategy produced results with a higher share of re-imports. Hence, the centralized strategy allowed an improved coordination of the district. The share of re-imports remained higher for the centralized design strategy, even when electricity production is increased in the district (Figure 5.1b). To decrease the annual OPEX below 12 CHF/m², electrical storage systems were used, demonstrating another benefit of the centralized approach: whereas re-import share further decreased to 0 when using the decentralized strategy, the coordinated operation allowed the share of re-imports to be increased to 30%. The minimum TOTEX obtained both optimization strategies is marked on the Pareto-optimal frontiers in Figure 5.1 and further discussed in the following paragraphs.

Single-objective optimization SOO resulted in similar objective values (TOTEX minimization) using both strategies, as shown in Figure 5.2. The objective value is similar for both optimization strategies. The centralized strategy led to an annual TOTEX 1.1% lower than the decentralized strategy. However, the use of the centralized strategy significantly changed other KPIs, including a lower CAPEX investment, a 25% lower PVP, and a 10% lower SS.

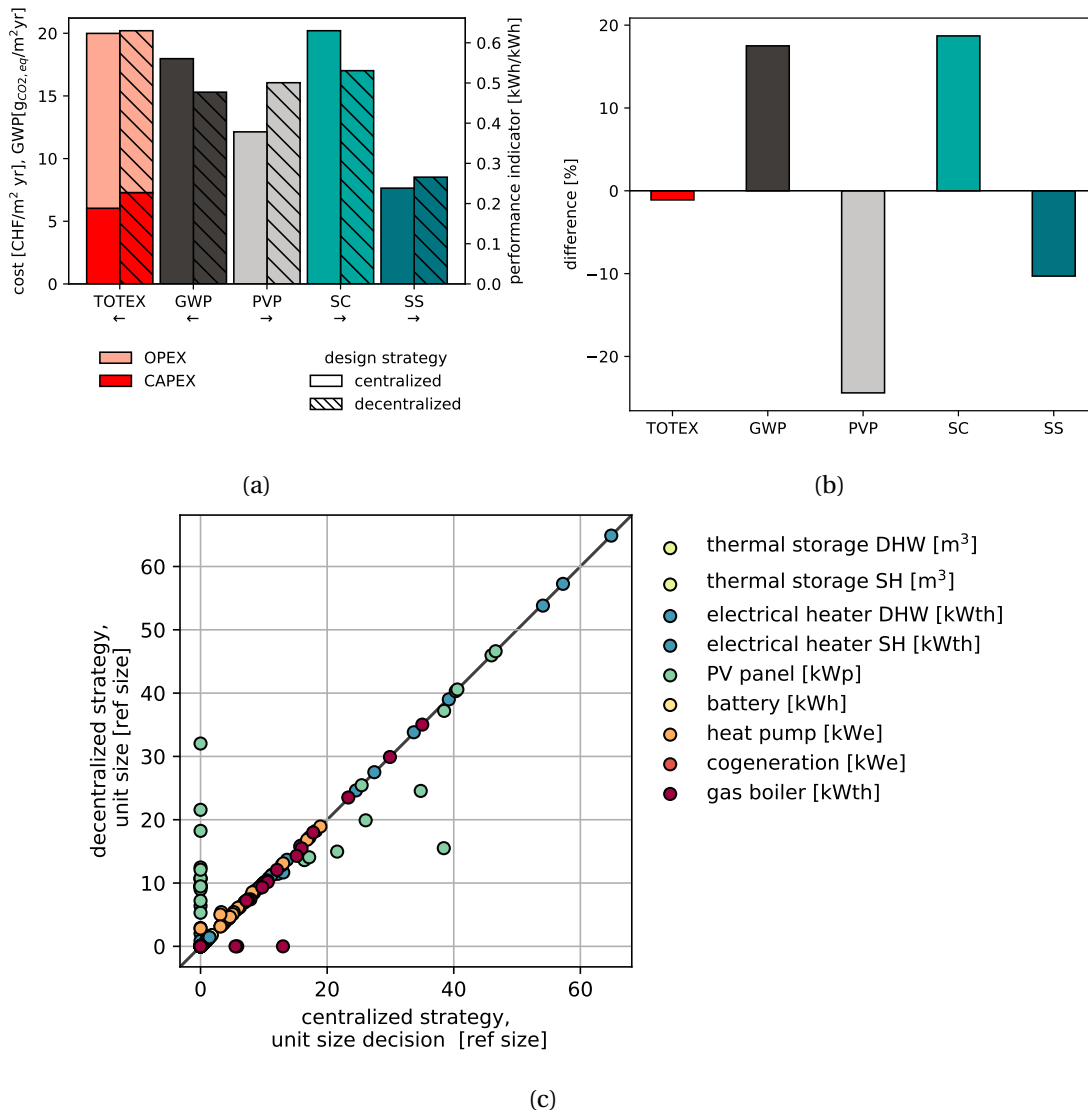


Figure 5.2 – Single-objective optimization (SOO) of a residential district with 31 buildings. Comparison of centralized and decentralized design strategy according to a) objective value (total expenses (TOTEX) and key performance indicators (KPIs): global warming potential (GWP), photovoltaic penetration (PVP), self-consumption (SC), and self-sufficiency (SS). b) Relative difference between the decentralized and centralized methods c) Installed units.

Comparing the configurations of the optimized renewable energy hubs (Figure 5.2c) gives further insight to the two solutions and confirms the analysis of the KPIs. Whereas the majority of the nine unit decision for each of the 31 buildings were identical, more PV panels were installed when the decentralized system was used. The decentralized investment strategy was developed from renewable energy hub at the building scale and does not take investment decisions for the community into account. The surface that is chosen for installing PV panels can be sub-optimal, as there might

5.3. Results

be better-oriented surfaces in the district available. Therefore, the optimization of the renewable energy hub at the district scale resulted in fewer but larger PV investment decisions.

The two gas boilers that are additionally installed in the optimum obtained using the centralized strategy (Figure 5.2c) accounted most of the 20% increase in the GWP (Figure 5.2a). The electricity exchange at the transformer also contributed to the GWP. Whereas the electricity import at the transformer was almost identical in both cases (Figure 5.3a), more electricity was exported in the result obtained using the decentralized strategy, which also had a higher PVP and lower SC.

The variation in electricity exchange and allocated OPEX from the two perspectives analyzed are shown in Figure 5.3.

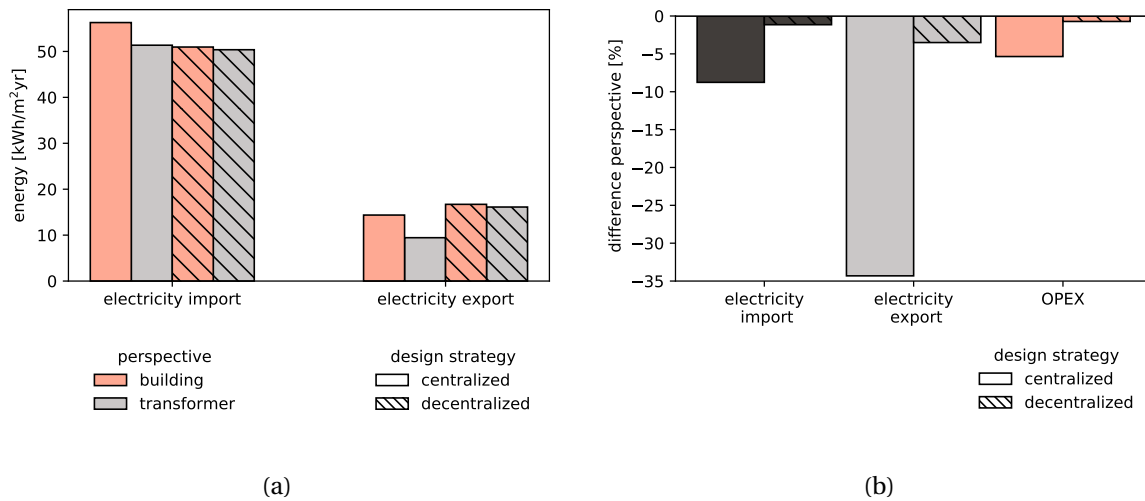


Figure 5.3 – Electricity exchange in the district from the perspective of the buildings and the transformer for each design strategy. a) Absolute exchange values. b) Relative difference between perspectives.

The difference between these two perspectives was, in general, much larger for the centralized design strategy. Almost 35% of the electricity exported at building level remained within the district and was not exported at transformer level, which confirms the analysis regarding re-imports in Figure 5.1b). This electricity met 10% of the total electricity demand of the buildings thereby decreasing the electricity import at transformer level by 10%. This difference in electricity exchange led to a monetary difference in OPEX. To be able to compare this difference in OPEX the same electricity tariffs were assumed for feed-in and demand at the transformer and buildings. The result of the centralized strategy shows OPEX which are 5.4% reduced, when accounted at the transformer. This saving can be directly translated into the benefit of centralized strategy. The saving of the decentralized design strategy at the district scale is 0.7%.

Previously, the resulting optimum using two different design strategies were compared. Although

their objective value (TOTEX) were similar, they were not the same. In MILP optimization, even a small difference in objective values can lead to very different system configurations. To have a clearer picture of the potential of the centralized design strategy, the previous analysis was repeated with identical objective values. As the centralized strategy was non-dominated along the Pareto (Figure 5.1a), the accepted value of the objective of the centralized strategy was increased to meet the identified minimum TOTEX of the decentralized strategy.

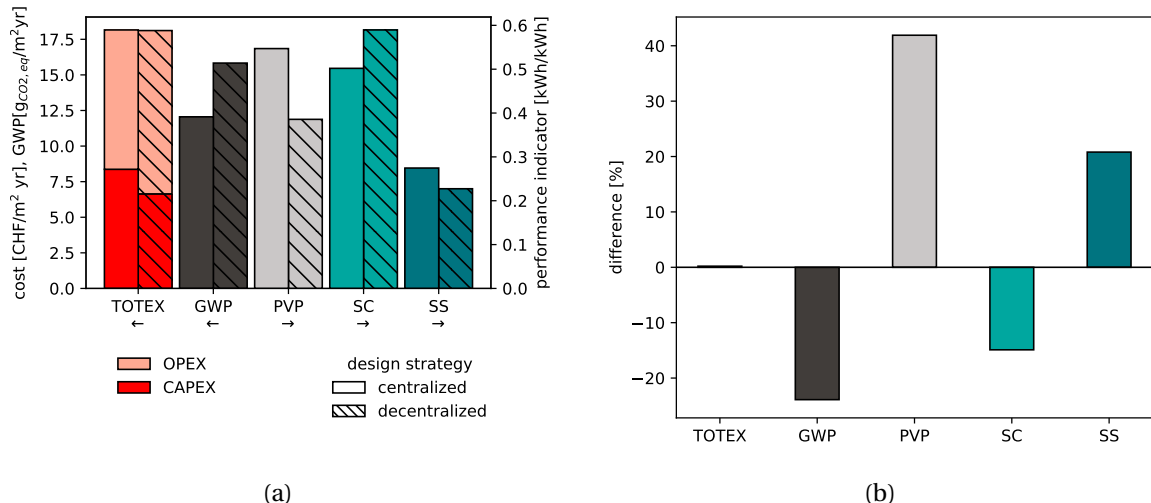


Figure 5.4 – Comparison of optimal solutions with identical TOTEX for a residential district with 31 buildings. Comparison according to key performance indicators: GWP, PVP, SC and SS. a) Absolute comparison. b) Relative difference between the methods.

5

The KPIs obtained from this analysis are shown Figure 5.4. The PVP and SS of the centralized solution was 40% and 20% higher than the solution identified using the decentralized strategy, respectively. The centralized design strategy of the distributed energy system allowed a reduction of the GWP of more than 20% for the same TOTEX. A comparison of both energy system designs, visualized in Figure 5.5, provides one part of the explanation for the decrease in the GWP and the increase in the PVP. The coordinated investment strategy of PV panels and the improved utilization of generated electricity allowed for an electrification of the system without increasing the TOTEX. The centralized design strategy improved PV inclusion, thereby increasing the size of PV modules using surfaces in the district. To use a higher share of locally generated electricity, the size of natural gas boilers was reduced and the size of the heat pumps was increased.

Electrifying the renewable energy hub reduced the gas demand by 40% and increased the electricity export by 80% (Figure 5.6). Analyzing optimal systems with the same TOTEX but different optimization strategies revealed another benefit of the centralized design strategy: an improved and increased inclusion of renewable energy technologies in the district. Therefore, the PV investment strategy that was identified with the coordinated, centralized design strategy is further analyzed in the next section.

5.3. Results

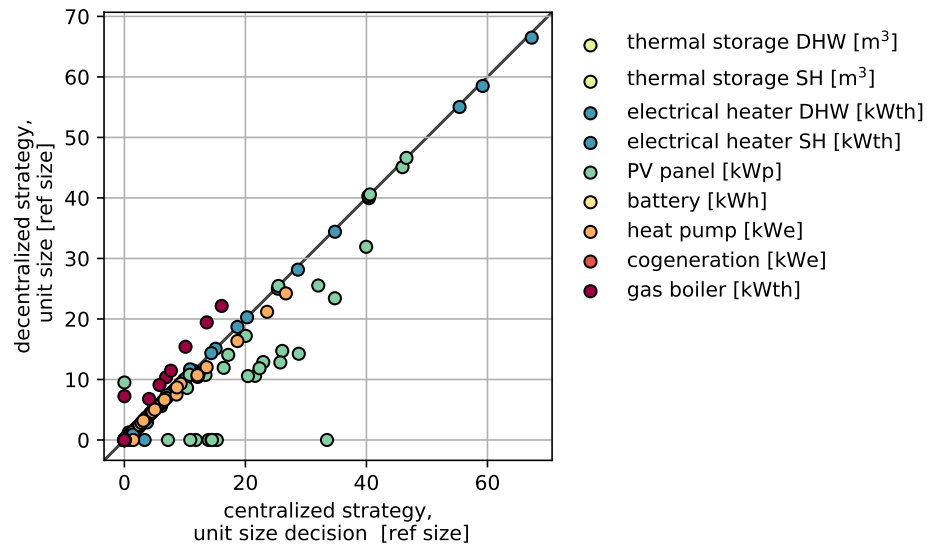


Figure 5.5 – Comparison of optimal unit decisions for solutions with identical TOTEX but different design strategies.

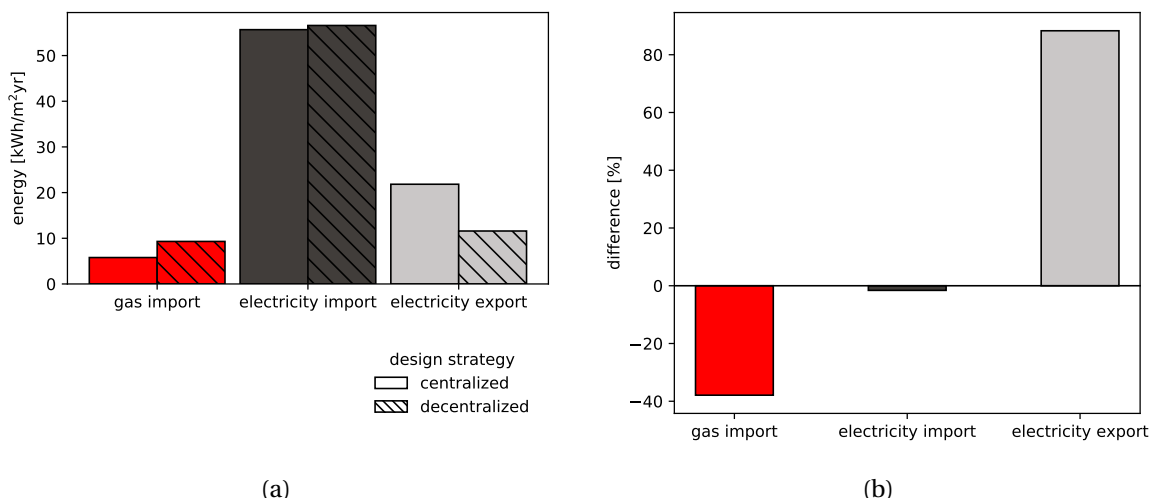


Figure 5.6 – Resource exchange of a residential district with 31 buildings. Comparison of optimal solutions with identical TOTEX but different design strategies. a) Absolute values b) Relative difference between the design strategies.

5.3.2 Optimal investment strategy for photovoltaic panels

Optimizing a renewable energy hub requires a holistic approach that accounts for both electricity demand and generation opportunities. Thereby, one challenge is to close the gap between the temporal availability of the generation and demand of electricity. The economic feasibility of PV panel investment strategies can be analyzed by asking two questions: (1) Which surfaces are optimal for PV panel installations? (2) What portion of these surfaces are economically convenient to cover and what is the influence of grid tariffs? Additionally, the required PV coverage to reach SS or carbon neutrality in the district is then discussed.

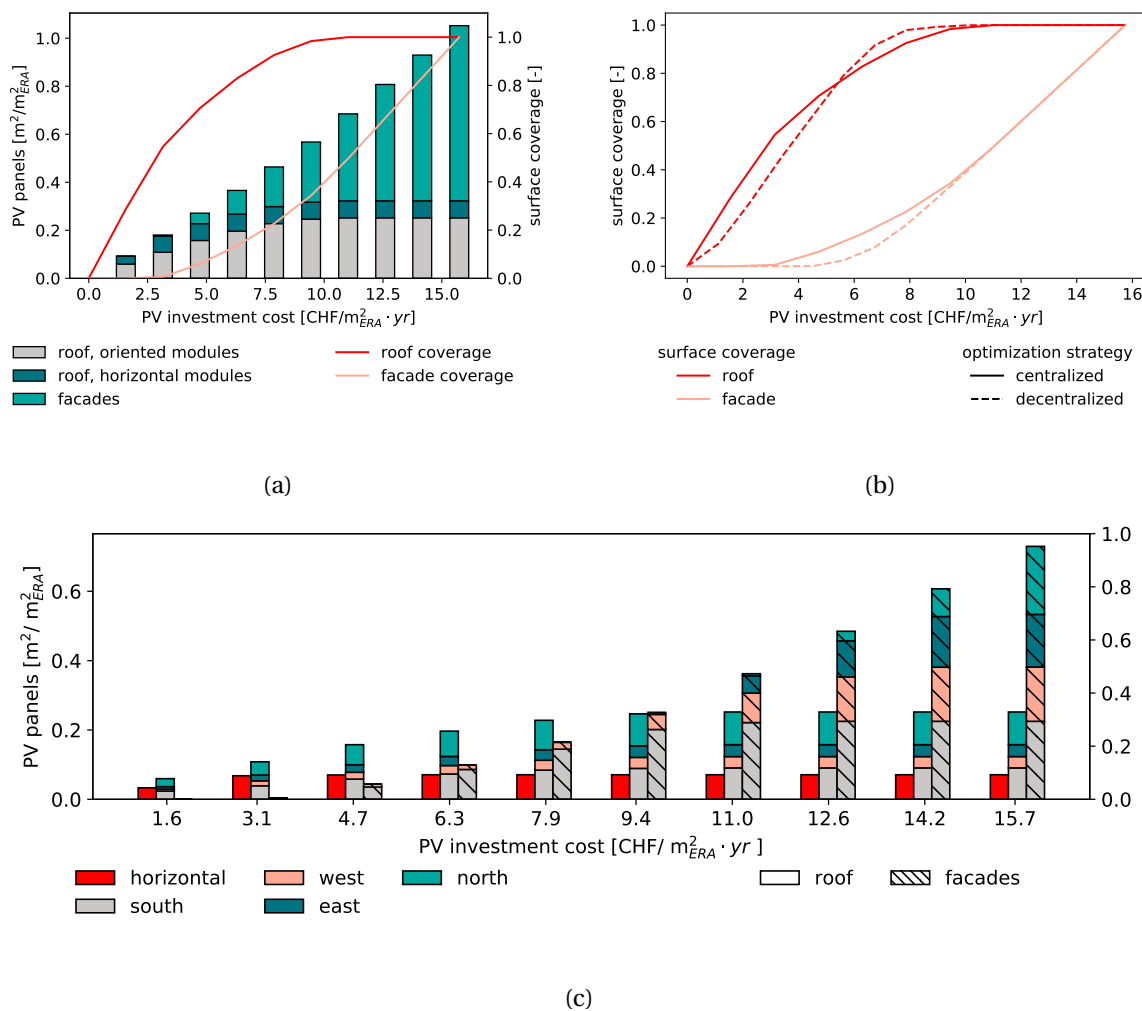


Figure 5.7 – Economic analysis of PV installations in the district a) Economic area covered with PV modules according to surface type. PV modules with tilt = 0°are horizontal, tilt angles = 90°are facades, oriented modules summarize all other tilt and azimuth angles. b) Comparison of the investment strategy with decentralized district optimization (compare to Figure 3.6) c) Orientation of economically PV installation.

Which surfaces are optimal for PV installations? The PV panel installation order with increasing investment cost is shown in Figure 5.7. As detailed in Figure 5.7a), horizontal and oriented roofs were selected first. For a given investment, the surface covered is not necessarily the same as the area of purchased PV modules. The surface coverage also accounts for the space between rows of oriented modules on flat roofs. At a roof coverage of 50%, facades started to be identified as the best choice economically. 40% of the facades were filled before the last roof was covered with PV panels. This is clearly against the strategy to pick the surface with highest solar potential. Only south-oriented facades had a higher annual potential than north-oriented roofs (see Figure 3.5). However, when the sun is lower in the sky during winter, when the heating demand is highest, the solar potential of facades can exceed that of roofs.

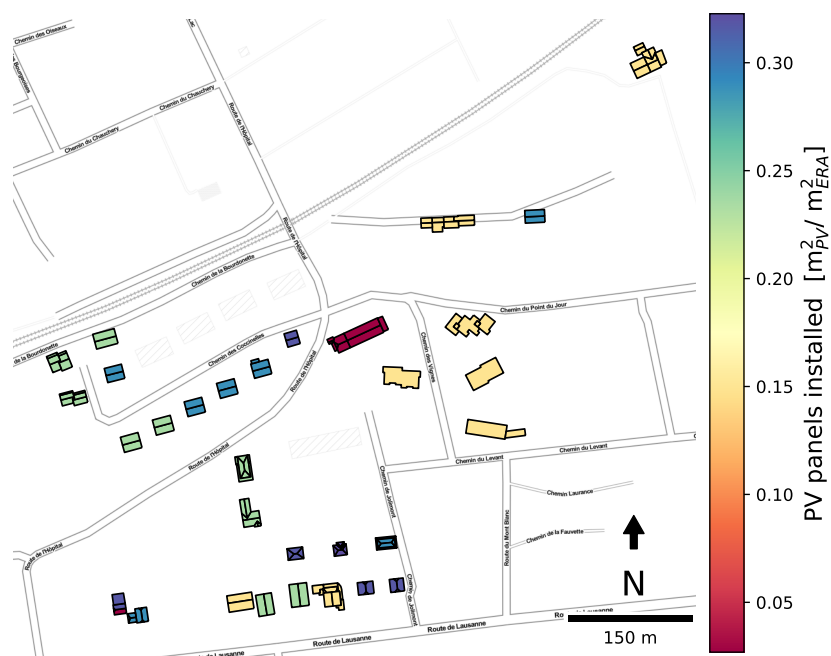


Figure 5.8 – Order of optimal PV panel installations on roofs in case study district. All buildings are connected to the same low-voltage transformers. The colors indicate at which level of PV integration the roofs are chosen for the first time.

When the decentralized optimization strategy was employed, nearly 90% of roofs were filled before considering PV modules on facades (Figure 3.6). In early investment stages, the centralized strategy allowed for a greater surface to be covered, as shown in Figure 5.7b. In these early stages of PV integration, little distinction seems to have been made between different roof orientations (Figure 5.7c). Whereas building owners would start by investing in PV panels on southern-oriented surfaces (see Figure 3.6c), analysis from the district perspective indicates that the entire roof should be covered. On a typical pointed roof choosing a southern-oriented surface would thus lead to use north-oriented surface areas, which have a much lower solar potential but optimizes fixed installation costs. Thus, for the same investment cost, more surfaces are covered with PV modules.

Along with the tilted south (and connected north-facing) roofs, horizontal roofs were fully covered.

The order in which roofs were chosen is shown in Figure 5.8. The optimal strategy for the roof coverage was as follows. 1) Big roof with large south oriented surfaces were identified. The entire roof was used, regardless orientation of remaining surfaces. 2) Horizontal roofs were then fully exploited. 3) The remaining roofs were chosen in the order of their solar potential, south-facing facades were preferred to north-facing roofs. 4) The optimal placement of facades modules was according to their solar potential: in order, south, west, east, and north.

How much PV solar energy can be generated locally and cost-efficiently? During the MOO, the operation and investment of the entire renewable energy hub was considered. To increase the share of renewable energy sources, the economically feasible range of solar energy in the district is a matter of interest. From the perspective of the investors, this includes the number of PV panels that can be fully paid back by the end of their lifetime. From the perspective of policymakers, this translates into the question, how to establish energy tariffs to create incentives for a desired PVP in the electricity grid.

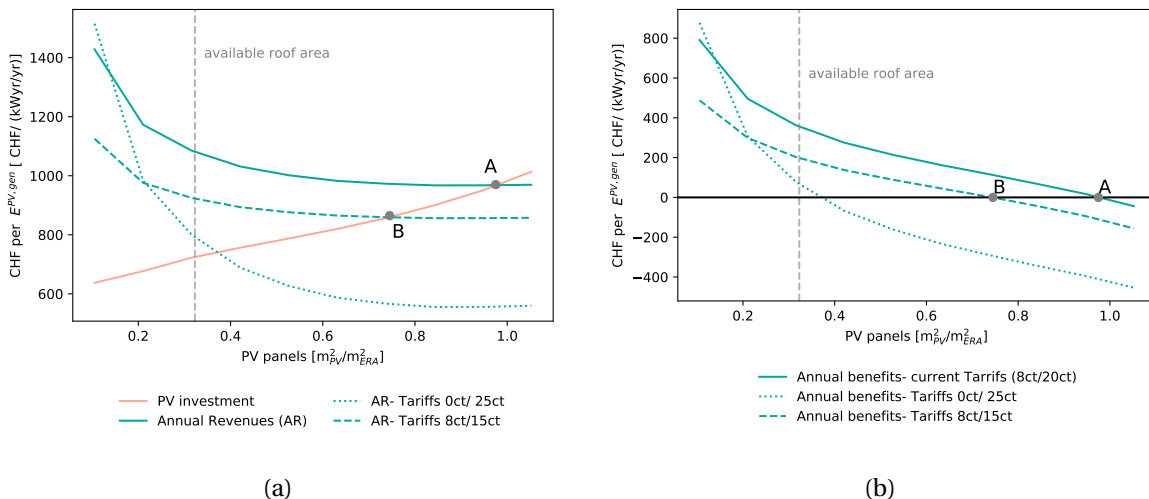


Figure 5.9 – a) PV investment per generated PV electricity E_{PV}^{gen} and implicit revenues for different feed-in and demand prices. Economic point: Investment in PV and connected revenues are balanced. Point A: current tariffs (8 ct feed-in, 20 ct demand price). Point B: break-even point for exemplary tariffs. b) Annual benefits, which are the annual revenues subtracted by the PV investment.

An economic analysis of PV panels in the district is summarized in Figure 5.9b. The cost of PV panels increased per generated kWyr electricity with the magnitude of PV investments. The first installed modules were cheapest per generated kWyr of electricity. In later investment stages, all profitable surfaces were covered and less profitable surfaces, like north-facing facades, were the only option left. At the same time, the annual revenues decreased with increasing investment into

5.3. Results

PV panels. This development can be explained by the higher self-consumption in the early stage. For investigated tariffs in Figure 5.9b, self-consumption was more beneficial than selling electricity, as it avoids paying higher prices to buy electricity from the grid. The last economically feasible point occurs when the investment cost of the PV panel and their revenues break-even. At current tariffs (20 and 8 ct/kWh), almost all surfaces in the district were financially sustainable in a centralized design strategy of the district. Lowering the electricity demand price by 5 ct/kWh reduced the economically feasible PV investment by 20%. The annual benefits depended on self-consumption in the scenario where no feed-in is reimbursed. Even if the electricity demand price is increased by 5 ct, much less PV investments are economically feasible.

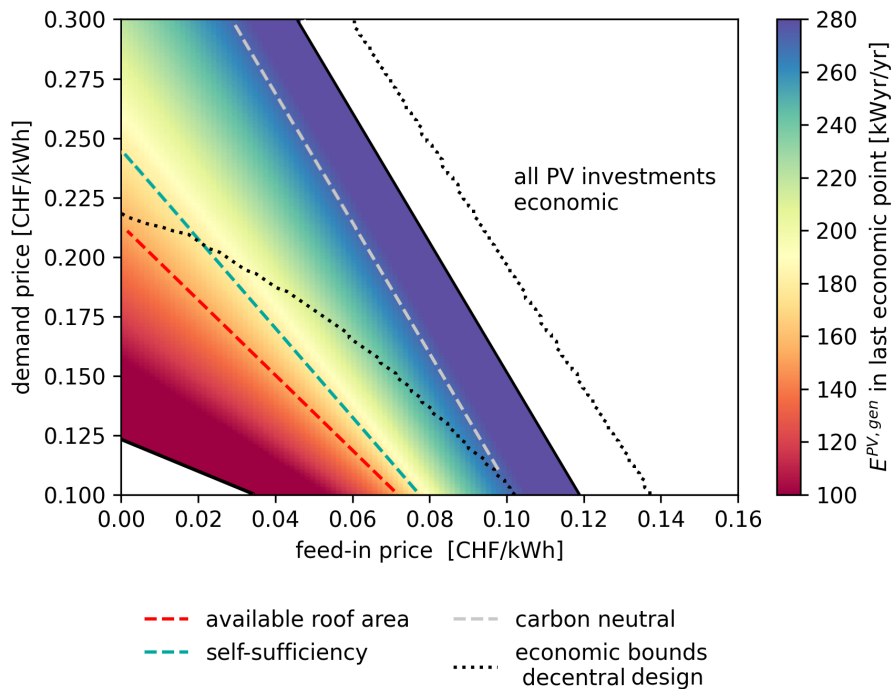


Figure 5.10 – Variation of the PV yearly generation to achieve break-even as a function of feed-in and demand prices of electricity. SS with ideal storage, round-trip efficiency $\eta = 100\%$. Carbon neutrality with dynamic emission profiles (Equation 5.9). Economic bounds from decentralized design strategy (see Figure 3.9b).

This economic analysis was extended to a wide range of tariffs in Figure 5.10. The analysis shows that PV investments became economically feasible at tariffs as low as 0 and 12 ct/kWh or 3 and 10 ct/kWh for feed-in and demand price, respectively. At a feed-in price of 12 ct/kWh, all PV installations were economically feasible, even at a demand price as low as 10 ct/kWh. The economic bounds of the decentralized design strategy are also indicated in Figure 5.10. The economically feasible region begins at much higher tariffs (10/10 ct/kWh and 0/22 ct/kWh), further demonstrating the benefit of a centralized, coordinated design strategy. Three points of interest are added in Figure 5.10:

available roof surfaces are fully covered, SS, and carbon neutrality are achieved. As the amount of electricity generated, was linearly correlated with the electricity tariffs, these points lie along a straight line. To achieve SS with PV panels alone, storage systems are required to balance the mismatch of electricity generation and consumption. The point of SS therefore depends on the round-trip efficiency of these storage systems. The SS was considered with ideal storage systems in Figure 5.10. More realistic cases of SS lie above the indicated line ($8/10$ ct/kWh and $0/25$ ct/kWh for combination of feed-in/demand price), and are discussed in more detail in the next section.

How much PV is needed to achieve self-sufficiency or carbon neutrality? Although PV panel installation has been demonstrated to be economically feasible, reaching electrical SS from PV panels requires the installation of storage capacities to overcome the mismatch of electricity generation and consumption.

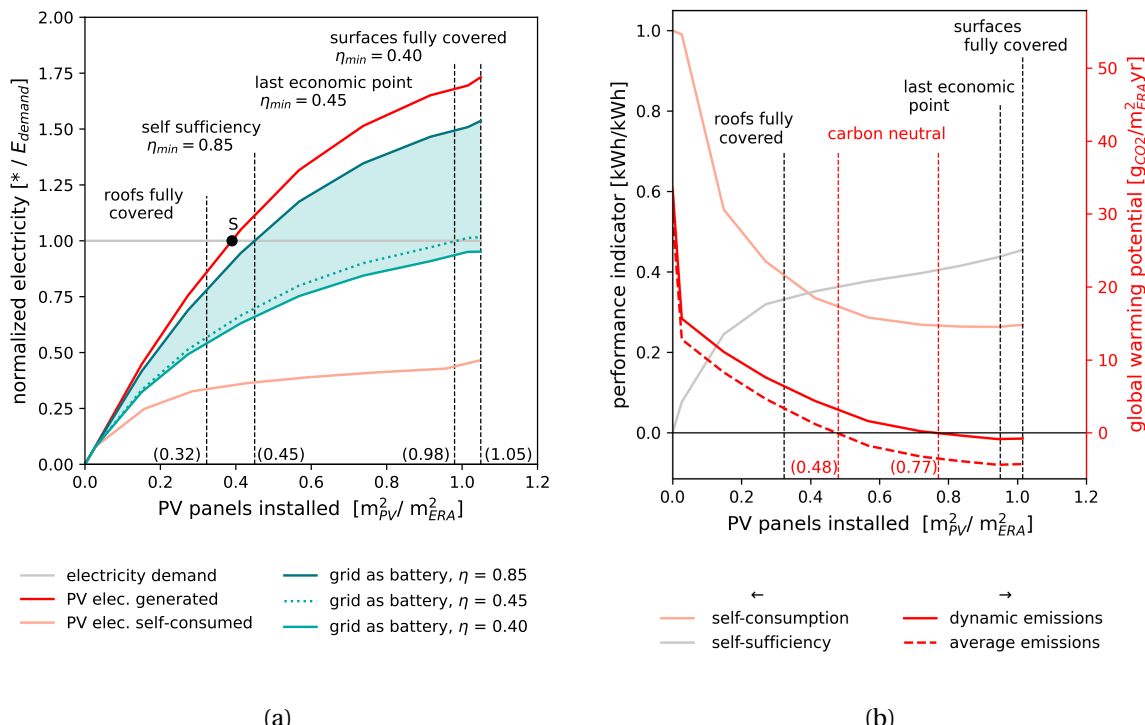


Figure 5.11 – Required PV panel installation to achieve a) self-sufficiency, using the grid as battery for different round-trip efficiencies η , and b) carbon neutrality. Point S: Self-sufficiency considering ideal storage with $\eta = 100\%$. Related emission intensity values based on the Swiss grid mix from 2019 [33].

Installing more PV panels, even in different sky orientations, cannot close this gap. Rather, SS could only be achieved using the grid as storage (i.e., by selling electricity to the grid to purchase it back at a later time), as shown in Figure 5.11a. All presented values are normalized to the electricity

5.3. Results

demand of the building. A maximum of 45% of the electricity demand can be covered by direct self-consumption of generated electricity; the difference must be re-imported from the grid. The minimum area of PV panels per ERA required to achieve SS was 0.4 for a round-trip efficiency of 100% (Point S). At this point, facades were already required. As the round-trip efficiency decreases, the required level of PV installation increases. In the case of highly efficient storage systems, such as lithium batteries, an efficiency of 85% was considered. In this case, the centralized and decentralized design strategies led to a required ratio of 0.45 m² PV panels per ERA. For the decentralized method, this value was identified slightly increased (0.53 m²_{PV}/m²_{ERA}, see Figure 3.10) for the decentralized design strategy. The difference between these two strategies here can be explained by the higher degree of pooling of electricity within the district involved in the centralized design strategy, which led to a smaller registered electricity demand at the transformer. The ratio of electricity generated per electricity demand was thus increased, reducing the required value for the point of SS. With current tariffs, the last point that was economically feasible was at 0.98 m²_{PV}/m²_{ERA} (Figure 5.9). To realize SS at that point, the round-trip efficiency of connected storage assets could be as low as 45%.

In case there is no storage system accounted for in the system, the SS reaches a maximum of 45% (Figure 5.11b), when covering all available surfaces with PV panels. In this case, the self-consumption saturates at around 27%. Carbon neutrality is defined as the point where the overall GWP becomes zero. The first drop seen in Figure 5.11 from 30 to 15 gCO₂/m²_{ERA} was mainly due to the electrification of the system, i.e, switching from natural gas boilers to heat pumps. Self-consumption of on-site generated electricity further reduced the GWP. However, as the SC decreasing with increasing PV installations, the share of GWP which is deduced due to the feed-in is gaining significance. When the carbon intensity of the electrical grid was considered volatile, 0.77 m² PV panels per m² ERA were necessary to achieve carbon neutrality. In contrast, assuming an annual average grid emission intensity required only 0.48 m²_{PV}/m²_{ERA} of installed PV panels to meet carbon neutrality. The carbon intensity of the grid is lowest during the day in summer. However, this is when the PV panels generate the most electricity. Hence, with average values the carbon emission were underestimated leading to a smaller required PV installation.

Given that the need of PV panel integration to achieve SS and carbon neutrality depends on the electricity demand of buildings, a reduction in the electricity demand would also reduce the required number of PV panels. The electricity demand can be lowered in multiple ways, such as improving the efficiency of energy conversion units, lowering the end-use demand of the buildings, or switching to other energy resources. The analysis presented was based on the current building stock until now; the identified points were all in high-CAPEX scenarios, where heat pumps were used for heat generation. The PV panel requirement found in this analysis can be influenced by: 1) to co-generating electricity with different equipment, 2) to refurbishing the building stock, and 3) to relying more on natural gas. The prior analysis was thus repeated considering these three scenarios; the resulting correlation between annual generated electricity and the area of required PV panels

for each scenario is detailed in Figure 5.12. Here, the ratio of electricity generated per area of PV module decreases as the solar potential of available surfaces decreases. In early PV investments, south-oriented roofs were available, in later investments, only north-facing facades were available.

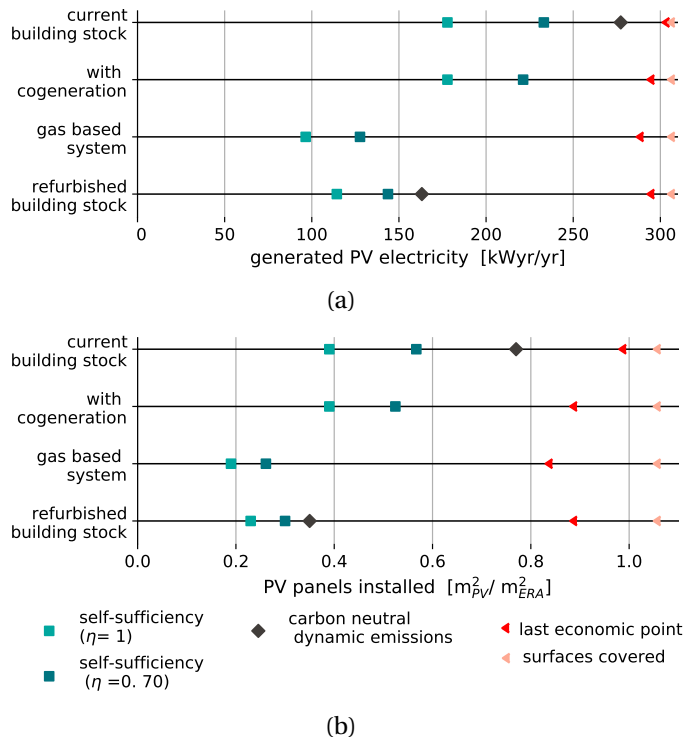


Figure 5.12 – Required PV panel integration for different district scenarios: current building stock, renovated building stock, and a scenario on the current building stock with cogeneration and gas boilers. a) Annual generated electricity from PV panels and b) area of installed PV modules per heated surface area.

Among the scenarios, the natural gas-based system required the smallest area of PV panels to become electrically self-sufficient (Figure 5.12). This energy system was based on a combination of heat pumps and gas boilers and resembles the BESSs of today. However, the requirements for natural gas were increased, which made it impossible to become carbon neutral. The most feasible path to reach carbon neutrality involved renovating the building stock and relying on an electric energy system. Refurbishing the building stock reduces the supply and return temperatures as well as the amount of heat required for space heating. This process reduces the electricity demand required by the heat pumps. Here, the annual electricity that is needed to achieve SS decreased by 35% with respect to the same installed system without renovating the building stock. This translates to a 40 % reduction of required PV panels to $0.29 A_{PV} / A_{ERA}$. To achieve carbon neutrality, the influence of the renovation is even greater. The PV panel installations could be reduced by 55% to $0.35 A_{PV} / A_{ERA}$. The inclusion of cogeneration in the form of solid oxide fuel cells (SOFCs) did not lead to a remarkable difference with respect to the scenario based on an electric system in the

5.3. Results

current building stock. With current tariffs (6 ct/ kWh natural gas, 8/24 ct/ kW electricity feed-in and demand) the SOFC was only used to cover peak loads. SOFCs only became optimal investments in high-investment scenarios after most well-oriented surfaces were covered with PV panels; only west, east, and north-facing facades were available at this point. Therefore, the SS point assuming ideal storage systems was identical (0.39 m^2_{PV} per heated surface), but SS requirements assuming a 70% round-trip efficiency were slightly reduced.

Table 5.2 – Limits and constraints for the integration of PV panels.

	available surfaces on roofs [$\text{m}^2_{PV} / \text{m}^2_{ERA}$]	available surfaces on facades [$\text{m}^2_{PV} / \text{m}^2_{ERA}$]	biggest economic PV installation [$\text{m}^2_{PV} / \text{m}^2_{ERA}$]	lowest round-trip efficiency [-]
current building stock	0.32	0.73	0.98	0.45
with cogeneration	0.32	0.73	0.88	0.31
gas based system	0.32	0.73	0.83	0.20
refurbished building stock	0.32	0.73	0.88	0.25

Reducing the electricity demand effects the bounds for economically feasible PV installation and the minimum round-trip efficiency to achieve SS (Table 5.2). For considered grid tariffs, self consumption was more beneficial than selling electricity. As the total self-consumption of kWh electricity decreased, the generated annual revenues equally decreased. For the same cost of PV modules per generated electricity, the last economical point reduced with the reduction of electricity demand. At the same time, the reduction of electricity demand requires less re-imports of electricity to achieve SS. The minimum required round trip-efficiency was thus reduced.

5

5.3.3 Grid-aware integration of renewable energy

Given that SS and carbon neutrality were demonstrated to require large but economically feasible capacities of PV panels, this section aims to identify the requirements of storage systems and analyze the feasibility of the integration of a large amount PV panels into the power grid.

What type of storage is needed? One benefit of centralized optimization is the inclusion of centralized units, which can be financed once for the entire district, rather than purchased by each

building. A central lithium battery that can be used for daily storage unit was added to the unit choices during MOO of the district.

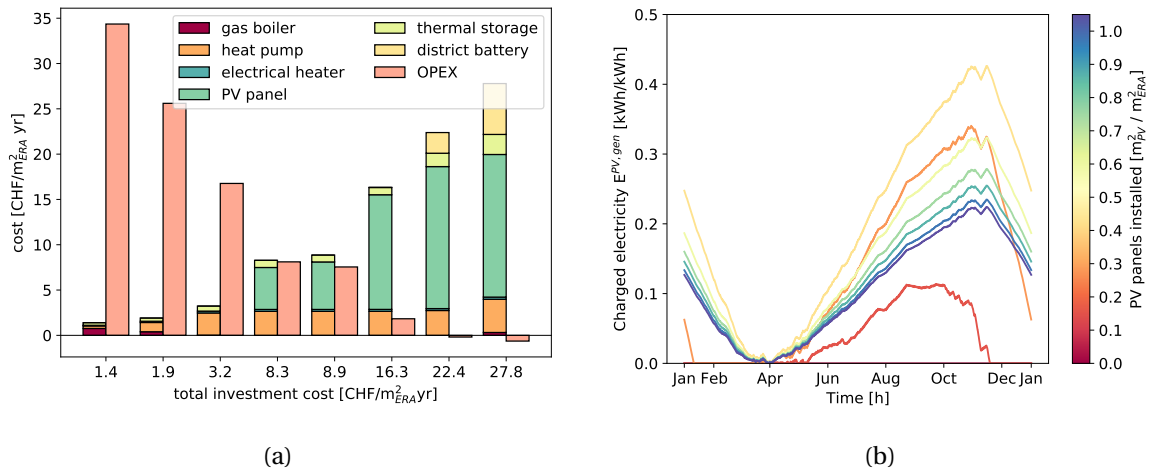


Figure 5.13 – Analysis of two storage systems: a) optimal investment strategy including daily district storage and b) state of charge of an ideal storage system aiming for SS for different levels of PV penetration.

The results of a MOO of the district, including a district storage system, are summarized in Figure 5.13a. The optimized result with the lowest CAPEX included natural gas boilers in combination with thermal storage tanks. The OPEX could be reduced by investing in heat pumps, followed by the investing in PV panels. The district battery was chosen as a last resort to further reduce the OPEX. Thus, the system did not profit from electricity storage enough to justify the investment at an earlier stage. As detailed in Figure 5.13b, this was due in part because the centralized storage should be a seasonal storage. The assumed storage system in Figure 5.13b had a round trip efficiency of 100% and was connected to the district. The state of charge is expressed as charged electricity per annual electricity generated from PV panels in the district. Different levels of PV integration were analyzed. Already at a low level of PV integration, excess electricity was charged in the summer months and discharged in autumn. The curve takes the form of a typical seasonal storage system, not a daily storage, like those included in the analyses visualized in Figure 5.13a. The curve reached its peak at 0.4 m² PV panel per m² ERA. At this point, more than 40% of the generated electricity was stored in the storage system. This point corresponds to the SS point with ideal storage (Figure 5.11a). A further expansion of PV systems was not needed to satisfy the electricity demand of the district. Hence, the level of stored electricity per generated electricity declined.

What is the influence of capacity constraints imposed from the electrical grid? Another benefit of the centralized design strategy is the possibility to include centralized requirements that concern the entire system, such as the maximum capacity of the local low-voltage transformer.

5.3. Results

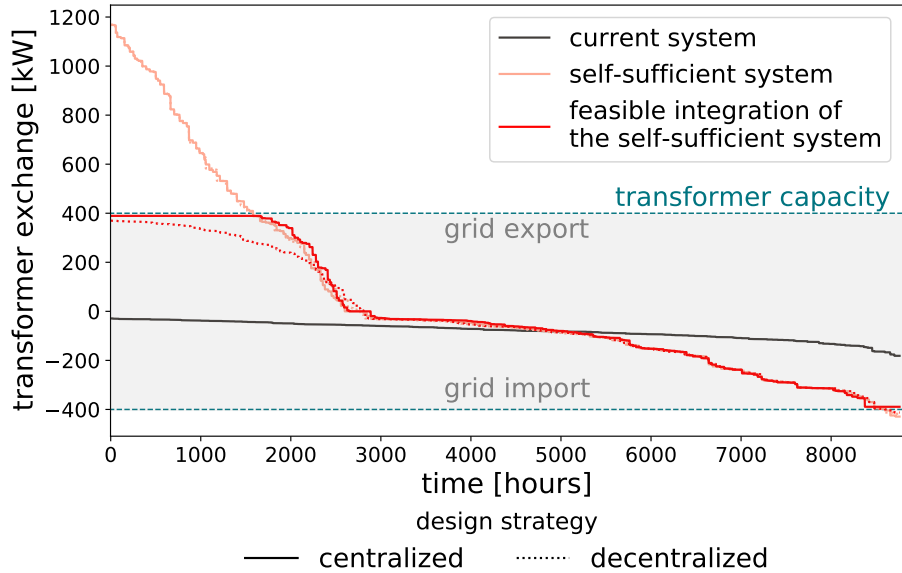


Figure 5.14 – Load duration curve on the local low-voltage transformer. Comparison of three different system scenarios: the current system, an identified self-sufficient system with a round-trip efficiency = 0.70%, and this latter system with modifications to be feasible at the transformer.

The load duration curve for different energy system scenarios is shown in Figure 5.14. The energy system design, which is currently installed in the district, lied clearly within the feasibility range of the transformer. The current system is characterized by the usage of gas boilers, a few heat pumps, and PV penetration so low that generated electricity is mainly consumed within the district. Aim of coming years is to drastically increase the level of PV integration, as it has been identified to be key on the way towards carbon neutrality [10]. Recent studies have demonstrated that the medium voltage level of the grid cannot host a large amount of PV installations [140]. Hence, the previously identified self-sufficient system including grid-aware PV integration and a storage system with a round-trip efficiency of $\eta = 0.7$ (Figure 5.12) is further analyzed here. With a peak feed-in of 1200 kW, the system exceeds the 400 kW capacity of the local transformer. A central grid constraint limiting the exchange to a maximum of 400 kW was imposed while maintaining the PV panel integration. This analysis provided feasible results using the centralized design strategy, as shown in Figure 5.14; however, this central constraint cannot be imposed using the decentralized design strategy. Therefore, the grid usage limit was split according to the magnitude of the uncontrollable load of the buildings (Equation 5.14). This procedure did lead to feasible solutions on the transformer but over-constrained the system. Imposing the transformer limits allowed feasible integration of PV, but came with certain costs, which are further detailed in Figure 5.15.

Peak reduction techniques are compared in Figure 5.15. The cost-optimal solution for the decentralized design strategy was to curtail excess electricity. More than 25% of PV electricity was curtailed,

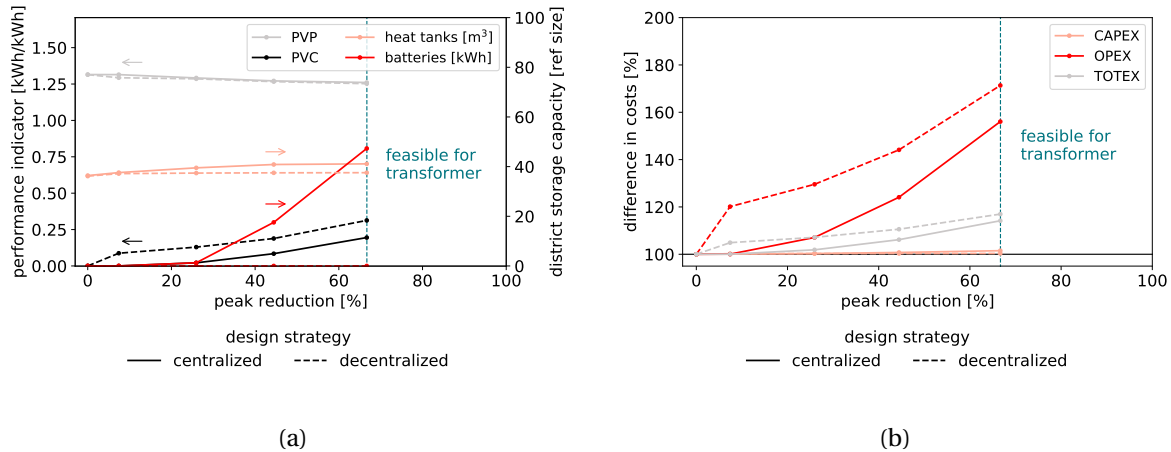


Figure 5.15 – Peak reduction for decentralized and centralized design strategy. a) Different measures for peak reduction: photovoltaic curtailment (PVC), resulting photovoltaic penetration (PVP) and storage system installations. b) Impact on related costs of the system.

5

which decreased the PVP by 4% and increased the OPEX by 70% at current feed-in tariffs of 8 ct/kWh. Using the centralized design strategy, however, allowed the peak exchange to be reduced by 25% by strategically operating the district, without requiring additional PVC or storage units. In this case, the capacity of the thermal tanks was marginally increased. The remaining reduction was achieved by a coordinated operation of the heat pumps, preheating the buildings, and using west-facing facades instead of south-facing facades as the preferred choice for PV panel installations. However, PV curtailment was still required, as this was not enough to be feasible at the transformer. However, the most cost-effective solution was not to curtail the excess completely, but purchase a central battery for peak shaving. This purchase increased the overall CAPEX of the energy system by less than 1% (Figure 5.15).

The baseline system is the already analyzed system, considering the current building stock with a high level of electrification. Additionally to this baseline scenario, the need of PV panels to become self-sufficient was analyzed for different district scenarios (Figure 5.12). The identified energy systems that are required to meet SS with a round-trip efficiency of 70% all exceeded the capacity of the transformer (Figure 5.16).

Furthermore, the capacity shortage of the transformer was correlated to the annual generated electricity within the district, as shown in Figure 5.16. The electricity demand of the baseline scenario and the scenario with cogeneration units installed was identical. However, part of the electricity demand was covered by cogeneration units instead of PV panels, which reduced the peak power and the annual capacity shortage marginally. The lowest capacity shortage was experienced using systems that reduced the overall electricity demand and, therefore, the amount of required PV panels to reach SS.

5.3. Results

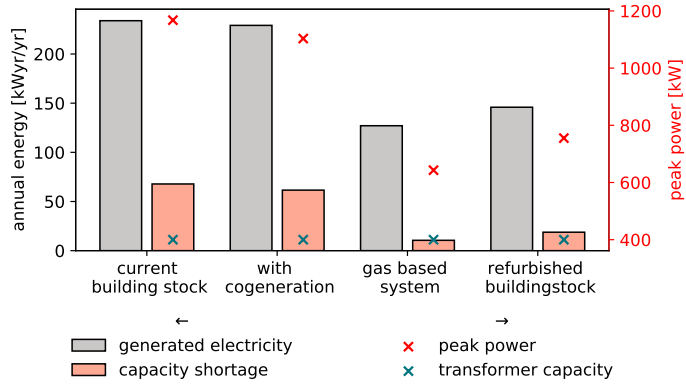


Figure 5.16 – Limitation imposed by the local transformer for different self-sufficient district scenarios with storage systems that have a round trip efficiency of 70% (see Figure 5.12).

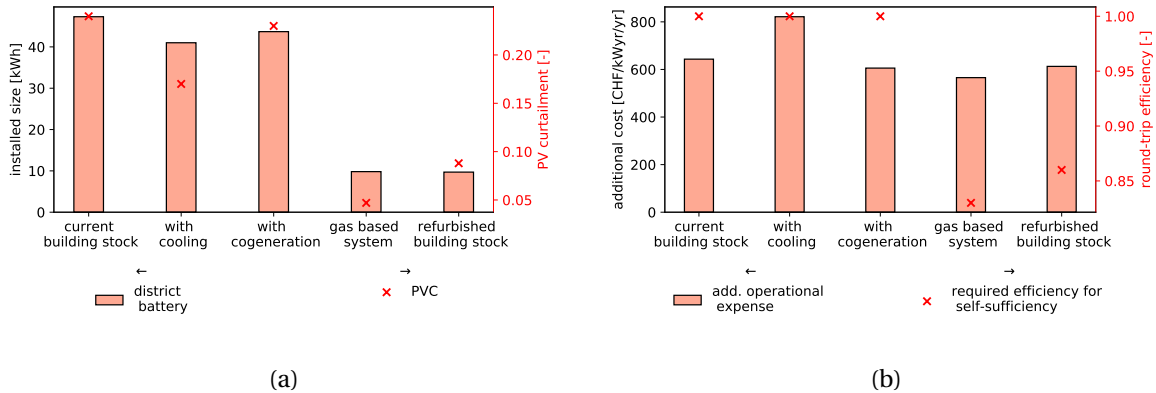


Figure 5.17 – Options for overcoming the local transformer limitation: a) required storage size for peak shaving and photovoltaic curtailment and b) additional efforts in terms of increased operation costs and round-trip efficiency for the district to remain self-sufficient.

Imposing transformer limitations during the centralized design of the district scenarios allowed solutions to be identified and the infeasibilities at the transformer to be overcome (Figure 5.17). The most economic solution involved installing a small district battery (size between 10 and 50 kWh) and curtailing remaining surplus electricity. The PV curtailment for the scenario with a renovated building stock was less than 10%, whereas the gas-based system required less than 5%. In contrast, 25% of all PV power was curtailed in the baseline scenario. Given that the curtailed electricity cannot be sold at feed-in price to the grid, the OPEX increased (Figure 5.17b). Regardless of the energy system, the cost increase was 600 CHF/kWyr/yr of capacity shortage at the transformer. This is a benchmark price for the reinforcement the system or for additional investments, which make a better use of the curtailed electricity. As electricity was curtailed in all analyzed systems, the round-tip efficiency needed to be increased to allow the system to remain self-sufficient. The baseline scenario required an ideal storage system to reach SS, whereas refurbishing the building

stock led to a more realistic required round-trip efficiency of 0.85 (Figure 5.17b). The PVC was the most economic solution. However, once the PV panels are purchased, curtailing the electricity or using it within the district has the same outcome. For example, the electricity can be used to power already installed heat pumps in reverse mode to supply cooling demand in summer. Since summer is when most solar peaks occur, the PVC decreased during this time by 10% (Figure 5.17a). As cooling must also be supplied during hours that are feasible at the transformer, the cost increase of this solution compared to the baseline scenario, without cooling is 800CHF/kWyr/yr(Figure 5.17b).

5.4 Conclusion

The aims of this chapter were two-fold: demonstrating the benefit of a strategic community-based design of distributed district energy systems and analyzing the grid-aware integration of solar energy in these renewable energy hubs at the district scale. To address the first of these aims, the proposed centralized design strategy was applied to a MOO framework of a typical central European residential district in Switzerland; the results were then compared with those obtained using a decentralized strategy, which focuses on the optimal design and operation of single buildings. The findings of a detailed analysis of the results are summarized below.

Objective The centralized strategy led to only non-dominated solutions on the Pareto frontier and outperformed the decentralized strategy in each scenario. This improvement was especially apparent in low-investment scenarios; Because the buildings become more independent from the community in high-investment scenarios, their results were more similar. To better compare these strategies no centralized units were considered, such as a combined heat and power plant, which led to the same unit investments in high-CAPEX and low-OPEX scenarios.

Unit selection and sizing The renewable energy hub with the lowest CAPEX was identical using both design strategies and was based on natural gas boilers. A similar approach was taken in both design strategies to reduce the OPEX of this system, i.e., switching from natural gas boilers to heat pumps. However, the centralized strategy allowed a better order of investment to be found: to achieve a 30% reduction in OPEX, the decentralized method required a 180% increase in CAPEX, whereas the centralized method required only a 5% increase in CAPEX. Moreover, the optimal sizing of units within the renewable energy hub was vastly improved by strategically sizing and placing the PV panels. Other equipment, such as heat pumps, electrical heaters, or distributed storage systems, could then be sized according to the computationally less-intensive decentralized optimization strategy.

Operation The centralized optimization of the operation led to an improved utilization of generated electricity in the district. Electricity pooling allowed for higher re-imports of electricity in all scenarios. For the same TOTEX, the centralized system led to a greater electrification of the system, increasing the PVP by 40% while reducing the total GWP by 20%.

The proposed method of analyzing grid-aware solar energy integration in renewable energy hubs at the district scale contributes to the state-of-the-art in district energy modeling, as entire low-voltage grids can be considered in a deterministic approach that includes the MOO of the thermal and electricity systems. Furthermore, the proposed centralized approach allows the consideration of centralized and distributed energy units in the district. Additionally, special focus was given here to highlight the needs and limitations of PV panel integration. The main findings are summarized below.

Placement strategy of PV panels The centralized strategy prioritized the largest, south-oriented surfaces in the district and filled the entire roof with PV panels, even if less optimal surfaces were present on the same roof. Horizontal roofs were then filled. The optimal surfaces were then chosen according to their solar potential: west, east, and finally north. South-facing facades were preferred to north-facing roofs.

Economic feasibility The price of PV panels per unit of generated electricity increased linearly as available surfaces in the district were filled. Less optimal surfaces were more costly than more optimal surfaces, such as south-oriented roofs. However, with the centralized, coordinated investment and operation strategy, PV panel installations were economically feasible for a wide range of tariffs, starting as low as 10 and 3 ct/kWh and 0 and 12.5 ct/kWh for feed-in and demand prices, respectively. This range was extended with respect to the decentralized strategy. At current tariffs, 93% of all surfaces were economically feasible, including all roof surfaces and almost all facades.

Achieving self-sufficiency and carbon neutrality PV panel integration can provide a route for the district to become carbon-neutral or self-sufficient. According to the presented results, both needs can be satisfied within the bounds of economic feasibility. Meeting SS using only PV panel installations requires the installation of storage systems. As the round-trip efficiency of the storage system increased from 45% to 100%, the required PV coverage decreased from 93% to 37%. Without storage systems, SS saturated at 45%. At this point, the SC was 27%. To achieve carbon neutrality, 73% of surfaces were covered with PV panels. This point was identified including a life cycle assessment of the equipment and hourly electricity grid-mix values from the year 2019.

The role of renovation Renovating the building stock drastically reduced the electricity demand, thereby decreasing the PV panel requirements and decreasing the economic bound by 10% to 84% ($0.88 A_{pv} / A^{ERA}$). Furthermore, the lowest possible round-trip efficiency required to meet SS within economic bounds decreased from 45% to 25%. District SS was reached by covering 25% to 84% of available surfaces with PV panels as the round-trip efficiency was decreased from 100% to 25%. Further, refurbishing the district allowed for a 55% reduction in the PV requirements to meet carbon neutrality (i.e., $0.35 A^{pv} / A^{ERA}$).

Technical feasibility The feasible integration of self-sufficient renewable energy hubs using the superior network as a storage system with a round-trip efficiency of 70% were then analyzed.

Additional to the baseline scenario, three different district scenarios were considered: a scenario with refurbished building stock, a system with additional cogeneration, and a system with an increased reliance on natural gas. The optimal, self-sufficient energy system for each scenario was infeasible at the district transformer without additional efforts. Necessary storage sizes for peak shaving ranged from 10 kWh to 40 kWh. Additionally, a PVC between 5% and 25% was required. These measures led to a cost increase of 600 CHF/kWyr/yr of capacity shortage, which is a benchmark price for the reinforcement of the system or for other investments.

Here, the only units considered as centralized units were daily storage systems. However, the presented analysis of the needs and limitations of solar integration demonstrate that seasonal storage systems with round-trip efficiency of greater than 0.45 for the current building stock and greater than 0.20 for a refurbished building stock would be required for the district to become self-sufficient. Thus, future work should consider the integration of seasonal storage systems or the inclusion of district heating and cooling network, which would allow centralized CHP units and thermal energy exchange between buildings. The charging infrastructure of electric vehicles could also be embedded in renewable energy hubs at the district scale. Additionally, the proposed approach also allows the investigation of tariffs or fees, when re-importing electricity from the community. These fees could be included in the economic analysis of investments at the district scale.

Conclusion

Overview

- General summary of developed methods
- Key answers to research questions
- Limitations and future perspectives

Although conclusions, including limitations and possible extension of the work, have been made in each chapter individually, the key findings and main perspectives are summarized in this chapter.

Chapter 1 "*How are renewable energy hubs defined at building scale?*" A mixed-integer linear programming (MILP) approach was used to define renewable energy hubs at the building scale. Energy carriers considered to satisfy the demand for space heating, domestic hot water, and electricity included solar irradiation, air, water, natural gas, and electricity. Air-water heat pumps, gas boilers, photovoltaic (PV) panels, electrical heaters and combined heat and power (CHP) units in the form of solid-oxide fuel cells were considered as conversion technologies. Electricity could be stored in batteries, thermal energy in separate a tank for space heat and domestic hot water, and in the building itself. The building was modeled according to the first-order dynamic building model (1R1C), with the a possibility to include a smart heating strategy in which the building is preheated in times of surplus electricity from renewable sources. Multi-objective optimization (MOO) was implemented to search the decision space of the renewable energy hubs, considering the objectives of minimizing operational expenses (OPEX), capital expenses (CAPEX), total expenses (TOTEX), and global warming potential (GWP) of the building energy system (BES), which was used to define the scope of the renewable energy hub at the building scale.

"What performance indicators should be used to describe renewable energy hubs?" Considering the state-of-the-art in BES modeling, 32 key performance indicators (KPIs) were collected, including controversial aspects, such as (i) appropriate system boundaries, (ii) resolution time, (iii) and the environmental impact of the energy conversion and storage units. The analysis of the measures was structured in two parts. In the first part, individual KPIs are investigated; in the second, an analysis of the correlation of KPIs is performed.

Conclusion

The analysis of KPIs in the context of the environmental impact provided three main findings. First, constructing modern, decentralized systems requires an analysis of emissions associated with construction, where these emissions can account >40% of the total GWP. This contrasts with the GWP associated with constructing basic renewable energy hubs (e.g., not comprising PV panels and batteries), which is often neglectable (<5% of the total GWP). Second, the grid mix has a great impact on the optimal strategy of renewable energy hubs. The lower the imported emissions of the electricity, the lower the incentives are to install independent, decentralized solutions, which rely on renewable energies and storage systems but are high in constructional GWP. Third, the usage of annual average values of the grid mix underestimates the GWP of renewable energy hubs by approximately 10%. Therefore, the GWP should be calculated including the constructional footprint of the energy system equipment and dynamic impact profiles of the grid.

Machine learning techniques, including principle component analysis and k-medoids clustering, were then applied to identify the major trends, thus supporting multi-criteria decision making. Several measures (e.g., OPEX) were identified to contribute more to the defined design of renewable energy hubs than others (e.g., levelized cost of electricity). An examination of the correlation between the identified KPI clarified that the performance of a renewable energy hub can be evaluated using three indicators.

Chapter 2 "*What is the impact of the orientation of PV panels on renewable energy hubs and the grid?*" Researchers in the field of BES optimization have mainly considered horizontal PV modules and based purchasing decisions on global irradiation without shadowing effects. The influence of including different panel orientations, both from the perspective of the individual building and of the grid, was analyzed and used to provide a methodology for selecting which roofs should be covered first. Incident solar irradiation was modeled by discretizing the skydome into 145 patches, each containing information about the irradiation density in a given time horizon. This approach was based on an anisotropic irradiation model that accounts for direct and diffuse irradiation. On horizontal roofs, shadow casting among rows of PV modules was also taken into account. The results confirmed the relevant influence of PV panels' azimuth and tilt on the performance of the renewable energy hub. Whereas south-oriented panels remains the preferred choice, west-oriented panels better match the demand when compared with east-oriented panels. Apart from the direct benefits for renewable energy hubs at the building scale, the interaction with the overlaying grid was also analyzed. When combined with appropriate scheduling, rotating the panels 20° westwards can reduce the peak power of the exchange between the renewable energy hub and the power grid by 50% while increasing the TOTEX by only 8.3%. Including a more detailed modeling of the PV energy generation demonstrated that assuming horizontal surfaces can lead to inaccuracies of up to 20% when calculating operating expenses and electricity generated, particularly for high levels of PV penetration.

Chapter 3 "*What is the role and potential of facades in decentralized energy hubs?*" To address this question, the assessment of the solar irradiation on facades, including the shadow cast from the surrounding buildings was assessed. The incoming solar irradiation was considered in two aspects: generating electricity on facade-mounted PV modules and the assessingng solar heat gains. The proposed approach was applied to a typical, central European, peri-urban district located in Switzerland. The district was considered as a decentralized collection of renewable energy hubs at the building scale. In the proposed approach, buildings interact with each other: 1) by contributing to the overall electricity balance of the district, both consuming and generating electricity, and 2) by shading neighboring surfaces and roofs, thus influencing the actual potential for local solar generation. The results indicated that the district could achieve carbon neutrality based on PV energy alone, but that this requires covering all the available district's rooftops and part of the district's facades with PV panels. Whereas facades are generally disregarded due to their lower generation potential, facade-mounted PV panels can be economically convenient for a wide range of electricity prices, including those currently used by the Swiss grid operators. Achieving self-sufficiency at in the district is challenging, as it would require approximately 42% to 100% of all available surfaces to be covered (including facades) as the round trip efficiency decreases from 100% to 50%. These results underline the importance of storage for achieving self-sufficiency: even with 100% round trip efficiency for the storage, the required ratio of area covered in PV modules to the energy reference area (ERA) was $A_{pv}/A_{ERA} = 0.44$. In this case, 16% of available facades in the district were needed to be covered with PV modules. However, energy demand reduction through renovation would allow self-sufficiency to be reached with only half of this PV and storage capacity.

Chapter 4 "*What is the best method to overcome runtime issues when generating centralized energy hub designs?*" Two methods were considered to tackle the computational reduction for centralized energy hubs at the district scale. The first one is a novel approach involving the time-series aggregation (TSA) of input data that evaluates the performance of the renewable energy hub rather than the one of the clustering algorithm. Although this approach has been able to reduce computational effort by 90% while diverting less than 2% from Pareto-optimal solutions, it is not suitable to tackle large-scale problems. The second method involves the decomposition of the compact model formulation into several smaller, connected problems. A literature review revealed the Dantzig-Wolfe decomposition method as the most promising for this purpose. This decomposition method uses one master problem on the network level and several sub problems, one for each building energy system. The method leverages on the concept of duality, which communicates the centralized design strategy from the master problem to the sub problems. This approach is as highly scalable, robust to integer decisions in the sub problems, and able to track interactions among the distributed energy hubs in the district. An additional contribution to the state-of-the-art is the implementation of MOO, which so allowed an improvement in the initialization of the decomposition algorithm. Validating the decomposed formulation against the compact formulation showed an error of less than 0.02% and identical unit decisions.

Chapter 5 "*What are the potential and limitations of centralized renewable energy hubs at the district scale?*" To answer this research question, the decomposition method developed and validated in Chapter 4 was applied to the same peri-urban district investigated in Chapter 3, thus allowing a direct comparison between the centralized and decentralized district design strategies. In all scenarios along the Pareto frontier, the centralized strategy outperformed the decentralized one. The coordinated investment strategy in low-CAPEX scenarios and the improved interaction among buildings were especially apparent. For the same TOTEX, the centralized system led to a greater electrification of the system, increasing the PV penetration by 40% while reducing the total GWP by 20%. Unlike in the decentralized strategy, where only optimal surfaces were selected (see Chapter 3), the centralized approach instead tended to select entire roofs to be covered, regardless of the requirements of that specific building, thereby better utilizing the district's surface resources and reducing the CAPEX per building overall. As a result, the economic feasibility range was expanded for PV installations for the renewable energy hub at the district scale. The round-trip efficiency, required to achieve self-sufficiency must also be considered; using the centralized approach, the coordinated operation in the district allows this efficiency to be 25%, whereas the decentralized approached required a minimum round-trip efficiency of 45%.

Furthermore, considering renewable energy hubs at the district scale allows centralized units and constraints to be included in the approach. By considering the local grid transformer limitations, it was shown that further efforts are required to include a high share of renewable energies. To reach electrical self-sufficiency, the economically best solution involves installing central storage systems for peak shaving and between 5% and 25% curtailment of the PV electricity. This solution requires an improved round-trip efficiency to the district to remain self-sufficient. The only feasible solution that also had the potential to be carbon neutral required renovating the building stock and increasing the round-trip efficiency from 70% to 85%.

Limitations and future perspectives

In the introduction, future perspectives about the goal of PV deployments using Switzerland as an example were stated, and questions on the impact of these goals on building energy systems were raised. These questions were then addressed through the proposal and application of an analysis method. In Chapter 5, PV panel integration requirements were demonstrated for different district scenarios.

Comparing these results with the goals set by the Swiss Federal Office of Energy (SFOE; [11]) and the Association of Swiss Solar Energy Professionals (Swissolar; [12]) demonstrated that the goal stipulated by the SFOE is not sufficient reach self-sufficiency or carbon neutrality in the building sector, even if the entire building stock is renovated (Figure 5.18). However, combining Swissolar's goal with refurbishing the building stock, would allow both principles; however, reaching carbon neutrality

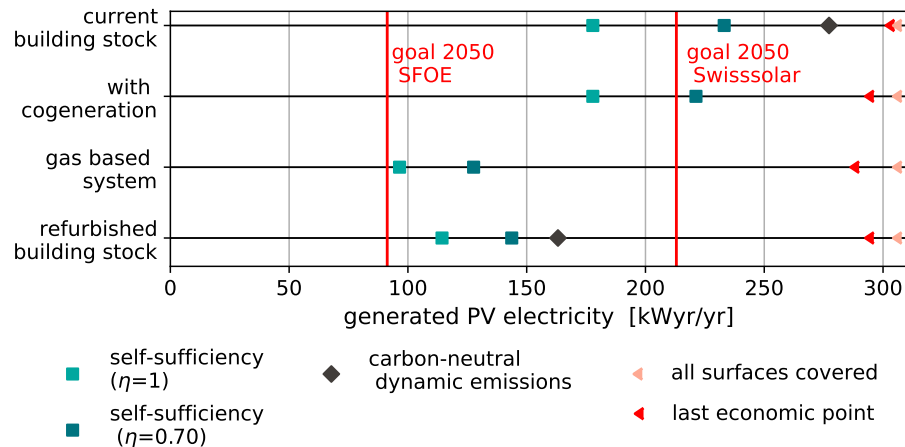


Figure 5.18 – Impact of the Swiss goals for 2050 for PV deployment. Goals according to Swiss Federal Office of Energy (SFOE) [11] and Swissolar, the Swiss Solar Energy Professionals Association [12]. These goals involve an exploited capacity of 30% and 70%, respectively.

would require a reduction in the natural gas demand of building energy systems (Figure 5.18).

In the presented results, renewable energy sources were optimally integrated based on the concept of renewable energy hubs at the district scale. This process demonstrated, that a high share of renewable energy sources are economically feasible but not necessarily technically feasible. However, the integration of renewable energies can be further improved. The developed method allows the consideration of thermal networks in the district. In this case, central CHP units and thermal exchanges among the buildings enhance further exploration of the renewable energy hub at the district scale. Further, an analysis of storage requirements demonstrated that seasonal storage should be considered, which can be also integrated in proposed approach.

The developed method was based on the typical building categories detailed by the national standard norm SIA [31]. However, the case study only considered a residential peri-urban area. This method should be applied to more diverse city districts, including those containing a higher share of industrial, public, or office buildings, as such an application might reveal interesting correlations and synergies among the diverse prosumers in the district. Analyzing more diverse energy prosumers would also allow renewable energy hubs to be defined at the national or regional scale, with typical renewable energy hubs at the district scale as a collection of sub systems.

In the future, extreme weather events are likely to increase and the average temperature is expected to increase [43]. This aspect could be reflected in the definition of typical time periods; here, they were defined based on one typical year, although the project horizon was on the magnitude of multiple decades. The ambient weather impacts the thermal demand and cooling demand is

Conclusion

expected to gain importance. Additionally, charging of electric vehicles will become a challenge that can be investigated in district energy systems.

Appendix

(Chapter 1)

Table A.1 – Global warming potential (GWP) and renewable energy share (RES) impact factors related to the grid, yearly average values of the profiles derived from the method provided by Kantor et al. [33].

	GWP	RES	ref.
electricity mix, Switzerland ⁺	0.134 kg _{CO₂} /kWh	0.42	[33]
electricity mix, France ⁺	0.072 kg _{CO₂} /kWh	0.20	[33]
electricity mix, Poland ⁺	0.933 kg _{CO₂} /kWh	0.13	[33]
electricity mix, Germany ⁺	0.508 kg _{CO₂} /kWh	0.40	[33]
natural gas [†]	0.214 kg _{CO₂} /kWh	0	[193]
heating oil [†]	0.322 kg _{CO₂} /kWh	0	[193]
thermal solar [†]	0.034 kg _{CO₂} /kWh	1	[193]
electricity from photovoltaic (PV) panels [*]	0.043 kg _{CO₂} /kWh	1	[194]

⁺ Values associated to consumption, reference year: 2019

[†] Reference: useful heat. Further details in Table A.2

^{*} Reference: final energy. Including life cycle assessment (LCA) of the technologies. Used only for calculating current state of the system.

A

Table A.2 – GWP factor g^{ng} of transmission and combustion of natural gas in Switzerland [34]

combustion emissions	g _{CO₂-eq} /m ³	1837
transmission emission	g _{CO₂-eq} /m ³	484
heating value	MJ/m ³	39
GWP factor g^{ng}	g _{CO₂-eq} /kWh	214

Appendix A. (Chapter 1)

Table A.3 – Performance efficiencies for assessing current operating cost based on demand values. Considered services: space heating (SH) and domestic hot water (DHW). Reference resource costs: natural gas 10 ct, electricity from the grid 20 ct, electricity from PV panels 0ct, heating oil 11ct, solar heat 0ct.

technology	service	η^{min}	η^{max}
gas boiler	SH	0.8	0.85
oil boiler	SH	0.8	0.85
district heating gas	SH	0.93	0.97
electric boiler	SH	0.93	0.97
air/water heat pump (HP)	SH	2.8	3.7
ground/water HP	SH	3.4	4.4
water/water HP	SH	3.4	4.7
solar heat	SH	1	1
electric boiler	DHW	0.9	0.95
gas boiler	DHW	0.8	0.85
oil boiler	DHW	0.8	0.85
district heating gas	DHW	0.93	0.97
air/water HP	DHW	2.2	3
solar heat	DHW	1	1
dhw storage and distribution	DHW	0.55	0.75

Table A.4 – Parameter data for modeling photovoltaic panels.

description	symbol	value	unit	ref.
panel height	h^{pv}	1	m	-
panel width	w^{pv}	1.6	m	-
inverter efficiency	η_{inv}	0.97	-	-
reference efficiency	$\eta^{ref,pv}$	0.17	-	[125]
temperature coefficient	δ^{pv}	0.0012	K^{-1}	[22]
absorption coefficient	ν^{pv}	0.9	-	[22]
module heat transfer coefficient	U^{pv}	29.1	W/m^2K	[22]
cost parameter	$i^{c1,pv}$	6556	CHF	[125]
cost parameter	$i^{c2,pv}$	1978	CHF/kWp	[125]
baremodule	b^{pv}	1.0	-	[22]
lifetime	l^{pv}	20	yr	[22]

Table A.5 – Global warming potential to the construction of energy system technologies. Linearized according to values taken from ecoinvent [34], fixed impact factor i^{g1} , continuous impact factor i^{g2} , see Equation 1.20

technology [r]	$i^{g1} [\text{kgCO}_2]$	$i^{g2} [\text{kgCO}_2/\text{r}]$
batteries [kg]	0	7.8106
cogeneration unit [kWe]	460.55	0
electrical heater [kWth]	2.04	0.41
gas boiler [kWth]	253.27	11.62
heat pump [kWe]	0	138
photovoltaic panels [m ²]	0	78.711
thermal storage [m ³]	0	1204

Table A.6 – Economic parameters of energy system technologies according to Stadler [22], lifetime l_u , baremodule b_u , fixed cost factor i^{c1} , continuous cost factor i^{c2} , see cost equations 1.16

technology [◊]	$i^{c1} [\text{CHF}]$	$i^{c2} [\text{CHF}/◊]$	$b^u [-]$	$l_u [\text{yr}]$
gas boiler [kWth]	3800	105	1.8	20
cogeneration [kWe]	15442	2100	1.8	20
heat pump [kWe]	5680	1240	1.8	20
electrical heater [kWth]	968	13	1	20
thermal storage SH [m ³]	760	1040	1.87	20
thermal storage DHW [m ³]	295	6100	1.68	20
batteries [kWh]	620	970	1.33	10

Table A.7 – Bounds of the unit sizes of the energy system technologies, see sizing equations 1.1.

technology	ref. unit	F^{\min}	F^{\max}
heat pump	kWe	1.5	1e5
gas boiler	kWe	0.1	1e5
cogeneration	kWe	0.7	2.5
battery	kWh	0.1	100
thermal storage (SH)	m ³	0.1	10
thermal storage (DHW)	m ³	0.06	10
electrical heater	kW _{th}	0	100

A

Appendix A. (Chapter 1)

Table A.8 – Considered second law efficiency for different temperature levels of the heat pump. Temperatures in °C.

T^{source}	-20	-15	-10	-7	-2	2	7	10	15	20
$T^{sink} = 35$	0.0	0.464	0.458	0.458	0.469	0.462	0.435	0.416	0.370	0.307
$T^{sink} = 45$	0.0	0.445	0.463	0.464	0.460	0.446	0.439	0.436	0.430	0.396
$T^{sink} = 55$	0.0	0.0	0.0	0.421	0.423	0.416	0.439	0.436	0.412	0.395

Table A.9 – Considered part load limit for different temperature levels of the heat pump. Temperatures in °C.

T^{source}	-20	-15	-10	-7	-2	2	7	10	15	20
$T^{sink} = 35$	0.00	0.62	0.65	0.65	0.65	0.65	0.68	0.68	0.68	0.68
$T^{sink} = 45$	0.00	0.74	0.74	0.74	0.76	0.79	0.82	0.82	0.79	0.79
$T^{sink} = 55$	0.00	0.00	0.00	0.91	0.94	0.97	0.97	0.97	1.00	1.00

Table A.10 – Annual uncontrollable load E , annual demand for space heating Q^{SH} , annual demand for domestic hot water Q^{dhw} for different building categories and types according to national standard norms [31] and [131]. All values in [kWh/m²].

affiliation	type	standard			existing		
		E	Q^{SH}	Q^{dhw}	E	Q^{SH}	Q^{DHW}
multi-family home	I	20	18	17.8	21.7	103.3	17.8
single-family home	II	19.2	28.8	13.5	21.8	172.7	13.5
administration	III	44.4	12.7	2.1	61.8	56.9	2.1
school	IV	26.6	22	3.2	27.2	101.8	3.2
shop	V	140.4	6.5	1.51	160.5	37.1	1.5
restaurant	VI	85.2	23.7	65.5	109.5	117.2	65.5
assembly hall	VII	45.1	20.2	4.5	57.6	101.3	4.5
hospital	VIII	40.6	14.8	34	40.1	79	34
industry	IX	52.9	18.2	1.8	74.5	82.4	1.8
warehouse	X	21.6	16.9	0.9	20.3	76.3	0.9
gymnasium	XI	24.6	17.8	37	20.7	78.8	37
swimming pool	XII	39.9	27.9	104.7	47	114	105
hall	XIII	22	18	0.9	19	85	0.9

Table A.11 – Building details of the case study. Building category according to standard norm [131], energy reference area (ERA) A^{era} in [m^2], current installed resources for SH and DHW, ground area A^{gr} in [m^2], design supply/return temperature $T_0^{s/r}$ in $^\circ\text{C}$, overall heat transfer factor U in [$\text{W}/(\text{m}^2 \text{K})$], heat capacity factor C in [$\text{Wh}/(\text{m}^2 \text{K})$], solar gain factor ϕ . Source: databases of the national building stock [44, 45]. Temperatures and heat transfer parameters [23].

ID	date	category	type	A^{era}	SH ^{res}	DHW ^{res}	A^{gr}	T_0^r	T_0^s	C	U	ϕ
1	1974	existing	I	1123	oil	oil	225	50	65	120	2.09	0.078
2	1974	existing	I	1098	oil	oil	220	50	65	120	2.09	0.078
3	1981	existing	I	1544	oil	oil	386	50	65	120	1.52	0.048
4	1981	existing	I	842	oil	oil	211	50	65	120	1.52	0.048
5	1981	existing	I	848	oil	oil	212	50	65	120	1.52	0.048
6	1972	existing	I	1531	oil	oil	383	50	65	120	2.09	0.078
7	1935	existing	I	333	oil	oil	111	50	65	120	2.02	0.074
8	1995	existing	I	719	gas	gas	240	50	65	120	1.52	0.048
9	2013	standard	I	609	hp	solar	213	33.9	41.5	120	0.83	0.012
10	2014	standard	I	598	gas	solar	250	33.9	41.5	120	0.83	0.012
11	1940	existing	II	1158	oil	oil	386	50	65	120	1.52	0.048
12	1960	existing	II	412	gas	gas	206	50	65	120	2.02	0.074
13	2001	existing	II	263	gas	gas	131	50	65	120	1.52	0.048
14	2005	existing	II	260	elec.	elec.	87	50	65	120	1.52	0.048
15	1985	existing	II	267	elec.	elec.	89	50	65	120	1.52	0.048
16	1982	existing	II	157	elec.	elec.	78	50	65	120	1.52	0.048
17	1982	existing	II	157	elec.	elec.	79	50	65	120	1.52	0.048
18	1985	existing	II	267	elec.	elec.	89	50	65	120	1.52	0.048
19	1980	existing	II	199	elec.	elec.	66	50	65	120	2.09	0.078
20	1980	existing	II	202	elec.	elec.	67	50	65	120	2.09	0.078
21	1980	existing	II	201	elec.	elec.	67	50	65	120	2.09	0.078
22	1981	existing	II	202	elec.	elec.	67	50	65	120	1.52	0.048
23	2003	existing	II	456	elec.	elec.	152	50	65	120	1.52	0.048
24	1920	existing	II	129	oil	oil	65	50	65	120	1.81	0.063
25	2004	existing	II	204	elec.	elec.	68	50	65	120	1.52	0.048
26	1908	existing	II	372	oil	elec.	124	50	65	120	1.81	0.063
27	1910	existing	II	251	gas	gas	125	50	65	120	1.81	0.063
28	1900	existing	II	580	gas	gas	193	50	65	120	1.81	0.063
29	1955	existing	II	422	oil	oil	211	50	65	120	2.02	0.074
30	1977	existing	II	183	gas	gas	92	50	65	120	2.09	0.078
31	1930	existing	II	210	oil	oil	105	50	65	120	2.02	0.074
32	1936	existing	II	228	gas	gas	114	50	65	120	2.02	0.074
33	1991	existing	II	328	gas	gas	109	50	65	120	1.52	0.048
34	1999	existing	II	491	hp	hp	164	50	65	120	1.52	0.048
35	1994	existing	II	271	oil	oil	90	50	65	120	1.52	0.048
36	1790	existing	II	310	gas	gas	155	50	65	120	1.81	0.063
37	2013	standard	II	519	elec.	elec.	158	33.9	41.5	120	0.83	0.012
38	2007	standard	II	294	elec.	elec.	98	33.9	41.5	120	0.83	0.012
39	2009	standard	II	527	elec.	elec.	67	33.9	41.5	120	0.83	0.012
40	2012	standard	II	435	elec.	elec.	67	33.9	41.5	120	0.83	0.012

A

Table A.12 – Weather data clustering results.

Period	Frequency [d/yr]	Period duration [h]	Date
1	59	24	02/22
2	46	24	02/14
3	23	24	02/09
4	35	24	05/01
5	40	24	10/05
6	37	24	04/06
7	16	24	05/14
8	42	24	08/26
9	24	24	09/18
10	43	24	08/17
11	1	1	-
12	1	1	-

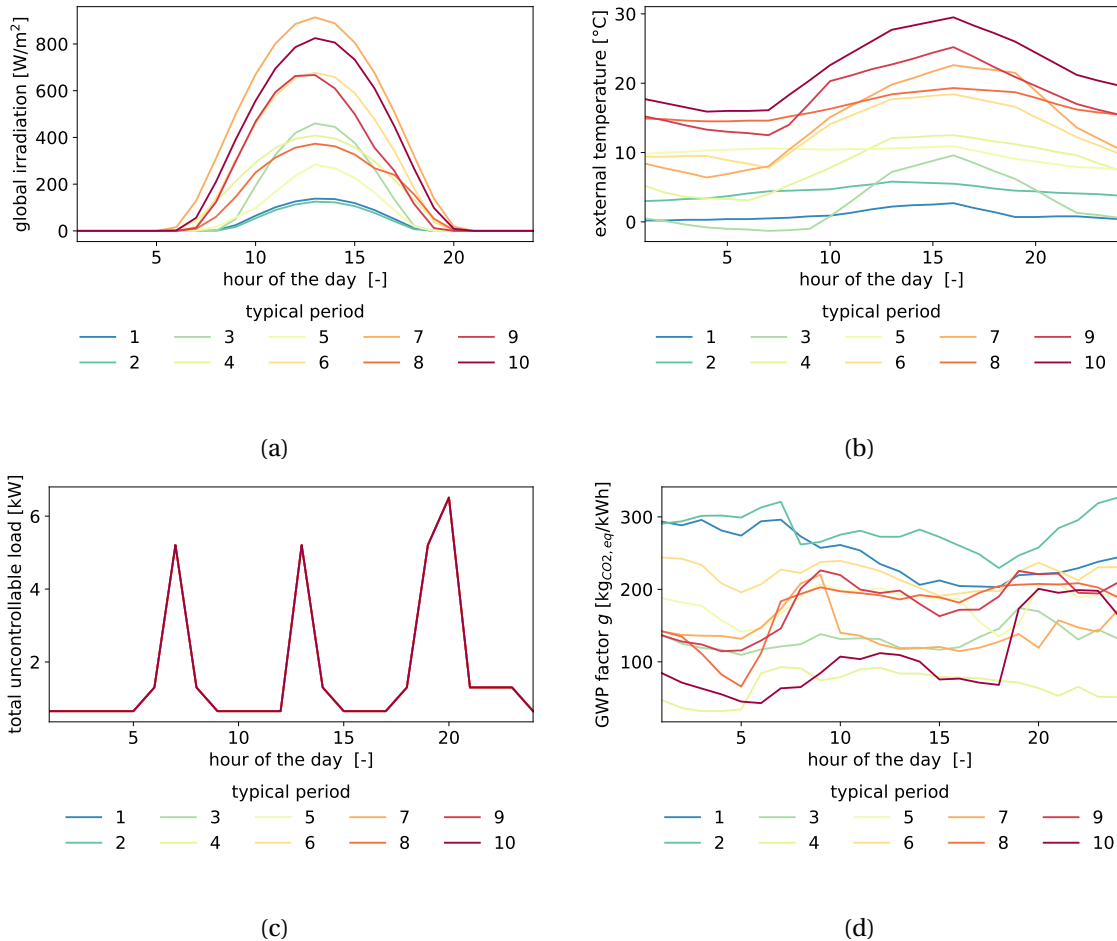


Figure A.1 – Relevant building data for different typical days: a) global irradiation [48], b) a)external temperature [48] c) uncontrollable load of one building according to [31], d) emission impact factors of the grid [33].

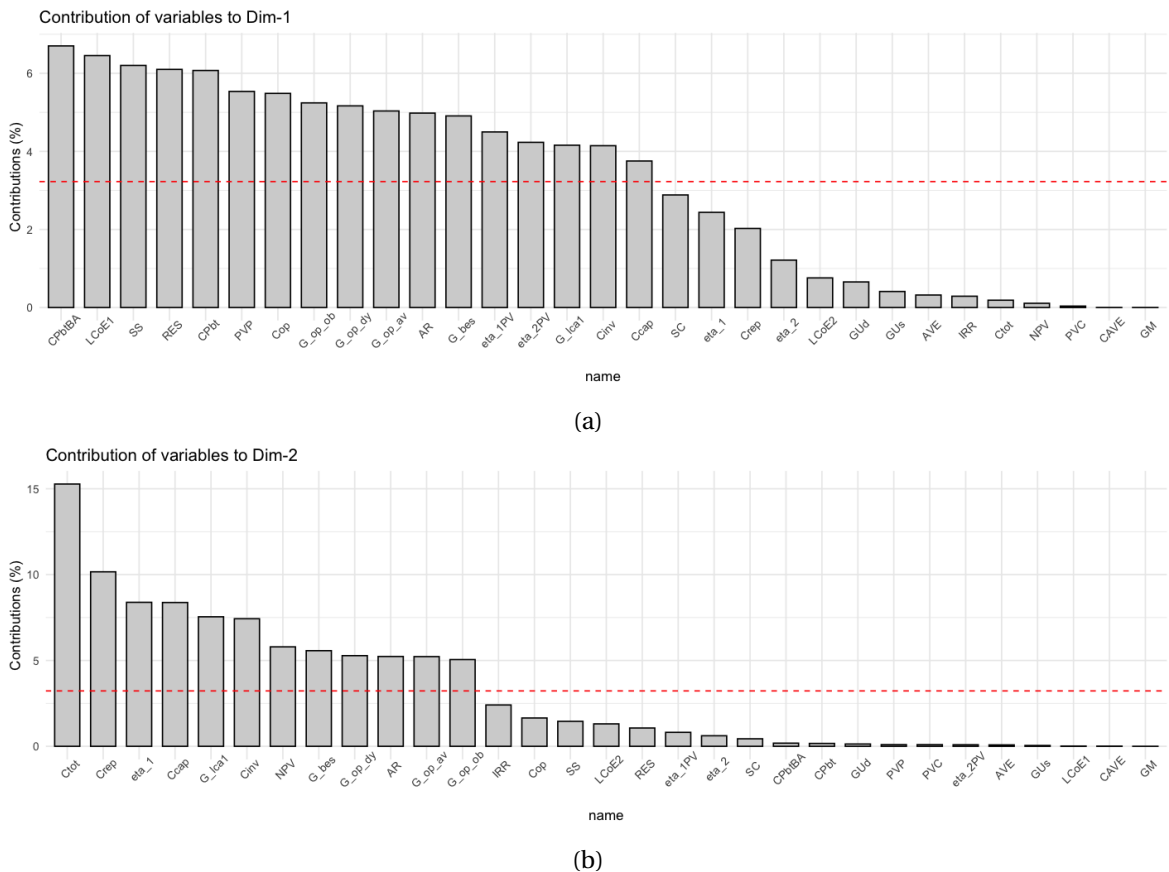


Figure A.2 – Contribution of each key performance indicator (KPI) a) to dimension 1 b) dimension 2 of the principal component analysis. For details about the abbreviations and the KPI , see Table 1.2.

A

A

(Chapter 2)

The limiting angle along the y-axis on the panel is decreasing from β^{design} to zero degree (Figure 2.3). Equation B.1 gives the limiting angle for each position along the y-axis on the panel.

$$\tan(\beta) = \frac{(1-y)}{\frac{1}{\tan(\beta^\alpha)} + \frac{y}{\tan(\gamma_{pv})}} = \frac{(1-y)}{\frac{1}{\cos(\alpha_{pt}-\alpha_{pv}) \cdot \tan(\beta)} + \frac{y}{\tan(\gamma_{pv})}} \quad (\text{B.1})$$

Figure B.1a visualises Equation B.1 for a south oriented panel and the design limiting angle of 20°. For small tilt, below 5°, the limiting angle is dropping rapidly, while the other tilt angles show a nearly linear trend.

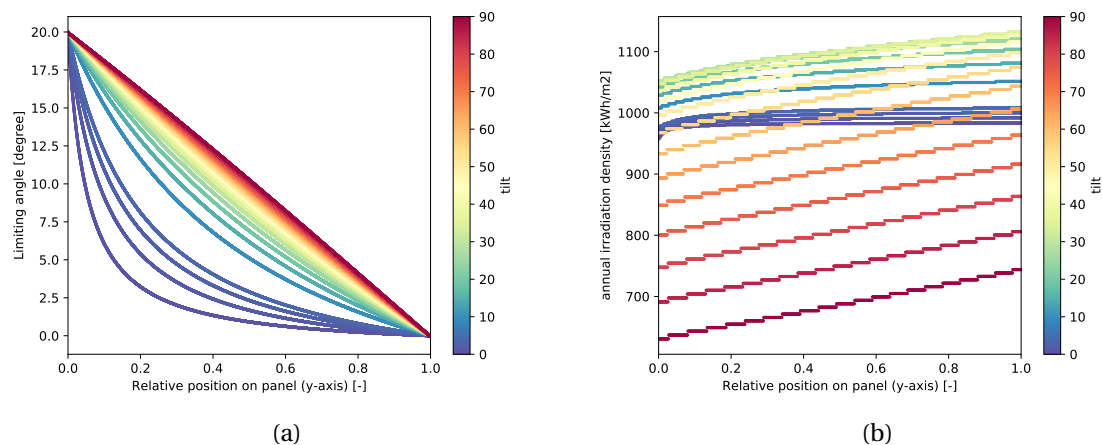


Figure B.1 – Influence of tilt angle orientation on partly shaded panel oriented azimuth 180° and $\beta^{design} = 20^\circ$, tilt in 1° steps for $\gamma_{pv} \in [1;5]$, in 5° steps for $\gamma_{pv} \in [5;90]$; Figure B.1a: Limiting angle along y-axis (see Figure B.2) Figure B.1b: Annual irradiation density along y-axis.

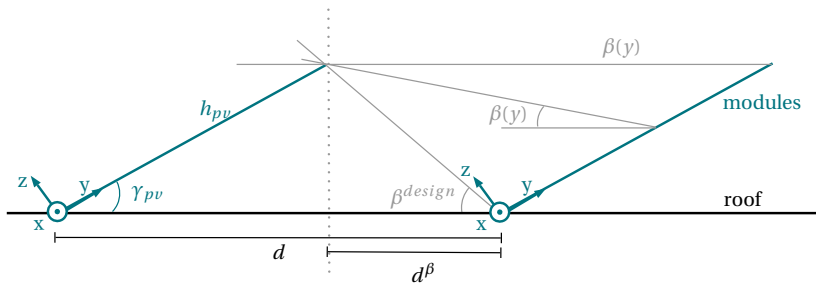


Figure B.2 – Footprint of PV panels on roof, visualization of changing limiting angle β along panel.

Table B.1 – Weather data clustering results including weekdays.

Period	Frequency [d/yr]	Period duration [h]	Date	Weekday
1	35	24	02/20	0
2	74	24	12/28	1
3	47	24	03/14	1
4	22	24	03/28	1
5	20	24	03/12	0
6	28	24	09/03	0
7	35	24	04/07	1
8	37	24	08/26	1
9	22	24	08/07	0
10	45	24	08/16	1
11	1	1	-	-
12	1	1	-	-

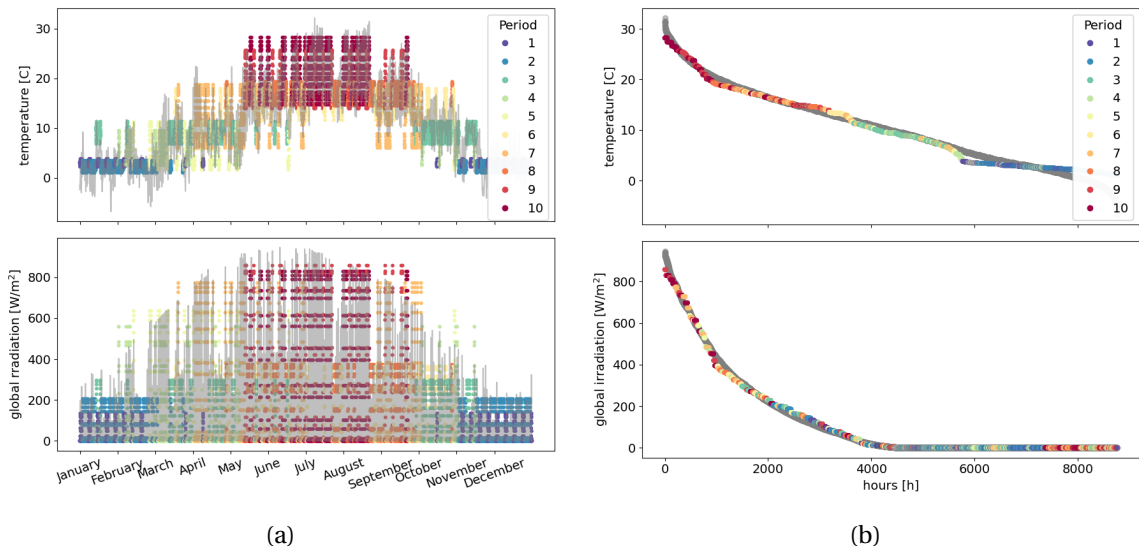


Figure B.3 – Clustering results for external temperature, global irradiation, and weekdays [48] a) classification of different periods over the year b) load duration curve.

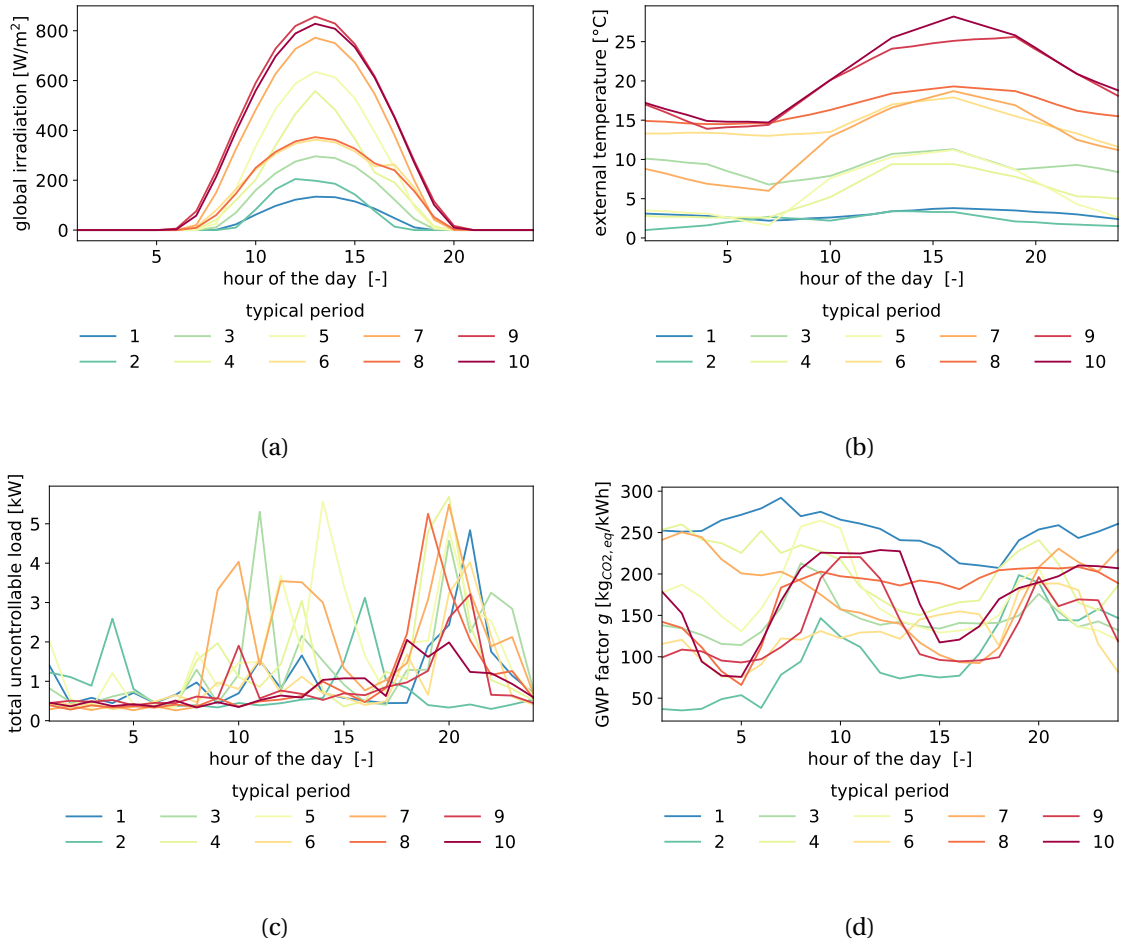


Figure B.4 – Relevant district data for different typical days: a) global irradiation [48], b) external temperature [48] c) uncontrollable load at transformer, disaggregated from measurements by [87], d) emission impact factors of the grid [33].

B

(Chapter 3)

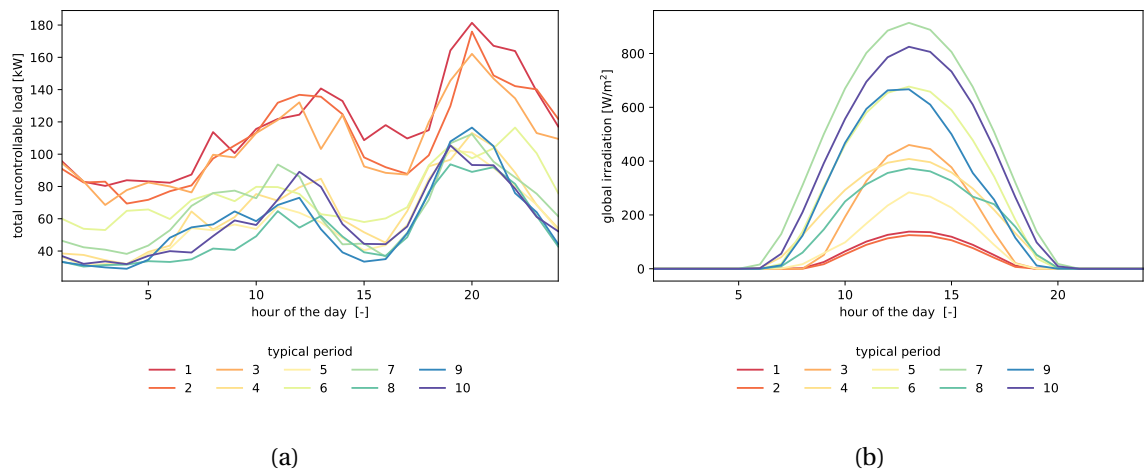


Figure C.1 – Relevant district data for different typical days a) uncontrollable load at transformer. Disaggregated from measurements by [87], d) global irradiation [195].

Appendix C. (Chapter 3)

Table C.1 – Building related data, building type and category according to [131], ERA A_{era} in [m^2], building height in [m^2], heat transfer factor U in [$\text{W}/\text{m}^2_{era}\text{K}$], heat capacity factor C in [$\text{Wh}/\text{m}^2_{era}\text{K}$], design supply temperature T_0^s in [$^\circ\text{C}$], design return temperature T_0^r n [$^\circ\text{C}$].

Building	type	category	period	A_{era}	h	U	C	T_0^s	T_0^r
1	II	existing	<1919	349	8	1.81	120	65	50
2	II	existing	<1919	346	11	1.81	120	65	50
3	I	existing	<1919	538	9	1.81	121	65	50
4	II	existing	1971-1980	257	12	2.09	120	65	50
5	II	existing	1919-1945	318	8	2.02	120	65	50
6	II	existing	1946-1960	589	8	2.02	120	65	50
7	II	existing	1971-1980	307	8	2.09	120	65	50
8	II	existing	1981-1985	376	9	1.90	120	65	50
9	I	existing	1981-1985	335	7	1.93	119	65	50
10	I	existing	1981-1985	479	9	1.49	118	65	50
11	I	existing	<1919	1217	9	1.55	112	65	50
12	II	existing	1991-1095	304	10	1.52	120	65	50
13	II	existing	<1919	1083	9	1.81	120	65	50
14	II	existing	1986-1990	244	9	1.52	120	65	50
15	II	existing	<1919	718	8	1.81	120	65	50
16	I	existing	1919-1945	428	5	1.69	106	65	50
17	I	standard	2011-2015	664	11	0.83	121	41.5	33.9
18	I	existing	1991-1095	893	11	1.52	121	65	50
19	II	existing	1946-1960	251	9	2.02	120	65	50
20	II	existing	1919-1945	293	10	2.02	120	65	50
21	I	existing	1919-1945	310	12	2.02	121	65	50
22	I	standard	2011-2015	700	10	0.83	121	41.5	33.9
23	II	existing	1981-1985	564	9	1.64	120	65	50
24	I	existing	1971-1980	1839	17	2.05	117	65	50
25	II	existing	1981-1985	227	9	1.83	120	65	50
26	II	existing	1981-1985	146	6	1.52	120	65	50
27	I	existing	1981-1985	1436	15	1.52	121	65	50
28	I	existing	1981-1985	1967	16	1.52	121	65	50
29	II	existing	1971-1980	283	6	2.09	120	65	50
30	II	existing	1996-2000	305	8	1.52	120	65	50
31	I	existing	1971-1980	2069	16	2.09	121	65	50

Table C.2 – Building related data, energy related values are annual. Electricity demand of building E^B in [kWh/m $^2_{net}$], space heating demand Q^{SH} in [kWh/m $^2_{era}$], demand for domestic hot water Q^{dhw} in [kWh/m $^2_{net}$], internal heat gains Q^{int} in [kWh/m 2], roof area A^{roof} in [m 2], surface area A^s in [m 2].

Building	E^B	Q^{SH}	Q^{dhw}	Q^{int}	A^{roof}	A^s
1	37	110	19	32	227	349
2	35	115	19	27	198	297
3	32	114	25	32	324	420
4	109	131	19	27	140	309
5	20	135	19	27	201	239
6	12	140	19	27	294	311
7	44	132	19	32	219	317
8	86	121	19	27	218	336
9	30	123	25	28	229	317
10	28	90	25	32	290	329
11	61	99	25	32	711	637
12	31	86	19	32	147	311
13	4	122	19	27	475	613
14	57	80	19	32	196	326
15	17	117	19	27	537	537
16	7	119	25	28	392	166
17	69	36	25	32	294	472
18	48	94	25	32	327	527
19	37	126	19	27	162	291
20	18	127	19	32	163	288
21	18	128	25	28	143	316
22	39	39	25	32	266	395
23	26	107	19	27	220	331
24	40	140	25	32	469	1062
25	226	102	19	32	228	336
26	202	74	19	32	286	248
27	57	92	25	28	411	1169
28	53	95	25	32	414	1079
29	30	141	19	27	220	210
30	84	87	19	32	263	291
31	35	138	25	32	476	1638

Table C.3 – Available surface share for PV installations on facades and roofs. [82]

	Facades	Roofs $\gamma \leq 10^\circ$	Roofs $\gamma > 10^\circ$
Single Family House	0.45	0.7	0.7
Multi Family House	0.60	0.6 · 0.7	0.7
MFH ≥ 1000 m 2 roof	0.60	0.6 · 0.8	0.7
All other buildings	0.55	0.7	0.7
All other buildings ≥ 1000 m 2 roof	0.55	0.8	0.7

C

(Chapter 4)

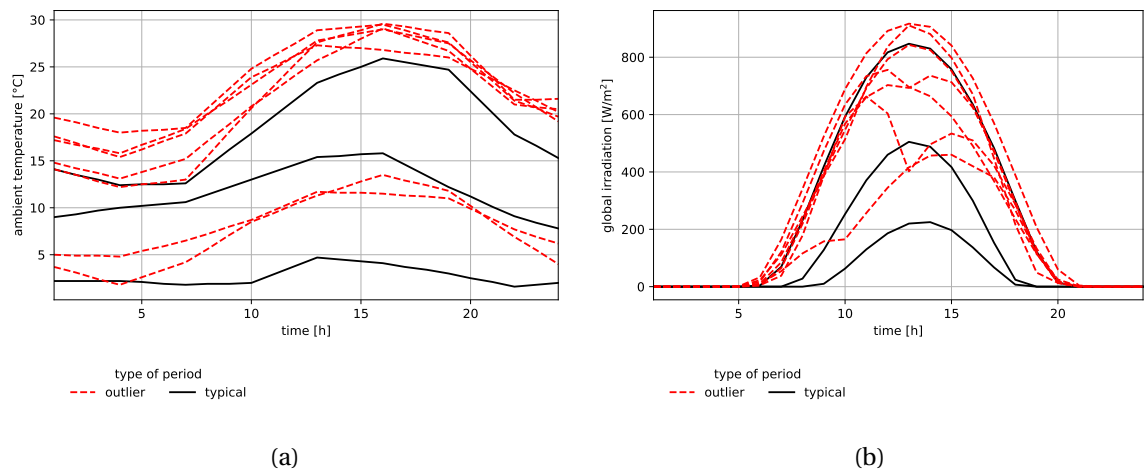


Figure D.1 – Details about detected typical days and outliers a)ambient temperature b) global irradiation

D

(Chapter 5)

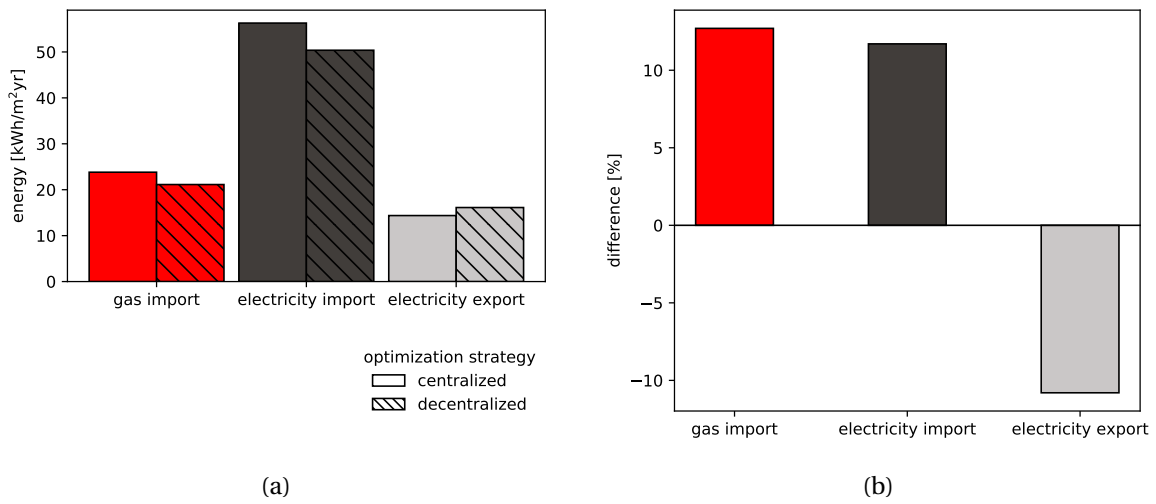


Figure E.1 – Resource exchanges at district level for the detected TOTEX optimum according to two different optimization strategies. District with 31 buildings. a) Absolute resource exchange at district level and b) relative difference between both design strategies.

Appendix E. (Chapter 5)

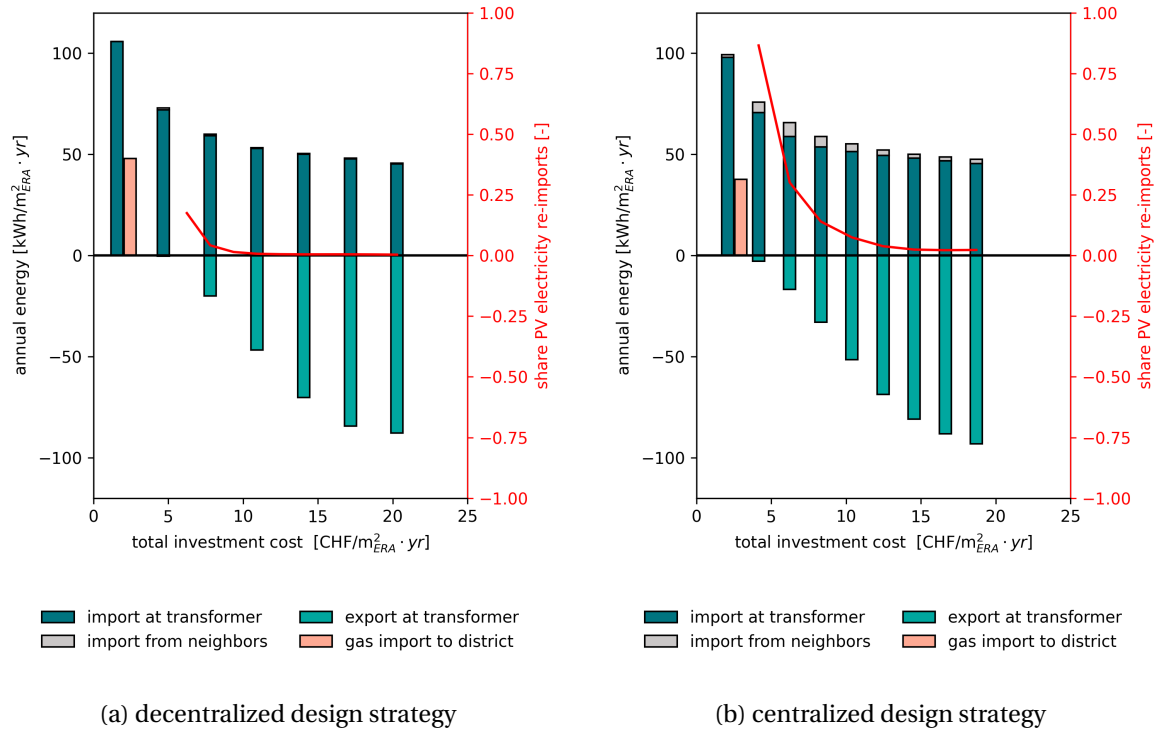


Figure E.2 – Resource exchange at transformer level for increasing investment cost. Renewable energy hub without electricity storage systems.

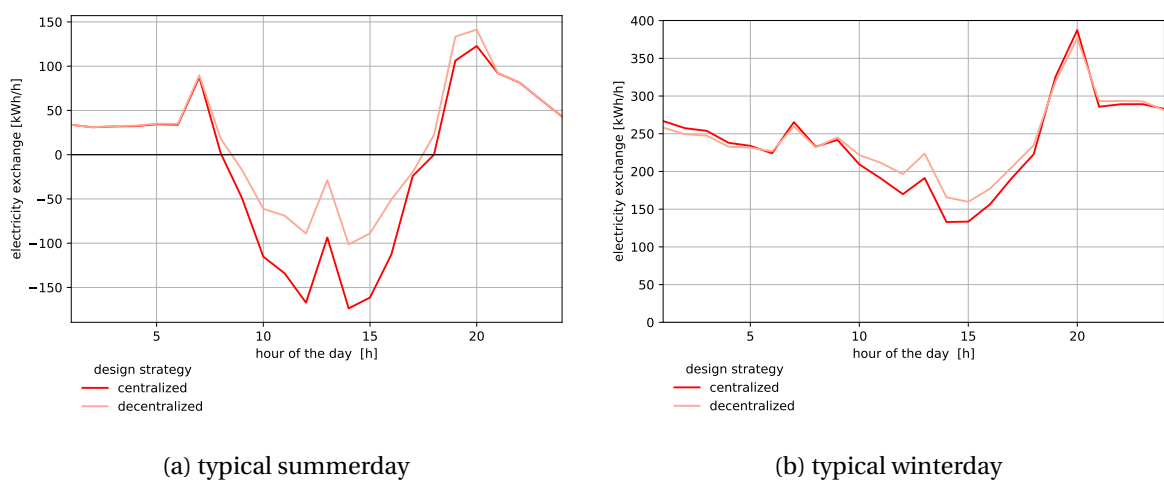


Figure E.3 – Electricity demand profile at the transformer for different typical days. Considered scenario: same TOTEX (= 17.5 CHF/m²) of both design strategies.

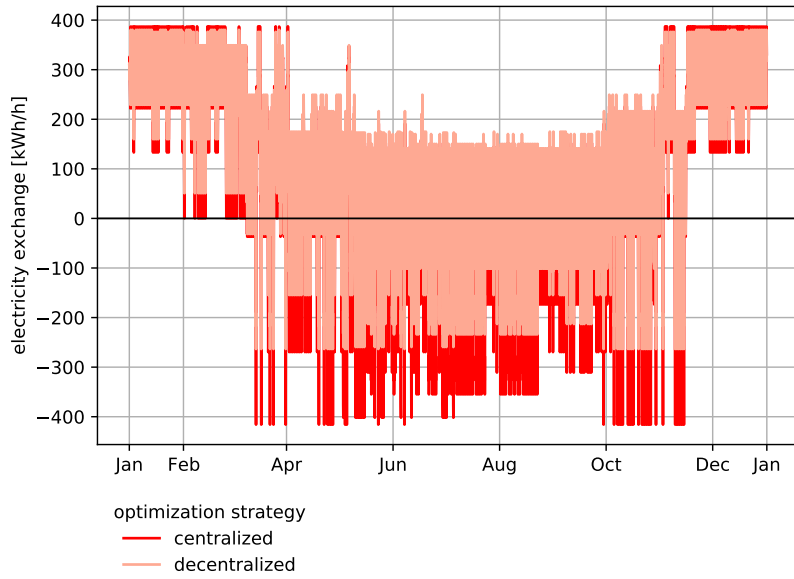


Figure E.4 – Annual electricity demand profile at the transformer. Considered scenario: same TOTEX (= 17.5 CHF/m²) of both design strategies.

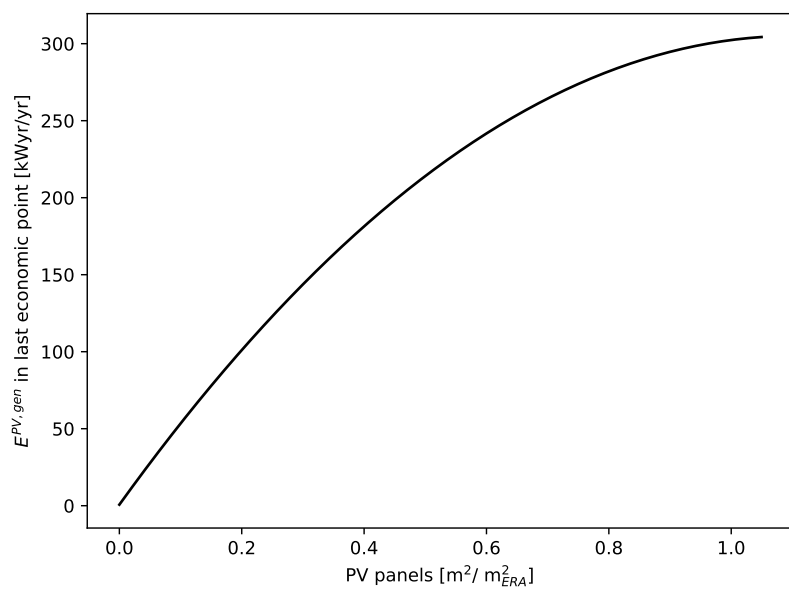


Figure E.5 – Annual generated electricity per installed area of PV panels.

Appendix E. (Chapter 5)

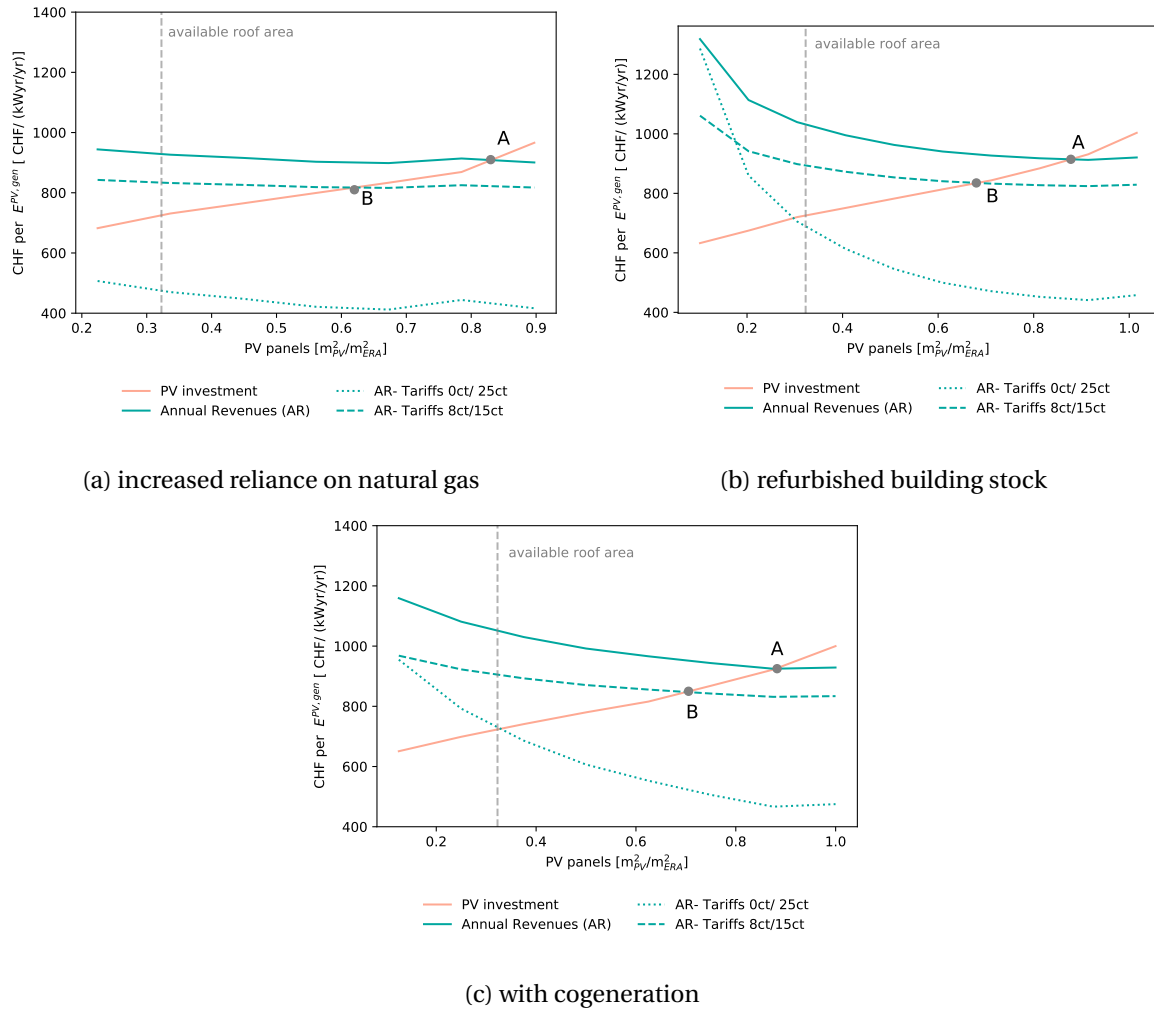


Figure E.6 – Economic analysis of PV panel installation following a centralized investment strategy for different scenarios. PV investment per generated PV electricity $E_{PV,gen}$ and implicit revenues for different feed-in and demand prices. Economic point: Investment in PV and connected revenues are balanced. Point A: current tariffs (8 ct feed-in, 20 ct demand price). Point B: break-even point for exemplary tariffs. Consideration of different district scenarios.

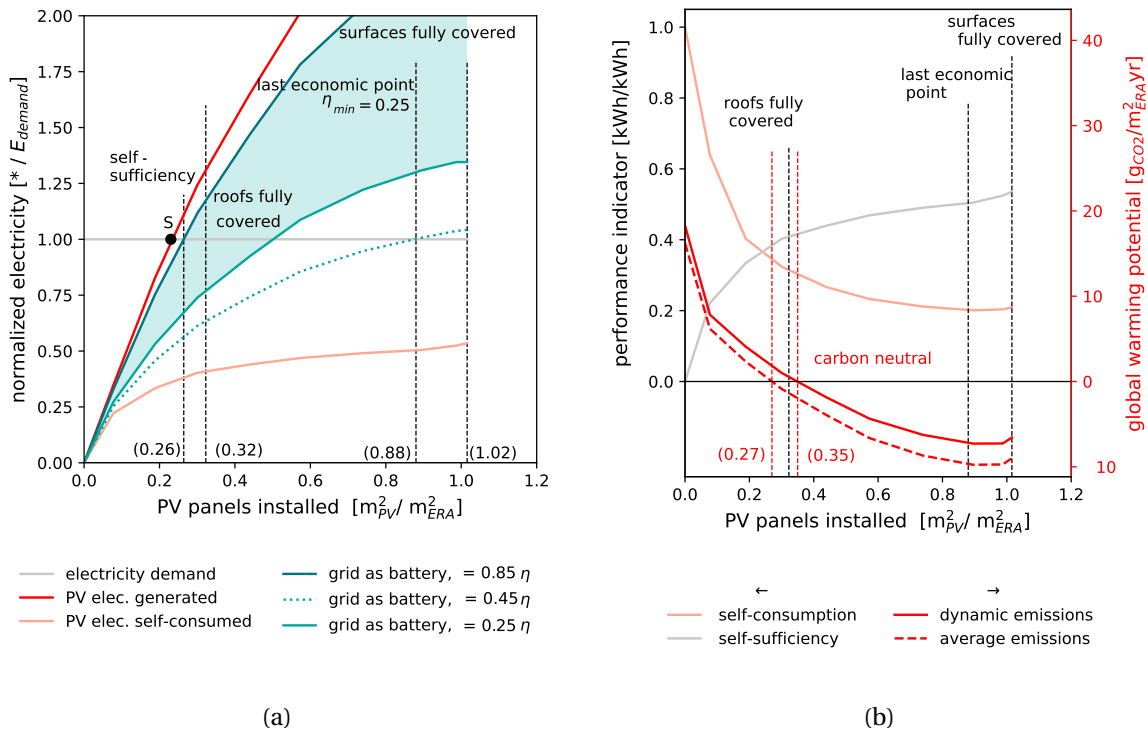


Figure E.7 – Required PV panel installation for the district scenario considering a refurbished building stock to achieve a) self-sufficiency, using the grid as battery for different round-trip efficiencies η , and b) carbon neutrality. Point S: Self-sufficiency considering ideal storage with $\eta = 100\%$. Related emission intensity values based on the Swiss grid mix from 2019 [33].

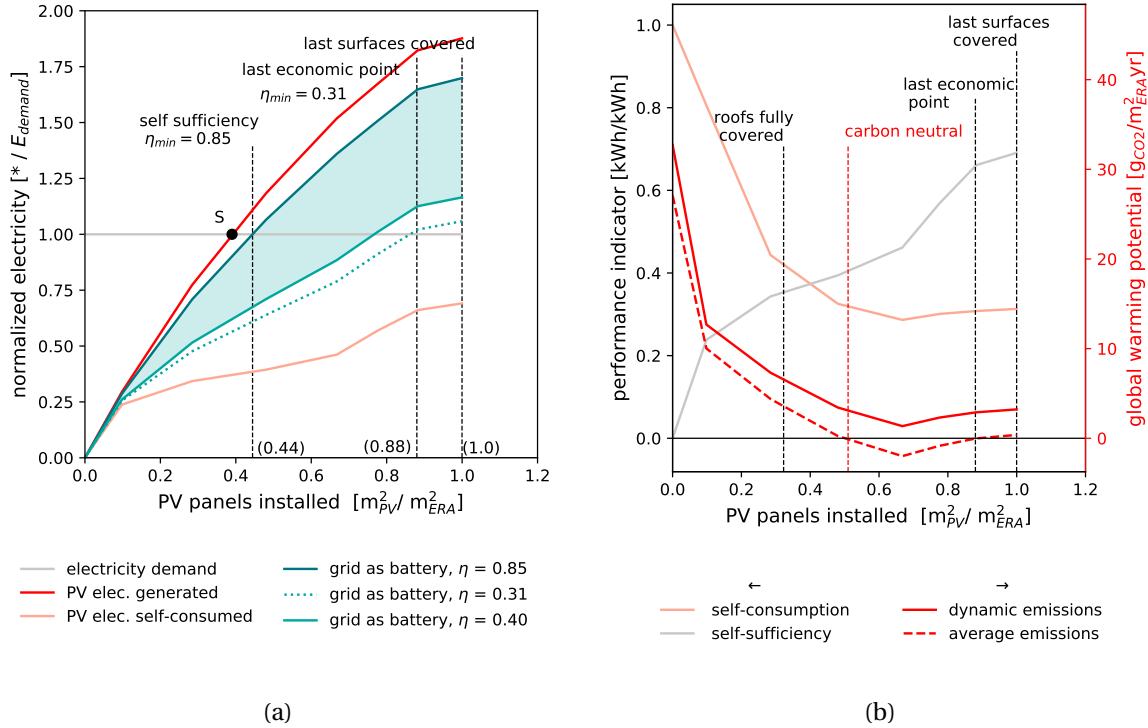


Figure E.8 – Required PV panel installation for the district including cogeneration to achieve a) self-sufficiency, using the grid as battery for different round-trip efficiencies η , and b) carbon neutrality. Point S: Self-sufficiency considering ideal storage with $\eta = 100\%$. Related emission intensity values based on the Swiss grid mix from 2019 [33].

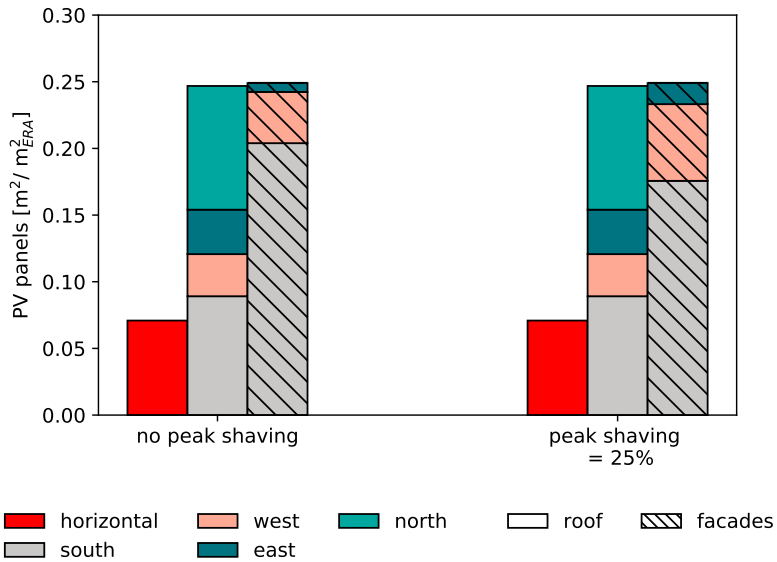


Figure E.9 – The influence of peak shaving on the optimal orientation of PV panels for the centralized design strategy.

Bibliography

- [1] RK Pachauri et al. *Climate Change 2014: Synthesis Report. Contribution of Working Groups I, II and III to the Fifth Assessment Report of the Intergovernmental Panel on Climate Change*. Ed. by RK Pachauri and L Meyer. Geneva, Switzerland: IPCC, 2014.
- [2] UNEnvironment. *2019 global status report for buildings and construction: Towards a zero-emission, efficient and resilient buildings and construction sector*. Tech. rep. Global Alliance for Buildings and Construction, International Energy Agency, UN environment programme, 2019.
- [3] O Lucon and et. al. “Buildings”. In: *Climate Change 2014: Mitigation of Climate Change. Contribution of Working Group III to the Fifth Assessment Report of the Intergovernmental Panel on Climate Change*. United Kingdom and New York: Cambridge University Press, 2014.
- [4] J Rogelj, D Shindell, K Jiang, S Fifita, P Forster, V Ginzburg, C Handa, H Kheshgi, S Kobayashi, E Kriegler, et al. “Mitigation pathways compatible with 1.5 C in the context of sustainable development”. In: *Global warming of 1.5° C*. Intergovernmental Panel on Climate Change, 2018, pp. 93–174.
- [5] D Gielen, R Gorini, R Leme, G Prakash, N Wagner, L Janeiro, S Collins, M Kadir, E Asmelash, R Ferroukhi, et al. *World Energy Transitions Outlook: 1.5° C Pathway*. Abu Dhabi: International Renewable Energy Agency, 2021.
- [6] S Bouckaert, AF Pales, C McGlade, U Remme, B Wanner, L Varro, D D'Ambrosio, and T Spencer. *Net Zero by 2050: A Roadmap for the Global Energy Sector*. International Energy Agency, 2021.
- [7] R Suciu, P Stadler, A Ashouri, and F Maréchal. “Towards energy-autonomous cities using CO₂ networks and Power to Gas storage”. In: *Proceedings of ECOS 2016*. 2016.
- [8] S Henchoz, C Weber, F Maréchal, and D Favrat. “Performance and profitability perspectives of a CO₂ based district energy network in Geneva’s City Centre”. In: *Energy* 85 (June 2015), pp. 221–235.

Bibliography

- [9] T Lang, E Gloerfeld, and B Girod. “Dont just follow the sun – A global assessment of economic performance for residential building photovoltaics”. In: *Renewable and Sustainable Energy Reviews* 42 (Feb. 2015), pp. 932–951.
- [10] R Nordmann. *Sonne für den Klimaschutz: ein Solarplan für die Schweiz*. ger. 1. Auflage. Basel: Zytglogge, 2019.
- [11] SFOoE SFOE. *Energy Strategy 2050*. en.
- [12] R Nordmann. “Stromversorgung sicherstellen - Sonne als zweiter Hauptpfeiler neben der Wasserkraft”. In: *Swissolar* (2020), p. 16.
- [13] M Geidl, G Koeppel, P Favre-Perrod, B Klockl, G Andersson, and K Frohlich. “Energy hubs for the future”. In: *IEEE Power and Energy Magazine* 5.1 (Jan. 2007), pp. 24–30.
- [14] M Mohammadi, Y Noorollahi, B Mohammadi-ivatloo, M Hosseinzadeh, H Yousefi, and ST Khorasani. “Optimal management of energy hubs and smart energy hubs – A review”. en. In: *Renewable and Sustainable Energy Reviews* 89 (June 2018), pp. 33–50.
- [15] MC Bozchalui, SA Hashmi, H Hassen, CA Canizares, and K Bhattacharya. “Optimal Operation of Residential Energy Hubs in Smart Grids”. In: *IEEE Transactions on Smart Grid* 3.4 (Dec. 2012), pp. 1755–1766.
- [16] M Zare Oskouei, B Mohammadi-Ivatloo, M Abapour, M Shafiee, and A Anvari-Moghaddam. “Techno-economic and environmental assessment of the coordinated operation of regional grid-connected energy hubs considering high penetration of wind power”. en. In: *Journal of Cleaner Production* 280 (Jan. 2021), p. 124275.
- [17] A Maroufmashat, A Elkamel, M Fowler, S Sattari, R Roshandel, A Hajimiragh, S Walker, and E Entchev. “Modeling and optimization of a network of energy hubs to improve economic and emission considerations”. en. In: *Energy* 93 (Dec. 2015), pp. 2546–2558.
- [18] N Nikmehr. “Distributed robust operational optimization of networked microgrids embedded interconnected energy hubs”. en. In: *Energy* 199 (May 2020), p. 117440.
- [19] D Huo, S Le Blond, C Gu, W Wei, and D Yu. “Optimal operation of interconnected energy hubs by using decomposed hybrid particle swarm and interior-point approach”. en. In: *International Journal of Electrical Power & Energy Systems* 95 (Feb. 2018), pp. 36–46.
- [20] L Middelhauve, A Santecchia, L Girardin, and F Marechal. “Key Performance Indicators for Decision Making in Building Energy Systems”. In: *Proceedings of ECOS 2020*. June 2020.
- [21] L Middelhauve, L Girardin, F Baldi, and F Maréchal. “Potential of Photovoltaic Panels on Building Envelopes for Decentralized District Energy Systems”. In: *Frontiers in Energy Research* 9 (Oct. 2021), pp. 689–781.
- [22] PM Stadler. “Model-based sizing of building energy systems with renewable sources”. PhD thesis. EPFL, 2019.

Bibliography

- [23] L Girardin. "A GIS-based Methodology for the Evaluation of Integrated Energy Systems in Urban Area". PhD thesis. EPFL, 2012.
- [24] DS Kourkoumpas, G Benekos, N Nikolopoulos, S Karellas, P Grammelis, and E Kakaras. "A review of key environmental and energy performance indicators for the case of renewable energy systems when integrated with storage solutions". In: *Applied Energy* 231 (Dec. 2018), pp. 380–398.
- [25] J Holweger, L Bloch, C Ballif, and N Wyrsch. "Mitigating the impact of distributed PV in a low-voltage grid using electricity tariffs". In: *arXiv:1910.09807 [cs, eess]* (Oct. 2019). arXiv: 1910.09807.
- [26] R Wu, G Mavromatidis, K Orehounig, and J Carmeliet. "Multiobjective optimisation of energy systems and building envelope retrofit in a residential community". In: *Applied Energy* 190 (Mar. 2017), pp. 634–649.
- [27] AJ McEvoy, T Markvart, and L Castañer, eds. *Practical handbook of photovoltaics: fundamentals and applications*. 2nd ed. OCLC: ocn714729581. Waltham, MA: Academic Press, 2012.
- [28] J Keirstead. "Towards Urban Energy System Indicators". In: *Imperial College London Urban Energy Systems* (2007), p. 68.
- [29] R Turton, ed. *Analysis, synthesis, and design of chemical processes*. 4th ed. Upper Saddle River, NJ: Prentice Hall, 2012.
- [30] A Girardin. "Thermal storage aiming at increasing the share of used heat rejected from a cooling process". In: (2012).
- [31] SIA. "2024:2025 Raumnutzungsdaten für die Energie- und Gebäudetechnik". In: *Schweizerischer Ingenieur und Architektenverein* (2015).
- [32] SIA. "SIA 385/2:2015 Anlagen für Trinkwarmwasser in Gebäuden - Warmwasserbedarf, Gesamtanforderungen und Auslegung". In: *Schweizerischer Ingenieur und Architektenverein* (2015).
- [33] Kantor Ivan and A Santecchia. "D5.7 – Report on LC assessment tools based on the results of MORE and EPOS". In: *Coordinated Production For Better Resource Efficiency* (May 2019).
- [34] G Wernet, C Bauer, B Steubing, J Reinhard, E Moreno-Ruiz, and B Weidema. "The ecoinvent database version 3 (part I): overview and methodology". In: *The International Journal of Life Cycle Assessment* 21.9 (Sept. 2016), pp. 1218–1230.
- [35] L Borel and D Favrat. *Thermodynamics and energy systems analysis. Vol. 1: From energy to exergy*. 1. ed. Engineering sciences Mechanical engineering. OCLC: 845717782. Lausanne: EPFL Press, 2010.
- [36] D Favrat, F Marechal, and O Epelly. "The challenge of introducing an exergy indicator in a local law on energy". In: *Energy* 33.2 (Feb. 2008), pp. 130–136.

Bibliography

- [37] R Luthander, J Widén, D Nilsson, and J Palm. "Photovoltaic self-consumption in buildings: A review". In: *Applied Energy* 142 (Mar. 2015), pp. 80–94.
- [38] P Stadler, L Girardin, A Ashouri, and F Maréchal. "Contribution of Model Predictive Control in the Integration of Renewable Energy Sources within the Built Environment". In: *Frontiers in Energy Research* 6 (May 2018).
- [39] Y Fan and X Xia. "A multi-objective optimization model for energy-efficiency building envelope retrofitting plan with rooftop PV system installation and maintenance". In: *Applied Energy* 189 (Mar. 2017), pp. 327–335.
- [40] M Hartner, D Mayr, A Kollmann, and R Haas. "Optimal sizing of residential PV-systems from a household and social cost perspective". en. In: *Solar Energy* 141 (Jan. 2017), pp. 49–58.
- [41] K Branker, M Pathak, and J Pearce. "A review of solar photovoltaic levelized cost of electricity". In: *Renewable and Sustainable Energy Reviews* 15.9 (Dec. 2011), pp. 4470–4482.
- [42] B Metz and IP on Climate Change, eds. *IPCC special report on carbon dioxide capture and storage*. OCLC: ocm64949778. Cambridge: Cambridge University Press, for the Intergovernmental Panel on Climate Change, 2005.
- [43] IP on Climate Change and O Edenhofer, eds. *Climate change 2014: mitigation of climate change: Working Group III contribution to the Fifth Assessment Report of the Intergovernmental Panel on Climate Change*. OCLC: ocn892580682. New York, NY: Cambridge University Press, 2014.
- [44] Administration cantonale vaudoise. *Géodonnées Etat de Vaud , Registre cantonal des bâtiments (RCB)*. Office de l'information sur le territoire (OIT), 2019.
- [45] Federal Statistical Office. *Federal Register of Buildings and Dwellings (RBD)*. 2019.
- [46] M Hoffmann, L Kotzur, D Stolten, and M Robinius. "A Review on Time Series Aggregation Methods for Energy System Models". en. In: *Energies* 13.3 (Feb. 2020), p. 641.
- [47] T Schütz, MH Schraven, M Fuchs, P Remmen, and D Müller. "Comparison of clustering algorithms for the selection of typical demand days for energy system synthesis". In: *Renewable Energy* 129 (2018), pp. 570–582.
- [48] DOE. *Weather Data | EnergyPlus*, U.S. Department of Energy's (DOE) Building Technologies Office (BTO) and National Renewable Energy Laboratory (NREL). <https://energyplus.net/weather>. Mar. 2020.
- [49] *wcKMedoids function - RDocumentation*.
- [50] R Sangi and D Müller. "Exergy-based approaches for performance evaluation of building energy systems". In: *Sustainable Cities and Society* 25 (Aug. 2016), pp. 25–32.
- [51] *prcomp function - RDocumentation*.

Bibliography

- [52] L Middelhauve, F Baldi, P Stadler, and F Maréchal. “Grid-Aware Layout of Photovoltaic Panels in Sustainable Building Energy Systems”. In: *Frontiers in Energy Research* 8 (Feb. 2021), p. 573290.
- [53] L Middelhauve, F Baldi, PM Stadler, L Bloch, and F Marechal. “Influence of photovoltaic panel orientation on modern energy systems in residential buildings”. In: *Proceedings of ECOS 2019*. June 2019.
- [54] M Jennings, D Fisk, and N Shah. “Modelling and optimization of retrofitting residential energy systems at the urban scale”. In: *Energy* 64 (Jan. 2014), pp. 220–233.
- [55] T Ma, J Wu, L Hao, WJ Lee, H Yan, and D Li. “The optimal structure planning and energy management strategies of smart multi energy systems”. In: *Energy* 160 (Oct. 2018), pp. 122–141.
- [56] M Stadler, M Groissböck, G Cardoso, and C Marnay. “Optimizing Distributed Energy Resources and building retrofits with the strategic DER-CAModel”. In: *Applied Energy* 132 (Nov. 2014), pp. 557–567.
- [57] B Morvaj, R Evins, and J Carmeliet. “Optimising urban energy systems: Simultaneous system sizing, operation and district heating network layout”. In: *Energy* 116 (Dec. 2016), pp. 619–636.
- [58] R Jing, M Wang, H Liang, X Wang, N Li, N Shah, and Y Zhao. “Multi-objective optimization of a neighborhood-level urban energy network: Considering Game-theory inspired multi-benefit allocation constraints”. In: *Applied Energy* 231 (Dec. 2018), pp. 534–548.
- [59] JMF Rager. “Urban Energy System Design from the Heat Perspective using mathematical Programming including thermal Storage”. PhD thesis. EPFL, 2015.
- [60] JA Duffie and WA Beckman. *Solar engineering of thermal processes / John A. Duffie, William A. Beckman*. 4th ed. Hoboken: John Wiley, 2013.
- [61] A Ashouri. “Simultaneous Design and Control of Energy Systems”. PhD thesis. ETH Zurich, 2014.
- [62] J Lazar. *Teaching the "duck" to Fly, Second Edition*. Regulatory Assistance Project, 2016.
- [63] S van der Stelt, T AlSkaif, and W van Sark. “Techno-economic analysis of household and community energy storage for residential prosumers with smart appliances”. In: *Applied Energy* 209 (Jan. 2018), pp. 266–276.
- [64] G Litjens, E Worrell, and W van Sark. “Influence of demand patterns on the optimal orientation of photovoltaic systems”. In: *Solar Energy* 155 (Oct. 2017), pp. 1002–1014.
- [65] JD Mondol, YG Yohanis, and B Norton. “The impact of array inclination and orientation on the performance of a grid-connected photovoltaic system”. In: *Renewable Energy* 32.1 (Jan. 2007), pp. 118–140.

Bibliography

- [66] A Lahnaoui, P Stenzel, and J Linssen. "Tilt Angle and Orientation Impact on the Techno-economic Performance of Photovoltaic Battery Systems". In: *Energy Procedia* 105 (May 2017), pp. 4312–4320.
- [67] JI Laveyne, D Bozalakov, G Van Eetvelde, and L Vandeveld. "Impact of Solar Panel Orientation on the Integration of Solar Energy in Low-Voltage Distribution Grids". In: *International Journal of Photoenergy* 2020 (Feb. 2020), pp. 1–13.
- [68] SB Sadineni, F Atallah, and RF Boehm. "Impact of roof integrated PV orientation on the residential electricity peak demand". In: *Applied Energy* 92 (Apr. 2012), pp. 204–210.
- [69] JD Rhodes, CR Upshaw, WJ Cole, CL Holcomb, and ME Webber. "A multi-objective assessment of the effect of solar PV array orientation and tilt on energy production and system economics". In: *Solar Energy* 108 (Oct. 2014), pp. 28–40.
- [70] A Hafez, A Soliman, K El-Metwally, and I Ismail. "Tilt and azimuth angles in solar energy applications – A review". In: *Renewable and Sustainable Energy Reviews* 77 (Sept. 2017), pp. 147–168.
- [71] V Badescu, ed. *Modeling solar radiation at the earth's surface: recent advances*. OCLC: ocn209334629. Berlin: Springer, 2008.
- [72] YS Khoo, A Nobre, R Malhotra, D Yang, R Ruther, T Reindl, and AG Aberle. "Optimal Orientation and Tilt Angle for Maximizing in-Plane Solar Irradiation for PV Applications in Singapore". In: *IEEE Journal of Photovoltaics* 4.2 (Mar. 2014), pp. 647–653.
- [73] DA Chwieduk. "Recommendation on modelling of solar energy incident on a building envelope". In: *Renewable Energy* 34.3 (Mar. 2009), pp. 736–741.
- [74] K Shukla, S Rangnekar, and K Sudhakar. "Comparative study of isotropic and anisotropic sky models to estimate solar radiation incident on tilted surface: A case study for Bhopal, India". In: *Energy Reports* 1 (Nov. 2015), pp. 96–103.
- [75] S Freitas, C Catita, P Redweik, and M Brito. "Modelling solar potential in the urban environment: State-of-the-art review". In: *Renewable and Sustainable Energy Reviews* 41 (Jan. 2015), pp. 915–931.
- [76] M Bremer, A Mayr, V Wichmann, K Schmidtner, and M Rutzinger. "A new multi-scale 3D-GIS-approach for the assessment and dissemination of solar income of digital city models". In: *Computers, Environment and Urban Systems* 57 (May 2016), pp. 144–154.
- [77] L Ko, JC Wang, CY Chen, and HY Tsai. "Evaluation of the development potential of rooftop solar photovoltaic in Taiwan". In: *Renewable Energy* 76 (Apr. 2015), pp. 582–595.
- [78] A Verso, A Martin, J Amador, and J Dominguez. "GIS-based method to evaluate the photovoltaic potential in the urban environments: The particular case of Miraflores de la Sierra". In: *Solar Energy* 117 (July 2015), pp. 236–245.

Bibliography

- [79] A Vulkan, I Kloog, M Dorman, and E Erell. “Modeling the potential for PV installation in residential buildings in dense urban areas”. In: *Energy and Buildings* 169 (June 2018), pp. 97–109.
- [80] A Walch, N Mohajeri, and JL Scartezzini. “A critical comparison of methods to estimate solar rooftop photovoltaic potential in Switzerland”. In: *Journal of Physics: Conference Series* 1343 (Nov. 2019), p. 012035.
- [81] D Assouline, N Mohajeri, and JL Scartezzini. “Quantifying rooftop photovoltaic solar energy potential: A machine learning approach”. In: *Solar Energy* 141 (Jan. 2017), pp. 278–296.
- [82] D Klauser. *Solarpotentialanalyse für Sonnendach.ch Schlussbericht*. Tech. rep. Bern: Bundesamt für Energie BFE, Feb. 2016.
- [83] D Robinson and A Stone. “Irradiation modelling made simple: the cumulative sky approach and its applications”. In: (Jan. 2004).
- [84] R Perez, R Seals, and J Michalsky. “All-weather model for sky luminance distribution—Preliminary configuration and validation”. In: *Solar Energy* 50.3 (Mar. 1993), pp. 235–245.
- [85] A Martinez-Rubio, F Sanz-Adan, and J Santamaria. “Optimal design of photovoltaic energy collectors with mutual shading for pre-existing building roofs”. In: *Renewable Energy* 78 (June 2015), pp. 666–678.
- [86] A Mermoud. “Optimization of Row-Arrangement in PV Systems, Shading Loss Evaluations According to Module Positioning and Connexions”. In: *27th European Photovoltaic Solar Energy Conference and Exhibition; 4009-4013* (2012). Artwork Size: 5 pages, 2167 kb Medium: application/pdf Publisher: WIP, 5 pages, 2167 kb.
- [87] J Holweger, M Dorokhova, L Bloch, C Ballif, and N Wyrsch. “Unsupervised algorithm for disaggregating low-sampling-rate electricity consumption of households”. In: *Sustainable Energy, Grids and Networks* 19 (Sept. 2019), p. 100244.
- [88] T Hoffmann. *SunCalc sun position- und sun phases calculator*. Library Catalog: www.suncalc.org. 2020.
- [89] D Akinyele and R Rayudu. “Review of energy storage technologies for sustainable power networks”. In: *Sustainable Energy Technologies and Assessments* 8 (Dec. 2014), pp. 74–91.
- [90] TM Gür. “Review of electrical energy storage technologies, materials and systems: challenges and prospects for large-scale grid storage”. In: *Energy & Environmental Science* 11.10 (2018), pp. 2696–2767.
- [91] S Freitas, C Reinhart, and M Brito. “Minimizing storage needs for large scale photovoltaics in the urban environment”. In: *Solar Energy* 159 (2018), pp. 375–389.
- [92] P Redweik, C Catita, and M Brito. “Solar energy potential on roofs and facades in an urban landscape”. In: *Solar Energy* 97 (Nov. 2013), pp. 332–341.

Bibliography

- [93] C Catita, P Redweik, J Pereira, and M Brito. "Extending solar potential analysis in buildings to vertical facades". In: *Computers and Geosciences* 66 (2014), pp. 1–12.
- [94] E Walter and JH Kämpf. "A verification of CitySim results using the BESTEST and monitored consumption values". In: *Proceedings of the 2nd Building Simulation Applications conference*. 2015.
- [95] G Desthieux, C Carneiro, R Camponovo, P Ineichen, E Morello, A Boulmier, N Abdennadher, S Dervey, and C Ellert. "Solar energy potential assessment on rooftops and facades in large built environments based on lidar data, image processing, and cloud computing. Methodological background, application, and validation in geneva (solar cadaster)". In: *Frontiers in Built Environment* 4 (2018).
- [96] JH Kämpf, M Montavon, J Bunyesc, R Bolliger, and D Robinson. "Optimisation of buildings' solar irradiation availability". In: *Solar Energy* 84.4 (Apr. 2010), pp. 596–603.
- [97] M Brito, S Freitas, S Guimarães, C Catita, and P Redweik. "The importance of facades for the solar PV potential of a Mediterranean city using LiDAR data". In: *Renewable Energy* 111 (Oct. 2017), pp. 85–94.
- [98] C Chatzipoulka, R Compagnon, J Kaempf, and M Nikolopoulou. "Sky view factor as predictor of solar availability on building façades". In: *Solar Energy* 170 (2018), pp. 1026–1038.
- [99] N Rehman, T Anderson, and R Nates. "Diffuse Solar Potential of Facades in an Urban Context under Different Sky Conditions". In: (Dec. 2018).
- [100] S Aguacil, S Lufkin, and E Rey. "Active surfaces selection method for building-integrated photovoltaics (BIPV) in renovation projects based on self-consumption and self-sufficiency". In: *Energy and Buildings* 193 (2019), pp. 15–28.
- [101] Y Li and C Liu. "Techno-economic analysis for constructing solar photovoltaic projects on building envelopes". In: *Building and Environment* 127 (2018), pp. 37–46.
- [102] M Díez-Mediavilla, M Rodríguez-Amigo, M Dieste-Velasco, T García-Calderón, and C Alonso-Tristán. "The PV potential of vertical façades: A classic approach using experimental data from Burgos, Spain". In: *Solar Energy* 177 (2019), pp. 192–199.
- [103] S Horn, E Bagda, K Brandau, and B Weller. "Influence of building-integrated photovoltaics in façades for the energetic evaluation of buildings. Part 1: Potential of façade integration of photovoltaics". In: *Bauphysik* 40.2 (2018), pp. 68–73.
- [104] L Pantić, T Pavlović, D Milosavljević, D Mirjanić, I Radonjić, and M Radović. "Electrical energy generation with differently oriented photovoltaic modules as façade elements". In: *Thermal Science* 20.4 (2016), pp. 1377–1386.
- [105] R Zimmerman, A Panda, and V Bulović. "Techno-economic assessment and deployment strategies for vertically-mounted photovoltaic panels". In: *Applied Energy* 276 (2020).

Bibliography

- [106] L Mulcué-Nieto, L Mora-López, and a et al. “A novel methodology for the pre-classification of façades usable for the decision of installation of integrated PV in buildings: The case for equatorial countries”. In: *Energy* 141 (2017), pp. 2264–2276.
- [107] J Kanders, M Wall, and MC Dubois. “Development of a façade assessment and design tool for solar energy (FASSADES)”. In: *Buildings* 4.1 (2014), pp. 43–59.
- [108] J Gonçalves, T van Hooff, and D Saelens. “Simulating building integrated photovoltaic facades: Comparison to experimental data and evaluation of modelling complexity”. In: *Applied Energy* 281 (2021).
- [109] C Zomer, I Custódio, S Goulart, S Mantelli, G Martins, R Campos, G Pinto, and R Rüther. “Energy balance and performance assessment of PV systems installed at a positive-energy building (PEB) solar energy research centre”. In: *Solar Energy* 212 (2020), pp. 258–274.
- [110] A Buonomano, F Calise, A Palombo, and M Vicidomini. “BIPVT systems for residential applications: An energy and economic analysis for European climates”. In: *Applied Energy* 184 (2016), pp. 1411–1431.
- [111] AA Bayod-Rújula, Y Yuan, A Martínez-Gracia, J Wang, J Uche, and H Chen. “Modelling and Simulation of a Building Energy Hub”. In: *Proceedings* 2.23 (Nov. 2018), p. 1431.
- [112] S Xu, Z Huang, J Wang, T Mendis, and J Huang. “Evaluation of photovoltaic potential by urban block typology: A case study of Wuhan, China”. In: *Renewable Energy Focus* 29 (2019), pp. 141–147.
- [113] A Boccalatte, M Fossa, and C Ménézo. “Best arrangement of BIPV surfaces for future NZEB districts while considering urban heat island effects and the reduction of reflected radiation from solar façades”. In: *Renewable Energy* 160 (2020), pp. 686–697.
- [114] H Yesilmaden and A Dogru. “Finding the best locations for photovoltaic panel installation in urbanized areas”. In: *Fresenius Environmental Bulletin* 28.2 (2019), pp. 619–625.
- [115] J Esclapés, I Ferreiro, J Piera, and J Teller. “A method to evaluate the adaptability of photovoltaic energy on urban façades”. In: *Solar Energy* 105 (2014), pp. 414–427.
- [116] G Lobaccaro, M Lisowska, E Saretta, P Bonomo, and F Frontini. “A methodological analysis approach to assess solar energy potential at the neighborhood scale”. In: *Energies* 12.18 (2019).
- [117] ED Mehler, H Sarimveis, NC Markatos, and LG Papageorgiou. “A mathematical programming approach for optimal design of distributed energy systems at the neighbourhood level”. In: *Energy* 44.1 (Aug. 2012), pp. 96–104.
- [118] B Morvaj, R Evans, and J Carmeliet. “Optimization framework for distributed energy systems with integrated electrical grid constraints”. In: *Applied Energy* 171 (June 2016), pp. 296–313.
- [119] Y Yang, S Zhang, and Y Xiao. “Optimal design of distributed energy resource systems coupled with energy distribution networks”. In: *Energy* 85 (June 2015), pp. 433–448.

Bibliography

- [120] X Fang, X He, and J Huang. "A strategy to optimize the multi-energy system in microgrid based on neurodynamic algorithm". In: *Applied Soft Computing* 75 (Feb. 2019), pp. 588–595.
- [121] EA Martinez Cesena, P Mancarella, and a et al. "Energy Systems Integration in Smart Districts: Robust Optimisation of Multi-Energy Flows in Integrated Electricity, Heat and Gas Networks". In: *IEEE Transactions on Smart Grid* 10.1 (Jan. 2019), pp. 1122–1131.
- [122] T Schütz, X Hu, M Fuchs, and D Müller. "Optimal design of decentralized energy conversion systems for smart microgrids using decomposition methods". In: *Energy* 156 (Aug. 2018), pp. 250–263.
- [123] C Weber and N Shah. "Optimisation based design of a district energy system for an eco-town in the United Kingdom". In: *Energy* 36.2 (Feb. 2011), pp. 1292–1308.
- [124] NC Schüler. "Computational methods for multi-criteria decision support in urban planning". PhD thesis. EPFL, 2018.
- [125] EnergieSchweiz. *Simulation von Energiesystemen mit dem Tachion-Simulation-Framework*. Tech. rep. Bundesamt für Energie BFE, 2020.
- [126] R Perez, R Stewart, C Arbogast, R Seals, and J Scott. "An anisotropic hourly diffuse radiation model for sloping surfaces: Description, performance validation, site dependency evaluation". In: *Solar Energy* 36.6 (1986), pp. 481–497.
- [127] MS Roudsari and A Smith. "Ladybug: A parametric environmental plugin for grasshopper to help designers create an environmentally-conscious design". In: *Proceedings of BS2013*. Chambéry France, Aug. 2013.
- [128] D Perez. "A framework to model and simulate the disaggregated energy flows supplying buildings in urban areas". en. Publisher: Lausanne, EPFL. PhD thesis. 2014.
- [129] Federal Office of Topography swisstopo. *swissBUILDINGS3D 2.0 - 3D building models of Switzerland*. 2019.
- [130] Swiss Federal Office of Energy - Geoinformation - Sonnendach.ch. *3D data of roof area by the Swiss Federal Office of Topography swisstopo*. 2018.
- [131] SIA. "SIA 380/1:2016 Heizwärmebedarf". In: *Schweizerischer Ingenieur und Architektenverein* (2016).
- [132] J Remund, S Kunz, METEOTEST, and MSFO of Energy. *METEONORM - Global Meteorological Database for Engineers, Planners and Education*. 2003.
- [133] OpenStreetMap contributors. *Planet dump retrieved from https://planet.osm.org*. Published: <https://www.openstreetmap.org>. 2017.
- [134] Federal Office of Meteorology and Climatology MeteoSwiss. *Solar potential of all roofs and facades in Switzerland*. 2019.

Bibliography

- [135] Romande Energie SA. *Distribution networks database*. Published: www.romande-energie.ch. 2018.
- [136] F Domínguez-Muñoz, JM Cejudo-López, A Carrillo-Andrés, and M Gallardo-Salazar. “Selection of typical demand days for CHP optimization”. In: *Energy and Buildings* 43.11 (Nov. 2011), pp. 3036–3043.
- [137] CJ Barnhart. “Energy and Carbon Intensities of Stored Solar Photovoltaic Energy”. In: *A Comprehensive Guide to Solar Energy Systems*. Elsevier, 2018, pp. 351–360.
- [138] H Blanco and A Faaij. “A review at the role of storage in energy systems with a focus on Power to Gas and long-term storage”. In: *Renewable and Sustainable Energy Reviews* 81 (Jan. 2018), pp. 1049–1086.
- [139] KN Streicher, S Mennel, J Chambers, D Parra, and MK Patel. “Cost-effectiveness of large-scale deep energy retrofit packages for residential buildings under different economic assessment approaches”. In: *Energy and Buildings* 215 (May 2020), p. 109870.
- [140] R Gupta, F Sossan, and M Paolone. “Countrywide PV hosting capacity and energy storage requirements for distribution networks: The case of Switzerland”. In: *Applied Energy* 281 (Jan. 2021), p. 116010.
- [141] L Middelhauve, N Ljubic, J Granacher, L Girardin, and F Marechal. “Data reduction for mixed integer linear programming in complex energy systems”. In: *Proceedings of ECOS 2021*. June 2021.
- [142] L Middelhauve and F Maréchal. “About data reduction techniques and the role of outliers for complex energy systems”. In: *Proceedings of PSE 2021*. 2021.
- [143] L Middelhauve, C Terrier, and F Maréchal. “Decomposition strategy for districts as renewable energy hubs”. In: *IEEE Journal of Power and Energy in Review* (2022).
- [144] T Stocker. *Climate change 2013: the physical science basis: Working Group I contribution to the Fifth assessment report of the Intergovernmental Panel on Climate Change*. Cambridge university press, 2014.
- [145] L Kotzur, P Markewitz, M Robinius, and D Stolten. “Impact of different time series aggregation methods on optimal energy system design”. In: *Renewable Energy* 117 (Mar. 2018), pp. 474–487.
- [146] S Fazlollahi, SL Bungener, P Mandel, G Becker, and F Maréchal. “Multi-objectives, multi-period optimization of district energy systems: I. Selection of typical operating periods”. In: *Computers & Chemical Engineering* 65 (June 2014), pp. 54–66.
- [147] PG Brodrick, CA Kang, AR Brandt, and LJ Durlofsky. “Optimization of carbon-capture-enabled coal-gas-solar power generation”. In: *Energy* 79 (2015), pp. 149–162.

Bibliography

- [148] B Bahl, A Kümpel, H Seele, M Lampe, and A Bardow. “Time-series aggregation for synthesis problems by bounding error in the objective function”. In: *Energy* 135 (Sept. 2017), pp. 900–912.
- [149] N Baumgärtner, B Bahl, M Hennen, and A Bardow. “RiSES3: Rigorous Synthesis of Energy Supply and Storage Systems via time-series relaxation and aggregation”. In: *Computers & Chemical Engineering* 127 (2019), pp. 127–139.
- [150] P Gabrielli, M Gazzani, E Martelli, and M Mazzotti. “Optimal design of multi-energy systems with seasonal storage”. In: *Applied Energy* 219 (2018), pp. 408–424.
- [151] B Bahl. *Optimization-Based Synthesis of Large-Scale Energy Systems by Time-Series Aggregation; 1. Auflage*. en. Vol. RWTH Aachen University. Artwork Size: pages 1 Online-Ressource (XXI, 148 Seiten) : Illustrationen Pages: pages 1 Online-Ressource (XXI, 148 Seiten) : Illustrationen Publication Title: Dissertation. RWTH Aachen University, 2018.
- [152] H Liu, J Li, Y Wu, and Y Fu. “Clustering with Outlier Removal”. In: *arXiv:1801.01899 [cs, stat]* (Jan. 2018). arXiv: 1801.01899.
- [153] CPLEX Options for AMPL. <https://ampl.com/products/solvers/solvers-we-sell/cplex/options/>. Feb. 2020.
- [154] W Li, Y Zhou, K Cetin, J Eom, Y Wang, G Chen, and X Zhang. “Modeling urban building energy use: A review of modeling approaches and procedures”. en. In: *Energy* 141 (Dec. 2017), pp. 2445–2457.
- [155] S Lu, W Gu, J Zhou, X Zhang, and C Wu. “Coordinated dispatch of multi-energy system with district heating network: Modeling and solution strategy”. In: *Energy* 152 (June 2018), pp. 358–370.
- [156] T Wakui, M Hashiguchi, K Sawada, and R Yokoyama. “Two-stage design optimization based on artificial immune system and mixed-integer linear programming for energy supply networks”. en. In: *Energy* 170 (Mar. 2019), pp. 1228–1248.
- [157] O Erdinc and M Uzunoglu. “Optimum design of hybrid renewable energy systems: Overview of different approaches”. en. In: *Renewable and Sustainable Energy Reviews* 16.3 (Apr. 2012), pp. 1412–1425.
- [158] L Wang, M Lampe, P Voll, Y Yang, and A Bardow. “Multi-objective superstructure-free synthesis and optimization of thermal power plants”. en. In: *Energy* 116 (Dec. 2016), pp. 1104–1116.
- [159] G Mavromatidis, K Orehounig, LA Bollinger, M Hohmann, JF Marquant, S Miglani, B Morvaj, P Murray, C Waibel, D Wang, and J Carmeliet. “Ten questions concerning modeling of distributed multi-energy systems”. en. In: *Building and Environment* 165 (Nov. 2019), p. 106372.

Bibliography

- [160] IE Grossmann. "Advances in mathematical programming models for enterprise-wide optimization". en. In: *Computers & Chemical Engineering* 47 (Dec. 2012), pp. 2–18.
- [161] JR Tebboth. "A computational study of Dantzig-Wolfe decomposition". PhD thesis. University of Buckingham, 2001.
- [162] R Rahmaniani, TG Crainic, M Gendreau, and W Rei. "The Benders decomposition algorithm: A literature review". en. In: *European Journal of Operational Research* 259.3 (June 2017), pp. 801–817.
- [163] A Fakhri, M Ghatee, A Frakogios, and GK Saharidis. "Benders decomposition with integer subproblem". en. In: *Expert Systems with Applications* 89 (Dec. 2017), pp. 20–30.
- [164] A Ondock, TF Edgar, and M Baldea. "A multi-scale framework for simultaneous optimization of the design and operating strategy of residential CHP systems". en. In: *Applied Energy* 205 (Nov. 2017), pp. 1495–1511.
- [165] G Rius-Sorolla, J Maheut, S Estellés-Miguel, and JP Garcia-Sabater. "Coordination mechanisms with mathematical programming models for decentralized decision-making: a literature review". en. In: *Central European Journal of Operations Research* 28.1 (Mar. 2020), pp. 61–104.
- [166] TH Summers and J Lygeros. "Distributed model predictive consensus via the Alternating Direction Method of Multipliers". en. In: *2012 50th Annual Allerton Conference on Communication, Control, and Computing (Allerton)*. Monticello, IL, USA: IEEE, Oct. 2012, pp. 79–84.
- [167] C Conte, T Summers, MN Zeilinger, M Morari, and CN Jones. "Computational aspects of distributed optimization in model predictive control". en. In: *2012 IEEE 51st IEEE Conference on Decision and Control (CDC)*. Maui, HI, USA: IEEE, Dec. 2012, pp. 6819–6824.
- [168] C Chen, B He, Y Ye, and X Yuan. "The direct extension of ADMM for multi-block convex minimization problems is not necessarily convergent". en. In: *Mathematical Programming* 155.1-2 (Jan. 2016), pp. 57–79.
- [169] L Sokoler, L Standardi, K Edlund, N Poulsen, H Madsen, and J Jørgensen. "A Dantzig–Wolfe decomposition algorithm for linear economic model predictive control of dynamically decoupled subsystems". In: *Journal of Process Control* 24.8 (Aug. 2014), pp. 1225–1236.
- [170] GM Kopanos and EN Pistikopoulos. "Reactive Scheduling by a Multiparametric Programming Rolling Horizon Framework: A Case of a Network of Combined Heat and Power Units". en. In: *Industrial & Engineering Chemistry Research* 53.11 (Mar. 2014), pp. 4366–4386.
- [171] J Silvente, GM Kopanos, EN Pistikopoulos, and A Espuña. "A rolling horizon optimization framework for the simultaneous energy supply and demand planning in microgrids". en. In: *Applied Energy* 155 (Oct. 2015), pp. 485–501.

Bibliography

- [172] GB Dantzig and P Wolfe. "Decomposition Principle for Linear Programs". In: *Operations Research* 8.1 (1960). Publisher: INFORMS, pp. 101–111.
- [173] V Punnathanam and Y Shastri. "Efficient optimization of a large-scale biorefinery system using a novel decomposition based approach". en. In: *Chemical Engineering Research and Design* 160 (Aug. 2020), pp. 175–189.
- [174] V Gunnerud, B Foss, and E Torgnes. "Parallel Dantzig–Wolfe decomposition for real-time optimization—Applied to a complex oil field". en. In: *Journal of Process Control* 20.9 (Oct. 2010), pp. 1019–1026.
- [175] R Cheng, J Fraser Forbes, and W Yip. "Dantzig–Wolfe decomposition and plant-wide MPC coordination". en. In: *Computers & Chemical Engineering* 32.7 (July 2008), pp. 1507–1522.
- [176] H Harb, JN Paprott, P Matthes, T Schütz, R Streblow, and D Müller. "Decentralized scheduling strategy of heating systems for balancing the residual load". en. In: *Building and Environment* 86 (Apr. 2015), pp. 132–140.
- [177] HP Williams. "Duality in mathematics and linear and integer programming". In: *Journal of Optimization Theory and Applications* 90.2 (Aug. 1996), pp. 257–278.
- [178] P Stadler, A Ashouri, and F Maréchal. "Model-based optimization of distributed and renewable energy systems in buildings". In: *Energy and Buildings* 120 (May 2016), pp. 103–113.
- [179] S Fazlollahi. "Decomposition optimization strategy for the design and operation of district energy systems". PhD thesis. EPFL, 2014.
- [180] N Abbasabadi and M Ashayeri. "Urban energy use modeling methods and tools: A review and an outlook". en. In: *Building and Environment* 161 (Aug. 2019), p. 106270.
- [181] C Wouters, ES Fraga, and AM James. "An energy integrated, multi-microgrid, MILP (mixed-integer linear programming) approach for residential distributed energy system planning – A South Australian case-study". en. In: *Energy* 85 (June 2015), pp. 30–44.
- [182] B Pickering and R Choudhary. "District energy system optimisation under uncertain demand: Handling data-driven stochastic profiles". en. In: *Applied Energy* 236 (Feb. 2019), pp. 1138–1157.
- [183] L Kotzur, P Markewitz, M Robinius, G Cardoso, P Stenzel, M Heleno, and D Stolten. "Bottom-up energy supply optimization of a national building stock". en. In: *Energy and Buildings* 209 (Feb. 2020), p. 109667.
- [184] X Liu, J Wu, N Jenkins, and A Bagdanavicius. "Combined analysis of electricity and heat networks". In: *Applied Energy* 162 (Jan. 2016), pp. 1238–1250.
- [185] M Geidl and G Andersson. "A modeling and optimization approach for multiple energy carrier power flow". In: *2005 IEEE Russia Power Tech*. St. Petersburg, Russia: IEEE, June 2005, pp. 1–7.

Bibliography

- [186] F Belfiore. "District heating and cooling systems to integrate renewable energy in urban areas". Publisher: Lausanne, EPFL. PhD thesis. 2021.
- [187] C MacRae, A Ernst, and M Ozlen. "A Benders decomposition approach to transmission expansion planning considering energy storage". en. In: *Energy* 112 (Oct. 2016), pp. 795–803.
- [188] A Rajaei, S Fattaheian-Dehkordi, M Fotuhi-Firuzabad, and M Moeini-Aghetaie. "Decentralized transactive energy management of multi-microgrid distribution systems based on ADMM". en. In: *International Journal of Electrical Power & Energy Systems* 132 (Nov. 2021), p. 107126.
- [189] J Chen, Z Lin, J Ren, W Zhang, Y Zhou, and Y Zhang. "Distributed multi-scenario optimal sizing of integrated electricity and gas system based on ADMM". en. In: *International Journal of Electrical Power & Energy Systems* 117 (May 2020), p. 105675.
- [190] J Tan, Q Wu, W Wei, F Liu, C Li, and B Zhou. "Decentralized robust energy and reserve Co-optimization for multiple integrated electricity and heating systems". en. In: *Energy* 205 (Aug. 2020), p. 118040.
- [191] T Wakui, M Hashiguchi, and R Yokoyama. "Structural design of distributed energy networks by a hierarchical combination of variable- and constraint-based decomposition methods". en. In: *Energy* 224 (June 2021), p. 120099.
- [192] WJ Cole and A Frazier. *Cost Projections for Utility-Scale Battery Storage*. en. Tech. rep. NREL/TP-6A20-73222, 1529218. June 2019, NREL/TP-6A20-73222, 1529218.
- [193] KBOB. *Ökobilanzdaten im Baubereich 2009/1:2016*. Koordinationskonferenz der Bau- und Liegenschaftsorgane der öffentlichen Bauherren. 2016.
- [194] R Frischknecht, P Stolz, L Krebs, MD Wild-Scholten, and P Sinha. "Life Cycle Inventories and Life Cycle Assessments of Photovoltaic Systems 2020 Task 12 PV Sustainability". In: (2020). Publisher: International Energy Agency (IEA).
- [195] Meteonorm. *Global Meteorological Database-Handbook Part II: Theory, Version 7.3.4*. Bern: Meteotest, 2020.

Luise Middelhauve

EDUCATION

PhD Energy / Feb 2018 – Feb 2022

*Swiss Federal Institute of Technology Lausanne (EPFL),
Industrial Process and Energy Systems Engineering (IPES)*
PhD thesis: "On the role of districts as renewable energy hubs"

MSc Energy Engineering/Oct 2014 – Dec 2016

RWTH Aachen University, DE
Master thesis: "Robust optimization of thermal energy systems on city district scale"

Power Engineering/Oct 2014 – Feb 2016

National Tsing Hua University, TW
Master courses in Energy

BSc Mechanical Engineering/Oct 2011 – Sep 2014

Hamburg University of Technology (TUHH), DE
Bachelor thesis: "Modeling of a diesel-combined-cycle power plant for the provision of tertiary control reserve in energy systems with large share of renewable energy sources"

EXPERIENCE

Project manager/Sep 2017 – Feb 2018

Innogy SE, Essen DE
Department New Technologies, Grid & Infrastructure

Research assistant/May 2015 – Sept 2015

RWTH Aachen University, DE
Institute for Combustion Engines (vka)
Simulation of Coolant Circuits for Fuel Cells

Student assistant/Nov 2013 – Sept 2014

MAN Diesel& Turbo, Hamburg DE
Department Instruments & Controls

Internship/ Apr 2011 – Oct 2011

Bentley Motors Limited, Crewe UK
Chassis Development, Vehicles Dynamics

TEACHING

Teaching assistant/Feb 2018 – Feb 2021
Swiss Federal Institute of Technology Lausanne (EPFL)
ME-454 Modelling and optimization of energy systems

Teaching assistant/Sep 2018 – Sep 2021
Swiss Federal Institute of Technology Lausanne (EPFL)
ME-409 Energy conversion and renewable energy

Supervisor master & semester projects/Feb 2018 – Sep 2021

Swiss Federal Institute of Technology Lausanne (EPFL)

- Optimal design and operation of district energy systems using Dantzig-Wolfe decomposition
- Surrogate models for energy system simulation
- Modeling & integration of new technologies for energy system optimization
- Cost estimation of a technology
- Data reduction for mixed integer linear programming in complex energy systems evaluated on objective function and integer decisions
- Evaluation of a biogas and power to gas combined plant as a storage solution for a building energy system
- Solutions for optimal biogas integration in the Sogaval network

PUBLICATIONS

Journal article

- [L Middelhauve](#), C Terrier, and F. Maréchal. (in Review). Decomposition strategy for districts as renewable energy hubs. IEEE Journal of Power and Energy
- [Middelhauve, L.](#), Baldi, F., Girardin, L., and Maréchal, F. (2021). Potential of Photovoltaic Panels on Building's envelope for Decentralized District Energy Systems Frontiers in Energy Research
- [Middelhauve, L.](#), Baldi, F., Stadler, P., and Maréchal, F. (2021). Grid-Aware Layout of Photovoltaic Panels in Sustainable Building Energy Systems. Frontiers in Energy Research

Conference proceedings

- [Middelhauve, L.](#) and Maréchal, F. About data reduction techniques and the role of outliers for complex energy systems. In Proceedings of PSE 2021+
- [Middelhauve, L.](#), Ljubic N., Granacher J., Girardin L., and Maréchal, F. Data reduction for mixed integer linear programming in complex energy systems. In Proceedings of ECOS 2021
- [Middelhauve, L.](#), Santecchia, A., Girardin, L., and Marechal, F. (2020). Key Performance Indicators for Decision Making in Building Energy Systems. In Proceedings of ECOS 2020
- [Middelhauve, L.](#), Baldi, F., Stadler, P. M., Bloch, L., and Maréchal, F. (2019). Influence of photovoltaic panel orientation on modern energy systems in residential buildings. In Proceedings of ECOS 2019

Project reports

- [Middelhauve, L.](#), Girardin, L., (2021). SCCER FURIES- Report on the performance of the implemented solutions with guidelines for subsequent implementation
- Girardin, L., [Middelhauve, L.](#), Lo Cascio, E., Maréchal, F (2021). SCCER FURIES- Chapters on the best investment strategies when prosumer capacities are increased in the grid (REDemo) -
- Bloch, L., Girardin, L., Holweger, [Middelhauve, L.](#) (2020). SCCER JA-RED- A list of possible ancillary services for enhanced grid operation and implementation of the most effective ones at the RE demo site
- Niffeler, M., Schluck, T., Derungs, C., Girardin, L., [Middelhauve, L.](#), & Bloch, L. (2019). SCCER JA-RED-Analysis of initial case and identification of potential use for renewables and waste heat at the building and district level
- [Middelhauve, L.](#), Bloch, L., Holweger, J., Stadler, P. M., & Girardin, L. (2019). SCCER JA-RED-Detailed evaluation of the grid operation bottlenecks and load shifting potential for the reference system
- [Middelhauve, L.](#), Bloch, L., Girardin, L., Stadler, P. M., Holweger, J., & Tommasi, H. (2018). SCCER-FURIES- Design of Sizes for Buildings Energy Systems as a Function of the Grid Evolution